Signaling Proteins in the Post-Synaptic Density

Thesis by

Tinh Nghi Luong

In Partial Fulfillment of the Requirements for the

Degree of

Doctor of Philosophy

CALIFORNIA INSTITUTE OF TECHNOLOGY

Pasadena, California

2010

(Defended May 24, 2010)

Acknowledgments

I would like to thank Mary Kennedy, my advisor, for her support, and for challenging me to become a better scientist. This work would not have been possible without Holly Carlisle who collaborated on most aspects of both Densin and RasGRF1 projects. Andrew Medina-Marino led efforts to create the Densin knockout (KO) mouse after the DNA construct was made by Jenia Khorosheva. Leslie Schenker provided support and technical expertise and did virtually all the genotyping and managed the mice in BBB. Holly Beale analyzed RNA seq data from the forebrains of Densin KO and WT mice. I am grateful to members of the Kennedy Lab past and present including Tami Ursem, Edoardo Marcora, and Lori Washburn and those listed above who were always available for support, questions, and insightful discussions.

Many thanks to my committee members Ray Deshaies, Pamela Bjorkman, Steve Mayo, Paul Patterson, and Paul Sternberg for their constructive criticism and time. Paul Sternberg chaired my committee with great generosity. Paul Patterson collaborated with us on the behavioral characterization of the Denisn KO mouse, for which I am truly grateful, and provided expertise, in addition to training through his lab.

Keith Gunapala and Andrew Steele formally tested nest building in our behavioral cohort and monitored the activity of Densin KO and WT mice using the home cage monitoring system developed by Andrew Steele. They also did GFAP staining of brain sections. Dr. Devin Binder and Mike Hsu (UC Riverside) kindly met with me to evaluate the seizures that the Densin KOs were experiencing. Bruce Cohen and Henry

Lester ran preliminary EEG studies. Shirley Pease provided valuable advice on breeding and obtaining the behavioral cohort. Mona Shagholi and Jie Zhou provided mass spectrometry support for the studies in Chapter 5 and the article in the appendix. Jost Vielmatter, Mike Anaya and Inderjit Nangiana, (Caltech Protein Expression Center) were helpful in expressing RasGRF1 in HEK cells. Renata Zippel provided the RasGRF1-pCDNA3.1 construct. Nicole Tetreault kindly provided training and microscope time for imaging of brain sections. Margarita Behrens (Salk Institute, La Jolla) taught me how to prepare brain sections and stain them with the greatest patience. Natalie Verduzco, Naomi Fujita, Reyna Sauza, Amanda Updike, and Leah Gilera took very good care of our often very needy mice. Amber Southwell, Elaine Hsiao, Prabhat Kunwar, and the Mayo Lab provided access to and training on equipment.

I am grateful to the Biology Department, the Philanthropic Educational Organization (PEO), and Dean Joseph Shepherd and Graduate office for financial support. I am also thankful to Natalie Gilmore for her optimism and kindness.

I am thankful to the USC MD/Ph.D. Program, Dr. Robert Chow, Sandy Mosteller, and Roland Rapanot who always looked after my progress and well-being, and were invested in my success. Separate from the program, Jack Kirsch and Ichiro Matsumura provided career guidance, support, and wisdom.

Jesus Sanchez, Bonefacio Mazas constantly maintained my work habitat I stepped in everyday for years with great work ethics and attitudes. Jose Gonzales and

Bill Lease were always so cooperative with any research supply needs. Cheryl Gause and Liz Ayala provided administrative and moral support.

Julie Ferguson, Violet Delgadillo, and Kim Huynh made me get right back up after each fall and celebrated my successes with me no matter how small. Ellen and Everett Lundsberg have cheered me on since the second grade and were integral in getting me to where I am at today.

Last but not least, I would like to thank my parents, Buu Nhut Luong and Lay Cam Luu, who supported my education and choices above their own needs and made so many sacrifices so that I could succeed. My sister and brother, San and Kien Leung, supported my career and personal goals as did my uncle Lau Chun Man. Terence Heuston, my fiancé, provided video support, and ensured my well-being during my graduate years so that I was as happy as I could be.

Abstract

The ability of an organism to respond to its environment stems from synapses and signaling in the post-synaptic density (PSD). Neurological disorders often occur at the level of faulty signal transduction in the PSD. Here we describe the behavioral characterization of Densin 180, a PSD-enriched scaffold protein. We also report on the regulation of Ras guanine release factor1 (RasGRF1), a guanine exchange factor that promotes activation of Ras and thus the ERK pathway as part of an NMDA (N-methyl-D-aspartate) receptor complex with CaMKII (Ca^{2+}/calmodulin-dependent kinase). The Densin KO exhibits severe nest building deficits, elevated anxiety and aggressiveness, impaired sensorimotor gating, hyperlocomotion to novel objects, and short-term memory (hippocampal- and cortical- dependent) deficits. These behavioral abnormalities resemble schizophrenia and autism. Decreases in the schizophrenia susceptibility gene products, DISC1 and mGluR5, are observed in the KO relative to the WT and may be a result of a decrease in their common binding partner α-actinin. α-actinin is known to regulate mGluR5 surface levels. Cross-linking and stabilization of PSD protein architecture by scaffold proteins like Densin may contribute to some of the observed behavioral abnormalities. The Densin KO also has blunted activity-dependent gene expression. Steady-state levels of the immediate early genes Arc and c-fos are decreased in the hippocampus and cortex of brain sections. Levels of Arc induced in response to stimulation by the neurotrophin BDNF is significantly decreased in the Densin KO neurons after 8 hours of treatment. Impairments in BDNF signaling can lead to affective and cognitive disorder and has a role in cortical inhibition. Dysfunction in

BDNF signaling and DISC1 signaling have been previously implicated in autism. The Densin KO also is susceptible to seizures, in particular when injected with Nembutal, a GABA(A) agonist. One point of intersection between signaling pathways that involve DISC1, mGluR, and BDNF is at the level of ERK signaling, which if impaired may establish a hypoglutamatergic state in the Densin KO.

In addition to characterizing the Densin KO, we studied possible interactions of RasGRF1 and CaMKII with the NR2B subunit tail of the NMDA receptor. CaMKII phosphorylation sites on RasGRF1 were identified, including Ser916, by mass spectrometry. Immunoprecipitation from HEK cells revealed that RasGRF1 enhances CaMKII association with NR2B.

Chapter 1
The Post-synaptic Density and Synaptic Plasticity

The ability to act, think, and feel originates at neuronal synapses where transmission of information occurs between neurons at opposing pre- and post-synaptic structures. The presynaptic terminal releases neurotransmitters that diffuse across the synaptic cleft. A specialized cluster of proteins called the postsynaptic density (PSD) lies near the membrane in the postsynapse and responds to the chemical traffic (Kennedy, 2000) and Fig. 1.1). As one can imagine, orchestrating the signals from billions of these pre- and postsynaptic hubs into synchronized action potentials representing different networks is no small task. Each synapse maintains homeostasis but is also flexible and can modify the strength/efficacy of its connections. This "synaptic plasticity" is ultimately what allows an organism to respond to its environment.

Signal transduction mechanisms enable synaptic plasticity in both excitatory and inhibitory synapses. However, well-defined PSDs are only found in excitatory synapses. Receptors embedded in the PSD bind neurotransmitters and relay this information to signaling proteins intracellularly through protein-protein interactions, conformational changes, or post-translational modifications. In addition to signaling proteins, the PSD is comprised of layers of scaffolding proteins and cell adhesion complexes that collectively respond to changes in synaptic activity to strengthen or weaken communication at the synapse. Misregulation of the finely tuned, dynamic processes that occur in the PSD to maintain homeostasis and to respond to stimuli can lead to diseases of the central nervous system (Butler et al., 1995; Durand et al., 2007; Brandon et al., 2009; Yoshii and Constantine-Paton, 2010). Mechanisms that contribute to schizophrenia, affective

disorders, autism, and cognitive defects often overlap at the level of faulty signal transduction at excitatory and inhibitory synapses (Cohen and Greenberg, 2008; Brandon et al., 2009; Yoshii and Constantine-Paton, 2010).

Changes in Spine Morphology in Synaptic Plasticity

Spines are small protrusions averaging approximately 1 micron long and 0.5 microns wide, emanating from dendritic branches of neurons. Postsynaptic contacts and PSDs are usually situated near the tip of a spine. Spines assume different shapes, volumes, and lengths that reflect their functional state regulated by integrated signals coming through the PSD. Spines are categorized as mushroom, stubby, thin, or filopodial, based on the ratio of their head diameter to neck length (Fiala et al., 2002; Bourne and Harris, 2008). Mushroom spines are considered the most "mature." They have a bulbous head with a relatively large PSD and a thinner neck. Thin spines are believed to be less mature, having smaller heads and PSDs. The head of the spine undergoes large changes in size and shape as a result of synaptic plasticity (Bourne and Harris, 2007; Tanaka et al., 2008). The neck is also plastic and helps to contain ion fluxes and activated signaling cascades within the spine head, limiting spillover to the dendrite and neighboring synapses. Ca^{2+} transients, for instance, can reach higher concentrations in thin and filopodial spines (Bourne and Harris, 2008). Aberrant spine morphology and density is associated with disorders such as Fragile X (increase in filopodial spines), other forms of mental retardation, schizophrenia (decreased density), and epilepsy (Swann et al., 2000; Fiala et al., 2002; Ramakers, 2002). Longer spines, seen in the Densin KO, are

usually correlated with immaturity (Holly Carlisle, unpublished data). The Densin KO also has more mushroom and fewer stubby shaped spines (Holly Carlisle and Andrew Medina Marino, unpublished data), which is addressed further in Chapter 2 with implications for psychiatric disorders.

Remodeling of spines occurs with long term potentiation (LTP) and long term depression (LTD), two forms of synaptic plasticity that persistently increase and decrease the efficiency in postsynaptic response, respectively. Electrophysiologically, LTP is typically induced by high frequency stimulation (trains of 50-100 stimuli at 100 Hz or more) and LTD with low frequency stimulation (0.5-5 Hz) (Dudek and Bear, 1992; Bliss and Collingridge, 1993; Dudek and Bear, 1993; Malenka and Bear, 2004). During the consolidation phase of LTP, thin spines enlarge and expand into mushroom spines. Because thin spines are shorter lived and adjust more flexibly in response to changes, they have been hypothesized to act as "learning spines" that are converted to the more stable mushroom spines, which are considered to be "memory spines" (Bourne and Harris, 2007). Single spines, when activated with high frequency photo-uncaging of glutamate accompanied by postsynaptic spiking enlarge into mushroom spines within seconds, after which the neck gradually decreases in diameter and shortens over a period of ~1 hour (Tanaka et al., 2008). To adjust to its new functional state with induction of LTP, lipid-bound vesicles (amorphous vesicular clumps and endsomes) and polyribosomes are also transported into the spine from the shaft of the dendrite. The vesicular clumps provide lipids to expand the spine membrane to a bulbous head, whereas endsomes regulate trafficking of new proteins to the surface membrane, and

polyribosomes carry out local synthesis of new proteins (Park et al., 2006; Bourne and Harris, 2007).

A redistribution of the sizes and shapes of spines is also seen during the maturation of neurons. In particular, there is an increase in thin and mushroom spines with perforated PSDs from postnatal day 15 to adulthood (Harris et al., 1992). Perforations are ”holes” in the PSD observed at the tips of spines during spine maturation (Bourne and Harris, 2008). They are believed to reflect structural reorganization that takes place as the synapse matures. Along with growth of spines, pruning is also needed to prevent inappropriate synaptic connections. The process of appropriate pruning may be affected in diseases like schizophrenia (McGlashan and Hoffman, 2000). Shrinkage and retraction of spines is associated with LTD (Chen et al., 2004; Nagerl et al., 2004; Zhou et al., 2004), which is thought to decrease the transmission of information at the synapse and return the spine to a state that can be potentiated in the future (Bourne and Harris, 2007).

The mice in which the Densin gene has been knocked out have significantly longer spines than wild type (Holly Carlisle, unpublished data). Longer, thinner spines are often associated with immaturity (Fiala et al., 2002; Bourne and Harris, 2007; Bourne and Harris, 2008). The Densin KO also has a higher proportion of mushroom spines and fewer stubby spines (Holly Carlisle and Andrew Medina Marino, unpublished). The implications of these finding are addressed in Chapter 2 along with the implications for psychiatric disorders.

Signal transduction in the post synaptic density in synaptic plasticity

The morphological alterations associated with changes in synaptic strength are driven by rearrangements of PSD proteins and the actin cytoskeleton, as orchestrated by signaling transduction pathways. The two classes of glutamate receptors in the PSD, ionotropic and metabotropic, are distinguished by their mode of signaling, either by ionic flux or by coupling to G proteins as second messengers, respectively. The AMPA (α-amino-3-hydroxyl-5-methyl-4-isoxazole-propionate) and NMDA (N-methyl-D-aspartic acid) receptors are the most important of the ionotropic receptors. During the induction of LTP, the PSD expands along with the enlarging spine. This expansion is associated with increased levels of NMDA and AMPA receptors (Harris et al., 1992; Bourne and Harris, 2008), although AMPA receptor levels increase more dramatically (Nusser, 2000). Signaling from the synaptic cleft is relayed intracellularly to signal transduction molecules, many of which are clustered near the glutamate receptors. Stimulation of NMDA receptors leads to Ca^{2+} influx, which activates Ca^{2+}/calmodulin dependent protein kinase II (CaMKII), a key mediator of LTP (Lisman et al., 2002; Merrill et al., 2005). CaMKII phosphorylates a number of substrates including AMPA receptors. Phosphorylation of the AMPA receptor by CaMKII modulates the size of the current through the AMPA receptor (Soderling and Derkach, 2000). Phosphorylation of additional substrates by CaMKII leads to upregulation of surface levels of AMPA receptors on a time scale of several minutes, augmenting future responses to glutamate stimulation (Hayashi et al., 2000; Lee et al., 2003). Induction of LTD leads to increased removal of AMPA receptors by endocytosis (Malenka and Bear, 2004; Waung et al.,

2008). Thus, regulation of AMPA receptor trafficking to the membrane is a mechanism used in induction of both LTP and LTD to encode changes in synaptic transmission.

In addition to CaMKII, other Ca^{2+} sensors respond to stimulation of the NMDA receptor, including RasGRF1 (which activates the Ras-Erk pathway (Krapivinsky et al., 2003), adenylate cyclase (Chetkovich and Sweatt, 1993), calcineurin (Morishita et al., 2005), and nitric oxide synthase (Brenman and Bredt, 1997). These sensors mediate a variety of synaptic processes important in neuronal survival, maturation, and differentiation. The interactions of RasGRF1 and CaMKII with the NMDA receptor complex are described in Chapter 5. Signal transduction mechanisms involving LIM kinase (LIMK), cofilin and the ARP 2/3 complex control reorganization of the actin cytoskeleton that underlies the structural plasticity of spines (Carlisle and Kennedy, 2005). α-actinin, which is a binding partner of Densin, the NMDA receptor (NR2 and NR2B subunits), and αCaMKII, is thought to link the NMDA signaling machinery to the actin cytoskeleton (Wyszynski et al., 1997; Wyszynski et al., 1998; Krupp et al., 1999; Walikonis et al., 2001; Nakagawa et al., 2004).

Glutamate receptors and synaptic plasticity

In the Densin KO, induction of LTD is impaired and the amount of mGluR5 in the PSD is decreased (H. Carlisle, unpublished). These two findings may be linked because one form of LTD is mediated by mGluR. In the following section, I review the role and regulation of glutamate receptors in LTP and LTD.

The two major mechanisms for the regulation of AMPA receptors are phosphorylation of the GluR1 and GluR2, subunits of the AMPA receptor, and trafficking of the receptors into and out of the postsynaptic membrane. Phosphorylation of GluR1 subunits on Ser 831 by CaMKII and on Ser 845 by CaMKII and PKA (Hayashi et al., 2000; Lee et al., 2003) regulate the internalization of the receptor. Additional sites have been seen to alter channel properties (Soderling and Derkach, 2000). Both the number of AMPA receptors in the synaptic membrane and their channel properties influence the strength of synaptic transmission. Insertion of the receptor occurs by exocytosis chaperoned by stargazin-PSD-95 complexes (Schnell et al., 2002). Internalization of the receptor occurs via clathyrin endocytosis complexes containing endophilin and dynamin, a process that requires interaction with the immediate early gene, Arc (Chowdhury et al., 2006).

In LTD, spine volume is reduced, concomitant with the dismantling of actin and removal of AMPA receptors from the membrane surface. From a disease perspective, one purpose of LTD is to prevent damage from excitotoxicity that may result if too many synapses on a neuron are too highly potentiated for too long (Villmann and Becker, 2007). The two most studied forms of LTD are facilitated by two glutamate receptors: the ionotropic NMDA receptor, which produces Ca^{2+} influx that triggers LTD, and metabotropic glutamate receptors, which are coupled to G proteins and increase Ca^{2+} concentration by release from intracellular stores (Huber et al., 2001; Luscher and Huber, 2010).

Overstimulation of the NMDA receptor can lead to excitotoxcity (Villmann and Becker, 2007). However, a normal homeostatic mechanism results in synaptic depression in response to prolonged NMDA receptor activation and thus prevents excitotoxicity. This mechanism requires activation of calcineurin and protein phosphatase 1 (Morishita et al., 2005). NMDA-dependent LTD involves the decrease of surface AMPA receptors either through GluR1 dephosphorylation, or through increased removal of GluR2 from the synaptic membrane, the converse of what is seen in LTP, which is mediated by the same receptor. Dephosphorylation of GluR1 AMPA receptor at Ser 845, the PKA site, is correlated with LTD (reviewed in (Malenka and Bear, 2004)).

A second form of LTD that is distinct from that mediated by the NMDA receptor, depends on signaling through metabotropic glutamate receptors (mGluRs). In contrast to ionotropic glutamate receptors, mGluR receptors transmit signals through G-proteins that activate hydrolysis of phosphotidylinositol 4,5 bisphosphate (PIP2) by phospholipase C, yielding the messengers 1,4,5-trisphosphate (IP3) and diacylglycerol. Metabotropic glutamate receptors are classified into three groups (I, II, and III), of which Group I (which includes mGluRs 1 and 5) is the only one located in the postsynaptic density. Studies in the cerebellum and hippocampus have revealed that group I mGluRs participate in LTP and LTD, which is regulated by the complex of proteins anchored to it (Niswender and Conn, 2010). The immediate early gene and scaffold protein, Homer 1A links mGluRs to a meshwork of proteins linked to Shank's modular domains. The linkage produces a physical bridge that allows cross talk between Group I mGluR and NMDA receptors (Bertaso et al.; Ronesi and Huber, 2008). Moreover, α-actinin, a binding

partner of Densin, interacts directly with mGluRs and is thought to regulate their surface levels.

Scaffold proteins and synaptic plasticity

Scaffold proteins such as Densin and PSD-95 (discussed in Chapters 2, 3, 4, and the Appendix) contribute to synaptic plasticity by helping to adapt the PSD architecture to changes in synaptic strength. This can be accomplished by physically linking receptors to downstream signaling molecules, regulating endocytosis, shaping dendritic morphology, or creating an interface between the PSD and the actin cytoskeleton. PSD-95 associates directly with the carboxyl terminal tails of the NR2 subunits of the NMDA receptor (Kornau et al., 1995). Deletion of PSD-95 leads to alterations in the configuration of signaling proteins associated with the NMDA receptor. PSD-95 also regulates levels of AMPA receptors by playing a role in their trafficking through stargazin (Chen et al., 2000; El-Husseini et al., 2000; Schnell et al., 2002). The Homer family of proteins associates with mGluRs at the edges of the PSD and links them both to internal Ca2+ stores and to the PSD itself through its interaction with Shank (Tu et al., 1999; Sala et al., 2001). Shank is another prominent scaffold protein that forms bridges between the NMDA, mGluR, and AMPA receptor complexes through its modular domains (including a PDZ domain, an SH3 domain, a SAM domain, and ankyrin-like repeats) (Naisbitt et al., 1999).

Activity-dependent transcription and synaptic plasticity

Information about recent activity at the synapse can be transmitted to the cell body in order to direct long lasting adaptations by the neuron through increased transcription (Cohen and Greenberg, 2008). Defects in activity-dependent transcription, as may be present in the Densin KO (Chapter 2 and 3), can lead to neurological dysregulation. The immediate early genes are defined in the nervous system as those rapidly transcribed in response to neuronal stimulation. This family includes activity-regulated cytoskeletal protein (Arc), c-fos, Jun, Homer 1A, etc. Ca^{2+} signaling in spines and protein sensors in the PSD initiate signals that travel to the nucleus. One well-studied example of a transcription factor regulated by synaptic activity is cyclic AMP response element-binding protein (CREB). Several signaling pathways acting through at least four protein kinases (PKA, RSK, CaMKIV, CaMKII) converge on regulation of phosphorylation of CREB at Ser 133 (reviewed in (Cohen and Greenberg, 2008)). CREB helps to control the transcription of target genes, including many of the IEGs, by binding to a CRE sequence within their promoter. Mutation of activity-dependent transcription factors, or of any genes encoding proteins that contribute to activation of CREB, can cause mental disorders. It is also believed that the loss of any of the IEGs or other activity-dependent genes may result in some loss of cognitive ability (Cohen and Greenberg, 2008). In addition to CREB, NF-kB and Npas4 are activity-dependent transcription factors that respond to synaptic activity or membrane depolarization by increasing expression of a certain sets of genes. For both transcription factors, this group includes the gene encoding brain-derived neurotrophic factor (BDNF), which plays

an important role in regulating dendritic growth and synaptic plasticity (Waterhouse and Xu, 2009; Yoshii and Constantine-Paton, 2010).

Protein synthesis and synaptic plasticity

Although not always proportional, increased transcription often prompts increased protein translation from these transcripts. Lasting changes in the strength of the synapse, as in the consolidation of LTP and LTD, requires the synthesis of new proteins, which is regulated temporally and spatially (Frey et al., 1988; Huber et al., 2001). The administration of protein synthesis inhibitors (i.e. anisomycin) during and shortly after the initiation of LTP blocks the enlargement of spines and consolidation of late phase LTP (Frey et al., 1988; Tanaka et al., 2008). In addition to protein synthesis in the soma, translation in dendrites plays a prominant role. For example, local translation in activated dendrites has been proposed as a way for neurons to tag particular synapses based on experience (Frey and Morris, 1997). Polyribosomes have been observed by electron microscopy in dendrites near the base of spines (Steward and Levy, 1982; Sutton and Schuman, 2006) and within spines following induction of LTP (Ostroff et al., 2002).

Dendritic protein synthesis is important in encoding synaptic plasticity and molecular memory, although its precise role in tagging is still unclear (Frey and Morris, 1997; Sutton and Schuman, 2006). Supporting data have come from the use of drugs to block protein synthesis, studies with mutant mice, and study of synaptic transmission in dendrites physically disconnected from the soma after stimulation (Frey et al., 1988; Frey et al., 1989; Kang and Schuman, 1996; Sutton and Schuman, 2006). The list of

confirmed locally translated proteins is likely not complete, but the most studied and well known of them is CaMKII (Ouyang et al., 1999; Miller et al., 2002; Sutton and Schuman, 2006). Mice lacking the 3' untranslated region (UTR) that is responsible for directing nascent CaMKII mRNA to the dendrite have deficits in hippocampal-dependent and object recognition memory and in late phase LTP (Miller et al., 2002). The transcript of Arc is upregulated in response to synaptic activity and transported into active dendrites where it is translated and participates in synaptic regulation of AMPA receptor trafficking and rearrangments in the actin cytoskeleton (Ying et al., 2002; Waung et al., 2008). Neurotrophin induced plasticity, for example that induced by BDNF, is an example in which synaptic plasticity is depends on production of new protein (Kang and Schuman, 1996; Tanaka et al., 2008). Induction of LTP by BDNF in hippocampal dendrites that have been physically disconnected from the soma is impaired without local protein synthesis (Kang and Schuman 1996). It was later shown induction of plasticity by BDNF also requires expression of Arc, as addressed more extensively in Chapter 3 (Ying et al., 2002; Bramham et al., 2009).

LTD also requires protein translation, some of which occurs rapidly. Stimulation of metabotropic GluRs facilitates dendritic protein synthesis-dependent LTD that is distinct from that induced by NMDA receptor activation (Huber et al., 2000; Huber et al., 2001). mGluR-dependent LTD requires synthesis of Arc within 5 min. of stimulation, as well as translation of other proteins (Huber et al., 2000; Waung et al., 2008). Preincubation with anisomycin blocks LTD initated by the Group I mGluR agonist, DHPG (*RS*-3,5-dihydroxyphenylglycine) (Huber et al., 2000). mGluRs are thought to facilitate

LTD by regulation of endocytosis of AMPARs by a complex that includes Arc, dynamin, and endophilin (Chowdhury et al., 2006; Waung et al., 2008).

Activity-dependent degradation of proteins is also integrally involved in development, homeostasis, and synaptic plasticity. Protein degradation in the PSD occurs primarily through the activity of E3 ubiquitin ligases, ubiquitin-activating E1 enzymes, and ubiquitin-conjugating E2 enzymes (Segref and Hoppe, 2009). Increased degradation of Shank3, along with particular scaffold proteins, is stimulated by synaptic activity (Ehlers, 2003). Ubiquitination of PSD-95, for example, leads indirectly to decreases in levels of surface AMPA receptors and deficits in NMDA receptor-dependent LTD (Colledge et al., 2003). Mono-ubiquitination of receptors can direct them to lysosomes or recycling endosomes. Proteasomes have been observed in dendrites and can be transported into the spine where they bind to active CaMKII upon synaptic stimulation (Bingol et al., 2010).

Balance of inhibitory and excitatory inputs in synaptic plasticity

While the processes discussed above occur mostly in excitatory synapses, inhibitory synapses that use GABA (γ-aminobutyric acid) as their transmitter also contribute to brain plasticity. Within neuronal networks, inhibitory inputs refine the neuron's decision to fire or not. Unlike the PSDs of excitatory synapses, the postsynaptic membranes of inhibitory synapses are not situated on the ends of spines. In inhibitory synapses, the presynaptic bouton makes contact with the dendritic shaft. The postsynaptic protein complex contains some but not all of the components of the

PSD, and plasticity occurs by different mechanisms. Imbalance of inhibitory and excitatory tone in the brain contributes to the etiology of seizure disorders, and possibly in schizophrenia, autism, and mood disorders (Cline, 2005; Fritschy, 2008). This is further discussed in Chapter 4.

Neuronal networks and behavior

The formation of appropriate synapses is necessary to establish well-functioning neural circuits. Donald Hebb originally hypothesized that neurons that "fire together wire together" (Hebb, 1949). Research over the last 50 years has largely confirmed this prediction. Neurons become specialized for receiving inputs from other neurons after repeatedly adjusting synaptic transmission (Hebb, 1949). Problems with connectivity, sometimes resulting from miswiring during developmental, and over-excitability of particular neuronal networks, have been implicated in autism, schizophrenia and epilepsy. In schizophrenia, for instance, disruption in inhibitory tone in a subset of inhibitory, fast spiking interneurons containing parvalbumin results in aberrant network oscillation patterns (Belforte et al.; Jones 2010; Lodge et al., 2009). In epilepsy, inappropriate mossy fiber growth with kindling contributes to asynchronous firing that may occur by similar mechanisms that modulate synaptic plasticity (Morimoto et al., 2004).

Networks of neurons from different parts of the brain collaborate to control behavior. Behavioral studies of mouse models have established that either inappropriate responses to normal synaptic activity or lack of necessary responses

interferes with the ability of an organism to interact with its environment. While it is difficult to correlate mouse behavioral phenotypes with mental disorders in humans, many mouse behavioral abnormalities can be considered endophenotypes associated with a disorder. Together, these endophenotypes may constitute a syndrome that is representative of a particular disease (Takao et al., 2007). A disease model can also be created by mutating or deleting a known susceptibility gene for a human disease, such as the DISC1 (disrupted-in-schizophrenia) gene, arguably the leading genetic risk factor for schizophrenia (Blackwood et al., 2001). Mutation of even such a highly predisposing gene, however, can result in clinically heterogeneous symptoms that vary in severity due to environmental and genetic variability between individuals. This was exemplified by cases of recurring major depression, bipolar, and anxiety disorder seen with the chromosomal translocation in the Scottish family where DISC1 was identified. Increasingly, it appears that there is a biological continuum in the pathophysiology of mental diseases. This may also be true in the Densin KO (Chapter 2, 3, and 4), which exhibits schizophrenic-like endophenotypes compounded with anxiety and a susceptibility to seizures, the latter of which is often a comorbidity in the human schizophrenic population.

Summary of thesis

This thesis concerns the contributions to synaptic plasticity of the NMDA receptor signal transduction complex and the scaffold proteins, Densin and PSD-95. The behavioral characterization of the Densin KO mouse is described in Chapter 2. Possible

molecular links to epilepsy, anxiety, and schizophrenia are discussed with respect to the observed decrease in steady state levels of α-actinin, DISC1, mGluR, and Arc. Alterations in Arc and c-fos levels in the Densin KO are discussed in Chapter 3. Chapter 4 addresses the disruptions in the GABAergic system associated with the seizure phenotype in the Densin KO. Chapter 5 concerns the interaction of RasGRF1, an activator of Ras, with the NMDA receptor complex. Control of the ERK pathway via Ras is important for neuronal maturation, gene transcription, neuronal survival, and synaptic plasticity. Finally, the article in the Appendix contains the results of a collaboration with Dmitry Korkin and members of Andre Salij's lab that addressed regulation of the scaffold protein, PSD-95, by intramolecular interactions. Biochemical and mass spectrometry data were combined with computational "patch" analysis to determine the domains that comprise the stable core of the PSD-95 protein.

REFERENCES

Belforte JE, Zsiros V, Sklar ER, Jiang Z, Yu G, Li Y, Quinlan EM, Nakazawa K Postnatal NMDA receptor ablation in corticolimbic interneurons confers schizophrenia-like phenotypes. Nat Neurosci 13:76-83.

Bertaso F, Roussignol G, Worley P, Bockaert J, Fagni L, Ango F Homer1a-dependent crosstalk between NMDA and metabotropic glutamate receptors in mouse neurons. PLoS One 5:e9755.

Bingol B, Wang CF, Arnott D, Cheng D, Peng J, Sheng M (2010) Autophosphorylated CaMKIIalpha acts as a scaffold to recruit proteasomes to dendritic spines. Cell 140:567-578.

Blackwood DH, Fordyce A, Walker MT, St Clair DM, Porteous DJ, Muir WJ (2001) Schizophrenia and affective disorders--cosegregation with a translocation at chromosome 1q42 that directly disrupts brain-expressed genes: clinical and P300 findings in a family. Am J Hum Genet 69:428-433.

Bliss TV, Collingridge GL (1993) A synaptic model of memory: long-term potentiation in the hippocampus. Nature 361:31-39.

Bourne J, Harris KM (2007) Do thin spines learn to be mushroom spines that remember? Curr Opin Neurobiol 17:381-386.

Bourne JN, Harris KM (2008) Balancing structure and function at hippocampal dendritic spines. Annu Rev Neurosci 31:47-67.

Bramham CR, Alme MN, Bittins M, Kuipers SD, Nair RR, Pai B, Panja D, Schubert M, Soule J, Tiron A, Wibrand K (2009) The Arc of synaptic memory. Exp Brain Res.

Brandon NJ, Millar JK, Korth C, Sive H, Singh KK, Sawa A (2009) Understanding the role of DISC1 in psychiatric disease and during normal development. J Neurosci 29:12768-12775.

Brenman JE, Bredt DS (1997) Synaptic signaling by nitric oxide. Curr Opin Neurobiol 7:374-378.

Butler LS, Silva AJ, Abeliovich A, Watanabe Y, Tonegawa S, McNamara JO (1995) Limbic epilepsy in transgenic mice carrying a Ca2+/calmodulin-dependent kinase II alpha-subunit mutation. Proc Natl Acad Sci U S A 92:6852-6855.

Carlisle HJ, Kennedy MB (2005) Spine architecture and synaptic plasticity. Trends Neurosci 28:182-187.

Chen L, Chetkovich DM, Petralia RS, Sweeney NT, Kawasaki Y, Wenthold RJ, Bredt DS, Nicoll RA (2000) Stargazin regulates synaptic targeting of AMPA receptors by two distinct mechanisms. Nature 408:936-943.

Chen Y, Bourne J, Pieribone VA, Fitzsimonds RM (2004) The role of actin in the regulation of dendritic spine morphology and bidirectional synaptic plasticity. Neuroreport 15:829-832.

Chetkovich DM, Sweatt JD (1993) nMDA receptor activation increases cyclic AMP in area CA1 of the hippocampus via calcium/calmodulin stimulation of adenylyl cyclase. J Neurochem 61:1933-1942.

Chowdhury S, Shepherd JD, Okuno H, Lyford G, Petralia RS, Plath N, Kuhl D, Huganir RL, Worley PF (2006) Arc/Arg3.1 interacts with the endocytic machinery to regulate AMPA receptor trafficking. Neuron 52:445-459.

Cline H (2005) Synaptogenesis: a balancing act between excitation and inhibition. Curr Biol 15:R203-205.

Cohen S, Greenberg ME (2008) Communication between the synapse and the nucleus in neuronal development, plasticity, and disease. Annu Rev Cell Dev Biol 24:183-209.

Colledge M, Snyder EM, Crozier RA, Soderling JA, Jin Y, Langeberg LK, Lu H, Bear MF, Scott JD (2003) Ubiquitination regulates PSD-95 degradation and AMPA receptor surface expression. Neuron 40:595-607.

Dudek SM, Bear MF (1992) Homosynaptic long-term depression in area CA1 of hippocampus and effects of N-methyl-D-aspartate receptor blockade. Proc Natl Acad Sci U S A 89:4363-4367.

Dudek SM, Bear MF (1993) Bidirectional long-term modification of synaptic effectiveness in the adult and immature hippocampus. J Neurosci 13:2910-2918.

Durand CM et al. (2007) Mutations in the gene encoding the synaptic scaffolding protein SHANK3 are associated with autism spectrum disorders. Nat Genet 39:25-27.

Ehlers MD (2003) Activity level controls postsynaptic composition and signaling via the ubiquitin-proteasome system. Nat Neurosci 6:231-242.

El-Husseini AE, Schnell E, Chetkovich DM, Nicoll RA, Bredt DS (2000) PSD-95 involvement in maturation of excitatory synapses. Science 290:1364-1368.
Fiala JC, Spacek J, Harris KM (2002) Dendritic spine pathology: cause or consequence of neurological disorders? Brain Res Brain Res Rev 39:29-54.
Frey U, Morris RG (1997) Synaptic tagging and long-term potentiation. Nature 385:533-536.
Frey U, Krug M, Reymann KG, Matthies H (1988) Anisomycin, an inhibitor of protein synthesis, blocks late phases of LTP phenomena in the hippocampal CA1 region in vitro. Brain Res 452:57-65.
Frey U, Krug M, Brodemann R, Reymann K, Matthies H (1989) Long-term potentiation induced in dendrites separated from rat's CA1 pyramidal somata does not establish a late phase. Neurosci Lett 97:135-139.
Fritschy JM (2008) Epilepsy, E/I Balance and GABA(A) Receptor Plasticity. Front Mol Neurosci 1:5.
Harris KM, Jensen FE, Tsao B (1992) Three-dimensional structure of dendritic spines and synapses in rat hippocampus (CA1) at postnatal day 15 and adult ages: implications for the maturation of synaptic physiology and long-term potentiation. J Neurosci 12:2685-2705.
Hayashi Y, Shi SH, Esteban JA, Piccini A, Poncer JC, Malinow R (2000) Driving AMPA receptors into synapses by LTP and CaMKII: requirement for GluR1 and PDZ domain interaction. Science 287:2262-2267.
Hebb DO (1949) The Organization of Behavior: A neuropsychological theory. New York: Wiley.
Huber KM, Kayser MS, Bear MF (2000) Role for rapid dendritic protein synthesis in hippocampal mGluR-dependent long-term depression. Science 288:1254-1257.
Huber KM, Roder JC, Bear MF (2001) Chemical induction of mGluR5- and protein synthesis--dependent long-term depression in hippocampal area CA1. J Neurophysiol 86:321-325.
Jones MW Errant ensembles: dysfunctional neuronal network dynamics in schizophrenia. Biochem Soc Trans 38:516-521.
Kang H, Schuman EM (1996) A requirement for local protein synthesis in neurotrophin-induced hippocampal synaptic plasticity. Science 273:1402-1406.
Kennedy MB (2000) Signal-processing machines at the postsynaptic density. Science 290:750-754.
Kornau HC, Schenker LT, Kennedy MB, Seeburg PH (1995) Domain interaction between NMDA receptor subunits and the postsynaptic density protein PSD-95. Science 269:1737-1740.
Krapivinsky G, Krapivinsky L, Manasian Y, Ivanov A, Tyzio R, Pellegrino C, Ben-Ari Y, Clapham DE, Medina I (2003) The NMDA receptor is coupled to the ERK pathway by a direct interaction between NR2B and RasGRF1. Neuron 40:775-784.
Krupp JJ, Vissel B, Thomas CG, Heinemann SF, Westbrook GL (1999) Interactions of calmodulin and alpha-actinin with the NR1 subunit modulate Ca2+-dependent inactivation of NMDA receptors. J Neurosci 19:1165-1178.

Lee HK, Takamiya K, Han JS, Man H, Kim CH, Rumbaugh G, Yu S, Ding L, He C, Petralia RS, Wenthold RJ, Gallagher M, Huganir RL (2003) Phosphorylation of the AMPA receptor GluR1 subunit is required for synaptic plasticity and retention of spatial memory. Cell 112:631-643.

Lisman J, Schulman H, Cline H (2002) The molecular basis of CaMKII function in synaptic and behavioural memory. Nat Rev Neurosci 3:175-190.

Lodge DJ, Behrens MM, Grace AA (2009) A loss of parvalbumin-containing interneurons is associated with diminished oscillatory activity in an animal model of schizophrenia. J Neurosci 29:2344-2354.

Luscher C, Huber KM (2010) Group 1 mGluR-dependent synaptic long-term depression: mechanisms and implications for circuitry and disease. Neuron 65:445-459.

Malenka RC, Bear MF (2004) LTP and LTD: an embarrassment of riches. Neuron 44:5-21.

McGlashan TH, Hoffman RE (2000) Schizophrenia as a disorder of developmentally reduced synaptic connectivity. Arch Gen Psychiatry 57:637-648.

Merrill MA, Chen Y, Strack S, Hell JW (2005) Activity-driven postsynaptic translocation of CaMKII. Trends Pharmacol Sci 26:645-653.

Miller S, Yasuda M, Coats JK, Jones Y, Martone ME, Mayford M (2002) Disruption of dendritic translation of CaMKIIalpha impairs stabilization of synaptic plasticity and memory consolidation. Neuron 36:507-519.

Morimoto K, Fahnestock M, Racine RJ (2004) Kindling and status epilepticus models of epilepsy: rewiring the brain. Prog Neurobiol 73:1-60.

Morishita W, Marie H, Malenka RC (2005) Distinct triggering and expression mechanisms underlie LTD of AMPA and NMDA synaptic responses. Nat Neurosci 8:1043-1050.

Nagerl UV, Eberhorn N, Cambridge SB, Bonhoeffer T (2004) Bidirectional activity-dependent morphological plasticity in hippocampal neurons. Neuron 44:759-767.

Naisbitt S, Kim E, Tu JC, Xiao B, Sala C, Valtschanoff J, Weinberg RJ, Worley PF, Sheng M (1999) Shank, a novel family of postsynaptic density proteins that binds to the NMDA receptor/PSD-95/GKAP complex and cortactin. Neuron 23:569-582.

Nakagawa T, Engler JA, Sheng M (2004) The dynamic turnover and functional roles of alpha-actinin in dendritic spines. Neuropharmacology 47:734-745.

Niswender CM, Conn PJ Metabotropic glutamate receptors: physiology, pharmacology, and disease. Annu Rev Pharmacol Toxicol 50:295-322.

Nusser Z (2000) AMPA and NMDA receptors: similarities and differences in their synaptic distribution. Curr Opin Neurobiol 10:337-341.

Ostroff LE, Fiala JC, Allwardt B, Harris KM (2002) Polyribosomes redistribute from dendritic shafts into spines with enlarged synapses during LTP in developing rat hippocampal slices. Neuron 35:535-545.

Ouyang Y, Rosenstein A, Kreiman G, Schuman EM, Kennedy MB (1999) Tetanic stimulation leads to increased accumulation of Ca(2+)/calmodulin-dependent protein kinase II via dendritic protein synthesis in hippocampal neurons. J Neurosci 19:7823-7833.

Park M, Salgado JM, Ostroff L, Helton TD, Robinson CG, Harris KM, Ehlers MD (2006) Plasticity-induced growth of dendritic spines by exocytic trafficking from recycling endosomes. Neuron 52:817-830.

Ramakers GJ (2002) Rho proteins, mental retardation and the cellular basis of cognition. Trends Neurosci 25:191-199.

Ronesi JA, Huber KM (2008) Homer interactions are necessary for metabotropic glutamate receptor-induced long-term depression and translational activation. J Neurosci 28:543-547.

Sala C, Piech V, Wilson NR, Passafaro M, Liu G, Sheng M (2001) Regulation of dendritic spine morphology and synaptic function by Shank and Homer. Neuron 31:115-130.

Schnell E, Sizemore M, Karimzadegan S, Chen L, Bredt DS, Nicoll RA (2002) Direct interactions between PSD-95 and stargazin control synaptic AMPA receptor number. Proc Natl Acad Sci U S A 99:13902-13907.

Segref A, Hoppe T (2009) Think locally: control of ubiquitin-dependent protein degradation in neurons. EMBO Rep 10:44-50.

Soderling TR, Derkach VA (2000) Postsynaptic protein phosphorylation and LTP. Trends Neurosci 23:75-80.

Steward O, Levy WB (1982) Preferential localization of polyribosomes under the base of dendritic spines in granule cells of the dentate gyrus. J Neurosci 2:284-291.

Sutton MA, Schuman EM (2006) Dendritic protein synthesis, synaptic plasticity, and memory. Cell 127:49-58.

Swann JW, Al-Noori S, Jiang M, Lee CL (2000) Spine loss and other dendritic abnormalities in epilepsy. Hippocampus 10:617-625.

Takao K, Yamasaki N, Miyakawa T (2007) Impact of brain-behavior phenotypying of genetically-engineered mice on research of neuropsychiatric disorders. Neurosci Res 58:124-132.

Tanaka J, Horiike Y, Matsuzaki M, Miyazaki T, Ellis-Davies GC, Kasai H (2008) Protein synthesis and neurotrophin-dependent structural plasticity of single dendritic spines. Science 319:1683-1687.

Tu JC, Xiao B, Naisbitt S, Yuan JP, Petralia RS, Brakeman P, Doan A, Aakalu VK, Lanahan AA, Sheng M, Worley PF (1999) Coupling of mGluR/Homer and PSD-95 complexes by the Shank family of postsynaptic density proteins. Neuron 23:583-592.

Villmann C, Becker CM (2007) On the hypes and falls in neuroprotection: targeting the NMDA receptor. Neuroscientist 13:594-615.

Walikonis RS, Oguni A, Khorosheva EM, Jeng CJ, Asuncion FJ, Kennedy MB (2001) Densin-180 forms a ternary complex with the (alpha)-subunit of Ca2+/calmodulin-dependent protein kinase II and (alpha)-actinin. J Neurosci 21:423-433.

Waterhouse EG, Xu B (2009) New insights into the role of brain-derived neurotrophic factor in synaptic plasticity. Mol Cell Neurosci 42:81-89.

Waung MW, Pfeiffer BE, Nosyreva ED, Ronesi JA, Huber KM (2008) Rapid translation of Arc/Arg3.1 selectively mediates mGluR-dependent LTD through persistent increases in AMPAR endocytosis rate. Neuron 59:84-97.

Wyszynski M, Lin J, Rao A, Nigh E, Beggs AH, Craig AM, Sheng M (1997) Competitive binding of alpha-actinin and calmodulin to the NMDA receptor. Nature 385:439-442.

Wyszynski M, Kharazia V, Shanghvi R, Rao A, Beggs AH, Craig AM, Weinberg R, Sheng M (1998) Differential regional expression and ultrastructural localization of alpha-actinin-2, a putative NMDA receptor-anchoring protein, in rat brain. J Neurosci 18:1383-1392.

Ying SW, Futter M, Rosenblum K, Webber MJ, Hunt SP, Bliss TV, Bramham CR (2002) Brain-derived neurotrophic factor induces long-term potentiation in intact adult hippocampus: requirement for ERK activation coupled to CREB and upregulation of Arc synthesis. J Neurosci 22:1532-1540.

Yoshii A, Constantine-Paton M (2010) Postsynaptic BDNF-TrkB signaling in synapse maturation, plasticity, and disease. Dev Neurobiol 70:304-322.

Zhou Q, Homma KJ, Poo MM (2004) Shrinkage of dendritic spines associated with long-term depression of hippocampal synapses. Neuron 44:749-757.

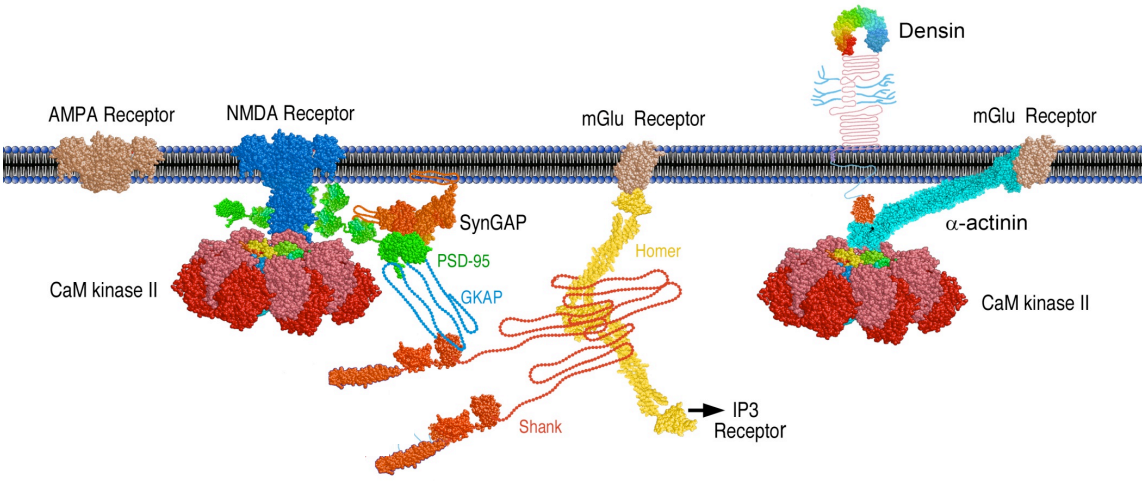

Figure 1.1. Key complexes surrounding ionic (AMPA and NMDA) and metabotropic glutamate (mGlu) receptors in the PSD. Densin is shown as a putative transmembrane protein and can a ternary interaction with a-actinin and CaMKII. Structures that contact each other indicate an interaction. The NMDA receptor is a docking site for CaMKII. PSD-95 serves to stabilize glutmate receptors in the PSD. Homer and Shank are major scaffolding proteins that form a mesh like structure and an assembly platform for other proteins. GKAP-guanylate kinase associated protein, GRIP = glutamate receptor interacting protein NMDAR = N-methyl-D-aspartate receptor, AMPAR = a-amino-3-hydroxyl-5-methyl-4-isoxazole-propionic acid receptor, CaMKII = Ca^{2+}/Calmodulin dependent kinase II, IP3 = Inositol triphosphate receptor, SynGAP = synaptic Ras GTPase activating protein. Figure by Holly Carlisle, Andrew Medina-Marino and Mary Kennedy.

Chapter 2
Behavioral Characterization of the Densin Knockout Mouse

INTRODUCTION

Densin-180 is a 180 kDa scaffold protein that is highly enriched in the PSD fraction; however relatively little is known about its functions. Hypotheses about the role of Densin in the PSD are based on its domain structure and on the roles of its binding partners in cell adhesion, bridging between receptor complexes, spine morphology, and participation in Ca^{2+} signaling. In this chapter I describe the characterization of motor, cognitive, sensorimotor, and affective behaviors of a mutant mouse line lacking Densin that was created by deletion of exon 3 (Andrew Medina-Marino's thesis). These KO mice exhibit a syndrome of schizophrenia/autistic-like behavior with anxiety, depression, and susceptibility to seizure as comorbidities (Seizure-Chapter 4). These symptoms are correlated with decreases in levels of certain PSD enriched proteins; including α-actinin, a direct binding partner of Densin, mGluR5, and DISC1. DISC1 and mGluR5 both interact with α-actinin, and are both implicated in schizophrenia, bipolar disorder, and depression (Blackwood et al., 2001; Brandon et al., 2009; Luscher and Huber, 2010). Additionally, the steady-state level of the immediate early gene arc (Chapter 3) is also decreased in brains of Densin KO mice. This may be due to defective BDNF signaling, which is associated with affective disorders. Decreased stimulation of the levels of Arc after treatment with BDNF, and a similar trend in levels of cfos and phosphoCREB are observed in cortical neurons cultured from the Densin KO

(Chapter 3). These molecular links offer clues about signal transduction pathways that may be compromised in the absence of Densin and how those disruptions may lead to behavioral abnormalities.

Densin Localization and Protein Domains

Densin is expressed in the forebrain, kidneys, testes, and pancreas (Apperson et al., 1996; Ahola et al., 2003; Heikkila et al., 2007; Lassila et al., 2007; Rinta-Valkama et al., 2007). In the forebrain, it is concentrated in the hippocampus at excitatory (Apperson et al., 1996) and inhibitory synapses (see Chapter 4). There are numerous splice variants that may be developmentally regulated (Strack et al., 2000b), but full length Densin contains an N-terminal leucine rich repeat (LRR), followed by a mucin homology domain, a putative transmembrane region and a C-terminal intracellular domain that includes a PSD-95/Dlg-A/ZO-1 (PDZ) domain (Apperson et al., 1996) (Fig. 2.1). Densin is membrane-associated and the LRR domains are targeted to the membrane when they are expressed alone in MDCK-II cells (Quitsch et al., 2005). However, there is not yet a consensus about whether Densin is a transmembrane protein, completely intracellular, or can assume both of these localizations. On one hand, biochemical evidence indicates that Densin is glycosylated and contains large polysialic acid chains that are normally found only extracellularly (Apperson et al., 1996). On the other hand, Thalhammer et al. found phosphorylated sites by mass spectrometric analysis on the previously suggested transmembrane region of Densin (Apperson et al., 1996; Thalhammer et al., 2009).

Theories about Densin Function based on Domain Homology and Protein-Protein Interactions

Structural homology

Densin has an arrangement of domains similar to other proteins that contain both LRR and PDZ domains, including Scribble and LET-43. These proteins have been christened LAP proteins (Santoni et al., 2002). Erbin, and Lano, *Drosophila melanogaster* Scribble and *Caenorhabditis elegans* LET-413, have roles in specifying apical-basal cell polarity and in regulating cell proliferation by maintaining an epithelial cell layer (Legouis et al., 2003). Mutants of Scribble and LET-413 also exhibit cell-cell junctions that are not properly aligned suggesting that Densin may be involved in synapse connectivity (Bilder & Perrimon, 2000, Borg et al 2000, Legouis et al., 2000). Densin also shares domain homology with the transmembrane protein GP1bα, a platelet cell adhesion molecule that binds von Willebrand factor, and the LRR domain of Toll-like receptors, implying it may mediate signal transduction by participating in cell-cell interaction (Apperson et al., 1996).

Interactions with cell adhesion molecules

Through its putative membrane proximal domain (amino acids 1249-1495), Densin is able to associate with directly with δ-catenin/NRAP, which is associated with cell adherens junctions (Izawa et al., 2002). Densin can also be immunoprecipitated with a nephrin-containing complex from the kidney (Ahola et al., 2003). The worm homolog for nephrin is SYG-2, which mediates synaptogenesis and when mutated leads to ectopic formation of synapses when mutated (Shen and Bargmann, 2003; Shen et al.,

2004). Because the kidney filtration cellular junction mimics the synapse architecturally in many surprising ways, it was also interesting to find that Densin is associated with β-catenin and N-cadherin in the kidney, but it is not known if these interactions are direct (Heikkila et al., 2007). It is possible that Densin may bind these proteins indirectly via delta catenin or α-actinin, which are also known to link these proteins to the cytoskeleton. In addition to its role in cell adhesion, N-cadherin internalization has repercussions for NMDA-induced synaptic plasticity (Tai et al., 2007; Mysore et al., 2008). Delta-catenin has roles in mediating neuronal branching, and similar to beta-catenin, can also act as a transcription factor. β-catenin participates in neurogenesis by enhancing transcription of target genes through a pathway in which its degradation is regulated by GSK3B and DISC1.

Densin interactions with scaffolding proteins

Densin interacts directly with Shank and with PSD-95 indirectly through MAGUIN (Ohtakara et al., 2002). Both are scaffold proteins that are largely responsible for the mesh-like quality of the PSD. They help to adapt the architecture of the PSD to changes in synaptic activity. Through binding to Densin's PDZ domain, MAGUIN links Densin to PSD-95, which has been suggested to stabilize the NMDA receptor in the PSD (Ohtakara et al., 2002). Shank is composed of a string of modular protein binding domains (N-terminal ankyrin repeats, SH3 and PDZ domains, conserved proline-rich clusters, and a SAM (sterile alpha motif) domain at its C-terminus) that can multimerize with themselves through SAM and helical regions (Naisbitt et al., 1999). Consequently, Shank is able to connect multiple receptor complexes to each other by its staggered layering

throughout the expanse of the PSD. Shank is linked to the mGluR receptor through Homer, indirectly to the NMDA receptor through GKAP, which in turn binds PSD-95, and to the AMPA receptor via GRIP or via GKAP, PSD-95 and stargazin. This dense stack of proteins is further connected to actin by Shank's ability to interact with F-actin and through α–actinin's crosslinking to F-actin, mGluR5, and Densin (Fig. 2.2). Many of these scaffold proteins that bind and stabilize GluR complexes are implicated in schizophrenia-like phenotypes, including Homer, which associates with mGluR receptors (Szumlinski et al., 2005).

Homer is a scaffold protein in the post-synaptic density that interacts with mGluR5, inositol triphosphate receptors, and Shank. Homer binds to the tail of the mGluR5 receptor and to Shank through Homer's N terminal EVH1 PDZ and C terminal coiled-coiled domain, respectively (Kammermeier et al., 2000). A shorter splice variant, Homer1A, is missing the C terminal coiled-coiled region and is able to interfere with protein interactions of the long form, including the mGluR5 receptor, in a dominant-negative manner (Tu et al., 1999; Kammermeier et al., 2000). Together Shank and Homer form a mesh-like structure and serve as an assembly platform for other complexes in the PSD (Hayashi et al., 2009).

The SH3 domain of Shank also can bind the C-terminus of Densin directly (Quitsch et al., 2005). The coexpression of Shank 1, 2, or 3 with Densin in HEK cells drives Densin into intracellular clusters, suggesting that Shank can contribute to the localization of Densin. Overexpression of Densin, particularly constructs including the LRR domain, in cultured hippocampal neurons leads to excessive branching of

hippocampal neurons and is hypothesized to be facilitated by delta-catenin. The excessive branching is countered if Shank is co-expressed with a Densin construct that contains the C-terminus (Quitsch et al., 2005). Because Shank interferes with binding of delta catenin to Densin-180 in pull-down assays, it is thought that Shank may block activation of Densin-180-dependent signaling pathways by delta-catenin. Delta-catenin promotes branching and neurite formation (Quitsch et al., 2005). Dissociated hippocampal neurons cultured from the Densin KO mouse appear to have normal branching patterns (Holly Carlilse, unpublished data); however it is unknown how the assembly of proteins surrounding Shank is altered in the absence of Densin.

Mutations in Shank 3 have been linked to both autism and schizophrenia (Durand et al., 2007; Gauthier et al., 2009; Gauthier et al., 2010), and these disorders share symptoms related to social and cognitive performance. *De novo* mutations R1117X and R536W were found in Shank 3 in two different families with a high incidence of schizophrenia (Gauthier et al., 2010). R1117X truncates Shank's C-terminus, which removes the Homer and cortactin binding sites. In zebrafish, this mutation results in defective morphology (smaller head, eyes, trunk) and behavior (inability to react to touch), and in defective neurite formation in cultured neurons. The effects of the R536W mutation, at a site in the protein adjacent to the Densin-binding SH3 domain, are more subtle (Gauthier et al., 2010).

Densin and Ca^{2+} Signaling

Densin may play a role in Ca^{2+} signaling by interacting with CaMKII, a key player in the induction of LTP and synaptic plasticity (Walikonis et al., 2001; Jenkins et al.,

2010). Autophosphorylation of CaMKII increases its affinity for Densin approximately ~100x (Walikonis et al., 2001). Densin colocalizes with CaMKII in neurons (Apperson et al., 1996) and may allow a subset of CaMKII molecules to dock near the mouth of the NMDA receptor. The affinity of CaMKII for the NR2B subunit of the NMDA receptor (K_d = 150-250 nM) is similar to its affinity for Densin *in vitro* (Strack and Colbran, 1998; Strack et al., 2000a; Strack et al., 2000b). A membrane-targeted minimized Densin peptide can recruit CaMKII to the membrane of HEK cells when the two proteins are cotransfected (Strack et al., 2000a). Pull-down experiments defined amino acids ~1354-1380 of Densin in the membrane-proximal region as being sufficient to bind CaMKII, while flanking regions potentiate Densin-CaMKII interaction. Densin is the only protein known to bind specifically to the association domain of CaMKII (Strack et al., 2000b; Walikonis et al., 2001)

Because of the important implications of obliterating a docking site in the PSD for a key facilitator of LTP, we assessed the localization of CaMKII in the PSD in cultured neurons from Densin KO and WT littermates (Carlisle and Medina-Marino, unpublished data). Colocalization of CaMKII with PSD-95 in immunostained hippocampal cultures was not altered in the Densin KO, supporting the conclusion that Densin is not required for CaMKII recruitment to the PSD. Furthermore, relative to the WT, the total amount of CaMKII in the Densin KO is unchanged in forebrain homogenates, and in synaptosomal and PSD fractions. However, in neurons cultured from double KOs lacking both NR1 and Densin, localization of CaMKII in the PSD is severely disrupted compared

to neurons from NR1 knockouts, indicating that the two molecules collaborate to localize CaMKII to the PSD (Carlisle and Medina-Marino, unpublished data).

In cultured neurons from the Densin KO, autophosphorylation of CaMKII is altered both basally and in response to synaptic activation. While basal autophosphorylation at T286 is decreased in hippocampal neurons cultured from the Densin KO, enhancement of synaptic transmission by treatment with bicucculine increases CaMKII autophosphorylation in the KO ~2 fold over the WT (H. Carlisle, unpublished data). This increased activation might explain the initial enhancement of post-tetanic potentiation seen in the KO (Carlisle, O'Dell, and Indersmitten, unpublished data). The initial response of CaMKII to Ca^{2+} influx through the NMDA receptor may be larger than in the WT. Otherwise, the electrophysiological profile of LTP in hippocampal slices from the KO is similar to that of the WT for the first hour. Furthermore, AMPA and NMDA receptor currents are normal in the Densin KO (Carlisle, O'Dell, and Indersmitten, unpublished data).

Recently, Densin has also been found to interact with $Ca_v1.3$ channels in the presence of CaMKII, and thus may form a link between these two proteins facilitating regulation by CaMKII (Jenkins et al., 2010). In a ternary complex with CaMKII, Densin is able to enhance Ca^{2+} transients by binding to this channel during high frequency stimulation, an ability that neither CaMKII nor Densin has when expressed by themselves (Jenkins et al. 2010). Hypoactivity of VSCC's has been linked with decreased expression of IEGs and with various forms of mental retardation (Greer and Greenberg, 2008).

Densin binds to α-actinin, which in turn binds to mGluR5 and DISC1

The PDZ domain of Densin binds the C-terminal TSV sequence of α-actinin, a cross linker of F-actin. Moreover, a ternary complex can be formed between Densin, α-actinin and CaMKII (Walikonis et al., 2001). α-actinin comprises an N-terminal actin binding domain and four tandem spectrin repeats with a C-terminal EF motif ending in a PDZ binding TSV sequence. It binds to NMDA and mGluR5 glutamate receptors, linking them to the cytsokeleton. Rearrangment of the actin cytoskeleton is critical for spine maturation and for normal alterations in spine morphology, both of which are disrupted in several neurological disorders (Fiala et al., 2002). Overexpression of α-actinin in hippocampal neurons in culture leads to an increase in motile filopodial spines (Nakagawa et al., 2004). Intriguingly, as identified by yeast two hybrid screens, DISC1 and mGluR5 are also binding partners of α-actinin (Millar et al., 2003; Cabello et al., 2007). α-actinin's direct interaction with mGluR5 regulates surface levels of the receptor and activation of ERK (Cabello et al., 2007).

Because of the cosegregation of mutations in mGluR5 and DISC1 with depression, cognitive, and mood disorders that resemble those in the Densin KO mouse, we probed for levels of both of these proteins and found them to be decreased in the PSD fraction of the KO. Group 1 mGluR5 receptors, which include mGluR1 and 5, are expressed in the cortex, hippocampus, striatum, lateral septal nucleus, olfactory bulb and nucleus accumbens. Metabotropic mGluR receptors are coupled to the $Ga_{q/11}$ proteins and facilitate a form of LTD that is dependent on protein synthesis and endocytosis of AMPA receptors and that involve rapidly translated Arc (Snyder et al.,

2001; Moult et al., 2006; Park et al., 2008; Waung et al., 2008; Luscher and Huber, 2010). mGluR deficient mice have decreased Prepulse Inhibition (PPI) and increased hyperlocomotion. Currently, a mGluR5 agonist is in clinical trials for potential use as an antipsychotic drug (Inta et al., 2009). Lack of the mGluR5 receptor has also been indicated in drug addiction and anxiety (Luscher and Huber, 2010).

Although schizophrenia is multifactorial and multigenetic disorder, DISC1 is presently considered a leading schizophrenia susceptibility gene. A 1,11 chromosomal translocation that truncates DISC1's C-terminus in a Scottish family predisposes them to schizophrenia and other affective disorders (Blackwood et al., 2001; Brandon et al., 2009). Mouse mutants with alterations in DISC1 also have schizophrenic-like endophenotypes (Shen et al., 2008; Kellendonk et al., 2009; Ayhan et al., 2010). Links to autism have also since been found with mutations in DISC1 (Kilpinen et al., 2008; Williams et al., 2009). The pathophysiology related to the DISC1 mutation is unclear but the protein appears to affect neuronal migration, proliferation, and arrangement of newly formed cells. Defects in these processes are predicted by the neurodevelopmental theory of schizophrenia (Ozeki et al., 2003; Pletnikov et al., 2008; Shen et al., 2008; Brandon et al., 2009). DISC1 may also participate in pathways that affect GluR signaling.

DISC1 is a coiled-coiled, PSD-enriched cytoplasmic protein that is particularly highly expressed in the hippocampus (especially Ammon's horn and the dentate granule cells) and is known to have five major functions (Meyer and Morris, 2008; Brandon et al., 2009). One of these is to inhibit hydrolysis of cAMP by phosphodiesterase (PDE 4B)

in the presence of low levels of cAMP (Millar et al., 2005; Millar et al., 2007). Second, DISC1 binds to kalirin and TNIK (Traf and nck interacting kinase) in the PSD, where it is believed to participate in rearrangement of the actin cytoskelton. Disc 1 restricts kalirin access to Rac1, which would constituitively decrease spine size. Kalirin is a Rac1-GTP exchange factor (GEF) that activates Rac1 and the PAK1 pathway to organize the actin cytoskeleton and spine morphology (Hayashi-Takagi et al., 2010). Decreased DISC1 is associated with decreased spine density in the dentate gyrus (Kvajo et al., 2008). The third function is in Wnt signaling, where DISC1 binds to the N-terminus of GSK3beta and inhibits GSK3beta activity, thus promoting the degradation of beta-catenin. Beta-catenin binds to the tail of Cadherin, a cell adhesion molecule. β-catenin can act as a transcription factor when it is released from cadherin. The result is increased neural stem cell proliferation. Through this pathway, knockdown of DISC1 with RNAi leads to a decrease in proliferation of progenitor cells in the dentate gyrus (Mao et al., 2009). Fourth, DISC1 can bind to the C-terminus of NDEL1 (nuclear distribution element like-1), and NDE1 in the dynein motor complex that organizes microtubules at the centrosome and plays a role in neurogenesis of hippocampal granule cells (Duan et al., 2007; Brandon et al., 2009). Last, DISC1 is a positive modulator of Erk signaling, which is one of the pathways downstream of activation of NMDA receptors (Hashimoto et al., 2006; Shinoda et al., 2007).

Densin and Spine Morphology

Compared to the WT, the Densin KO mouse has an increased number of mushroom spines at the expense of stubby spines (Carlisle and Medina-Marino,

unpublished data). The volumes of spine heads are similar but the length and thickness of the necks are altered. The density of spines is similar between the two genotypes. As we learn more about the intermediates along the path of formation and collapse of mushroom spines, we may learn what processes lead to a shift in the steady state to favor mushroom spines and how Densin might be involved in this regulation.

General Assessment of the Densin KO

The Densin knockout mouse was created by deletion of exon 3 of the gene through flox-Cre technology followed by breeding to Cre expressing mice (Medina-Marino, unpublished data). The KO mice are viable, born in Mendelian ratios, and are good breeders. Densin KO's and heterozyogtes appear to be good mothers; however, there is ~20% mortality of pups in their early weeks of life. At three weeks of age most of the KOs are runted and are typically ~50% of the weight of the WT (Medina-Marino, unpublished data). Because mutations in core components of the PSD can produce cognitive, mood and affect disorders, we characterized the behavior of the Densin KO. We discovered traits in the Densin KO mice that most resemble human schizoaffective disorder with anxiety, possible depression, and seizures. These traits are also consistent with autism. The seizures are described in more detail in Chapter 4. Human schizophrenia symptoms are difficult to assess in a mouse but certain endophenotypes are considered proxies of human symptoms in rodents (Takao et al., 2007; Inta et al., 2009). These endophenotypes have been characterized by studying phencyclidine- (PCP) and ketamine-induced psychosis in both humans and rodents, and by studying mouse models with altered human susceptibility genes. Finally, they have been

characterized by the ability to reverse the particular endophenotype by treatment with antipsychotics (Shen et al., 2008; Inta et al., 2009; Belforte et al., 2010).

METHODS

Breeding. The Densin KO mouse was generated by deletion of exon 3, which contains the transcriptional start site, by recombination of loxP sites by Cre recombinase *in utero* (described in Andrew Medina-Marino's thesis (2009)). All experiments were done with mice that had been outcrossed to C57Bl/6 twice, except for the behavioral cohort, which was outcrossed seven times. The Densin KO mouse is regularly maintained by Het x Het matings. Littermates from these crosses were usually used for comparison of wild type (WT) and KO phenotypes.

Genotyping of mice. Tail clippings or ear punches were harvested from individual mice at ~3-4 weeks of age. The tissue was lysed in 100 µL Viagen direct polymerase chain reaction (PCR) tail mix (Viagen®, Los Angeles) supplemented with Proteinase K overnight at 55-60˚C. The samples were then heated at 85˚ C for 40 min to inactivate the Proteinase K, and then centrifuged for 10 min at 16 k x g. Template DNA (2.5 µl) was amplified by PCR in 1x Coraload (Qiagen) PCR buffer, 0.625 mM $MgCl_2$, 0.3 mM dNTP, 1.25 units of Taq polymerase (Qiagen), and 1 pm/µL of the following primers: Lox Pray Up (5'-GAGATGCTCTCAAGATAGACATG-3), Lox Pray low (5'-CTCCAATTCTGAAGCCAGTAG-3'), and Posthygro2 (5'-ACAGAACTGGCTTCTGTCCAC- 3'). The temperature of the reaction was cycled according to the following protocol: 11 cycles of 95˚C 30 sec, 58˚C 30 sec, 72˚C 2 min, followed by 21 cycles of: 94˚C 40 sec, 56˚C 30 sec, 72˚C 2 minutes. A final extension at 72˚C for 5 min completed the protocol. PCR reaction products were

fractionated on a ~1.6% TBS agarose gel with ethidium bromide. A DNA band at 187 bp identifies a WT, 257 bp a KO, and both 187 and 257 bp bands a Het.

Fixation and Nissl staining. Knockout and wild type littermate pairs, aged 8-12 weeks, were perfused transcardially with fixative (4% formaldehyde, 15% saturated picric acid in 0.1 M phosphate buffered saline) for 20 min. Forebrains were dissected, postfixed overnight at 4° C, and then 50 μm coronal sections were cut with a vibratome and stored at -20 C in antifreeze reagent (50 mm phosphate buffer, 15% glucose, 30% ethylene glycol) until later processing. Sections were washed in PBS (10 mm NaHPO4, 120 mm NaCl, pH 7.4), mounted on Supermount Plus slides and allowed to dry overnight. Slides were then dipped in a series of decreasing ethanol solutions: 95% (15 min), 70% (1 min), and 50% (1 min) to remove lipids. After a 5 min water rinse, slides were submerged in cresyl violet staining solution (0.5% cresyl violet, 0.125% glacial acetic acid in distilled water) for 5 min followed by a 30 sec rinse in distilled water. The slices were destained in 96% ethanol/0.5% acetic acid for 5 min, fixed in isopropanol (5 min), followed by 5 min in isopropanol:xylene (1:2 parts), and dipped 4 times in xylene for 2 min each. Slides were sealed with Permount and allowed to dry at room temp ON before imaging. Slides were imaged at 2.5x (Plan-Neofluar 2.5x/NA 0,075) and 5x (objective) magnification.

Necropsy. Necropsy was performed by Gary Lawson at the University of California, Los Angeles. Two female runts, a male runt, and their WT male littermate (30 days old) were euthanized by CO_2, and fixed in 10% formalin at RT prior to delivery to Dr. Lawson. The

spinal cord was severed at the base of the brain to permit penetration of fixative and the thorax and peritoneum were opened to expose the abdominal organs to fixative.

PSD fractions. WT and KO PSD fractions were prepared from 7-8 mice pooled for each genotype that were matched by age (8-16 weeks) and sex. Data was quantified from 4 separate PSD preparations. Forebrains (excluding olfactory bulbs) were dissected from WT and KO mice sacrificed by cervical dislocation. Forebrains were rinsed in Buffer A (0.32 M sucrose, 1 mM $NaHCO_3$, 1 mM $MgCl_2$, 0.5 mM $CaCl_2$, 0.1 mM PMSF, 1 mg/l leupeptin) before homogenizing with 12 up and down strokes at 900 rpm in 14 mL Buffer A. The homogenates were diluted to 35 mL in Buffer A and then centrifuged at 1400 x g for 10 min. in an SS-34 rotor. The pellet was resuspended in 35 mL Buffer A, homogenized (3 strokes) and centrifuged at 710 g for 10 min. The supernatants were combined and centrifuged at 13,800 g (SS-34) for 10 min. The pellet was resuspended in 8 ml of Buffer B (0.32 M sucrose, 1 mM $NaHCO_3$), homogenized with 6 strokes and layered on top of a sucrose gradient comprising 10 mL each of 0.85 M, 1.0 M, and 1.2 M sucrose in 1 mM NaH_2CO_3 buffer. The sucrose gradient was centrifuged for 2 hours at 82,500 g in a swinging bucket rotor (SW-28). The resultant synaptosome-enriched layer between the 1.0 M and 1.2 M sucrose layers was collected, diluted to 15 mL with Solution B and added to an equal volume of Buffer B containing 1% Triton solution. The mixture was stirred for 15 min at 4˚C and centrifuged for 45 min at 36,800g. The pellet containing the PSD-enriched, Triton-insoluble fraction was resuspended in ~300 µL of 40 mM Tris pH 8 with a 25 gauge needle and 1 mL syringe, triturating ~25x. Samples were aliquoted, frozen in liquid nitrogen, and stored at -80° C.

Nembutal induced seizures. Densin KOs and WT littermate pairs (6-10 weeks old) were given i.p. injections of Nembutal (pentobarbital, 100 mg/kg). Injected mice were videotaped for later analysis of seizure type and severity and rated according to a common scale of seizure stages (staging described in detail in Chapter 4).

Behavioral studies. All mice were acclimated to cages in the behavioral facility for at least 2 weeks prior to behavioral testing. The male cohort consisted of 15 KO and 23 WT mice and the female cohort consisted of 9 KO and 14 WT mice. Mice from both cohorts had been backcrossed 7 times into a C57Bl/6 background. Females were housed in groups of 4. Initially, most of males were group housed, with an equal number of WT and KO males singly housed. As the experiments progressed, however, the majority of the males had to be separated due to fighting.

The behavioral tests proceeded in the following order: open field, short-term learning and memory (object recognition and place preference), motor tests (clasping, rotorod, and beam crossing), and prepulse inhibition. The cohort was tested during their light cycle (except for prepulse inhibition). During all intertrial periods, mice were returned to their home cages. Protocols were based on those described in Smith et al., (2007) and Southwell et al., (2009), or Current Protocols in Behavioral Neuroscience (Wiley).

Clasping. 24 KOs (15 males, 9 females) and 30 WTs (19 males, 11 females) were suspended by their tails for 1 min ~ 30cm above a table top and observed for hind- and forelimb clasping.

Rotarod. Mice were placed on an accelerating rotarod (~6 rpm to ~50 rpm in 240 sec) and the duration of time the mice remained on the rod was measured. Mice were trained on the rotarod for 2 consecutive days, 2 times each day separated by a 10' rest period. Mice were tested on the third day and the average of two trials was recorded. The maximum duration of a trial was 300 sec.

Beam crossing. Mice were placed at one end of a beam and the time required to cross to the escape box at the other end (80 cm away) was measured by motion detectors. Mice were trained on two beams (12 mm and 6 mm wide) on two 2 consecutive days. The mice rested for 10 min. in their home cages between training sessions on the two beams. Each mouse crossed each beam 3 times on training days, starting with the 12 mm and ending with the 6 mm beam. On test day, the times for two trials in which the mice did not stop while crossing the beam were averaged.

Open field. Mice were placed in the corner of a plastic 50 cm x 50 cm square box and allowed to explore the box for 10 min. Aerial video footage was captured using Picolo (frame grabber) with Media Cruise software. The path the mouse travelled and the duration of time spent in the center quadrant (25 cm x 25 cm) was analyzed using Ethovision 3.0 software.

Place preference. Each mouse was acclimated (10 min) to an open box (50 cm x 50 cm) and then returned to its home cage (5 min). It was then allowed to explore (5 min) the open box in which 2 objects had been placed in opposite corners (Fig. 2.6). Mice were returned to their homecages (10 min) and then reintroduced to the same box (5 min) where one of the objects had been moved to the opposite corner while the other object remained stationary (Fig. 2.6). The preference for the moved object was measured by calculating the number of investigations of the moved object as a percentage of the total number of investigations of both objects. Investigations were defined as head movements in the direction of the object where the tip of the nose was within 2 cm of the object.

Novel object recognition. 24 hours after the place preference test, mice were reacclimated to the testing box (10 min) and then returned to the home cage (5 min). The mice were then exposed to the same objects used in the place preference test (5 min). After a 5 min intertrial period, one of the objects was replaced with a novel object in the same location (Fig. 2.6) and the percentage of investigations of the novel object was assessed.

Prepulse inhibition (PPI). Prepulse inhibition is the diminished response to a startling sound if preceded by a sound of lower db. It is a measure of sensorimotor gating and, to some extent, distractability by filtering information. Mice were restrained in a cylindrical plexiglass tube on a platform situated in a chamber (SR Labs, San Diego) where the involuntary startle response is measured by an accelerometer underneath

the platform that the mice are resting on. The equipment was operated through "Startle" software to expose the mice to different trials comprising no startle noise, just the startle noise (120 db), or a prepulse (of 3 or 6 db over background) prior to the startle noise. Background noise was 65 db. The mice were acclimated in the plexiglass tube for 5 min prior to the start of the trials. To optimize for their natural circadian rhythm, the mice were tested starting an hour into the dark cycle. Prepulse inhibition is calculated as: 100% x ((startle.pulse)-(startle.prepulse))/(startle.pulse).

Aggression in the KO mice. During the course of the behavioral experiments, records were taken of cages where fighting was observed including which mouse acted as the aggressor. Determination of the aggressor was made by identifiying the mouse that was chasing, biting, or initiating the fight. Often the victim was confirmed by bite marks on the back and rear.

Nest building. A 2 x 2 inch square piece of cotton nesting material was placed in the wire food racks of singly caged KO and WT mice, low enough to be easily reached (Deacon, 2006). The unshredded nesting material remaining on the rack or on the cage floor was weighed at 12 hour intervals for up to 72 hours. These experiments were performed by Andrew Steele and Keith Gunapala (Caltech).

Freezing and average motion in an enclosed chamber. Mice were placed in a quiet room in their home cages for 30 min before being placed in a chamber commonly used

for fear-conditioning experiments (Med Associates Inc., Vermont). Mice were habituated in the chamber for 1 min without shock. The percentage of time spent freezing during the first minute was measured by infared detection of movement. The sampling rate was 30 frames per second (fps). The motion threshold was set at 18 arbitrary units. Minimum freezing duration was set at 30 frames.

Home cage activity. A home cage activity monitoring system with automated behavioral detection was developed and employed by Andrew Steele to look at the activity over light and dark cycles (Steele et al., 2007). The mice were monitored at 8, 10, and 12 weeks of age after acclimating to the facility for 2 weeks in single housing conditions.

Object recognition with extended training. Mice were trained as described in Object Recognition, above, except that they were exposed to 2 training sessions per day for 2 days, followed by a testing session with the novel object at the end of the second day.

RESULTS

The gross histology of the Densin KO forebrain is normal. Adult homozygous Densin KO mice do have no obvious abnormalities in the hippocampus or cortex (Fig. 2.3). Cell layers of the hippocampus and cortex appear to be normal: The arrangement, thickness, cell and density of cell body layers are similar in KO and WT forebrains. Staining for glial fibrillary acidic protein (GFAP) (Keith Gunapala, data not shown) revealed no abnormal gliosis in the KO brain.

At 4 weeks of age, Densin KO are reduced in size, have a small spleen and thymus, and may have malabsorption problems in the digestive tract. Dr. Gregory Lawson (Division of Laboratory Animal Medicine, UCLA) performed necropsies on WT and KO littermates. At this age, the KO mice were small in size and at least 20% of them had died. There were no lesions in the primary organs. The most striking finding was that the thymus was greatly reduced in size and was difficult to find. In addition, the spleen was small and pale in all three KO runts that were examined. The intestinal lumen had underdeveloped villi, which may have lead to difficulties with absorption and the small body size. The livers of KO mice were small and sharp-edged. The brains of the KO mice were smaller than the WT but constituted a larger percentage of the total body weight because of the small body size. The kidneys were indistinguishable from those of the WT.

The Densin KO mice "clasp" their hind- and forelimbs when suspended by their tails. WT mice usually splay their limbs out to the side when suspended by their tails. In contrast, 100% of the KO mice clasped their hind limbs and 96% their forelimbs as compared to 20% and 10% for WTs (Fig. 2.4). 96% of the KOs also clasped their hindlimbs when performing on the accelerating rotarod.

The Densin KO mice perform as well as the WTs on motor tests. The accelerating rotarod motor test measures motor coordination and learning and is also an indicator of time to fatigue. At 7.5-9.5 weeks old, the KO mice performed as well as the WTs on this

test (Fig. 2.5). When the rotarod was at higher speeds, the KO mice more often relied on their forelimbs to stay on the rod while their hindlimbs often clasped.

The KO mice performed similarly to WT on the 12mm beam (male WTs: 4.6 sec +/- 0.4, KOs: 3.9 sec +/- 0.4); female WTs-3.3 sec +/- 0.3, female KOs 3.5 sec +/- 0.3) and, outperformed the WT on the 6mm beam (6.8 sec +/- 0.7 average for WT versus 4.9 sec +/- 0.5 for KO males $p=0.03$, 5.9 sec +/- 0.5 for WTs and 4.1 sec +/- 0.4 for KO females $p=0.014$). Errors are reported as SEM.

Even though the KO mice performed as well or better than WT mice on test day, they required more training, especially on day 1. On the first training day on the beam, WT mice traversed the beam to the 'safe' box at the end with minimal prodding on their initial exposure to the beam. In contrast, KO mice frequently jumped off the beam, turned around, stalled, or tried to climb off the beam. When crossing the beam on the first day, KO mice frequently slipped and had to be assisted to complete the crossing. Surprisingly, the KO mice showed significant improvement 24 hours later; and began to perform similarly to the WT mice. We counted only the trials in which the mice did not stall on the beam.

The Densin KO mouse displays deficits in short-term hippocampal- and cortical-dependent memory. To test short-term memory, we used the place preference and novel object tests. The place preference task relies on hippocampal-dependent short-term memory of contextual cues about the position of an object within an environment. The novel object task relies on short-term memory of details about an object and is dependent on the perirhinal cortex (Murray and Richmond, 2001).

In the place preference task, the KO mice showed no preference for exploring an object that had been moved after its first presentation, whereas WT mice showed a significant preference (Fig. 2.6). Similarly, in the novel object test, the KO mice showed only a slight preference for the new object, whereas the WT mice preferred the new object by ~13% ($p<0.05$) over the more familiar object.

The Densin KO is hyperlocomotive to novel objects. We noticed in the novel place and novel object trials that the KO mice investigated all objects twice as frequently as WT mice (Fig. 2.6C and 2.6F). In both tests, the animals had limited exposure to the toys before the testing. Thus, the KO mice appear to display hyperlocomotion when placed in the presence of novel objects. This behavior is particularly striking because the KO mice are hypoactive in their home cage (see below).

The Densin KO has impaired prepulse inhibition. To test whether the KO mice have defective sensory filtering, we compared them to WT mice in a test for prepulse inhibition. Female KO mice have decreased prepulse inhibition compared to WT when tested with either a 68 or a 71 db prepulse (3 db and 6 db over background, respectively) (Fig. 2.7). The diminished prepulse inhibition (WT 49.5% (SEM=8.13), KO 30.5% (SEM=5.2), $p< 0.05$) is significant at the 3 db setting. The magnitude of startle to the 120 db stimulus exhibited by the KO mice was double that of the WT mice. Defective prepulse inhibition has been observed in human schizophrenics and in rodent schizophrenia models. The male KO mice showed no difference in perpulse inhibition compared to male WT mice; however the high level of aggression among male KO mice

compared to WT may be a confounding factor.

The Densin KO displays a deficit in nest building. (Fig. 2.8) When presented with a 2 x 2 inch square piece of compressed cotton, WT mice usually shred the material completely within 48 hours, and gather it to build a nest. In contrast, the KO mice left the material intact as long as 72 hours. This deficit was not observed in heterozygous KO mice.

The Densin KO mice are hypoactive. Littermates were monitored in their home cage with a computerized system. The KO mice were significantly less active than WT mice during both the light and dark cycles (Fig. 2.9). In addition, the KO mice spent much less time hanging vertically than WT mice. To differentiate whether the reduced vertical hanging was the result of a deficiency in motor motivation to hang or whether they are deficient in that particular motor skill, our collaborators Keith Gunapala and Andrew Steele, measured the time that KO and WT mice hung vertically on a wire cage flipped upside down. The KO mice spent much less time hanging vertically than WT mice in this context also. A confounding factor in these tests is whether the mice are capable of prolonged hanging or whether they are not motivated to do so even when they are forced to hang or fall. The KO mice also twitch, chew, and drink more frequently than WT mice.

The Densin KO displays increased anxiety. We compared the level of anxiety in KO and WT mice as measured in two tests: the open field test, and the response to a novel, enclosed chamber. The KO mice displayed increased anxiety in both tests (Figs. 2.10 and 2.11). In the open field test, KO mice spent significantly less time in the center

quadrant than WT mice (3 versus 10% over 2 min (SEM=1.3 and 1.4, p=0.002), 3.6 versus 14% over 4 min (SEM=0.98 and 1.8, p=0.0003), and 6.3 versus 15.3% over 8 min (SEM=1.8 and 0.4, p=0.01), respectively). The average latency to enter the center quadrant was longer for the KO mice (85 sec, SEM=25) compared to WT mice (23 sec, SEM=4.2, p=0.005). The KO mice also entered the center space less often than WT mice (1.4 (SEM=0.5) vs 6.4 (SEM=0.7) times during the test, respectively). The WTs traveled a greater distance during the test than the KO mice (897 cm (SEM=44) versus 658 (SEM=57) cm in the first 2 min (p=0.0018), and 1650 (SEM=60.8) versus 1416 (SEM=110) cm in the first 4 min (p=0.01), respectively). Mice freeze when they are placed into an environment that induces fear. We found a large difference between KO mice and WT mice in their freezing response to placement in a novel enclosed environment. This behavior is another measure of anxiety.

On average, KO mice exhibited 44% freezing (SEM=7.5) as compared to 0.2% (SEM=0.2) for their WT counterparts upon introduction into a novel enclosed box. When the behavior is expressed as average motion, KO mice scored 21 ± 8.4 and WT mice scored 260 ± 21 arbitrary units (see Methods for settings). These results are statistically significant ($p=3.8 \times 10^{-6}$ for freezing, and $p=3 \times 10^{-8}$ for average motion). The data for the males are similar: the percent freezing for KO males was 36% (SEM=8) compared to 0% for WT males. The average motion for the KO mice (70 (SEM=16)) was also significantly lower than that for the WTs (232 (SEM=11)). Average motion for the heterozygote cohort was 197 (SEM=13), which was not a dramatic difference from the WT behavior but was significant. The average percentage freezing (0%) in heterozygous

Densin KO mice was similar to that of WT mice, suggesting that total loss of densin is required to produce increased anxiety in this test. A confounding factor is that the heterozygote cohort had not experienced the previous tests and thus had more limited experience outside their home cages than the WT and KO cohorts.

The high rate of freezing upon introduction to an enclosed box prevented us from using conditioned fear of shock to test long-term memory. We were unable to reduce the level of initial freezing by habituating the KO mice to the enclosed box (1 min initial introduction, then 5 min per day).

Homozygous and heterozygous Densin KO mice display increased aggression. Both homozygous and heterozygous KO mice displayed heightened aggression toward their cagemates. We systematically recorded initiation of fighting in cages with different combinations of genotypes (Fig. 2.12). By this measure, heterozygous KO mice were more dominant than homozygous KO mice, which were more dominant than WT mice.

We observed fighting in 4 out of 5 cages where a homozygous KO mouse was housed with a heterozygote. In these cages, the heterozygote was the aggressor in every case. In 3 cages in which a homozygous KO mouse was housed with a WT mouse, the KO was the aggressor in every case. The heterozygotes might dominate homozygotes because they are larger than the homozygotes. An alternative explanation is that loss of one copy of Densin causes more aggressive behavior than loss of both copies.

Proteins associated with schizophrenia are reduced in the PSD fraction from forebrains of Densin KO mice compared to WT mice. As a first step in examining the

molecular basis for these behavioral phenotypes, we measured the levels of several proteins in PSD fractions from forebrains of KO and WT mice. The levels of most PSD proteins were unchanged in the KO mice, including the Densin interacting proteins δ-catenin and CaMKII. However, levels of four proteins were significantly decreased in KO compared to WT mice; α-actinin, a direct binding partner of Densin, the mGluR5 receptor, and DISC1, each by ~35% (Fig. 2.13). Arc is also decreased in homogenate, synaptosome, and PSD fractions in KO mice by 30%, 36%, and 25%, respectively (see Chapter 3). Changes in proteins associated with GABAergic systems are described in Chapter 4.

DISCUSSION

We have screened a cohort comprised of WT and homozygous Densin KO mice in a battery of tests to assess their motor and cognitive skills, as well as general affect. A literature search revealed that the phenotypes found in the Densin KO mice resembled those of other mouse models of schizophrenia, and thus are considered "endophenotypes of schizophrenia." Schizophrenia affects 1% of humans (Sullivan et al., 2003). It is most often diagnosed in juveniles or in early adulthood by the onset of cognitive impairments accompanied by negative and/or positive symptoms (Diagnostic and Statistical Manual of Mental Disorders (DSM IV)). Positive symptoms include hallucinations and psychosis. On the other hand, negative symptoms include the absence of traits that are usually found in the typical person. They include lack of social

interaction, apathy, and flattened affect. In addition, schizophrenic symptoms often include cognitive impairments, for example deficits in short-term or working memory.

The Densin KO mice have impaired short-term memory as measured in place preference and novel object tests. The KO mice are hyperlocomotive in response to novel objects, which is an endophenotype for positive symptoms of schizophrenia. Moreover, they exhibit asocial behavior, exemplified by their aggressiveness toward littermates. They do not build well-formed nests and are hypoactive in their home cage, which may correspond to a form of depression seen in chronic schizophrenia, characterized by the negative symptoms of amotivation and anhedonia. Negative symptoms in humans also include poor speech, reduced facial expressions, and flattened affect, traits that are impossible to assess in mice.

The schizophrenia-like traits in the Densin KO mice are accompanied by increased anxiety, aspects of depression, and seizures (Chapter 4). Importantly, the KO mice exhibit diminished prepulse inhibition indicative of altered sensorimotor gating, which is also observed in human schizophrenia. They have behaviors that could be interpreted as increased stereotypy, such as increased chewing and grooming. The endophenotypes of Densin KO mice are particularly reminiscent of the schizophrenic mouse model described in Belforte et al. (2010) in which NMDA-type glutamate receptors are deleted from a subset of fast spiking interneurons. These mice display enhanced aggression, anxiety, nest building deficits, novelty induced hyperlocomotion, and diminished prepulse inhibition (Belforte et al. 2010). The similarities may be due to decreased levels of PSD proteins that are known interactors of Densin.

General Assessment

The behavioral disorders in the Densin KO mice do not appear to be caused by neurodegeneration. Virtually all Densin KOs clasp their fore- and hindlimbs, a nonspecific indicator of neurological disease (Fig. 2.4). Clasping is seen in mouse models of Parkinson's and Huntington's disease, amongst others. Because of the possibility that lesions or loss of cells in particular parts of the brain might be responsible for these traits, we examined gross brain morphology by Nissl staining and found that the distribution of neurons appeared normal. We immunostained the sections for GFAP, which is a marker for gliosis that is often seen in neurodegenerative diseases, and did not find any obvious gliosis or lesions.

KO mice performed similarly to WT mice on motor tests (rotarod and beam) that measure balance and coordination. They compensated for clasping, and even outperformed the WTs on the more narrow 6 mm beam (Fig. 2.5). Thus, motor disabilities caused by the lack of Densin are not likely to confound the results of other behavioral tests. The difficulty in training the KO mice on the beam caused by their initial disorganized behavior may be a result of problems with procedural learning, lack of attention, and/or perceptual problems. By the second day of beam training, KO mice exhibited WT-like performance on both the 12 mm and 6 mm beams.

Cognitive Impairments

We observed impairments in hippocampal- and cortical-dependent short-term memory in the Densin KO mice. These cognitive deficits may relate to a deficit in LTD and aberrant spine morphology (H. Carlisle, unpublished data). It has been reported

that that recognition of the features of small objects involves induction of LTD in the perirhinal cortex, whereas presentation of new contexts devoid of objects results in induction of LTP (Massey et al., 2001; Warburton et al., 2003; Jo et al., 2006; Griffiths et al., 2008). One type of LTD is mediated by metabotropic glutamate receptors. Mice in which mGluR5 has been deleted perform poorly on learning and memory tests that rely on spatial cues (hippocampal-dependent) and on object recognition tests (perirhinal cortex-dependent) (Luscher and Huber, 2010). Blockade of Type 1 mGluR receptors, which include mGluR1 and mGluR5, is also known to disrupt object recognition memory (Barker et al., 2006). We hypothesize that the reduction in mGluRs in the PSD, and the deficits in induction of Arc (Chapter 3) may both be related to the impairment in LTD seen in the Densin KO mice because rapid synthesis of Arc is needed to facilitate mGluR-dependent LTD.

Positive Symptoms

Hyperlocomotion is one of the most common symptoms in mouse models of schizophrenia that involve mutation of GluR including mGluR5-deficient mice (Deltheil et al., 2008; Gray et al., 2009; Inta et al., 2009). (Table 2.1) Both hyperlocomotion in the open field and decreased PPI (negative symptom) are seen in mGluR5 deficient mice (Gray et al., 2009; Inta et al., 2009). Densin KO mice exhibit hyperlocomotion when presented with novel objects, but hypolocomotion in open field tests and in their home cage. General hyperactivity is the more classical representation of pscychosis in rodents, but novelty-induced hyperlocomotion and increased stereotypy have also been reported as behavioral proxies of schizophrenia-like traits (Inta et al., 2009; Belforte et

al., 2010). The hypolocomotion of the Densin KO mice in the open field may reflect their increased anxiety state.

The KOs are hypoactive in their home cage but exhibit increased stereotypy for particular activities including chewing, twitching, and grooming. Increased stereotypy has been observed in rats after administration of PCP and is often considered a proxy for positive symptoms of schizophrenia and is seen in autism (Sturgeon et al., 1979; Castellani and Adams, 1981; Crawley, 2007; Inta et al., 2009).

Negative Symptoms

We observed some endophenotypes associated with negative symptoms in the Densin KO mice. Deficits in PPI are also found in human schizophrenia, although the deficits are not synonymous with the disease. Decreased PPI is a hallmark of schizophrenia but is also seen in patients with autism, panic disorder Tourette's syndrome, bipolar disorder, Huntington's, and obsessive-compulsive disorder (Powell et al., 2009). PPI is used to test sensorimotor gating which is the ability to filter information from extraneous competing stimuli. Experimentally, PPI is measured as the decrease in an involuntary startle response when an auditory startle stimulus is presented following a quieter sound. With a prepulse sound of 3 db over background, the Densin KO mice exhibited ~20% less prepulse inhibition than WT mice.

Both homozygotes and heterozygotes diplay high aggression toward their cagemates, a sign of asocial behavior classified as a negative symptom of schizophrenia. We noticed that the instances of fighting were more frequent after the mice had been exposed to behavioral tests, suggesting an interplay between anxiety and aggression

(Neumann et al., 2010). The Densin KO mice also exhibit deficits in nest building, which can be interepreted as an endophenotype related to amotivation and anhedonia (Halene et al., 2009; Belforte et al., 2010).

Anxiety

Increased anxiety is the strongest and most penetrant phenotype in the Densin KO mice as demonstrated by their lack of time spent in the center quadrant of an open field and the increased freezing in the enclosed novel context relative to the WT (Fig. 2.11). Anxiety is consistent with other mouse models of schizophrenia and autism and is highly prevalent in these disorders (Crawley, 2007; Achim et al., 2009; Belforte et al., 2010; Mattila et al., 2010). An interplay of stress and anxiety with aggression may account for the fighting often observed in cages in which KOs and WTs were housed together after behavioral tests (Neumann et al., 2010). This is not surprising because the neural circuity for emotion in the orbital frontal cortex, amygdala, anterior cingulate cortex overlaps with that for aggression (Davidson et al., 2000).

Theories about the Causes of Schizophrenia

Four main theories about the pathology of schizophrenia include hyperdopaminergic, hyopglutamatergic, developmental, and GABAergic mechanisms. Our data thus far provide support for the latter three mechanisms. The GABAergic system will be described in relation to seizure susceptibility seen in the KO mouse in Chapter 4.

The hyperdopaminergic and hypoglutamatergic mechanisms are supported by both human pharmacological studies and by genetic manipulations in mouse models (Inta et al., 2009). The reversal of positive symptoms with antipsychotic drugs, which are virtually all dopaminergic antagonists, indicates that the presence of excessive dopamine at synapses or overstimulation of dopaminergic pathways may cause positive symptoms in schizophrenia such as delusions and hallucinations. A mouse in which the gene encoding catechol-O-methyl transferase (COMT), which normally degrades dopamine, was knocked out produced schizophrenic-like endophenotypes (Babovic et al., 2007; O'Tuathaigh et al., 2007).

Hypofunction of glutamatergic systems is believed to contribute to development of schizophrenia and manifests in positive symptoms, as well. Much information on this mechanism has come from recreational use of PCP, an NMDA receptor antagonist that produces schizophrenica-like symptoms, especially psychosis when it is abused. Ketamine, another NMDA receptor blocker, induces psychosis in healthy patients and aggravates it in schizophrenics. Mutant mice with hypoactive NMDA receptors have been created in particular parts of the brain and in subsets of neurons. For example, deletion of the NR1 subunit of the NMDA receptor, which is required for function, in cortical interneurons produces mice with schizophrenia endophenotypes (Inta et al., 2009; Belforte et al., 2010). Usually the NMDA receptor signals through the MAPK/ERK pathway, activating CREB, and thus transcription of neural plasticity genes. Reduction in mGluRs at excitatory synapses also contributes to schizophrenic symptoms in mice (Mohn et al., 1999).

Hypoglutamatergic Model

The reduction of mGluR5, DISC1, and α-actinin, in the PSDs (Fig. 2.13) of the Densin KO mice provides support for a hypoglutamatergic state through the MAPK/ERK pathway, which is a part of NMDA receptor signal transduction. Normally, both mGluR5 and DISC1 are able to enhance activation of MAPK/ERK (Hashimoto et al., 2006; Cabello et al., 2007) (Fig. 2.14). A significant reduction of these positive modulators of MAPK/ERK signaling in the Densin KO could effectively mimic a hypoglutamatergic state. MAPK/ERK activation normally promotes transcription of neural plasticity genes. The actual decrease in mGluR5 and DISC1 in the PSD might be related to the 35% reduction in α-actinin, a direct binding partner of both schizophrenia susceptibility gene products. α-actinin normally regulates the levels of surface mGluR5s and ERK signaling (Cabello et al., 2007). It is unknown if α-actinin stabilizes DISC1 in the PSD.

Developmental Theory

A decrease in DISC1 seen in the Densin KO would also support the neurodevelopmental model of schizophrenia. Schizophrenia is believed to be a disease of synaptic misconnectivity caused by developmental problems in neurogenesis, migration, and synapse formation (McGlashan and Hoffman, 2000). ERK signaling is again involved. Knockdown of DISC1 by siRNA decreases ERK signaling in the distal part of the axons and decreases axon elongation stimulated by neurotrophin. The requirement for DISC1 in neutrophin-induced axon elongation is through direct interaction with the adaptor protein Grb2 (Michailidis et al., 2007). Grb2 facilitates signaling between tyrosine kinase receptors, like the TrkB receptor, and activation of

ERK (Michailidis et al., 2007). Intriguingly, BDNF signaling, which occurs through binding to the TrkB receptor, is deranged in the Densin KO (Chapter 3). Moreover, another intersection of DISC1 with BDNF signaling is at the level of DISC1 inhibition of PDE4B degradation of cAMP through direct interactions (Millar et al., 2005).

Some traits exhibited by the Denisn KO fit more neatly than others within DSMIV categorization of negative and positive symptoms. In reality, clinical symptoms for schizophrenia are often hetereogeneous, vary in severity, and overlap or are comorbid with other diseases. This is illustrated by the presence of just as many, if not more cases of major recurrent depression, a few cases of bipolar disorder, and 2 cases of anxiety in addition to schizophrenia in the Scottish family that implicated DISC1 as a susceptibility gene (Blackwood et al., 2001). This overlap of disorders caused by a translocation that affects one gene suggests a common etiology (Blackwood et al., 2001; Brandon et al., 2009). We see possibly a similar spectrum of symptoms of the Densin KO mouse. While there is utility in recognizing the behavior of the Densin KO in terms of discrete schizophrenica-like categories, the lines dividing different diagnoses are often blurred. Schizophrenia mouse models are well-established, lending themselves to easier comparison in the literature.

The behavioral and molecular abnormalities seen with the Densin KO also resemble findings in autism, which is associated with dysfunctional social interaction, repetitive behavior, and deficits in communication (Crawley, 2007; Moy and Nadler, 2008). The asocial behavior, increased stereotypy (chewing, drinking, twitching), decreased prepulse inhibition, imbalance in excitation/inhibition and seizure

susceptibility, and cognitive deficits are consistent with this disorder (Crawley, 2007). Preliminary data show that the Densin KO mice are not exploratory if placed in a three-room container (A. Steele, personal communication) suggesting that they may be resistant to change. Increased anxiety and a susceptibility to seizures that we see in the Densin KO are commonly associated with autism (Crawley, 2007; Levisohn, 2007; Combi et al., 2010; Mattila et al., 2010). Mutations in DISC1 and BDNF have also been linked to the disorder (Kilpinen et al., 2008; Chapleau et al., 2009; Gadow et al., 2009; Williams et al., 2009).

Many aspects of the Densin KO that we describe as schizophrenia-like can also be bipolar-like or 'schizoaffective' (Craddock et al., 2010). One of the main differences between schizophrenia and bipolar disorder is that psychosis is a primary trait of the first disorder and secondary in the latter (Ivleva et al., 2008). Bipolar disorder is characterized by alternating phases of mania and depression often with elements of psychosis as well as cognitive deficits. From linkage studies, candidate genes for schizophrenia and mood disorder from linkage studies include NRG1, DTNBP1, DISC1, DAOA (G72), DAO, and RGS4, whereas those for bipolar disorder are DAOA(G72) and BDNF. Although DISC1 and BDNF are implicated in both schizophrenia and biopolar disorder, DISC1 appears to have a stronger association with the psychosis part of the spectrum, whereas BDNF is more strongly associated with dysfunctions in mood and affect (Craddock et al. 2010). These findings may be relevant to the Densin KO, which has disruptions in DISC1 and mGluR5 levels, as well as BDNF signaling (Chapter 3).

REFERENCES

Achim AM, Maziade M, Raymond E, Olivier D, Merette C, Roy MA (2009) How Prevalent Are Anxiety Disorders in Schizophrenia? A Meta-Analysis and Critical Review on a Significant Association. Schizophr Bull.

Ahola H, Heikkila E, Astrom E, Inagaki M, Izawa I, Pavenstadt H, Kerjaschki D, Holthofer H (2003) A novel protein, densin, expressed by glomerular podocytes. J Am Soc Nephrol 14:1731-1737.

Apperson ML, Moon IS, Kennedy MB (1996) Characterization of densin-180, a new brain-specific synaptic protein of the O-sialoglycoprotein family. J Neurosci 16:6839-6852.

Ayhan Y, Abazyan B, Nomura J, Kim R, Ladenheim B, Krasnova IN, Sawa A, Margolis RL, Cadet JL, Mori S, Vogel MW, Ross CA, Pletnikov MV (2010) Differential effects of prenatal and postnatal expressions of mutant human DISC1 on neurobehavioral phenotypes in transgenic mice: evidence for neurodevelopmental origin of major psychiatric disorders. Mol Psychiatry.

Babovic D, O'Tuathaigh CM, O'Sullivan GJ, Clifford JJ, Tighe O, Croke DT, Karayiorgou M, Gogos JA, Cotter D, Waddington JL (2007) Exploratory and habituation phenotype of heterozygous and homozygous COMT knockout mice. Behav Brain Res 183:236-239.

Barker GR, Bashir ZI, Brown MW, Warburton EC (2006) A temporally distinct role for group I and group II metabotropic glutamate receptors in object recognition memory. Learn Mem 13:178-186.

Belforte JE, Zsiros V, Sklar ER, Jiang Z, Yu G, Li Y, Quinlan EM, Nakazawa K (2010) Postnatal NMDA receptor ablation in corticolimbic interneurons confers schizophrenia-like phenotypes. Nat Neurosci 13:76-83.

Blackwood DH, Fordyce A, Walker MT, St Clair DM, Porteous DJ, Muir WJ (2001) Schizophrenia and affective disorders--cosegregation with a translocation at chromosome 1q42 that directly disrupts brain-expressed genes: clinical and P300 findings in a family. Am J Hum Genet 69:428-433.

Brandon NJ, Millar JK, Korth C, Sive H, Singh KK, Sawa A (2009) Understanding the role of DISC1 in psychiatric disease and during normal development. J Neurosci 29:12768-12775.

Cabello N, Remelli R, Canela L, Soriguera A, Mallol J, Canela EI, Robbins MJ, Lluis C, Franco R, McIlhinney RA, Ciruela F (2007) Actin-binding protein alpha-actinin-1 interacts with the metabotropic glutamate receptor type 5b and modulates the cell surface expression and function of the receptor. J Biol Chem 282:12143-12153.

Castellani S, Adams PM (1981) Acute and chronic phencyclidine effects on locomotor activity, stereotypy and ataxia in rats. Eur J Pharmacol 73:143-154.

Chapleau CA, Larimore JL, Theibert A, Pozzo-Miller L (2009) Modulation of dendritic spine development and plasticity by BDNF and vesicular trafficking: fundamental roles in neurodevelopmental disorders associated with mental retardation and autism. J Neurodev Disord 1:185-196.

Combi R, Redaelli S, Beghi M, Clerici M, Cornaggia CM, Dalpra L (2010) Clinical and genetic evaluation of a family showing both autism and epilepsy. Brain Res Bull 82:25-28.

Crawley JN (2007) Mouse behavioral assays relevant to the symptoms of autism. Brain Pathol 17:448-459.

Davidson RJ, Putnam KM, Larson CL (2000) Dysfunction in the neural circuitry of emotion regulation--a possible prelude to violence. Science 289:591-594.

Deacon RM (2006) Assessing nest building in mice. Nat Protoc 1:1117-1119.

Deltheil T, Guiard BP, Cerdan J, David DJ, Tanaka KF, Reperant C, Guilloux JP, Coudore F, Hen R, Gardier AM (2008) Behavioral and serotonergic consequences of decreasing or increasing hippocampus brain-derived neurotrophic factor protein levels in mice. Neuropharmacology 55:1006-1014.

Duan X, Chang JH, Ge S, Faulkner RL, Kim JY, Kitabatake Y, Liu XB, Yang CH, Jordan JD, Ma DK, Liu CY, Ganesan S, Cheng HJ, Ming GL, Lu B, Song H (2007) Disrupted-In-Schizophrenia 1 regulates integration of newly generated neurons in the adult brain. Cell 130:1146-1158.

Durand CM et al. (2007) Mutations in the gene encoding the synaptic scaffolding protein SHANK3 are associated with autism spectrum disorders. Nat Genet 39:25-27.

Fiala JC, Spacek J, Harris KM (2002) Dendritic spine pathology: cause or consequence of neurological disorders? Brain Res Brain Res Rev 39:29-54.

Gadow KD, Roohi J, DeVincent CJ, Kirsch S, Hatchwell E (2009) Association of COMT (Val158Met) and BDNF (Val66Met) gene polymorphisms with anxiety, ADHD and tics in children with autism spectrum disorder. J Autism Dev Disord 39:1542-1551.

Gauthier J, Spiegelman D, Piton A, Lafreniere RG, Laurent S, St-Onge J, Lapointe L, Hamdan FF, Cossette P, Mottron L, Fombonne E, Joober R, Marineau C, Drapeau P, Rouleau GA (2009) Novel de novo SHANK3 mutation in autistic patients. Am J Med Genet B Neuropsychiatr Genet 150B:421-424.

Gauthier J et al. (2010) De novo mutations in the gene encoding the synaptic scaffolding protein SHANK3 in patients ascertained for schizophrenia. Proc Natl Acad Sci U S A 107:7863-7868.

Gray L, van den Buuse M, Scarr E, Dean B, Hannan AJ (2009) Clozapine reverses schizophrenia-related behaviours in the metabotropic glutamate receptor 5 knockout mouse: association with N-methyl-D-aspartic acid receptor up-regulation. Int J Neuropsychopharmacol 12:45-60.

Greer PL, Greenberg ME (2008) From synapse to nucleus: calcium-dependent gene transcription in the control of synapse development and function. Neuron 59:846-860.

Griffiths S, Scott H, Glover C, Bienemann A, Ghorbel MT, Uney J, Brown MW, Warburton EC, Bashir ZI (2008) Expression of long-term depression underlies visual recognition memory. Neuron 58:186-194.

Halene TB, Ehrlichman RS, Liang Y, Christian EP, Jonak GJ, Gur TL, Blendy JA, Dow HC, Brodkin ES, Schneider F, Gur RC, Siegel SJ (2009) Assessment of NMDA

receptor NR1 subunit hypofunction in mice as a model for schizophrenia. Genes Brain Behav 8:661-675.

Hashimoto R et al. (2006) Impact of the DISC1 Ser704Cys polymorphism on risk for major depression, brain morphology and ERK signaling. Hum Mol Genet 15:3024-3033.

Hayashi MK, Tang C, Verpelli C, Narayanan R, Stearns MH, Xu RM, Li H, Sala C, Hayashi Y (2009) The postsynaptic density proteins Homer and Shank form a polymeric network structure. Cell 137:159-171.

Hayashi-Takagi A, Takaki M, Graziane N, Seshadri S, Murdoch H, Dunlop AJ, Makino Y, Seshadri AJ, Ishizuka K, Srivastava DP, Xie Z, Baraban JM, Houslay MD, Tomoda T, Brandon NJ, Kamiya A, Yan Z, Penzes P, Sawa A (2010) Disrupted-in-Schizophrenia 1 (DISC1) regulates spines of the glutamate synapse via Rac1. Nat Neurosci 13:327-332.

Heikkila E, Ristola M, Endlich K, Lehtonen S, Lassila M, Havana M, Endlich N, Holthofer H (2007) Densin and beta-catenin form a complex and co-localize in cultured podocyte cell junctions. Mol Cell Biochem 305:9-18.

Inta D, Monyer H, Sprengel R, Meyer-Lindenberg A, Gass P (2009) Mice with genetically altered glutamate receptors as models of schizophrenia: a comprehensive review. Neurosci Biobehav Rev 34:285-294.

Ivleva E, Thaker G, Tamminga CA (2008) Comparing genes and phenomenology in the major psychoses: schizophrenia and bipolar 1 disorder. Schizophr Bull 34:734-742.

Izawa I, Nishizawa M, Ohtakara K, Inagaki M (2002) Densin-180 interacts with delta-catenin/neural plakophilin-related armadillo repeat protein at synapses. J Biol Chem 277:5345-5350.

Jenkins MA, Christel CJ, Jiao Y, Abiria S, Kim KY, Usachev YM, Obermair GJ, Colbran RJ, Lee A (2010) Ca2+-dependent facilitation of Cav1.3 Ca2+ channels by densin and Ca2+/calmodulin-dependent protein kinase II. J Neurosci 30:5125-5135.

Jo J, Ball SM, Seok H, Oh SB, Massey PV, Molnar E, Bashir ZI, Cho K (2006) Experience-dependent modification of mechanisms of long-term depression. Nat Neurosci 9:170-172.

Kammermeier PJ, Xiao B, Tu JC, Worley PF, Ikeda SR (2000) Homer proteins regulate coupling of group I metabotropic glutamate receptors to N-type calcium and M-type potassium channels. J Neurosci 20:7238-7245.

Kellendonk C, Simpson EH, Kandel ER (2009) Modeling cognitive endophenotypes of schizophrenia in mice. Trends Neurosci 32:347-358.

Kilpinen H, Ylisaukko-Oja T, Hennah W, Palo OM, Varilo T, Vanhala R, Nieminen-von Wendt T, von Wendt L, Paunio T, Peltonen L (2008) Association of DISC1 with autism and Asperger syndrome. Mol Psychiatry 13:187-196.

Kvajo M, McKellar H, Arguello PA, Drew LJ, Moore H, MacDermott AB, Karayiorgou M, Gogos JA (2008) A mutation in mouse Disc1 that models a schizophrenia risk allele leads to specific alterations in neuronal architecture and cognition. Proc Natl Acad Sci U S A 105:7076-7081.

Lassila M, Juhila J, Heikkila E, Holthofer H (2007) Densin is a novel cell membrane protein of Sertoli cells in the testis. Mol Reprod Dev 74:641-645.

Legouis R, Jaulin-Bastard F, Schott S, Navarro C, Borg JP, Labouesse M (2003) Basolateral targeting by leucine-rich repeat domains in epithelial cells. EMBO Rep 4:1096-1102.

Levisohn PM (2007) The autism-epilepsy connection. Epilepsia 48 Suppl 9:33-35.

Luscher C, Huber KM (2010) Group 1 mGluR-dependent synaptic long-term depression: mechanisms and implications for circuitry and disease. Neuron 65:445-459.

Mao Y, Ge X, Frank CL, Madison JM, Koehler AN, Doud MK, Tassa C, Berry EM, Soda T, Singh KK, Biechele T, Petryshen TL, Moon RT, Haggarty SJ, Tsai LH (2009) Disrupted in schizophrenia 1 regulates neuronal progenitor proliferation via modulation of GSK3beta/beta-catenin signaling. Cell 136:1017-1031.

Massey PV, Bhabra G, Cho K, Brown MW, Bashir ZI (2001) Activation of muscarinic receptors induces protein synthesis-dependent long-lasting depression in the perirhinal cortex. Eur J Neurosci 14:145-152.

Mattila ML, Hurtig T, Haapsamo H, Jussila K, Kuusikko-Gauffin S, Kielinen M, Linna SL, Ebeling H, Bloigu R, Joskitt L, Pauls DL, Moilanen I (2010) Comorbid Psychiatric Disorders Associated with Asperger Syndrome/High-functioning Autism: A Community- and Clinic-based Study. J Autism Dev Disord.

McGlashan TH, Hoffman RE (2000) Schizophrenia as a disorder of developmentally reduced synaptic connectivity. Arch Gen Psychiatry 57:637-648.

Meyer KD, Morris JA (2008) Immunohistochemical analysis of Disc1 expression in the developing and adult hippocampus. Gene Expr Patterns 8:494-501.

Michailidis IE, Helton TD, Petrou VI, Mirshahi T, Ehlers MD, Logothetis DE (2007) Phosphatidylinositol-4,5-bisphosphate regulates NMDA receptor activity through alpha-actinin. J Neurosci 27:5523-5532.

Millar JK, Christie S, Porteous DJ (2003) Yeast two-hybrid screens implicate DISC1 in brain development and function. Biochem Biophys Res Commun 311:1019-1025.

Millar JK, Mackie S, Clapcote SJ, Murdoch H, Pickard BS, Christie S, Muir WJ, Blackwood DH, Roder JC, Houslay MD, Porteous DJ (2007) Disrupted in schizophrenia 1 and phosphodiesterase 4B: towards an understanding of psychiatric illness. J Physiol 584:401-405.

Millar JK, Pickard BS, Mackie S, James R, Christie S, Buchanan SR, Malloy MP, Chubb JE, Huston E, Baillie GS, Thomson PA, Hill EV, Brandon NJ, Rain JC, Camargo LM, Whiting PJ, Houslay MD, Blackwood DH, Muir WJ, Porteous DJ (2005) DISC1 and PDE4B are interacting genetic factors in schizophrenia that regulate cAMP signaling. Science 310:1187-1191.

Mohn AR, Gainetdinov RR, Caron MG, Koller BH (1999) Mice with reduced NMDA receptor expression display behaviors related to schizophrenia. Cell 98:427-436.

Moult PR, Gladding CM, Sanderson TM, Fitzjohn SM, Bashir ZI, Molnar E, Collingridge GL (2006) Tyrosine phosphatases regulate AMPA receptor trafficking during metabotropic glutamate receptor-mediated long-term depression. J Neurosci 26:2544-2554.

Moy SS, Nadler JJ (2008) Advances in behavioral genetics: mouse models of autism. Mol Psychiatry 13:4-26.

Murray EA, Richmond BJ (2001) Role of perirhinal cortex in object perception, memory, and associations. Curr Opin Neurobiol 11:188-193.

Mysore SP, Tai CY, Schuman EM (2008) N-cadherin, spine dynamics, and synaptic function. Front Neurosci 2:168-175.

Naisbitt S, Kim E, Tu JC, Xiao B, Sala C, Valtschanoff J, Weinberg RJ, Worley PF, Sheng M (1999) Shank, a novel family of postsynaptic density proteins that binds to the NMDA receptor/PSD-95/GKAP complex and cortactin. Neuron 23:569-582.

Nakagawa T, Engler JA, Sheng M (2004) The dynamic turnover and functional roles of alpha-actinin in dendritic spines. Neuropharmacology 47:734-745.

Neumann ID, Veenema AH, Beiderbeck DI (2010) Aggression and anxiety: social context and neurobiological links. Front Behav Neurosci 4:12.

O'Tuathaigh CM, Babovic D, O'Meara G, Clifford JJ, Croke DT, Waddington JL (2007) Susceptibility genes for schizophrenia: characterisation of mutant mouse models at the level of phenotypic behaviour. Neurosci Biobehav Rev 31:60-78.

Ohtakara K, Nishizawa M, Izawa I, Hata Y, Matsushima S, Taki W, Inada H, Takai Y, Inagaki M (2002) Densin-180, a synaptic protein, links to PSD-95 through its direct interaction with MAGUIN-1. Genes Cells 7:1149-1160.

Ozeki Y, Tomoda T, Kleiderlein J, Kamiya A, Bord L, Fujii K, Okawa M, Yamada N, Hatten ME, Snyder SH, Ross CA, Sawa A (2003) Disrupted-in-Schizophrenia-1 (DISC-1): mutant truncation prevents binding to NudE-like (NUDEL) and inhibits neurite outgrowth. Proc Natl Acad Sci U S A 100:289-294.

Park S, Park JM, Kim S, Kim JA, Shepherd JD, Smith-Hicks CL, Chowdhury S, Kaufmann W, Kuhl D, Ryazanov AG, Huganir RL, Linden DJ, Worley PF (2008) Elongation factor 2 and fragile X mental retardation protein control the dynamic translation of Arc/Arg3.1 essential for mGluR-LTD. Neuron 59:70-83.

Pletnikov MV, Ayhan Y, Nikolskaia O, Xu Y, Ovanesov MV, Huang H, Mori S, Moran TH, Ross CA (2008) Inducible expression of mutant human DISC1 in mice is associated with brain and behavioral abnormalities reminiscent of schizophrenia. Mol Psychiatry 13:173-186, 115.

Quitsch A, Berhorster K, Liew CW, Richter D, Kreienkamp HJ (2005) Postsynaptic shank antagonizes dendrite branching induced by the leucine-rich repeat protein Densin-180. J Neurosci 25:479-487.

Rinta-Valkama J, Aaltonen P, Lassila M, Palmen T, Tossavainen P, Knip M, Holthofer H (2007) Densin and filtrin in the pancreas and in the kidney, targets for humoral autoimmunity in patients with type 1 diabetes. Diabetes Metab Res Rev 23:119-126.

Santoni MJ, Pontarotti P, Birnbaum D, Borg JP (2002) The LAP family: a phylogenetic point of view. Trends Genet 18:494-497.

Shen K, Bargmann CI (2003) The immunoglobulin superfamily protein SYG-1 determines the location of specific synapses in C. elegans. Cell 112:619-630.

Shen K, Fetter RD, Bargmann CI (2004) Synaptic specificity is generated by the synaptic guidepost protein SYG-2 and its receptor, SYG-1. Cell 116:869-881.

Shen S, Lang B, Nakamoto C, Zhang F, Pu J, Kuan SL, Chatzi C, He S, Mackie I, Brandon NJ, Marquis KL, Day M, Hurko O, McCaig CD, Riedel G, St Clair D (2008) Schizophrenia-related neural and behavioral phenotypes in transgenic mice expressing truncated Disc1. J Neurosci 28:10893-10904.

Shinoda T, Taya S, Tsuboi D, Hikita T, Matsuzawa R, Kuroda S, Iwamatsu A, Kaibuchi K (2007) DISC1 regulates neurotrophin-induced axon elongation via interaction with Grb2. J Neurosci 27:4-14.

Snyder EM, Philpot BD, Huber KM, Dong X, Fallon JR, Bear MF (2001) Internalization of ionotropic glutamate receptors in response to mGluR activation. Nat Neurosci 4:1079-1085.

Strack S, Colbran RJ (1998) Autophosphorylation-dependent targeting of calcium/ calmodulin-dependent protein kinase II by the NR2B subunit of the N-methyl- D-aspartate receptor. J Biol Chem 273:20689-20692.

Strack S, McNeill RB, Colbran RJ (2000a) Mechanism and regulation of calcium/calmodulin-dependent protein kinase II targeting to the NR2B subunit of the N-methyl-D-aspartate receptor. J Biol Chem 275:23798-23806.

Strack S, Robison AJ, Bass MA, Colbran RJ (2000b) Association of calcium/calmodulin-dependent kinase II with developmentally regulated splice variants of the postsynaptic density protein densin-180. J Biol Chem 275:25061-25064.

Sturgeon RD, Fessler RG, Meltzer HY (1979) Behavioral rating scales for assessing phencyclidine-induced locomotor activity, stereotyped behavior and ataxia in rats. Eur J Pharmacol 59:169-179.

Szumlinski KK, Lominac KD, Kleschen MJ, Oleson EB, Dehoff MH, Schwarz MK, Seeburg PH, Worley PF, Kalivas PW (2005) Behavioral and neurochemical phenotyping of Homer1 mutant mice: possible relevance to schizophrenia. Genes Brain Behav 4:273-288.

Tai CY, Mysore SP, Chiu C, Schuman EM (2007) Activity-regulated N-cadherin endocytosis. Neuron 54:771-785.

Takao K, Yamasaki N, Miyakawa T (2007) Impact of brain-behavior phenotypying of genetically-engineered mice on research of neuropsychiatric disorders. Neurosci Res 58:124-132.

Thalhammer A, Trinidad JC, Burlingame AL, Schoepfer R (2009) Densin-180: revised membrane topology, domain structure and phosphorylation status. J Neurochem 109:297-302.

Tu JC, Xiao B, Naisbitt S, Yuan JP, Petralia RS, Brakeman P, Doan A, Aakalu VK, Lanahan AA, Sheng M, Worley PF (1999) Coupling of mGluR/Homer and PSD-95 complexes by the Shank family of postsynaptic density proteins. Neuron 23:583-592.

Walikonis RS, Oguni A, Khorosheva EM, Jeng CJ, Asuncion FJ, Kennedy MB (2001) Densin-180 forms a ternary complex with the (alpha)-subunit of Ca2+/calmodulin-dependent protein kinase II and (alpha)-actinin. J Neurosci 21:423-433.

Warburton EC, Koder T, Cho K, Massey PV, Duguid G, Barker GR, Aggleton JP, Bashir ZI, Brown MW (2003) Cholinergic neurotransmission is essential for perirhinal cortical plasticity and recognition memory. Neuron 38:987-996.

Waung MW, Pfeiffer BE, Nosyreva ED, Ronesi JA, Huber KM (2008) Rapid translation of Arc/Arg3.1 selectively mediates mGluR-dependent LTD through persistent increases in AMPAR endocytosis rate. Neuron 59:84-97.

Williams JM, Beck TF, Pearson DM, Proud MB, Cheung SW, Scott DA (2009) A 1q42 deletion involving DISC1, DISC2, and TSNAX in an autism spectrum disorder. Am J Med Genet A 149A:1758-1762.

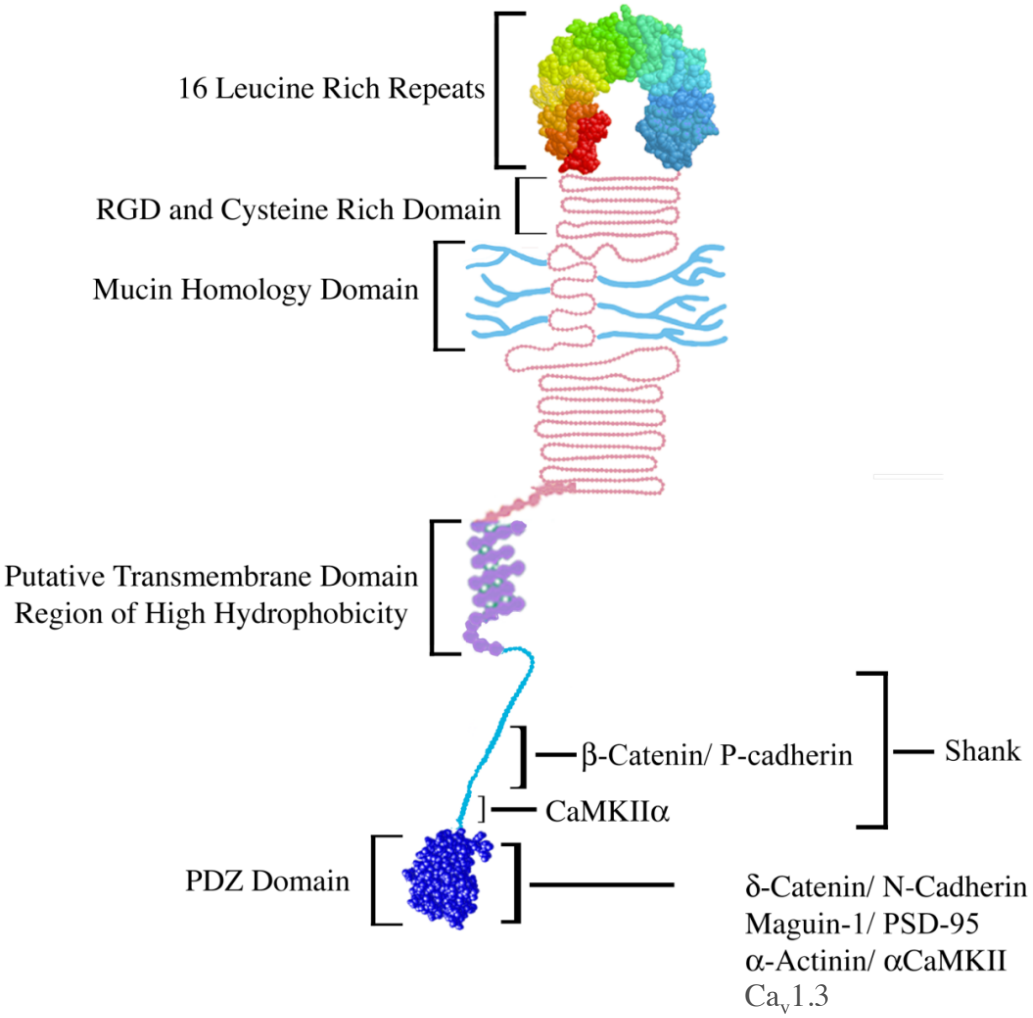

Figure 2.1. Schematic showing Densin protein domains and known interactors with to the C-terminus of Densin. Densin is comprised of an N-terminal LRR domain, a mucin homology domain, an RGD (Arg-Gly-Asp) sequence and cysteine rich domain, a putative transmembrane domain, and a C-terminal PDZ domain (Apperson et al., 1996). Binding studies show that the major isoform of densin is connected to the PSD through the formation of a complex with maguin-1 and PSD-95 and through its binding to the scaffold protein, shank (Quitsch et al., 2005, Ohtakara, et al., 2002). It also forms a high affinity ternary complex with CaMKII and alpha-actinin (Walikonis et al., 2000). Densin binds directly to delta-catenin and can be found in a complex with beta-catenin/ P cadherin through interactions with the PDZ adjacent and PDZ domain, respectively (Inagaki et al., 2002, Heikkila, et al., 2007). The voltage gated calcium channel, $Ca_v1.3$, binds Densin in the presence of CaMKII (Jenkins et al., 2010). Figure adapted from Medina-Marino (2009).

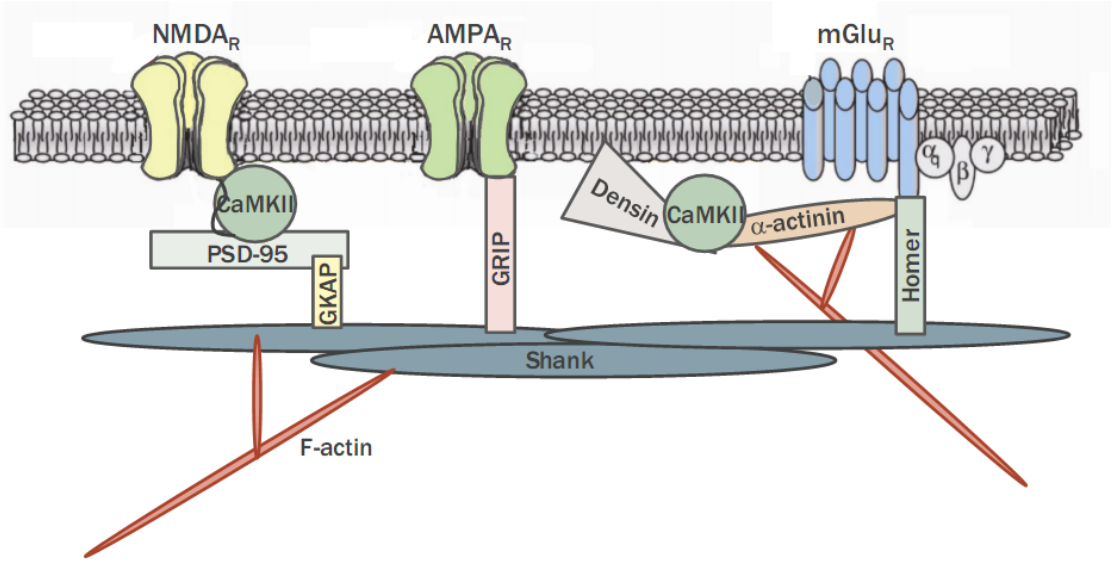

Figure 2.2. Diagram of ionotropic ($NMDA_R$ and $AMPA_R$) and metabotropic glutamate receptors (mGluR) binding to multimerized scaffold proteins that link the PSD to the actin cytoskeleton. mGluR receptors are coupled to G proteins while ionotropic receptors allow influx of Na^+ and/or Ca^{2+}. Shank is connected to $NMDA_R$, $AMPA_R$, and mGluR receptors through PSD-95/GKAP, GRIP, and Homer, respectively. Shank can multimerize with itself through SAM and helical domains. Alpha-actinin binds to the C terminal domain of the mGluR5b receptor (Cabello, 2007). Densin can interact with alpha-actinin and CaMKII in a ternary complex. GKAP = guanylate kinase associated protein, GRIP = glutamate receptor interacting protein $NMDA_R$ = N-methyl-D-aspartate receptor, $AMPA_R$ = α-amino-3-hydroxyl-5-methyl-4-isoxazole-propionic acid receptor, CaMKII = Ca^{2+}/ Calmodulin dependent kinase II. Figure by Holly Carlisle.

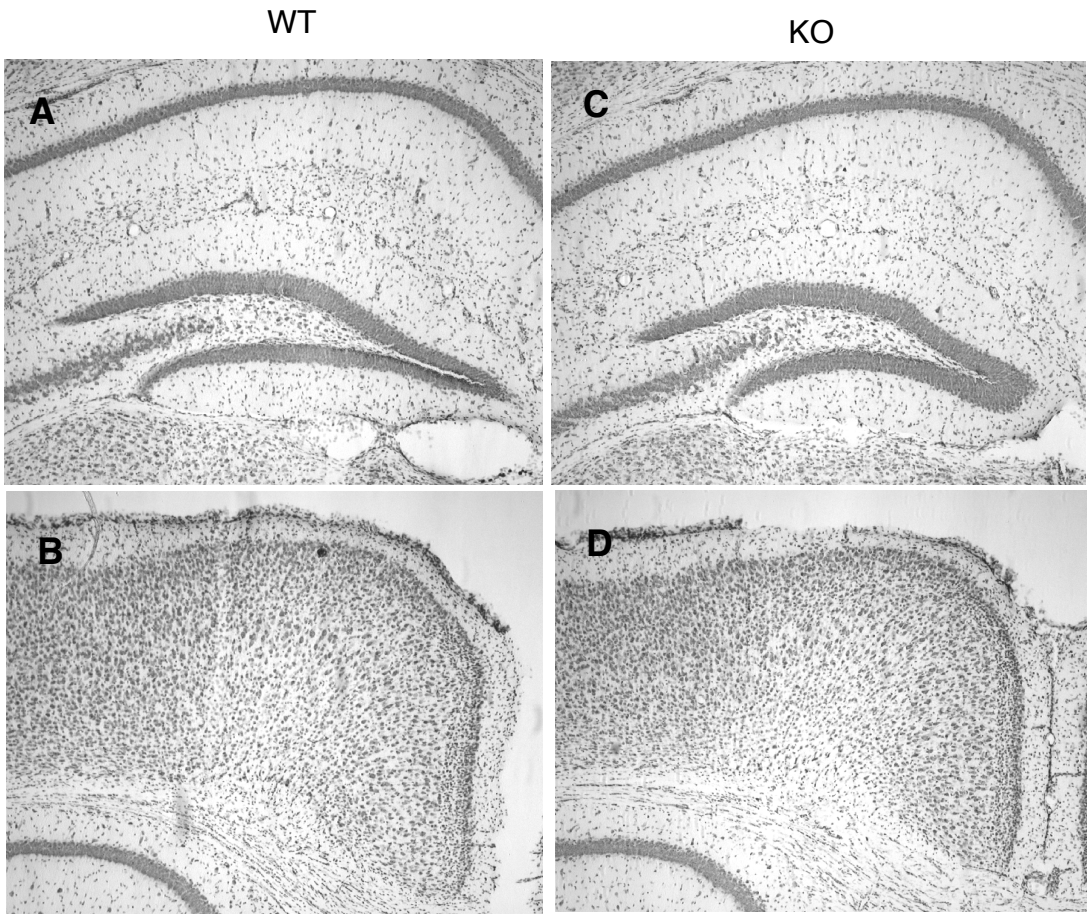

Figure 2.3. Brains from Densin KO mice have normal gross neuroanatomy. Representative Nissl stained images (5x magnification) from coronal sections of WT (left panels) and Densin KO (right panels) from hippocampus (A,C) and cortex (B,D). n=3 WT, 3KO.

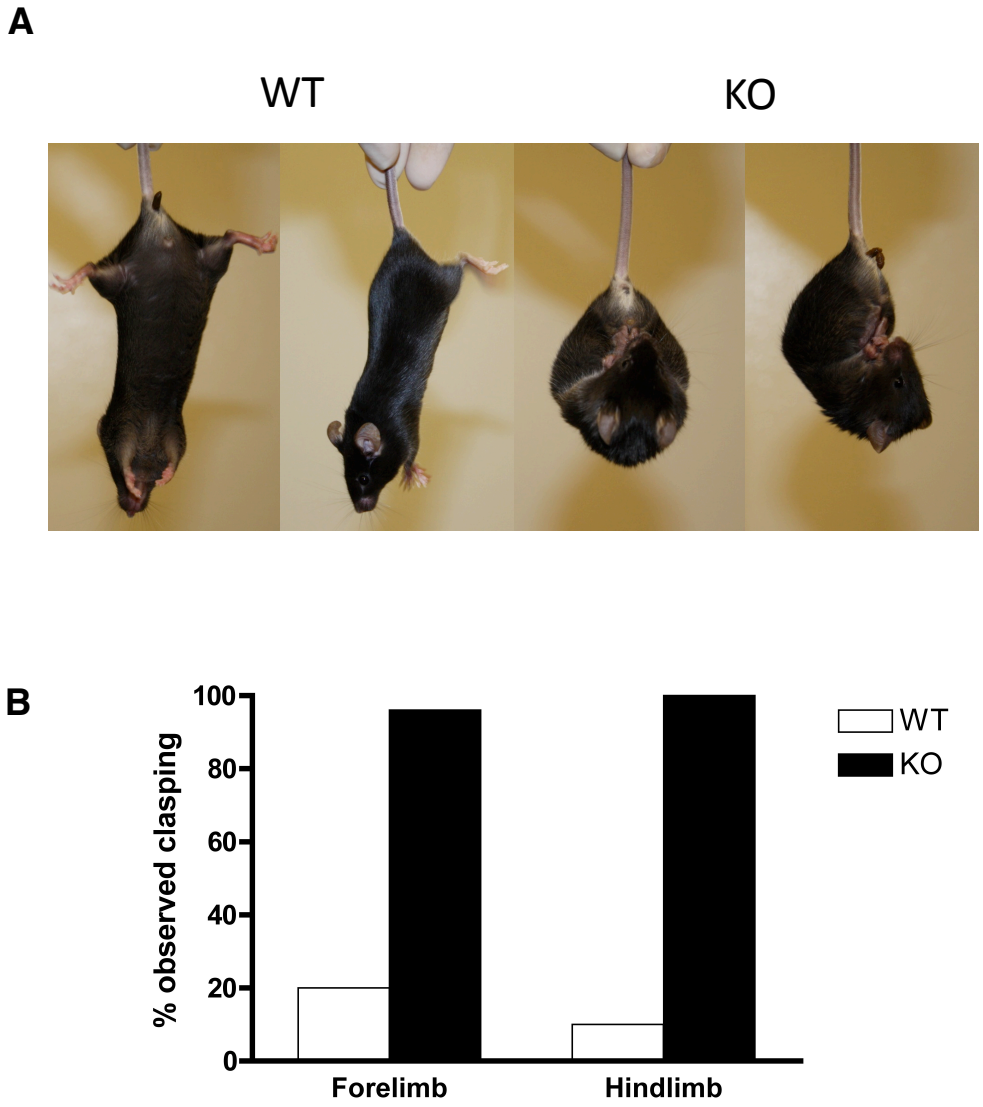

Figure 2.4. Densin KOs clasp their hind and fore limbs when suspended by the tail. (A) Representative pictures of front and side views of WT (left) and KO (right) mice. (B) Densin KO mice show a dramatic increase in front and hind limb clasping compared to WT mice (n= WT 15 males, 9 WT females, 19 KO males, KO 11 females; 9-11 weeks old).

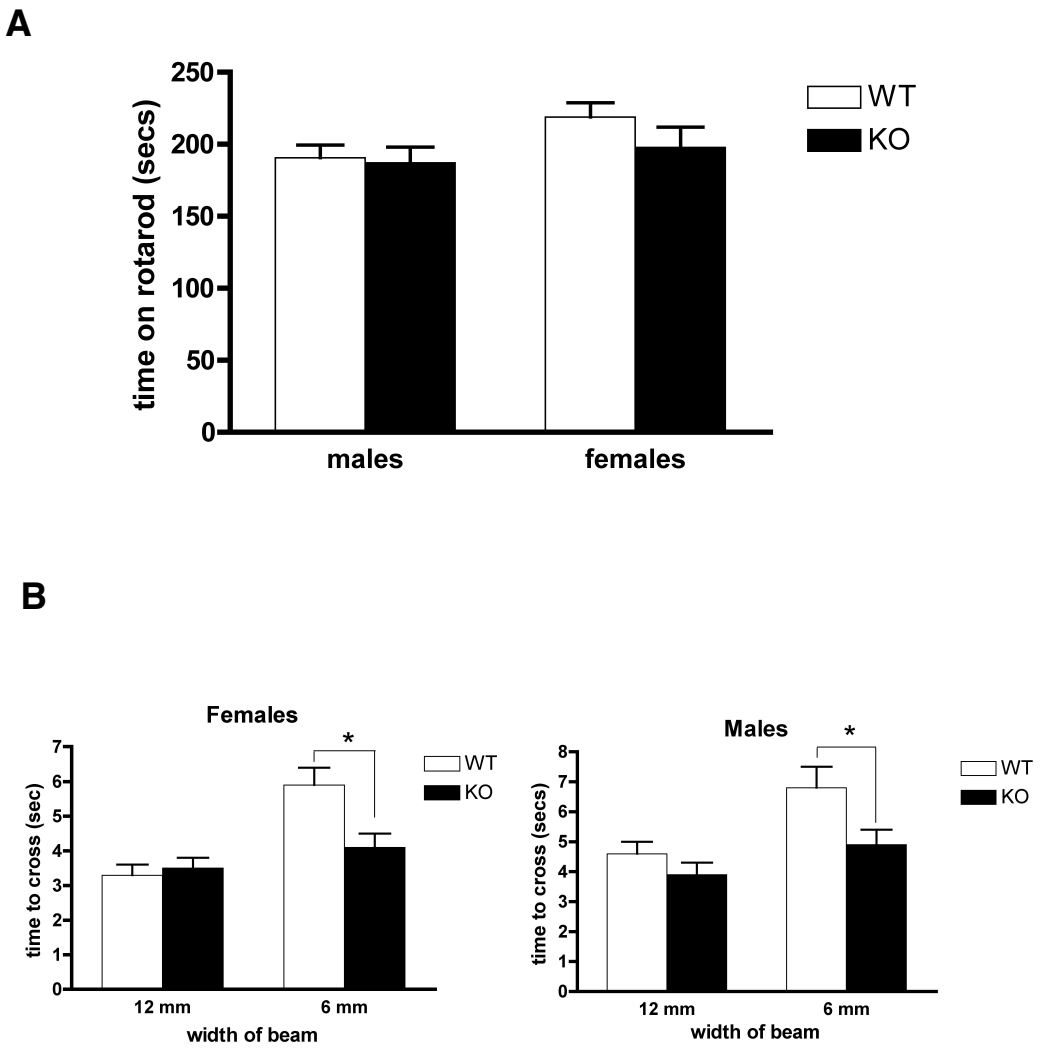

Figure 2.5. Densin KOs have normal motor abilities on the rotorod and beam crossing tasks. (A) Both WT and KO mice remained on the accelerating rotarod (5 to 50 rpm over 240 secs) for approximately 200 sec (n = 20 WT males, 11 WT females, 15 KO males, 9 KO females; 8-10 weeks old). (B) WT and KO cohorts crossed the 12mm beam with similar speeds (n = 15 WT males, 11 WT females, 13 KO males, 9 KO females). KO mice crossed the 6 mm beam significantly faster than the WT cohort (n=13 WT males, 10 WT females, 11 KO males, 9 KO females; 9-11 weeks old). Statistical significance measured by 2-tailed t-test (*p<.0.05). All error bars show SEM.

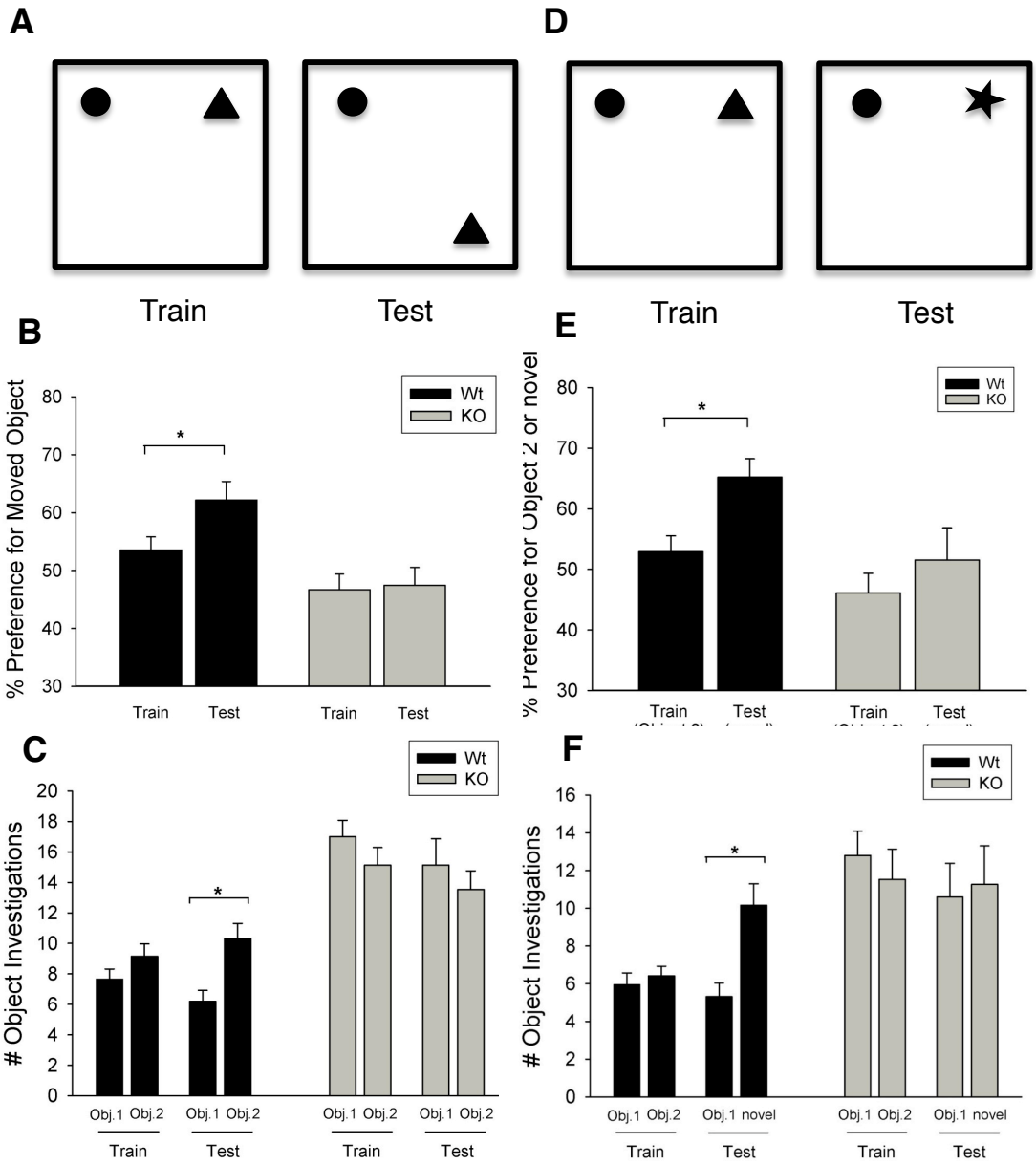

Figure 2.6. Densin KOs have deficient short-term hippocampal and cortical dependent memory as measured by place preference and novel object recognition tests. Diagrams of place preference and object recognition tests are shown in (A) and (D). In both tests, mice were exposed to two objects for 5 min, removed from the box for 10 min, and then their preference for the moved object (A-C) or the novel object (D-F) was measured by the number of times the mice investigated each object during a 5 min test period. Wild type mice (black bars) show a significant increase in the percent of investigations of the moved compared to the stationary object in the place preference test (B) and the novel object in the object recognition test (E), whereas KO mice (grey bars) showed no preference for the moved or novel objects. KOs investigated the objects approximately twice as frequently as the WTs during the place preference (C) and object recognition (E) tests, despite showing no preference for the moved or novel objects (n = 20 WT, 15 KO males, 8-10 weeks old). Significance was assessed by 2-tailed t-test (*$p<0.05$). All error bars represent SEM.

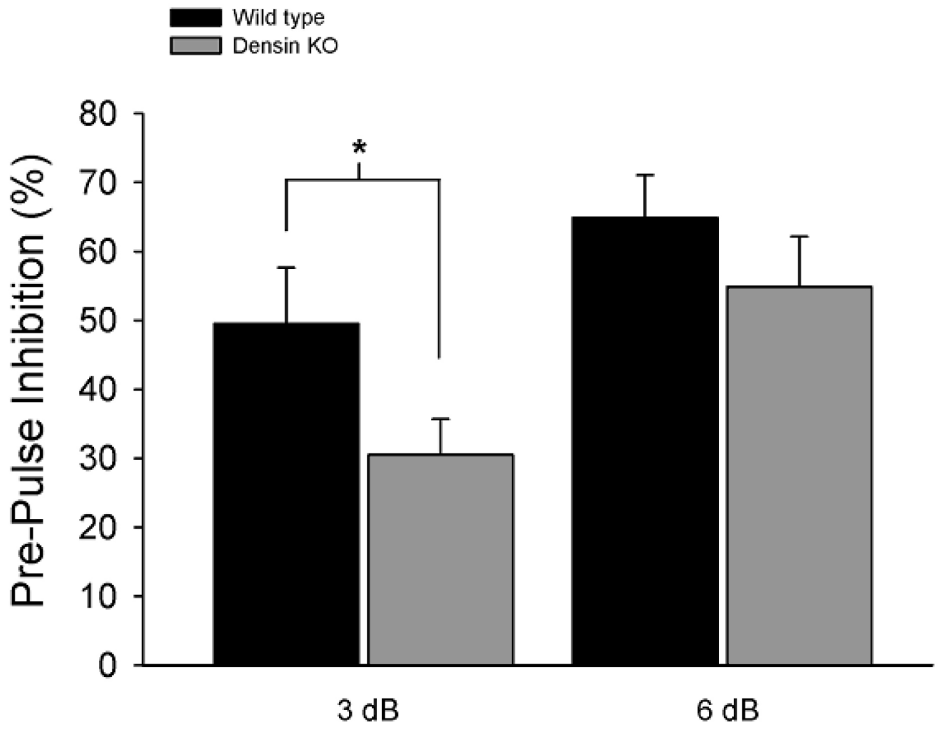

Figure 2.7. Prepulse inhibition of startle is decreased in the Densin KO mice. The startle reflex was measured by an accelerometer and reported as the percent decrease in the startle response to a 120 db pulse of sound when preceded by a mild acoustic prepulse (3 or 6 db over background) compared to the startle response in the absence of the prepulse (n= 13 WT, 10 KO females 15-17 weeks old). Significance was measured with 2-tailed t-test (*$p < 0.05$). Error bars represent SEM.

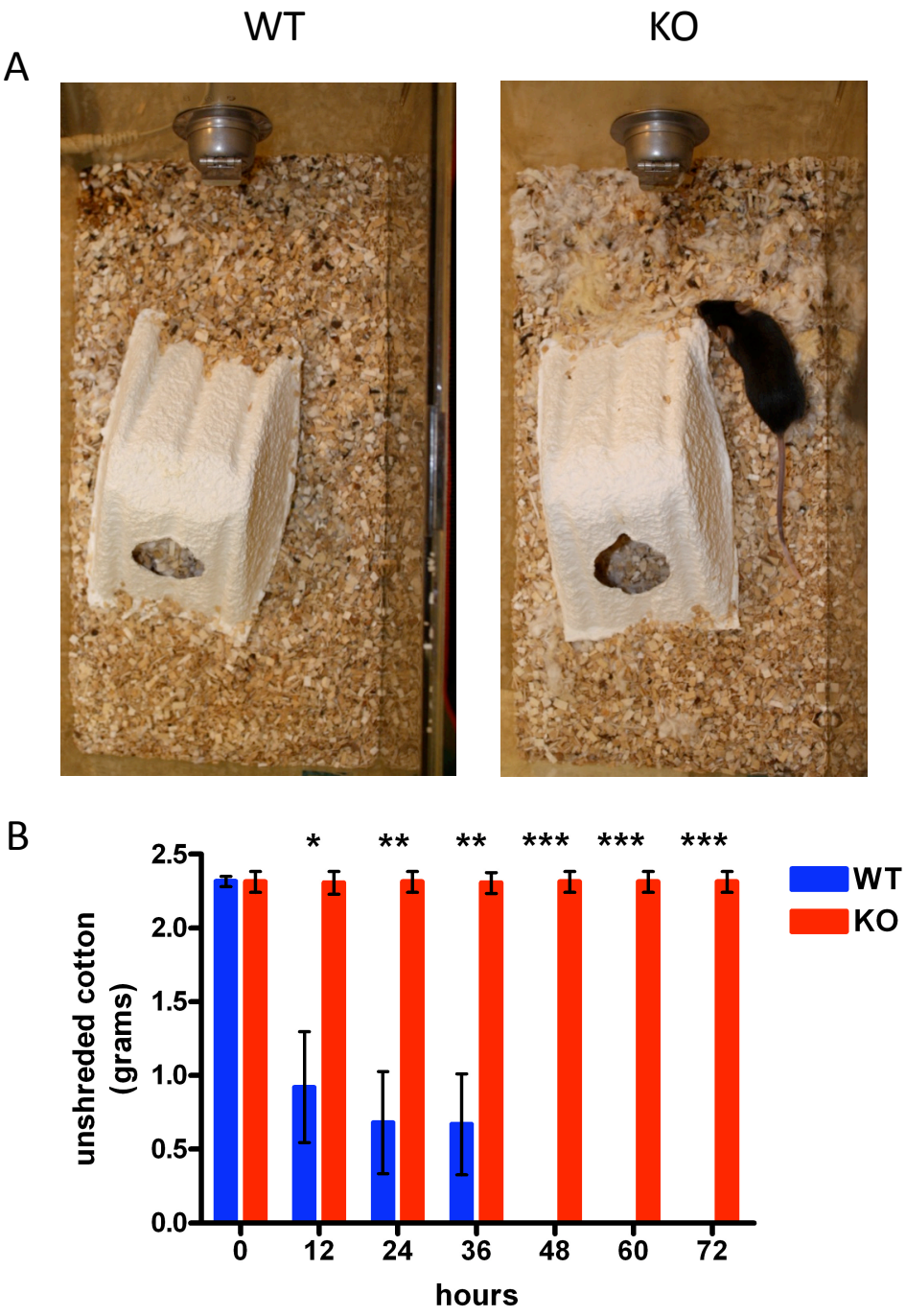

Figure 2.8. Densin KOs exhibit nest building deficits. (A) Representative cages of WT (left) and KO (right) nests. WT nests were formed within the cardboard houses whereas KOs tended to scatter the cotton on the cage floor. (B) A 2 x 2 inch piece of cotton was placed in the wire food rack and the unshredded cotton was weighed every 12 hours for 72 hours. Wild types made fully formed nests within 24 hours whereas none of the KO mice shredded any of the cotton even after 72 hours (n = 10 WT, 11 KO males 20-22 weeks old). Significance measured by Mann-Whitney test with two-tail p value (*p<0.05, **p<0.01, ***p<0.001). Error bars represent SEM. Data collected by Keith Gunapala.

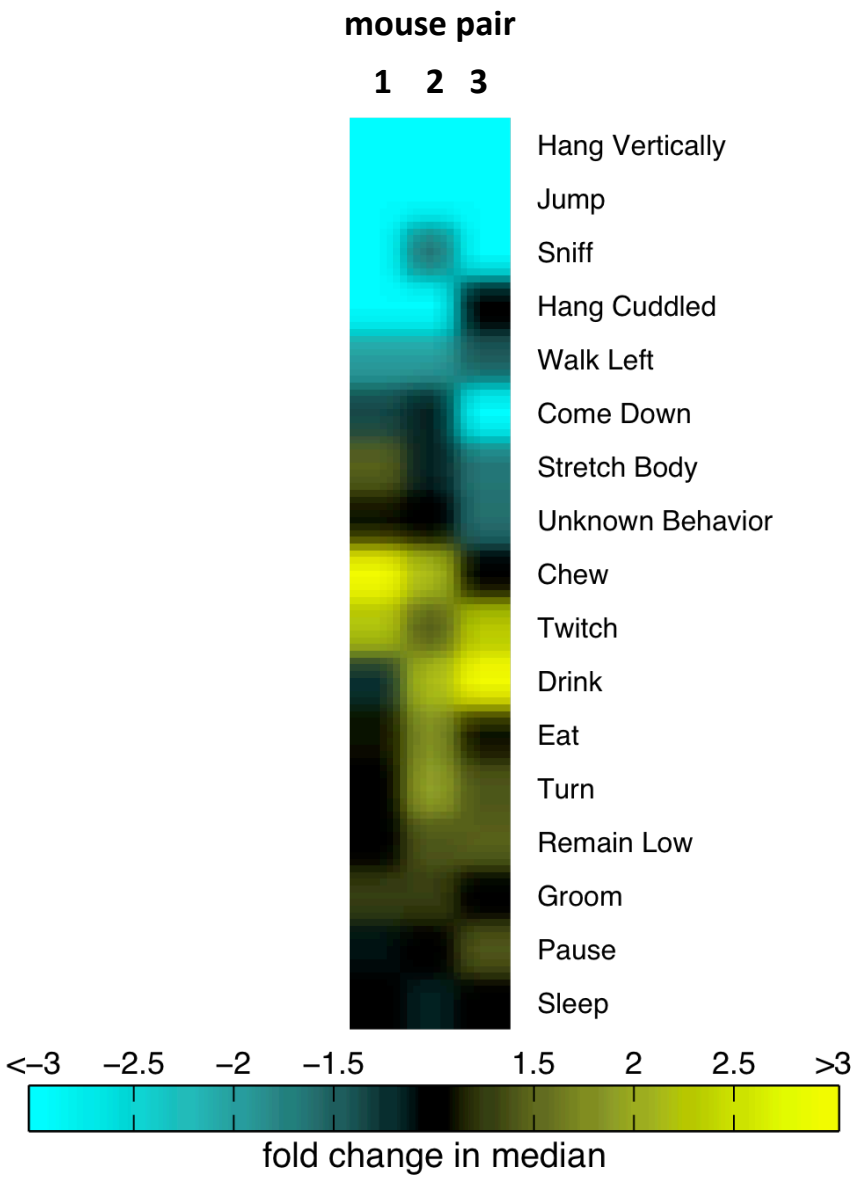

Figure 2.9. The Densin KOs are hypoactive. The activity of the Densin KO and WT mice was assessed in the light and dark cycle at 8, 10, and 12 weeks for 24 hours at each age using an automated home cage monitoring system. The fraction of frames in which specific behaviors were performed was calculated. The fold change in the median in the KO relative to the WT is reported from 3 separate WT-KO pairs. Underactive behaviors are shown in teal and overactive behaviors are shown in yellow. Descriptions of each behavior are described in Steele et al, 2007. Data collected by Andrew Steele and Keith Gunapala.

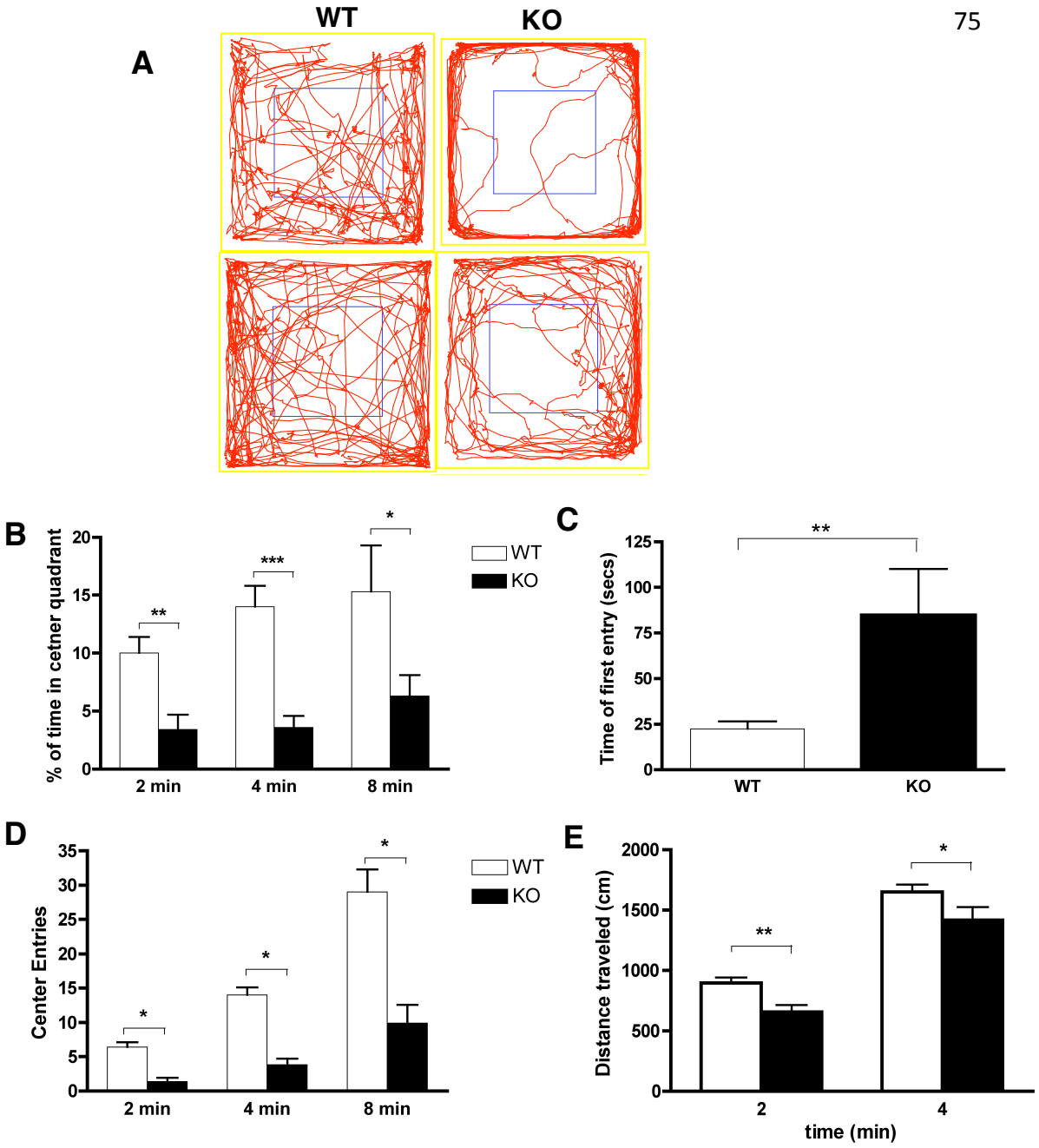

Figure 2.10: Densin KOs are more anxious than WTs in the open field test. (A) Shows representative paths of WT and KO mice during a 10 min exploratory session in an open field. The outer rim of the box (50 x 50 cm) is outlined in yellow, and the center quadrant in blue (25 x 25 cm). (B) The percentage of time that the KO mice spent in the center quadrant is significantly less than the WTs after 2, 4 and 8 min of exploration. KOs also showed a longer latency to enter into the center (C) and the frequency of entries into the center quadrant was also significantly lower for the KOs after 2, 4 and 8 minutes (D). KOs also travelled a significantly shorter distance (cm) after 2 and 4 minutes than WTs (E). WT and KO data are displayed as white and black bars, respectively. Error bars show SEM. Statistical significance was measured by 2-tailed t-test (*p <0.05 , **p <0.005 ,***p <0.0005). Mice were 8-10 weeks old.

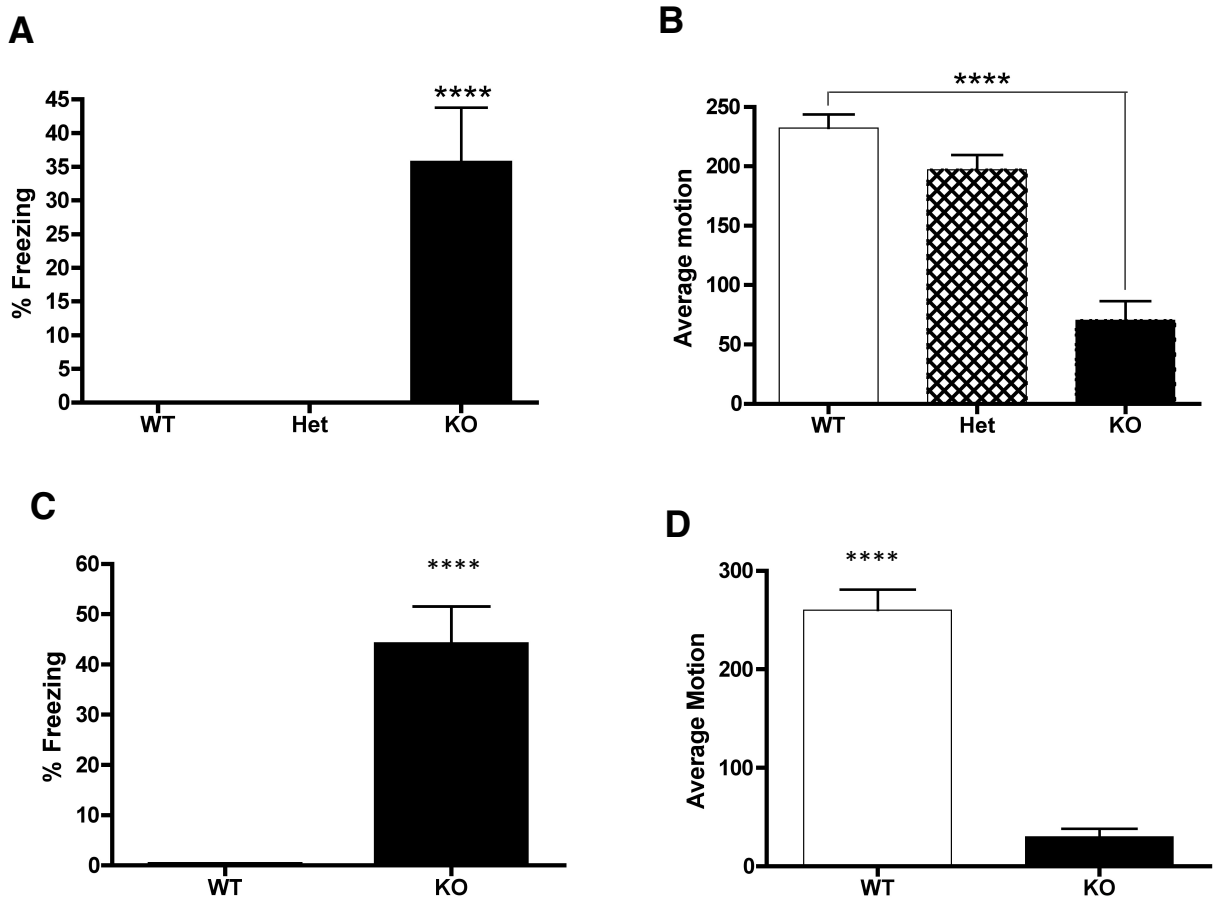

Figure 2.11: Densin KOs spend more time freezing and are less motile in a novel enclosed chamber than WTs. Percentage freezing and average motion was measured for male (A,B) and female (C,D) cohorts by infrared detection of movement in a fear conditioning chamber in which no shock was delivered. (A,C) Both male and female KO mice spent 30-40% of the 5 min exploration period freezing, whereas male and female WTs as well as male HETs spent 0% of the time freezing. (B) Male WT mice showed significantly higher levels of motion than the HET and KO males (n = 20 WT, 9 HET, 15 KO males). (D) Female WT mice were also more mobile compared to female KO mice (n = 11 WT, 9 KO females). Mice were 10-12 weeks old. Statistical significance was determined with ANOVA in A,B and 2-tailed t-test in C,D (****$p<0.0001$). Error bars represent SEM.

	WT	HET	KO
KO	**75%** n=4 cages KO	**80%** n=5 cages HET	**100%** n=2 cages KO
WT	**0%** n=4 cages	**67%** n=3 cages HET	

Figure 2.12: Densin KOs and HETs are aggressive with their littermates with assertion of dominance in the following order: HET>KO>WT. The table shows the genotypes that were housed together and the frequency of fighting among the different genotypes. The genotype of the aggressor is shown in red. Mice were assessed for fighting by 14-16 weeks of age.

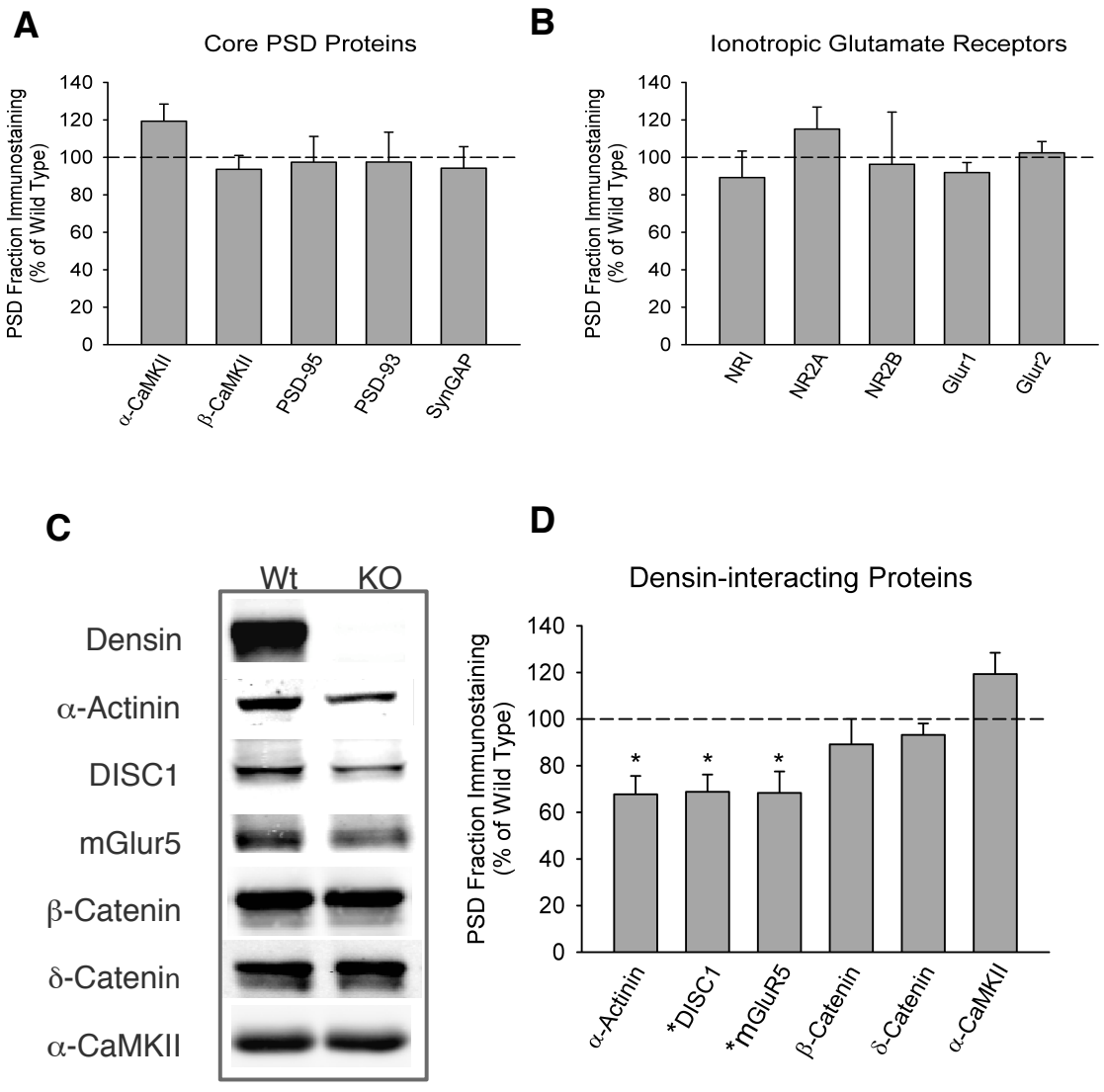

Figure 2.13: Loss of Densin results in decreased levels of alpha-actinin, DISC1, and mGluR5 in PSD fractions. Relative amounts of core PSD proteins (A) and ionotropic glutamate receptors (B) were unchanged in PSD fractions from KO compared to WT mice. The levels of direct and indirect (*) binding partners of Densin in PSD fractions from Densin KO mice are shown in (C). Significantly less alpha-actinin, DISC1, and mGlur5 was detected in PSD fractions from Densin KO mice compared to WT PSD fractions. Representative immunoblots are shown in (C). Statistical significance was assessed by one-sample t-tests with a theoretical mean of 100 (*$p < 0.05$; n=3-4 PSD fractions each prepared from 7 or 8 age and sex-matched mice of each genotype). Error bars represent SEM.

	Human Symptoms	Rodent Proxy
Cognitive dysfunction	impaired short-term memory impaired working memory	impaired short-term memory impaired working memory
Positive symptoms	hallucinations / delusions	locomotor hyperactivity
Negative symptoms	pre-pulse Inhibition reduced emotional expression poverty of speech asocial behavior anhedonia	pre-pulse inhibition no proxy no proxy aggression impaired social memory deficits in nest building reduced sucrose consumption

Table 2.1. Comparison of human symptoms of schizophrenia and endophenotypes described in mouse models of schizophrenia (table based on review by Inta et al., 2009).

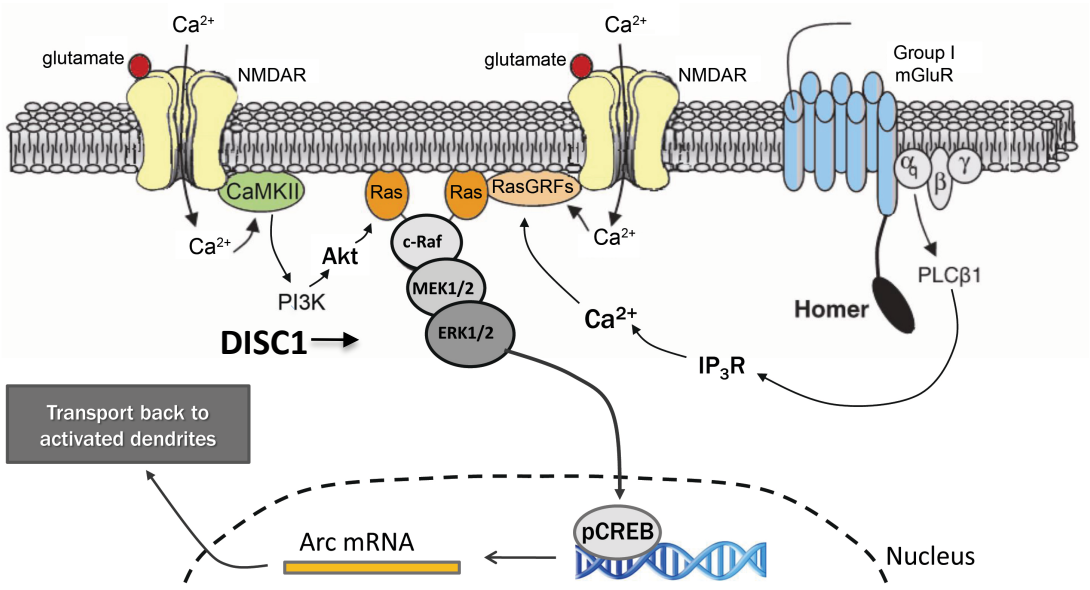

Figure 2.14. Working model showing how DISC1 and mGLUR1 signaling pathways positively regulate ERK signaling to promote activity dependent transcription. Stimulated Group 1 mGluR (mGluR1 and mGluR5) receptors act through G coupled proteins to facilitate Ca^{2+} signaling by phosphlipase C b1 (PLCb1) and IP3R, promoting activation of Ras and downstream ERK signaling which leads to CREB activation by phosphorylation at Ser133. siRNA knockdown of DISC1 has been shown to reduce phosphorylation of ERK (Hashimoto et al., 2006). Phosphorylated CREB (pCREB) enhances transcription of target genes, including Arc, whose transcript is then transported to activated dendrites. NMDA receptor signaling via Ca^{2+} influx also activates ERK signaling pathways. Figure by Holly Carlisle.

Chapter 3
Arc Protein Levels and BDNF Signaling are Deranged in the Densin KO

Communication between the synapse and the nucleus is an integral part of synaptic plasticity. Disruption of activity-induced transcription and translation has been linked to defects in cognition, affect, and anxiety levels (Cohen and Greenberg, 2008). Interestingly, relative to the WT, a number of transcripts for immediate early genes (IEGS), including Arc/Arg3.1, are decreased in the Densin KO relative to the WT (RNA seq data, Holly Beale's thesis). To extend these findings, we assessed the abundance of Arc protein in brain homogenate, synaptosome, and PSD fractions by immunoblot assays. We also assessed the localization of Arc in the hippocampus and cortex by immunohistochemistry. Furthermore, we investigated signaling pathways that normally induce Arc expression such as those mediated by the neutrotrophin BDNF. BDNF stimulation for 2, 4, or 8 hours in cortical cultures results in reduced Arc protein levels in KO compared to WT cells. Preliminary data show that levels of c-fos, another IEG, and phosphoSer133 CREB are also decreased in BDNF stimulated cortical cultures in the KO relative to the WT over the same time course. PhosphoSer133 is the active form of CREB, which enhances expression of many genes including c-fos and Arc. Impaired BDNF signaling cosegregates with mood and developmental disorders (Craddock et al., 2005; Ivleva et al., 2008; Chapleau et al., 2009; Yoshii and Constantine-Paton, 2010), consistent with the behavioral abnormalities of the Densin KO mouse. The decrease in Arc levels may also be related to a reduction in mGluR5 seen in the PSD fraction of the KO mouse. mGluR5 normally mediates a form of LTD that requires the rapid synthesis of Arc (Park et al., 2008).

Arc/Arg3.1

Like many of the IEGs, Arc is induced in response to a variety of stimuli including seizure, high frequency electrical stimulation, neurotransmitters, and neurotrophins (BDNF) (Link et al., 1995; Lyford et al., 1995; Ying et al., 2002). On a behavioral level, experiences such as exposure to a novel environment and training in spatial recognition of objects leads to increased Arc transcription (Guzowski et al., 2001; Steward and Worley, 2001; Soule et al., 2008). Unlike other IEGs, the activity-induced Arc transcripts are transported to activated dendrites where they are locally translated within 30 minutes, allowing Arc to serve as a transient geographical tag for recently activated synapses (Steward et al., 1998; Guzowski et al., 1999). Induction and proper localization of Arc mRNA is dependent on NMDA activity, actin polymerization, and Erk phosphorylation (Link et al., 1995; Steward and Worley, 2001; Huang et al., 2007). It is not completely clear what Arc actually does once it arrives in the active dendrite or in the PSD, where it is enriched, but its domain homology to spectrin is consistent with Arc's ability to modulate the expansion and contraction of the spine cytoskeleton through its indirect association with F-actin (Lyford et al., 1995; Donai et al., 2003; Plath et al., 2006). Arc is essential in the consolidation of different types of late-LTP (i.e. NMDA and BDNF driven) and facilitates mGluR-LTD by AMPA receptor trafficking (Chowdhury et al., 2006; Rial Verde et al., 2006; Shepherd et al., 2006; Waung et al., 2008).

Arc protein and transcript levels are altered in the Densin KO mouse, and Arc and Densin KO mice have electrophysiological and behavioral similarities. Both have normal

AMPA and NMDA currents with impaired LTD and early enhancement of LTP (Carlisle, O'Dell, and Indersmitten, unpublished data). In addition, the Arc KO mouse displays deficits in late phase LTP, which remains to be examined in the Denisn KO. These late LTP deficits are consistent with the need for translation of Arc and protein synthesis during this phase, and correlate with long-term memory deficits in novel object recognition and taste aversion seen in the Arc KO (Plath et al., 2006).

Arc's Role in Long-Term Potentiation

Arc is involved in the consolidation of LTP, which is dependent on new protein synthesis and is coupled to rearrangement of the actin cytoskeleton to expand the PSD and spine (Guzowski et al., 2000; Huang et al., 2007). The window of Arc activity in LTP was deduced from infusion of antisense oligonucleotides into the hippocampus to block Arc induction after initiation of LTP (Guzowski et al., 2000; Messaoudi et al., 2007). Antisense oligonucleotides specific for Arc mRNA interfered with the maintenance but not induction of LTP. Moreover, these animals exhibited problems in long, but not short-term spatial memory tasks, indicating that Arc is required in the consolidation, but not induction of LTP (Guzowski et al., 2000).

Arc may facilitate actin rearrangement in LTP through indirect regulation of cofilin, which severs actin and promotes its depolymerization. Cofilin is rendered inactive by phosphorylation by LIMK (LIM domain kinase). LIMK is regulated by PAK and Rho GTPases. Administration of antisense oligonucleotides specific for Arc mRNA after high frequency stimulation is correlated with dephosphorylation of cofilin, a decrease in Arc, and loss of actin at the synapse. Stabilization of F-actin by jasplakinolide reverses

this effect, underscoring the importance of cytoskeletal changes regulated by Arc for LTP consolidation (Messaoudi et al., 2007).

Both NMDA-LTP and BDNF-LTP are mediated by Arc, the latter through the TrkB receptor (Link et al., 1995; Lyford et al., 1995; Ying et al., 2002). There is crosstalk between these two pathways. Erk activity is important for both BDNF and NMDA-dependent LTP, leading to activation of CREB by phosphorylation at Ser133, thereby enhancing transcription of neural plasticity genes (Ying et al., 2002).

BDNF Signaling and Arc in LTP

We have found that BDNF signaling is impaired in Densin KO neurons. BDNF is secreted pre- and post synaptically in an activity-dependent manner and binds the TrkB receptor. An unprocessed form, proBDNF, is thought to be able to bind the p75NTR receptor, which has less clear effects. Stimuli that cause BDNF to be released into the synaptic cleft include NMDA activation and high frequency stimulation (Waterhouse and Xu, 2009). BDNF (found in both pre- and post sides of the synapse) has roles in neuroprotection, maturation, regulation of cortical inhibition, and is involved with early and late phases of LTP (Hong et al., 2008; Tanaka et al., 2008; Waterhouse and Xu, 2009; Yoshii and Constantine-Paton, 2010). Late phase LTP is differentiated by the requirement for protein synthesis. Importantly, the BDNF gene is considered a risk locus for mood and bipolar disorder as determined by genotyping single nucleotide polymorphisms (SNPs), and haplotyping studies from families with bipolar disorders (Sklar et al., 2002). Derangements in BDNF signaling may partially explain the increased anxiety, decrease in cognition, and possible depression in the Densin KO mouse. A

human single nucleotide polymorphism, Val66Met, in the 5' pro region of BDNF, which results in decreased activity-dependent secretion and trafficking of BDNF, confers risk for cognitive and affective problems (Egan et al., 2003; Chapleau et al., 2009; Yoshii and Constantine-Paton, 2010).

In the consolidation of LTP, BDNF facilitates protein synthesis-dependent expansion of singly activated spine heads created by actin rearrangement (Tanaka et al., 2008). Treatment of hippocampal slice cultures for 2-3 days with 250ng/mL BDNF leads to an increase in miniEPSPs and in spine density, favoring stubby spines over mushroom and thin spines (Tyler and Pozzo-Miller, 2003). Blocking TrkB receptors with TrkB-IgG in Purkinje cells increases the length of the neck of spines (Shimada et al., 1998). Together, these results suggest that dysfunctional BDNF signaling in the Densin KO could play a role in the loss of stubby spines with increased prevalence of mushroom spines with unusually long necks observed in this mutant (H. Carlisle, unpublished data).

Signaling from the TrkB receptor, by recruitment of proteins to its autophosphorylated tyrosine kinase tail, affects transcription and translation via three main pathways: 1) phospholipase Cγ (PLCγ) which generates IP3 and diacylgycerol (DAG), the latter activating PKC. IP3 triggers Ca^{2+} release from intracellular stores, which increases adenyl cyclase (AC) activity required for the formation of the PSD-TrkB complex and localization to the PSD. AC also regulates CREB, which can enhance transcription plasticity genes like Arc, c-fos, and BDNF itself (see Figure 3.5); 2) phosphatidylinositol 3-kinase (PI3K), which promotes formation of the PSD95-TrkB complex that is thought to localize the receptor to the PSD, and regulates translation via

Grb2 binding to Ras and activation of the AKT-mTor pathway; and 3) the MAPK/ERK pathway which increases transcription of activity-dependent genes through activation of CREB. The connection between the TrkB receptor and MAP/ERK is through Shc, which can bind to TrkB autophosphorylated at Tyr515. Shc interacts with the adaptor protein Grb and SOS, which activates Ras. MAP/ERK can also regulate translation by phosphorylation of the translation machinery, including eukaryotic initiation factor 4E (eIF4E), 4E binding protein 1 (4E-BP1), and ribosomal protein S6 (Chapleau et al., 2009; Waterhouse and Xu, 2009; Yoshii and Constantine-Paton, 2010).

Arc's Role in mGluR-mediated LTD

Arc also has a role in induction of LTD by mGluR signaling (Fig. 3.1). mGluR stimulation upregulates translation of Arc, which then increases internalization of AMPA receptors, thus decreasing synaptic transmission. Induction of mGluR-LTD requires rapid synthesis of Arc (within 5 min. upon stimulation). Based on the short time course of the response and studies examining where the protein localizes after mGluR5 stimulation, it is likely that rapid translation is from preexisting Arc mRNA in the dendritic shaft (Park et al., 2008; Waung et al., 2008). In contrast, NMDAR-mediated LTD is a separate and parallel process that does not require synthesis of IEGs. The increase in translation seen in mGluR-mediated LTD is accomplished by activation of the elongation factor kinase (eEF2K). eEF2K is inhibited when bound to mGluR5, but this complex dissociates when mGluR5 is stimulated. eEF2K then phosphorylates EF2 which inhibits elongation of the most nascent protein polypeptide. This process may make the translation machinery more available for those transcripts not inhibited by EF2, such as

Arc. mGluR signaling also increases Arc synthesis rapidly by dephosphorylation of FMRP (Fragile mental retardation protein), a process that releases constitutive repression of basal translation (Park et al., 2008).

Increases in Arc promote LTD by increasing internalization of AMPA receptors. Specifically, Arc interacts with endophilin and dynamin in clathrin complexes to regulate AMPA trafficking (Chowdhury et al., 2006; Waung et al., 2008). In Arc KO neurons, surface levels of GluR1 of the AMPA receptor are more abundant than usual (Chowdhury et al., 2006; Shepherd et al., 2006). The converse is also true in that overexpressing Arc results in decreased surface GluR1 subunit of the AMPA receptor (Chowdhury et al., 2006; Shepherd et al., 2006). It may seem counterintuitive that a protein involved in LTP would also have the ability to down-regulate AMPA receptors and participate in LTD. However, the ability of Arc to participate in both directions of plasticity may represent a negative feedback mechanism to maintain homeostasis (Rao et al., 2006; Shepherd et al., 2006).

The Densin KO brain displays decreased mGluR5 in the PSD fraction relative to WT, consistent with the observation of impaired LTD in the KO. The decrease in mGluR5 in the Densin KO may be due to reduced α-actinin, a binding partner of both Densin and mGluR5. α-actinin regulates surface mGluR5 levels and signaling between mGluR5 and ERK (Cabello et al., 2007). Reduced mGluR5 may be prominent among causes of the Densin KO phenotype. Both mGluR5 and Densin KOs have behavioral abnormalities such as decreased prepulse inhibition and hyperlocomotion. The importance of the centrality of mGluR in human mental disorders is evidenced by the mGluR agonists

currently in clinical trials for schizophrenia and psychosis (Luscher and Huber, 2010).

METHODS

PSD preparation: (described in Chapter 2).

Arc and c-fos immunohistochemistry. Sections were immunostained for Arc using peroxidase DAB substrate visualization, as previously described (Peng and Houser, 2005). Sections were blocked in 10% normal goat serum 0.3% Triton X-100, 0.1M TBS , ~ 13 µg/mL avidin. Brain slices were incubated with primary antibody specific for Arc (Santa Cruz sc-17839) diluted 1:1000 in 2% normal goat serum, 0.1 M Tris (0.15 M NaCl), ~3.7 µg/mL biotin overnight at room temperature. Following 3 washes 5 min each with TBS, sections were incubated with biotinylated goat anti-mouse (Vector Labs) secondary antibody in 2% NRS, 0.1 M Tris (0.15 M NaCl) for 1 hour at room temp. Staining was visualized by incubating with avidin-biotin peroxidase complex followed by 3,3 Diaminobenzidine (DAB) substrate for 3.5 min. Signal was enhanced with nickel (Vector labs). To stop the reaction, sections were washed repeatedly (3 x 1mL each) with H_2O. Sections were mounted onto SuperPlus slides (Fisher), dried and then defatted and cleared with the sequential incubations: 2 x 1 min 95% ethanol, 2 x 1 min 100% ethanol, 3 x 3 min xylene. Sections were sealed with Permount. Sections were imaged using light microscopy using a 2.5x objective. Sections were probed for c-fos as described above using the primary antibody Gt anti-cfos Ab 1:500 (sc-52G, Santa Cruz Biotechnology) and incubating with DAB-Ni substrate for 10 min.

ImageJ was used to quantitate the intensity of the stratum radiatum, pyramidale, and oriens of hippocampi from light microscope images of KO and WT brain sections of similar Bregma. Intensity of Arc staining across the statum pyramidale and its apical and basal dendrites were measured at a line (i.e. indicated in blue) drawn two-thirds of the way from CA1 to CA2 collateral, perpendicular to the stratum pyramidale. Sections were imaged using a 2.5x objective. The intensities were aligned so that values for the stratum pyramidale were set at 0 microns.

Bicuculline and BDNF induction of Arc expression in neuronal cultures. 14-16 day old WT and KO neuronal cultures were treated with 40 µM bicuculline (Tocris Cat: 2503) or 100 ng/mL BDNF (Human, Invitrogen Cat: 10908-010) for 2, 4, and 8 hours and analyzed by Western blot as compared to an untreated control. Bicuculline (solubilized in H_2O) and BDNF (in H_2O) were added directly to the media in each well at times that permitted all samples to be lysed within minutes of each other. Samples from each well of the 24 well plate were lysed in 35-50 µL of lysis solution (20mM Tris pH 7.5, 10mM EGTA, 40mM Beta-glycerophosphate, 3% SDS 2.5 mM $MgCl_2$, Sigma phosphatase, inhibitors 1 and 2, complete protease inhibitor tablet (Roche), 0.025 U/µL of benzonase (Sigma)). Samples were heated to 95˚C for 5'. Protein concentrations of the lysates were measured with the BCA assay. Equal amounts (15 or 20 µg) of protein were loaded and separated on an 8% or 10% SDS acrylamide gel and transferred onto a PVDF membrane (Millipor). The blot was blocked in Licor Blocking Buffer for a few hours at room temp, and incubated in primary antibody rocking at room temp overnight. Primary antibodies, diluted in Licor Blocking buffer, included: Ms anti-Arc (1:500, Santa Cruz), Rb anti-cfos

(1:500, Santa Cruz), Rb or Ms phosphoSer133-Creb (1:1000, Cell signaling and Chemicon, respectively). Ms anti-MAP2 (1:1000, Chemicon), and Ms anti-GAPDH (1:20,000, Sigma). Increases in Arc and cfos protein has been seen with such a protocol in the past (Rao et al., 2006). GAPDH and MAP2 antibody staining were used as loading controls and also to assess relative health of cultures. The intensity of bands was normalized to that of GAPDH.

Cardiac perfusion. Densin knockouts and wildtypes were anesthetized with 100 mg/kg body weight Nembutal prior to cardiac perfusion. 30-45 min elapsed before perfusion took place. The mice were infused with 10 mM sodium phosphate buffer with 0.136 M NaCl, followed by 4% formaldehyde, 15% by volume of saturated 1.3% picric acid in 0.15 M sodium phosphate. Dissected brains were fixed in formaldehyde over night and then transferred to PBS before sectioning 50 µM coronal slices using a vibratome in PBS. Slices were stored in 11 mM NaH_2PO_4, 20 mM Na_2HPO_4, 30% ethylene glycol, and 30% glycerol, pH 7.5 at -20˚C. Tail biopsies were performed to confirm genotype.

RESULTS

Arc protein is decreased in the Densin KO brain. A decrease in Arc protein was seen in the KO relative to WT in two experimental preparations: 1) the homogenate, synaptosome, and PSD fractions prepared from mouse forebrain (Fig. 3.2) and 2) in the hippocampal and cortex immunohisotchemistry.

Arc is decreased in the total homogenate (72% (SEM =1) of WT, $p=1.6 \times 10^{-7}$), synaptosome (64% of WT (SEM=6), p=0.001), and PSD fractions (78% (SEM=4.5) of WT,

p=0.03), respectively. The protein appears to be more depleted in the synaptosome than it is in the PSD, but this is not yet significant.

In three pairs of WT-KO littermates, the intensity of Arc staining is reduced in the KO hippocampus and cortex compared to the WT (Fig. 3.3). In WT hippocampi, Arc staining is less prominent in the soma (stratum pyramidale) than in adjacent layers. In contrast, Arc staining in KO hippocampi is more intense in the stratum pyramidale than the dendrites that extend from that layer into the stratum oriens and radiatum. In the distal dendrites (i.e. -30 and 30 microns from the stratum pyramidale), Arc staining is up to 1.5-fold more intense than the similar region for the KOs.

In WT hippocampus, the most intense Arc staining was visible in a small population of cells in the granule cell layer of the dentate gyrus (DG), in agreement with previous observations (Link et al., 1995; Lyford et al., 1995). In Densin KO hippocampus (2 mice), a greater proportion of granule cells in the DG stained intensely for Arc. A third Densin KO mouse had fewer intensely stained granule cells in the DG than the WT littermate. This difference could be reflective of variable seizure activity.

BDNF-induced Arc protein expression is decreased in Densin KO cortical cultures. To distinguish which Arc induction pathway is perturbed in the Densin KO, neuronal cortical cultures were stimulated with drug treatments known to induce Arc expression by different mechanisms: BDNF (Fig. 3.4) or bicuculline. In both WT and KO, Arc expression peaks four hours after treatment with BDNF. The Densin KO cells were, however, deficient in inducing Arc expression after stimulation with BDNF. Arc protein

levels are significantly lower (35%, p=0.04) in KO cells relative to the WT after 8 hours of BDNF treatment (Fig. 3.4). Preliminary data also show trends of decreased c-fos and phosphoSer133 CREB protein levels after BDNF induction. The differences between WT and KO are approaching significance at 8 hours.

Because abnormalities in Arc protein induction can be pathway-specific, the levels of Arc protein were also measured in response to treatment with bicuculline, a GABA(A) receptor antagonist that enhances synaptic activity by release of inhibition at synapses. WT and KO protein Arc levels are not significantly different with bicuculline treatment (data not shown).

c-fos and Arc expression are decreased in the Densin KO. Arc and c-fos levels were measured by immunohistochemistry in sections prepared from the brains of 3 WT/KO littermate pairs anesthetized with Nembutal. Immunostaining for Arc and c-fos was decreased in the KO compared to the WT in brain sections from 3 pairs of mice that had been injected with Nembutal. The sections examined were at intervals of every ~200 μm in the forebrain.

DISCUSSION

Decreased levels of Arc were seen in the Densin KO at steady state in brain homogenate, and synaptosomal and PSD fractions. Additionally, BDNF-induced Arc expression is lower (by 35%) relative to WT at 8 hours. A similar trend is seen in BDNF-induced c-fos and phosphoCREB levels, where the differences between KO and WT

levels are most apparent after 8 hours of BDNF stimulation. This is consistent with decreased steady state levels of Arc and c-fos. Arc protein levels are correlated with the decrease in mGluR5 (See Chapter 2 Figure 2.13), which facilitates rapid synthesis of Arc in LTD. In WT mice, application of an mGluR5 agonist causes increased Arc expression and reduced surface AMPA receptor levels (Park et al., 2008; Waung et al., 2008).

Dysregulation of Arc and other IEGs was first observed in the RNA-Seq comparison of transcript in the forebrain of Densin KO and WT mice, which demonstrated that abundance of transcripts for IEGs is decreased in the Densin KO relative to the WT (H. Beale, unpublished data). The Arc KO phenotype is similar to the Densin KO phenotype. Both have reduced LTD and early enhancement in LTP, although the impairment with the Densin KO mouse is not as severe as that observed in the Arc KO mouse. Although Arc KO mice have some memory impairments such as delays in finding a hidden platform in the Morris water maze, the Arc KO was indistinguishable form the WT in the short-term novel object learning and memory test. In contrast, the Densin KO performed worse than WT on the novel object test (Chapter 2 and Figure 2.6). Thus, the decrease in Arc observed in the Densin KO does not account for the entirety of the abnormal behavior.

Nevertheless, Arc may still play a role in other mechanisms underlying the Densin KO phenotype. Derangements of BDNF signaling are linked to mood disorders, Alzheimer's, autism spectrum disorder and other neurodevelopmental diseases (i.e. Rett syndrome and Tuberous sclerosis) (Chapleau et al., 2009; Gadow et al., 2009; Yoshii and Constantine-Paton, 2010). A natural polymorphism of BDNF, Val66Met, in

humans leads to increased risk of anxiety, cognitive, learning and memory defects, and depression (Bramham and Messaoudi, 2005; Bramham, 2007; Gadow et al., 2009). Normally, BDNF signaling leads to gradual enlargement of spines with changes in spine neck volume (Tanaka et al., 2008). The prevalence of mushroom spines at the expense of stubby spines seen in the Densin KO (H. Carlisle, unpublished data) could be a reflection of the dysfunction in BDNF signaling that we observe (Shimada et al., 1998; Tyler and Pozzo-Miller, 2003).

Decreases in Arc may contribute to impaired mGluR-LTD consistent with the abnormal induction of LTD seen in the Densin KO. Protein synthesis-dependent LTD, which is mediated by mGluR activation, requires rapid increase of Arc protein and results in the increased endocytosis of AMPA receptors (Waung et al., 2008). In future experiments, neuronal cultures can be treated with 3,5 DHPG, an agonist of mGluR5, to assess ERK activation and Arc induction in the KO versus WT.

The dysregulation of the cytoskeleton in the Densin KO may also involve Arc. Of relevance to the cytoskeletal changes is that the direct binding partner of Densin, α-actinin, is decreased in the Densin KO. α-actinin usually regulates levels of mGluR5 (Cabello et al., 2007). Appropriate actin dynamics and ERK signaling are needed for both induction and localization of the protein and mRNA (Huang et al., 2007). In the Densin KO, α-actinin a cross-linker of actin that directly interacts with Densin, is decreased by ~35%. α-actinin allows actin filaments to be cross-linked, a conformation that may be advantageous for arranging layers of PSD proteins. There may be an association between the loss of α-actinin seen in the Densin KO and the decrease in Arc that may

not allow for proper transformation of spine morphology in response to stimuli. Decreased levels of α-actinin may disrupt actin polymerization and the localization of Arc to active dendrites. Importantly, α-actinin is also a binding partner to the mGluR receptors, in particular Group 1, which is thought to mediate LTD through the Arc induction described above. Impairments in mGluR-LTD (Chapter 2) may also explain some of the behaviors in the Densin KO.

Our results indicate that the decrease in Arc protein levels observed in the Densin KO may be due to alterations in Arc regulation at several levels: transcription, localization and translation. RNA seq analysis of the forebrains of Densin KO mice (H. Beale and A. Medina-Marino, unpublished data) show that transcripts for Arc and to a lesser extent c-fos are decreased, which could partially explain the decrease in proteins. The trend in decreased phosphoCREB with BDNF stimulation in the KO also suggests that enhancement of Arc transcription by upstream activation of CREB is problematic. Measurement of transcripts by quantitative RT-PCR shortly after stimulation by different paradigms would supplement information about the mechanism by which Arc levels are decreased in the KO.

Alterations in Arc localization may increase or decrease stability of the transcript or protein. Evidence of the mislocalization of Arc is seen in the trend towards a greater loss of Arc in the synaptosome as opposed to the PSD or homogenate as a whole. More compelling are comparisons of Arc staining in the hippocampus of forebrain sections from WT and KO (Fig. 3.4). The intensity of Arc staining in the KO is reduced compared to the KO. Intriguingly, in the KO, the staining for Arc is significantly more intense in the

stratum pyramidale layer, which is composed of cell bodies, relative to the dendrites (apical in stratum radiatum, basal in stratum oriens) that emanate from the layer. In contrast, the WT Arc staining is more even between the dendrites and soma. This may be due to problems involving transport of Arc transcript, translation, and/or stability of transcript and protein in the dendrites of the KO hippocampal neurons. These brain sections were obtained from mice anesthetized with pentobarbital (Nembutal) where seizures were a side effect (see Chapter 4). Nonetheless, seizures would be expected to increase, rather than decrease staining of Arc.

Another IEG, c-fos, also has reduced protein levels in the Densin KO. c-fos is a transcription factor that is also used as an indicator of neuronal activity because of its ability to rapidly respond to different chemical and electrical stimuli. In association with Jun, it forms an AP-1 complex that binds DNA to regulate transcription. Mice deficient in c-fos lack proper behavioral responses to stimulation and to adapt. These mice have deficits in long-term memory and NR2A-dependent plasticity (Fleischmann et al., 2003; Cohen and Greenberg, 2008)

Lastly, a decrease in DISC1 in the PSD (Chapter 2 and Figure 2.13) could also contribute to decreased Arc protein levels through regulation of cAMP levels. DISC1 inhibits phosphodiesterase 4B (PDE4B) degradation of cAMP by directly interacting with PDE4B (Fig. 3.5) (Millar et al., 2005). The two proteins dissociate when cAMP levels are high, suggesting that DISC1 restricts PDE4B's degradation of cAMP to activated states in the cell (Millar et al., 2005; Millar et al., 2007). cAMP normally enhances Arc expression

by its direct effect on CREB and also more indirectly by promoting the trafficking of the TrkB receptor to the surface, likely through TrkB interactions with PSD-95 (Ji et al., 2005). Abnormally low levels of intracellular cAMP in the Densin KO may result from a decrease in DISC1 that releases inhibition of PDE4B activity. Decreased levels of cAMP also decreases BDNF enhancement of spine density (Ji et al., 2005). Deletion of the C-terminus of DISC1 that contains the binding site for PDE4B, as well as chromosomal translocation of the PDE4B gene, both cosegregate with schizophrenia and mood disorders (Millar et al., 2005; Millar et al., 2007). DISC1 also positively modulates the ERK pathway that promotes transcription of Arc, c-fos and other IEGs (Hashimoto et al., 2006; Shinoda et al., 2007).

Another level of cross talk between BDNF and DISC signaling is through modulation of the MAPK/ERK signaling (Chapter 2) which can lead to changes in IEG levels. DISC1 is required for neurotrophin-induced axonal elongation through its binding to the Grb2 adaptor protein and ERK activation. Grb2 facilitates signaling between tyrosine kinase receptors, such as the TrKB receptor and the ERK pathway (Michailidis et al., 2007).

Deficiencies in long-term memory are apparent in the Arc KO as tested by contextual fear conditioning and taste aversion by Plath et al., (2006). The Densin KO exhibits other impairments in addition to its shortcomings with Arc protein, which made long-term memory difficult to test. For example, contextual fear conditioning is limited by excessive freezing behaviors by the Densin KO mouse. An alternate approach, such

as a long-term taste aversion or analysis of late-LTP electrophysiology in slices, may be required to test long-term memory.

Other Considerations

The behavioral phenotype of the Densin KO mice may be partially due to diminished activity-induced transcription. Expression of IEGs is also perturbed in conditions that inhibit L-type voltage sensitive calcium channels (VSCCs), one of which ($Ca_v1.3$) binds Densin in the presence of CaMKII (Murphy et al., 1991; Bading et al., 1993; Cohen and Greenberg, 2008; Jenkins et al., 2010). There are other similarities between the two perturbations: mutation of VSCCs causes deficits in spatial tests and protein synthesis-dependent LTP, which are associated with mental retardation and other cognitive and affective disorders (Moosmang et al., 2005; Cohen and Greenberg, 2008). To test for overlap in the signal transduction underlying these phenotypes, promising future experiments could use agonists to activate VSCCs in Densin KO neuronal cultures to assess IEG induction relative to the WT.

References

Bading H, Ginty DD, Greenberg ME (1993) Regulation of gene expression in hippocampal neurons by distinct calcium signaling pathways. Science 260:181-186.

Bramham CR (2007) Control of synaptic consolidation in the dentate gyrus: mechanisms, functions, and therapeutic implications. Prog Brain Res 163:453-471.

Bramham CR, Messaoudi E (2005) BDNF function in adult synaptic plasticity: the synaptic consolidation hypothesis. Prog Neurobiol 76:99-125.

Cabello N, Remelli R, Canela L, Soriguera A, Mallol J, Canela EI, Robbins MJ, Lluis C, Franco R, McIlhinney RA, Ciruela F (2007) Actin-binding protein alpha-actinin-1 interacts with the metabotropic glutamate receptor type 5b and modulates the cell surface expression and function of the receptor. J Biol Chem 282:12143-12153.

Chapleau CA, Larimore JL, Theibert A, Pozzo-Miller L (2009) Modulation of dendritic spine development and plasticity by BDNF and vesicular trafficking: fundamental roles in neurodevelopmental disorders associated with mental retardation and autism. J Neurodev Disord 1:185-196.

Chowdhury S, Shepherd JD, Okuno H, Lyford G, Petralia RS, Plath N, Kuhl D, Huganir RL, Worley PF (2006) Arc/Arg3.1 interacts with the endocytic machinery to regulate AMPA receptor trafficking. Neuron 52:445-459.

Cohen S, Greenberg ME (2008) Communication between the synapse and the nucleus in neuronal development, plasticity, and disease. Annu Rev Cell Dev Biol 24:183-209.

Craddock N, O'Donovan MC, Owen MJ (2005) The genetics of schizophrenia and bipolar disorder: dissecting psychosis. J Med Genet 42:193-204.

Donai H, Sugiura H, Ara D, Yoshimura Y, Yamagata K, Yamauchi T (2003) Interaction of Arc with CaM kinase II and stimulation of neurite extension by Arc in neuroblastoma cells expressing CaM kinase II. Neurosci Res 47:399-408.

Egan MF, Kojima M, Callicott JH, Goldberg TE, Kolachana BS, Bertolino A, Zaitsev E, Gold B, Goldman D, Dean M, Lu B, Weinberger DR (2003) The BDNF val66met polymorphism affects activity-dependent secretion of BDNF and human memory and hippocampal function. Cell 112:257-269.

Fleischmann A, Hvalby O, Jensen V, Strekalova T, Zacher C, Layer LE, Kvello A, Reschke M, Spanagel R, Sprengel R, Wagner EF, Gass P (2003) Impaired long-term memory and NR2A-type NMDA receptor-dependent synaptic plasticity in mice lacking c-Fos in the CNS. J Neurosci 23:9116-9122.

Gadow KD, Roohi J, DeVincent CJ, Kirsch S, Hatchwell E (2009) Association of COMT (Val158Met) and BDNF (Val66Met) gene polymorphisms with anxiety, ADHD and tics in children with autism spectrum disorder. J Autism Dev Disord 39:1542-1551.

Guzowski JF, McNaughton BL, Barnes CA, Worley PF (1999) Environment-specific expression of the immediate-early gene Arc in hippocampal neuronal ensembles. Nat Neurosci 2:1120-1124.

Guzowski JF, Setlow B, Wagner EK, McGaugh JL (2001) Experience-dependent gene expression in the rat hippocampus after spatial learning: a comparison of the immediate-early genes Arc, c-fos, and zif268. J Neurosci 21:5089-5098.

Guzowski JF, Lyford GL, Stevenson GD, Houston FP, McGaugh JL, Worley PF, Barnes CA (2000) Inhibition of activity-dependent arc protein expression in the rat hippocampus impairs the maintenance of long-term potentiation and the consolidation of long-term memory. J Neurosci 20:3993-4001.

Hashimoto R et al. (2006) Impact of the DISC1 Ser704Cys polymorphism on risk for major depression, brain morphology and ERK signaling. Hum Mol Genet 15:3024-3033.

Hong EJ, McCord AE, Greenberg ME (2008) A biological function for the neuronal activity-dependent component of Bdnf transcription in the development of cortical inhibition. Neuron 60:610-624.

Huang F, Chotiner JK, Steward O (2007) Actin polymerization and ERK phosphorylation are required for Arc/Arg3.1 mRNA targeting to activated synaptic sites on dendrites. J Neurosci 27:9054-9067.

Ivleva E, Thaker G, Tamminga CA (2008) Comparing genes and phenomenology in the major psychoses: schizophrenia and bipolar 1 disorder. Schizophr Bull 34:734-742.

Jenkins MA, Christel CJ, Jiao Y, Abiria S, Kim KY, Usachev YM, Obermair GJ, Colbran RJ, Lee A (2010) Ca2+-dependent facilitation of Cav1.3 Ca2+ channels by densin and Ca2+/calmodulin-dependent protein kinase II. J Neurosci 30:5125-5135.

Ji Y, Pang PT, Feng L, Lu B (2005) Cyclic AMP controls BDNF-induced TrkB phosphorylation and dendritic spine formation in mature hippocampal neurons. Nat Neurosci 8:164-172.

Link W, Konietzko U, Kauselmann G, Krug M, Schwanke B, Frey U, Kuhl D (1995) Somatodendritic expression of an immediate early gene is regulated by synaptic activity. Proc Natl Acad Sci U S A 92:5734-5738.

Luscher C, Huber KM (2010) Group 1 mGluR-dependent synaptic long-term depression: mechanisms and implications for circuitry and disease. Neuron 65:445-459.

Lyford GL, Yamagata K, Kaufmann WE, Barnes CA, Sanders LK, Copeland NG, Gilbert DJ, Jenkins NA, Lanahan AA, Worley PF (1995) Arc, a growth factor and activity-regulated gene, encodes a novel cytoskeleton-associated protein that is enriched in neuronal dendrites. Neuron 14:433-445.

Messaoudi E, Kanhema T, Soule J, Tiron A, Dagyte G, da Silva B, Bramham CR (2007) Sustained Arc/Arg3.1 synthesis controls long-term potentiation consolidation through regulation of local actin polymerization in the dentate gyrus in vivo. J Neurosci 27:10445-10455.

Michailidis IE, Helton TD, Petrou VI, Mirshahi T, Ehlers MD, Logothetis DE (2007) Phosphatidylinositol-4,5-bisphosphate regulates NMDA receptor activity through alpha-actinin. J Neurosci 27:5523-5532.

Millar JK, Mackie S, Clapcote SJ, Murdoch H, Pickard BS, Christie S, Muir WJ, Blackwood DH, Roder JC, Houslay MD, Porteous DJ (2007) Disrupted in schizophrenia 1 and phosphodiesterase 4B: towards an understanding of psychiatric illness. J Physiol 584:401-405.

Millar JK, Pickard BS, Mackie S, James R, Christie S, Buchanan SR, Malloy MP, Chubb JE, Huston E, Baillie GS, Thomson PA, Hill EV, Brandon NJ, Rain JC, Camargo LM, Whiting PJ, Houslay MD, Blackwood DH, Muir WJ, Porteous DJ (2005) DISC1 and PDE4B are interacting genetic factors in schizophrenia that regulate cAMP signaling. Science 310:1187-1191.

Moosmang S, Haider N, Klugbauer N, Adelsberger H, Langwieser N, Muller J, Stiess M, Marais E, Schulla V, Lacinova L, Goebbels S, Nave KA, Storm DR, Hofmann F, Kleppisch T (2005) Role of hippocampal Cav1.2 Ca2+ channels in NMDA receptor-independent synaptic plasticity and spatial memory. J Neurosci 25:9883-9892.

Murphy TH, Worley PF, Baraban JM (1991) L-type voltage-sensitive calcium channels mediate synaptic activation of immediate early genes. Neuron 7:625-635.

Park S, Park JM, Kim S, Kim JA, Shepherd JD, Smith-Hicks CL, Chowdhury S, Kaufmann W, Kuhl D, Ryazanov AG, Huganir RL, Linden DJ, Worley PF (2008) Elongation factor 2 and fragile X mental retardation protein control the dynamic translation of Arc/Arg3.1 essential for mGluR-LTD. Neuron 59:70-83.

Peng Z, Houser CR (2005) Temporal patterns of fos expression in the dentate gyrus after spontaneous seizures in a mouse model of temporal lobe epilepsy. J Neurosci 25:7210-7220.

Plath N et al. (2006) Arc/Arg3.1 is essential for the consolidation of synaptic plasticity and memories. Neuron 52:437-444.

Rao VR, Pintchovski SA, Chin J, Peebles CL, Mitra S, Finkbeiner S (2006) AMPA receptors regulate transcription of the plasticity-related immediate-early gene Arc. Nat Neurosci 9:887-895.

Rial Verde EM, Lee-Osbourne J, Worley PF, Malinow R, Cline HT (2006) Increased expression of the immediate-early gene arc/arg3.1 reduces AMPA receptor-mediated synaptic transmission. Neuron 52:461-474.

Shepherd JD, Rumbaugh G, Wu J, Chowdhury S, Plath N, Kuhl D, Huganir RL, Worley PF (2006) Arc/Arg3.1 mediates homeostatic synaptic scaling of AMPA receptors. Neuron 52:475-484.

Shimada A, Mason CA, Morrison ME (1998) TrkB signaling modulates spine density and morphology independent of dendrite structure in cultured neonatal Purkinje cells. J Neurosci 18:8559-8570.

Shinoda T, Taya S, Tsuboi D, Hikita T, Matsuzawa R, Kuroda S, Iwamatsu A, Kaibuchi K (2007) DISC1 regulates neurotrophin-induced axon elongation via interaction with Grb2. J Neurosci 27:4-14.

Sklar P, Gabriel SB, McInnis MG, Bennett P, Lim YM, Tsan G, Schaffner S, Kirov G, Jones I, Owen M, Craddock N, DePaulo JR, Lander ES (2002) Family-based association study of 76 candidate genes in bipolar disorder: BDNF is a potential risk locus. Brain-derived neutrophic factor. Mol Psychiatry 7:579-593.

Soule J, Penke Z, Kanhema T, Alme MN, Laroche S, Bramham CR (2008) Object-place recognition learning triggers rapid induction of plasticity-related immediate early genes and synaptic proteins in the rat dentate gyrus. Neural Plast 2008:269097.

Steward O, Worley PF (2001) Selective targeting of newly synthesized Arc mRNA to active synapses requires NMDA receptor activation. Neuron 30:227-240.

Steward O, Wallace CS, Lyford GL, Worley PF (1998) Synaptic activation causes the mRNA for the IEG Arc to localize selectively near activated postsynaptic sites on dendrites. Neuron 21:741-751.

Tanaka J, Horiike Y, Matsuzaki M, Miyazaki T, Ellis-Davies GC, Kasai H (2008) Protein synthesis and neurotrophin-dependent structural plasticity of single dendritic spines. Science 319:1683-1687.

Tyler WJ, Pozzo-Miller L (2003) Miniature synaptic transmission and BDNF modulate dendritic spine growth and form in rat CA1 neurones. J Physiol 553:497-509.

Waterhouse EG, Xu B (2009) New insights into the role of brain-derived neurotrophic factor in synaptic plasticity. Mol Cell Neurosci 42:81-89.

Waung MW, Pfeiffer BE, Nosyreva ED, Ronesi JA, Huber KM (2008) Rapid translation of Arc/Arg3.1 selectively mediates mGluR-dependent LTD through persistent increases in AMPAR endocytosis rate. Neuron 59:84-97.

Ying SW, Futter M, Rosenblum K, Webber MJ, Hunt SP, Bliss TV, Bramham CR (2002) Brain-derived neurotrophic factor induces long-term potentiation in intact adult hippocampus: requirement for ERK activation coupled to CREB and upregulation of Arc synthesis. J Neurosci 22:1532-1540.

Yoshii A, Constantine-Paton M (2010) Postsynaptic BDNF-TrkB signaling in synapse maturation, plasticity, and disease. Dev Neurobiol 70:304-322.

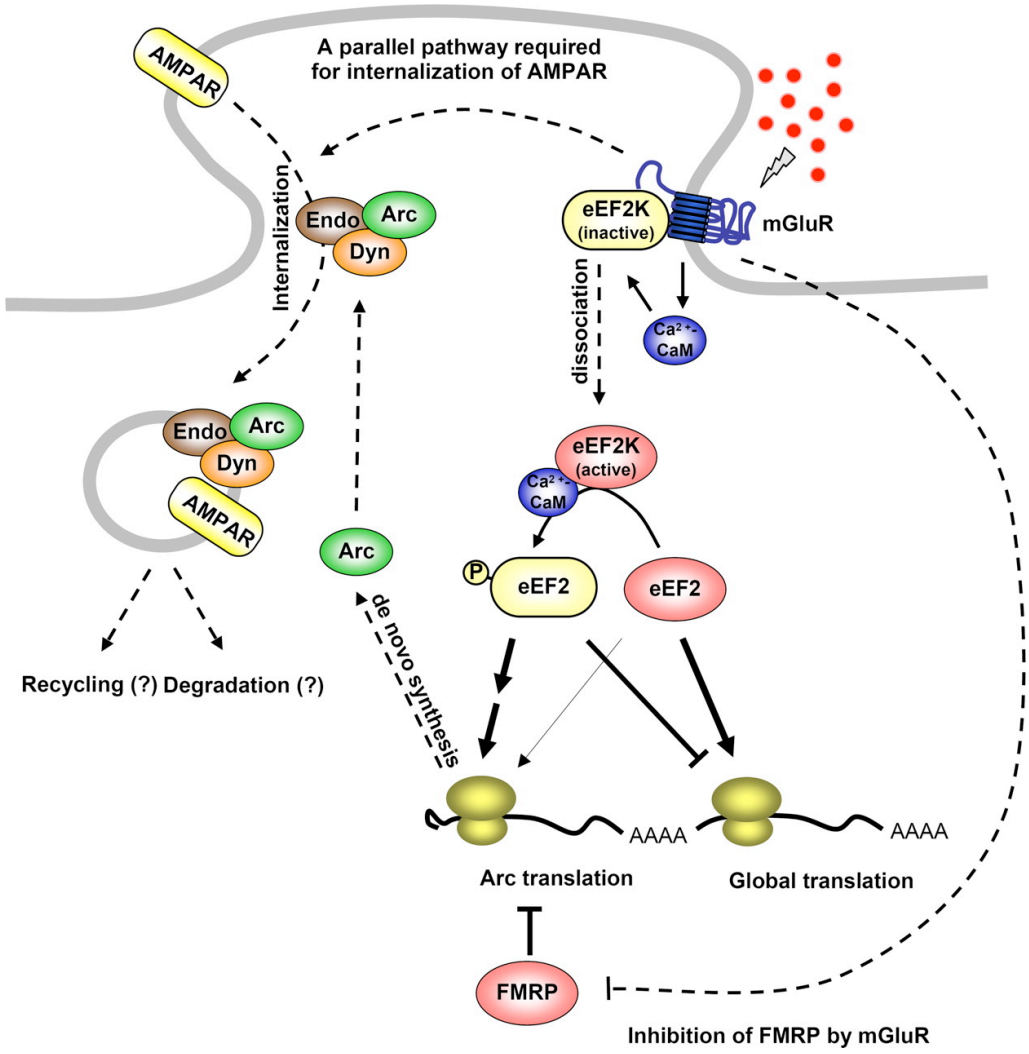

Figure 3.1. Arc has a role in induction of LTD by mGluR signaling. Induction of mGluR-LTD requires rapid synthesis of Arc (within 5 min. upon stimulation). The increase in translation seen in mGluR-mediated LTD is accomplished by activation of the elongation factor kinase (eEF2K). eEF2K is inhibited when bound to mGluR5, but this complex dissociates when mGluR5 is stimulated. eEF2K then phosphorylates EF2 which inhibits elongation of the most nascent protein polypeptide. This process may make the translation machinery more available for those transcripts not inhibited by EF2, such as Arc. mGluR signaling also increases Arc synthesis rapidly by dephosphorylation of FMRP (Fragile mental retardation protein), a process that releases constitutive repression of basal translation (Park et al., 2008). Increases in Arc promote LTD by increasing internalization of AMPA receptors. Specifically, Arc interacts with endophilin and dynamin in clathrin complexes to regulate AMPA. Reprinted from Park et al. Copyright (2008), with permission from Elsevier.

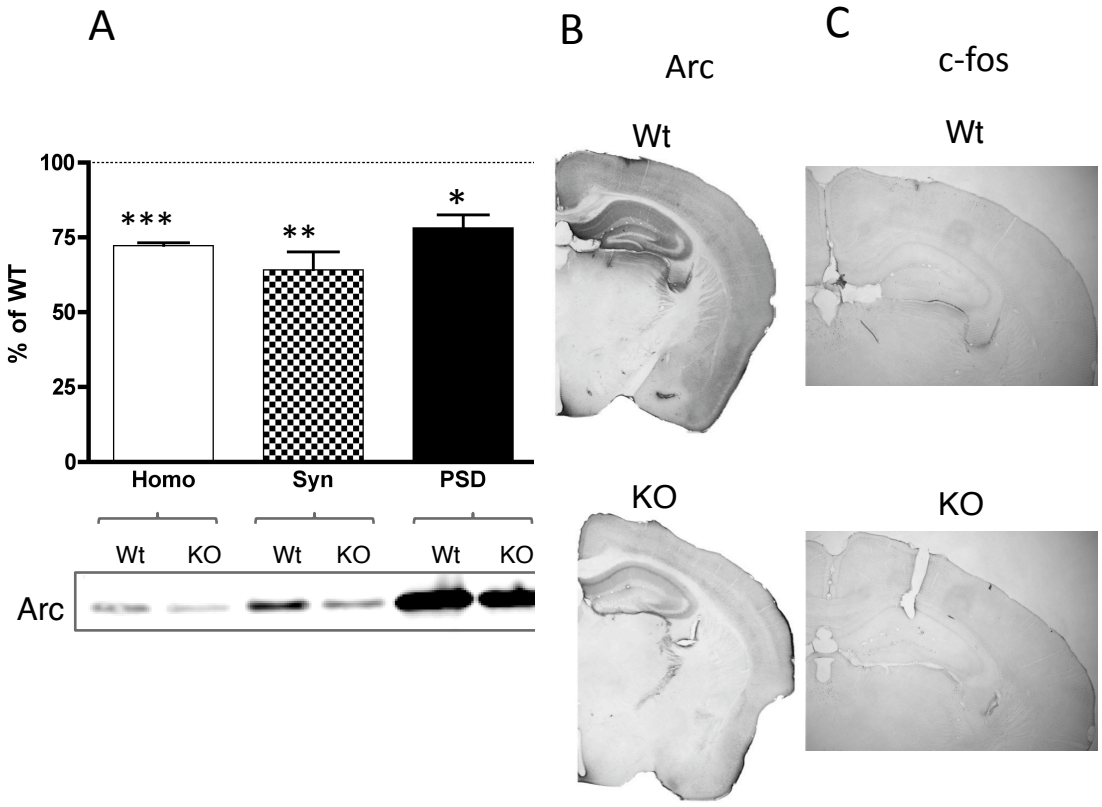

Figure 3.2. The Densin KO exhibits decreased steady state levels of c-fos and Arc. (A) Samples from forebrain homogenate, synaptosome and PSD fractions that were immunobloted with an Arc specific antibody show a significant decrease in Arc protein. The abundance of Arc protein is expressed as percentage of WT (standardized as 100% (dotted line)). A representative immunoblot detecting Arc in each of the labeled fractions is shown. Statistical significance was assessed by one-sample t-tests with a theoretical mean of 100 (*$p < 0.05$ **$p<0.005$ ***$p<0.00001$, t test; n=4 PSD fractions each prepared from 7 or 8 age and sex-matched mice of each genotype). Error bars represent SEM. (B) Representative WT and KO coronal brain sections including the cortex and hippocampus immunostained with an Arc specific antibody and visualized with peroxidase DAB-NI staining. (C) Representative coronal sections imaged at 2.5x magnification showing the hippocampus and part of the cortex from WT and KO immunostained with an antibody specific for c-fos and visualized through peroxidase DAB-Ni staining.

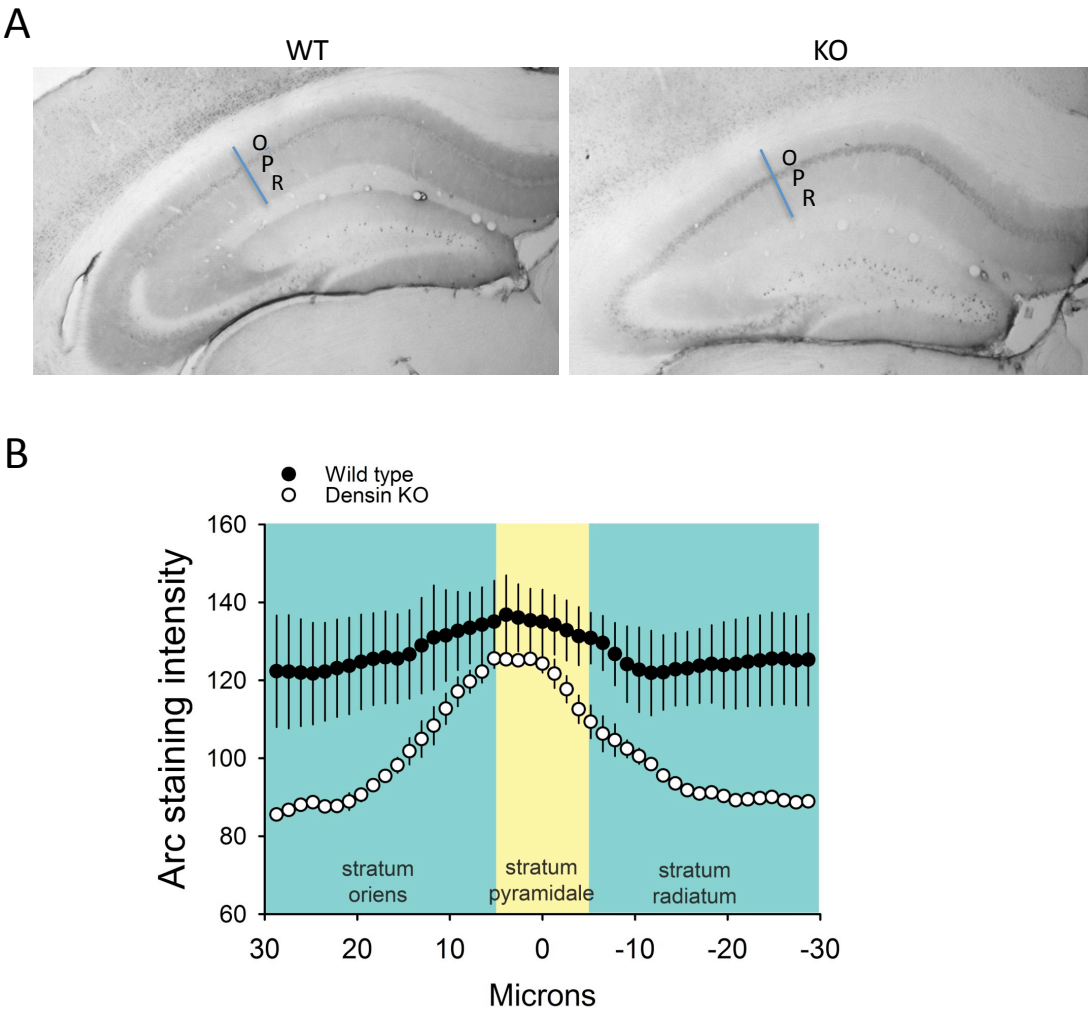

Figure 3.3. Arc protein is decreased in the Densin KO and concentrated in the soma of the stratum pyramidale relative to the basal and apical dendrites (found in stratum oriens and radiatum, respectively) that emanate from s. pyramidale. (A) Representative coronal sections of hippocampi from WT and KO mice immunostained with Arc antibody and visualized with peroxidase-DAB-Ni substrate. "P" indicates the stratum pyramidale cell body layer. "O" marks the stratum oriens and "R" the stratum radiatum. Intensity of Arc staining across all three layers were measured at a line (i.e. indicated in blue) drawn two-thirds of the way from CA1 to CA2 collateral, perpendicular to the stratum pyramidale. (B) Average staining intensity of each hippocampal layer labeled are plotted (+/- SEM) with the stratum pyramidale set as 0 microns. The intensity of the cell bodies in the s. pyramidale, and its basal and apical dendrites in the s. oriens, and s. radiatum, respectively, were quantitated (using Image J). Intensities were measured from both hippocampi from 4 different sections of 3 WT-KO pairs.

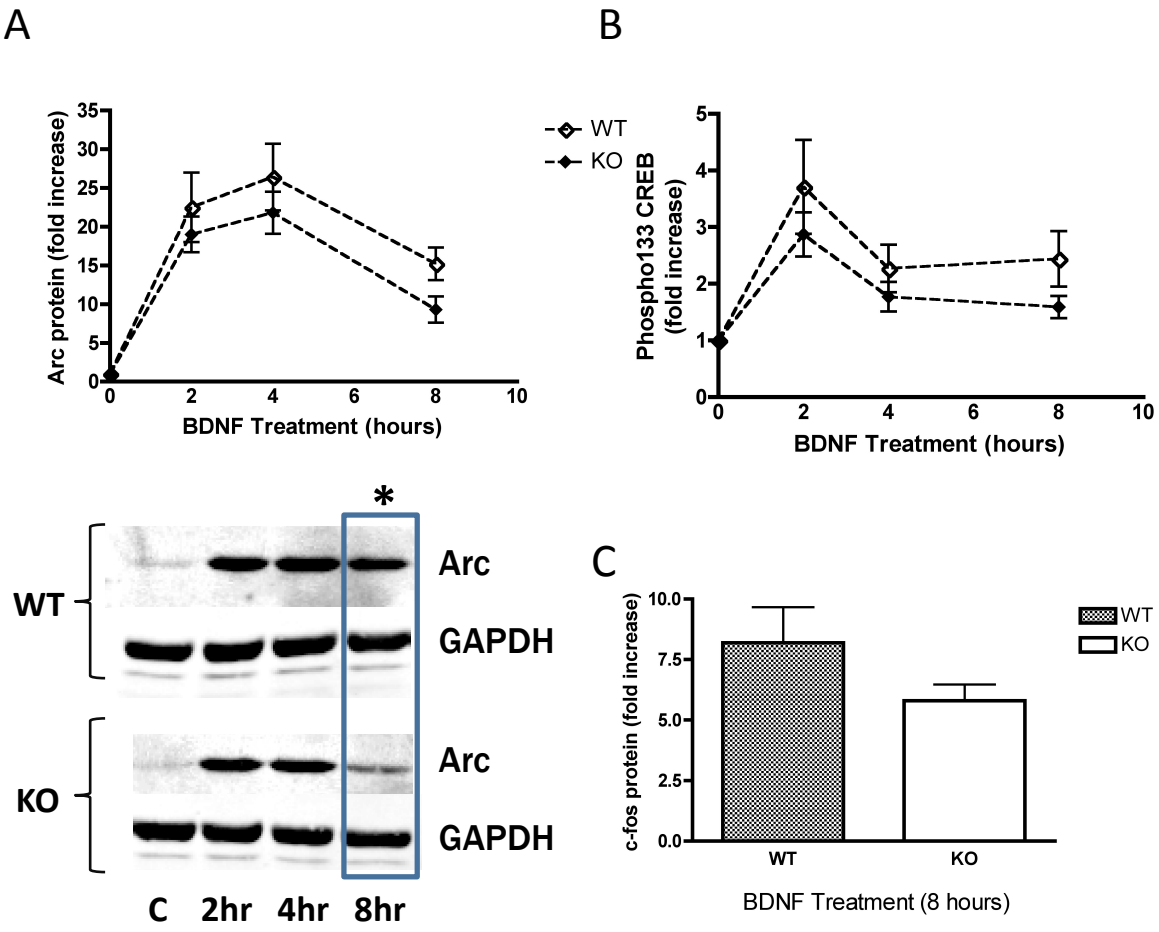

Figure 3.4 Arc induction by 100 ng/mL BDNF treatment is reduced in the Densin KO, which is significant at 8 hours. (A) Induction of Arc protein relative to control (indicated as C in the Western blots below it) based on quantitation of integrated intensities of Western blots where Arc was detected in lysates of 15-16 day old dissociated cortical cultures treated with BDNF for 0, 2, 4, and 8 hours. n=9 WTs, n=10 KOs. *=p<0.05. Data were normalized to GAPDH loading control. (B) and (C) Trend showing decreased induction of active CREB phosphorylated at 133 (n=7 WTs, n=7 KOs, p=0.13) and c-fos protein after treatment with BDNF. Fold increase in c-fos relative to the control is only reported for 8 hours n=7 WTs, n=7 KOs, p=0.16. Other time points are similar between the WT and KO for c-fos and are not shown due to scaling.

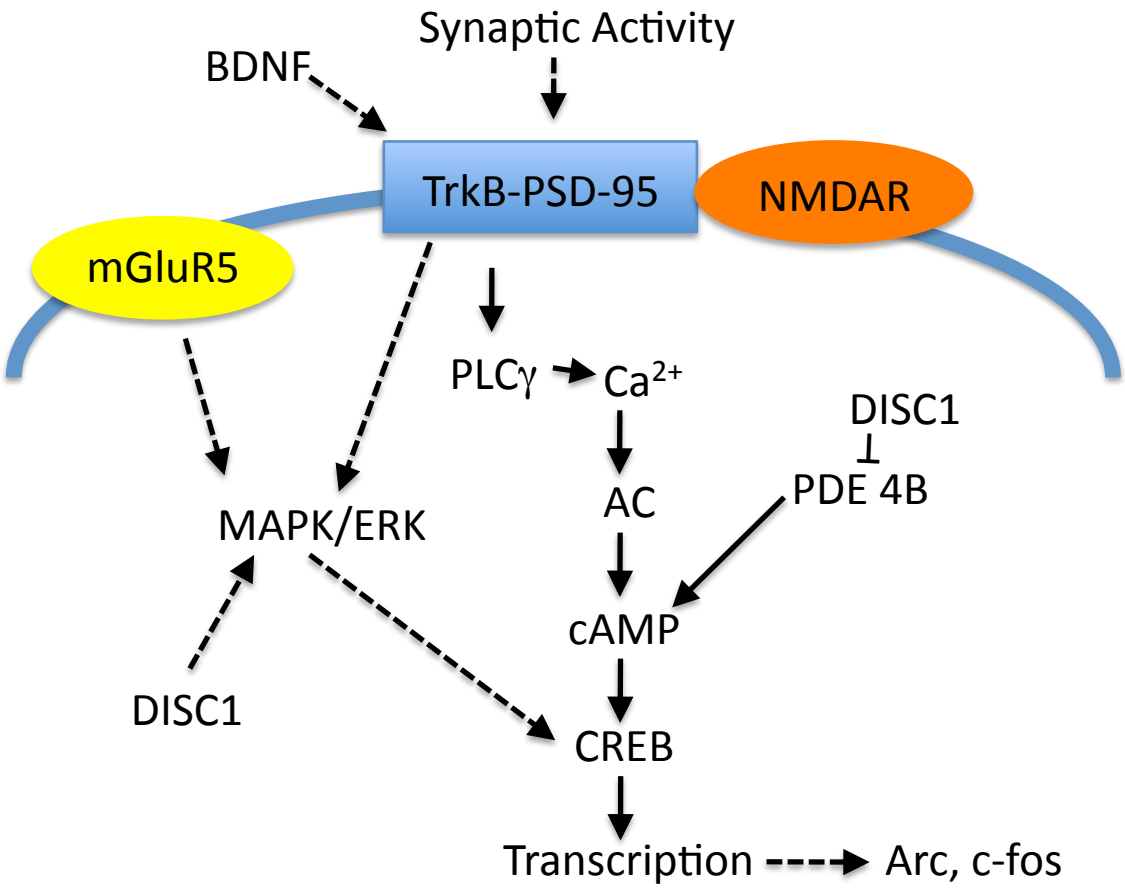

Figure 3.5. BDNF signaling through the TrkB receptor involves PLCγ and MAP/ERK activity as well as regulation of cAMP. Activation of PLCγ indirectly activates adenylate cyclase (AC) which generates cAMP. Importantly, Phosphodiesterase 4B (PDE4B) degrades cAMP but is inhibited by DISC1 (Millar et al., 2005, Millar et al., 2007). Perturbations in cAMP levels are linked to psychiatric illness (Millar et al., 2007). mGluR5 and NMDA mediated signaling act through the MAPK/ERK pathway, of which DISC1 is also a positive modulator. cAMP and activated ERK promote CREB activity leading to transcription of genes (like Arc and c-fos) that play a role in synaptic plasticity. cAMP also promotes the formation of TrkB-PSD95 complexes (Yoshii and Constantine-Paton (2010). Not shown is TrkB signaling through PI3K (Akt-mTOR pathway which influences translation and the formation of the synaptic TrkB-PSD95 complex) and the impact of these pathways on translation.

Chapter 4
Densin KO is Susceptible to Seizures

An unexpected phenotype in the Densin KO suggests a linkage between Densin function and a pre-disposition to seizures. The KO mice have violent tonic clonic seizures within two minutes of injection with pentobarbital, a GABA(A) receptor agonist, which usually sedates WT mice. Preliminary observations also suggest that the KO mice are predisposed to spontaneous seizures. This chapter describes the seizures and discusses molecular and physiological mechanisms known that might underly.

Seizures are often comorbid with mental retardation, neurodevelopmental disorders, and autism spectrum disorder (Rubenstein and Merzenich, 2003; Qin et al., 2005; Levisohn, 2007; Kanner et al., 2008; Cascella et al., 2009; Hagerman and Stafstrom, 2009; Combi et al., 2010). In epilepsy patients, there is a higher prevalence of schizophrenia (Qin et al., 2005; Cascella et al., 2009). Often the causes of a seizure, some of which are inheritable, are unknown. Molecular processes that enable brain plasticity, can, in pathologic situations, lead to epileptogenesis (McNamara et al., 2006; Scharfman, 2007; Rakhade and Jensen, 2009).

Inhibition and Excitation

Most of the inherited causes of epilepsy in humans involve genes that encode channels (i.e. potassium and sodium) or receptors that regulate ion flux (i.e. GABA receptors) (Noebels, 2003). Researchers have found that depolarizing GABA activity can contribute to pathology, and is critical for the interictal epileptic activity seen in the subiculum from patients with temporal lobe epilepsy (Cohen et al., 2002). GABA

provides the inhibitory inputs for the brain, but can also be excitatory, especially in the neonatal brain because of differences in Cl^- conductance due to expression of developmentally regulated Cl^- channels. Intracellular Cl^- concentrations are higher in the immature brain due to the presence of NKCC1 that cotransports Cl^- into the cell, along with Na^+ and K^+ (reviewed in (Ben-Ari, 2002; Kahle et al., 2008). NKCC1 creates an E_{Cl} that is more positive with respect to the membrane potential. When GABA(A) receptors are activated, the flow of Cl^- out of the cell increases, leading to depolarization of the neuron. In mature neurons, the KCC2 channel takes over as the main Cl^- transporter. In contrast to NKCC1, KCC2 extrudes intracellular K^+ and Cl^- to outside the cell. When GABA receptors are activated, Cl^- flows into the cell down its electrochemical gradient, leading to the inhibition that is typically associated with GABA from hyperpolarization. Stimulation of GABA(A) ionotropic receptors by binding of GABA neurotransmitter increases the conductance for Cl^- into the cell resulting in neuronal hyperpolarization, and thus inhibition of action potentials. Abnormal inhibitory function can lead to aberrant firing of neurons and networks (Morimoto et al., 2004; Scharfman, 2007). Problems in neuronal maturity or channel expression that lead to abnormal gene expression and ion flux, might conceivably alter whether GABA is excitatory or inhibitory in the mature organism (Ben-Ari, 2002; Kahle et al., 2008; Minkeviciene et al., 2009). Alternatively, disruptions in other ion channels (i.e. potassium leak channels) may allow for altered membrane potential such that GABA would be excitatory.

GABA(A) Receptors in Seizures

Alterations in abundance and distribution of GABA(A) receptors and innervation patterns of inhibitory neurons, can result in GABA being excitatory rather than inhbitory. These activity-dependent changes are the result of dynamic processes that may involve regulation of transcription, translation and the transport and internalization of receptors from the cell surface (Fritschy, 2008). The GABA(A) receptor is a pentamer made up of most commonly a combination of alpha (α1-α6), beta (β1-β3), and gamma (γ1-γ3) subunits. Some subunits are naturally more abundant in certain areas of the brain (Sieghart and Sperk, 2002; Voss et al., 2008) and certain subsets of neurons than others (Sieghart and Sperk, 2002). The distribution and abundance of GABA(A) receptors on a subset of inhibitory neurons that act on other inhibitory neurons can result in overexcitation due to disinhibition of excitatory neurons. (DeLorey et al., 1998; Bacci et al., 2003; Bacci et al., 2005; Voss et al., 2008). Changes in inhibitory interneuron populations and topography can alter firing rates and proper integration of neuronal networks (Santhakumar and Soltesz, 2004). Changes in GABA(A) receptors are also seen in schizophrenia (Charych et al., 2009).

In the mature brain, GABA input in the soma or axon initiation segment is inhibitory whereas both depolarizing and hyperpolarizing effects of GABA have been observed in dendrites (Gulledge and Stuart, 2003; Stein and Nicoll, 2003; Marty and Llano, 2005). Increases in the amount of GABA receptors, allowing for greater GABA input in the dendrites relative to the soma may be enough to change the reversal potential such that a GABA agonist would be excitatory. Spill over of GABA during intense activation from synaptic sites, can also be depolarizing at extrasynaptic sites

(Alger and Nicoll, 1982). Temporal factors also influence the effect of GABA as a switch. An opportunely timed GABA input within ~5-10 ms of a subthreshold excitatory depolarization facilitates an action potential, whereas either alone does not. This has to do with the changes in the resting potential relative to that of the reversal potential for Cl^-. However, a similarly timed GABA input at the soma has the opposite effect, leading to neuronal inhibition (Gulledge and Stuart, 2003; Stein and Nicoll, 2003; Marty and Llano, 2005). Very recently, it was reported that presynaptic GABA(A) receptors at hippocampal mossy fiber synapses (dentate granule cells) can be paradoxically excitatory rather than inhibitory, enhancing transmission and LTP induction (Ruiz et al., 2010).

Nembutal-induced Seizures in the Densin KO Mouse

We find that the GABA(A) receptor agonist, Nembutal (pentobarbital) paradoxically acts as a convulsant after i.p injection of the Densin KO mouse. Pentobarbital is a barbiturate that induces conformational changes in GABA(A) receptors to increase the duration of Cl^- influx, usually leading to hyperpolarization of the cell. We hypothesized that these Nembutal-induced seizures may be a consequence of a lowered threshold for seizure induction or a specific alteration in the number/pattern of GABAergic inputs. It is known that Densin is expressed in excitatory neurons. To see whether Densin is additionally expressed in inhibitory neurons, immunohistochemistry of neuronal cultures was done. We also determined the relative abundance of GABA(A) receptors and GABAergic markers in brain homogenate,

synaptosome, and PSD fractions in the KO relative to the WT. Imbalances in excitation and inhbition are a shared component of numerous disorders such as schizophrenia, autism, biopolar disorder, and anxiety, and may therefore reflect some shared pathogenesis (Rubenstein and Merzenich, 2003; Qin et al., 2005; Levisohn, 2007; Cascella et al., 2009). Interestingly, pentobarbital is also anxiolytic and the Densin KO exhibits anxious behavior (Chapter 2), suggesting this phenotype may have shared aspects of the pathophysiology in synaptic plasticity.

METHODS

Preparation of neuronal cultures for imaging on coverslips. Coverslips were washed with water, etched in 1M HCl, washed again in water, and ethanol, placed in 24 well plates and treated with poly-D-lysine (0.5 mg/mL in NaBorate buffer) in the 37˚C incubator overnight and washed with water before incubated with laminin (15 µg/mL in PBS). E15-E17 embryos were dissected from Densin Het x het timed matings for their hippocampi or cortices in Hanks dissection buffer (HEPES + Na pyruvate in HBSS) and triturated ~25-30x. Neuronal cultures grown on coverslips were plated in plating media (ß-mercaptoethanol, B27, glutamax, glutamate in neurobasal media). On day 2-3, 0.3 mL of plating media was replaced with 0.3 mL of feeding media (B27, glutamax, in neurobasal media). On day ~11, 0.175 mL of the media was replaced with 0.2mL feeding media.

Immunohistochemistry. Coverslips were rinsed in PBS and then fixed in 4˚C methanol for 20', which was replaced by -20˚C methanol and incubated for 20 min. After a 15

min wash with ice cold HBSS + HEPES, the samples were blocked in 5% normal goat serum with 0.25% Triton X-100 for 1 hour or overnight at 4˚C. Coverslips were incubated with primary antibody in preblock overnight at 4˚C, washed with preblock 3x, and incubated with secondary antibody (Alexa Fluor) for 1 hour at room tempertaure in preblock. Primary antibodies used were at the following dilutions: Densin CT245 or M3 (Kennedy Lab) 1:200-250, GAD65 and GAD67 (Chemicon). The samples were washed once with preblock and 2x with PBS followed by a 10 min postfix in 2% formaldehyde in PBS. Coverslips were washed 3x with PBS and mounted with Prolong® mountant (from Molecular Probes through Invitrogen) with Dap1 stain, and allowed to dry overnight at room temp. Coverslips were sealed with clear nail polish. Slides were stored at 4˚C or -20˚C if not imaged right away.

Nembutal induced seizures in the Densin KO. 9 WT and 8 KO mice (4 to 7.5 months of age) were injected with 100mg/kg body weight of Nembutal intraperitoneally. Seizures were videorecorded and analyzed in terms of stages. The following modification of the Racine scheme was used for description of stages: Stage 0-Normal behavior, Stage 1-Immobility, Stage 2-Forelimb and tail extension giving appearance of rigid posture, Stage 3-Automatisms: repetitive scratching, circling, or head bobbing, Stage 4-Forelimb clonus and rearing and falling, Stage 5-Repeated forelimb clonus and rearing and falling, Stage 6-Severe tonic clonic seizures, Stage 7-death (Racine, 1972).

Arc, c-fos, and GAD67 peroxidase staining of brain sections with DAB-Ni visualization. To attempt to identify the foci of seizure activity in the Densin KO, brain slices from 3

pairs of WT and KO mice that were injected with 100 µg/g body weight of Nembutal were probed for c-fos and Arc. Arc and more frequently, c-fos, have been used by others to correlate specific regions of the brain with seizure activity or at least neuronal activity. The mice were perfused ~30-45 min after injection with Nembutal. In the pilocarpine model of epilepsy, c-fos immunostaining peaked after 30 min (Peng and Houser, 2005).

Immunostaining for c-fos using peroxidase DAB substrate visualization was done based on Peng et al. (Peng and Houser, 2005) as described in Chapter 3 Methods. GAD67 staining was also done with the protocol above on sections from brains of mice that were injected ketamine/xylazine prior to cardiac perfusion. GAD67 antiserum (Ms, Chemicon) was incubated with brain sections at a 1:2000 dilution in goat serum and incubation with DAB-NI substrate was only for 1.5 min.

Cardiac perfusion. Densin knockouts and wildtypes were anesthetized with 125/10 mg/kg body weight ketamine/xylazine prior to cardiac perfusion. The mice were infused with 10 mM sodium phosphate buffer with 0.136 M NaCl, followed by 4% formaldehyde, 15% by volume of saturated 1.3% picric acid in 0.15 M sodium phosphate. Dissected brains were fixed in formaldehyde over night and then transferred to PBS before sectioning 50 µM coronal slices using a vibratome in PBS. Sections were stored in 11 mM NaH_2PO_4, 20 mM Na_2HPO_4, 30% ethylene glycol, and 30% glycerol, pH 7.5 at -20˚C. Mice were also retailed to confirm genotype.

PSD preparation. (See protocol in Chapter 2 Methods)

RESULTS

Nembutal induces seizures in the Densin KO mouse. The Densin KO mouse was created by deletion of exon 3 through flox-Cre technology and subsequent breeding to Cre expressing mice (Medina-Marino thesis). We found that the anesthetic Nembutal induces tonic clonic seizures in these mice. Half of the 8 Densin KOs tested reached stage 6, within 2 minutes after IP injection of 100 mg/kg body weight of Nembutal. The other 4 KOs tested displayed an abnormal jittery behavior. No convulsions were seen in any of the 9 WT littermates that were also injected with the same dose of Nembutal. No sex differences were seen in responses. A sequence of still images comparing the KO and WT with staging at different time points after injection is shown in Figure 4.1.

Similar seizures were also seen with a lower dose (50 mg/kg) of Nembutal and 2% Isoflurane, an inhaled anesthetic that acts on a number of pathways including GABA (Bruce Cohen, personal communication). However, the KO does not seize in response to every drug administered by i.p. injection: a ketamine/xylazine mixture (125/10 mg/kg of body weight) that was used to anesthetize for perfusions, did not induce seizures in any of the 9 KOs tested. We have not injected with ketamine alone to eliminate the possibility that xylazine, a muscle relaxant, may mask seizures.

We injected KOs and WTs (7^{th} outcross with C57) with Euthasol (pentobarbital plus phenytoin) to see if this combination would eliminate the seizures seen with pentobarbital alone. If it did, it would be a useful anesthetic for future perfusions. Interestingly, the 3 out of 3 KOs injected had Stage 6 tonic clonic seizures even though phenytoin is an antiepileptic that acts by stabilizing the inactive form of voltage gated

Na^+ channels. However, the seizures with Euthasol seem to be shorter in duration and less violent in nature than the seizures seen with the same concentration of pentobarbital alone. 2 of the 3 WTs exhibited mild twitching after the i.p. injection with Euthasol (~Stage 2/3). It appears that the seizure phenotype is more penetrant in the C57 background. The 2nd outcross of KO mice all had seizures with pentobarbital but only half went to stage 6 tonic clonic ones, while the other half were just jittery.

Densin is expressed in inhibitory neurons. Densin is enriched in the PSD of excitatory glutamatergic synapses (Apperson et al., 1996). Double staining for Densin and GAD 67, a marker for GABAergic neurons, in dissociated hippocampal cultures revealed that Densin is also expressed in at least a subset of inhibitory neurons (Fig. 4.2). This finding suggests that both inhibitory and excitatory neurons and their innervation patterns may be affected by the lack of Densin in the KO. It is unknown whether Densin is expressed in a particular subset of inhibitory neurons, such as the parvalbumin positive cells that are responsible for high frequency oscillation.

GABA(A) receptors and KCC2 are unaltered in homogenate and synaptosome fractions for Densin KO mice. PSD preparations from WT and KO mice were analyzed to determine whether the abundance of particular proteins is altered in the KO. Because Nembutal is an agonist of GABA(A) receptors, we hypothesized that GABA(A) receptors might be affected. Mutations of particular GABA(A) receptors are associated with certain types of epilepsy and with schizophrenia (Charych et al., 2009; Chen et al., 2009;

Zai et al., 2009). GABAAr (a1, b3, a2) levels were, however, not altered in homogenate or synaptosome fractions relative to WT (Fig. 4.3).

Because misregulation in the levels of KCC2 might contribute to changing the reversal potential in the KO relative to the WT such that the GABA agonists are inhibitory rather than excitatory, we probed for KCC2 in our protein preparations but found no change (Fig. 4.3). KCC2 is a potassium chloride cotransporter channel that is more highly expressed in the adult, mediating the developmental switch from depolarizing to hyperpolarizing effect that we typically see with GABA.

Some GABAergic markers are increased in the homogenate and synaptosome fractions of Densin KO brains. To see if other markers of the GABAergic system are altered, we probed for GAD67, GAD65, and parvalbumin (PV) in the homogenate and synaptosome fractions from Densin KO and WT forebrains. Signficantly, abundance of GAD65 and PV in the synaptosomal fraction are 125% (SEM=9.6, p=0.04) and 124% (SEM=5.5, p=0.005) of the WT, respectively (Fig. 4.4). A trend of increased GAD67, GAD65, and PV was also seen in the homogenate. GAD67 and GAD65 are decarboxylases that participate in the rate-limiting step of GABA synthesis. PV marks a high spiking subset of inhibitory neurons.

A seizure focus was not found but c-fos and Arc expression are decreased in the Densin KO. To determine which part of the brain is affected in Nembutal induced seizures, brain sections from KO and WT mice injected with Nembutal were stained for c-fos and Arc protein. Activity-induced transcription of IEGs are normally correlated

with areas that exhibit neuronal activity such as electrical and chemical stimulation or in response to brain injury (Cole et al., 1990; Herrera and Robertson, 1996; Hughes et al., 1999). c-fos, along with Jun, is part of a transcriptional complex called AP-1, that promotes the transcription of a set of genes in response to such stimuli. Changes in levels of c-fos protein detected by immunostaining in brain slices after spontaneous seizures reflect regions that are affected in the pilocarpine mouse model of temporal lobe epilepsy (Fabene et al., 2004; Harvey and Sloviter, 2005; Peng and Houser, 2005). RNAseq study of KO and WT mice performed showed that transcripts of a group of IEGs, including c-fos, are higher in the hippocampus in the Densin KO versus WT (H. Beale and Medina-Marino, unpublished data). This result indicates that the hippocampus is a potential site of overactivity.

We did not observe an obvious focus of seizure activity from staining brain sections for c-fos and Arc from WT and KO mice injected with 100 μg/mL Nembutal and fixed 30-45 minutes after injection. However, after immunostaining brain sections from 3 pairs of mice that had been injected with Nembutal with antibodies specific for these IEGs, we found that both c-fos and Arc levels are decreased in the KO compared to the WT. There is a loss in Arc protein in both the hippocampus and cortex in the Densin KO (Chapter 3). Western blots of Arc expression of the homogenate, synaptosome, and PSD fractions from PSD preps were consistent with the results seen from immunostaining brain sections.

DISCUSSION

Along with the increased anxiety and schizophrenic traits found in the Densin KO is a susceptibility to seizures. The Densin KO has paradoxical seizures in response to the GABA agonists Nembutal and isoflurane (Bruce Cohen, personal communication). These seizures rank as stage 6 in severity on a Racine scale. Such seizures in humans would be generalized meaning that they involve nearly all of the brain as opposed to partial seizures, which are more focused. The addition of the antiepileptic, phenytoin, to pentobarbital (in the form of Euthasol, 100 μg pentobarbital and 12.8 μg/g mouse weight), which stabilizes the inactive state of voltage gated sodium channels, seems to mitigate the duration and severity of the seizure; however, the seizures remain at stage 6. The Nembutal-induced seizures seem to be more penetrant in mice outcrossed to the C57 background 7 times. 3/3 of the 7^{th} outcrossed KO mice that were injected had stage 6 seizures whereas about half of the 2^{nd} outcross had stage 6 seizures. Barbiturates and benzodiazepines are also anxiolytics. Benzodiazepines can decrease anxiety by increasing the inhibitory effects that the lateral septum has on the amgydala (Yadin et al., 1993). The increased anxiety seen in the Densin KO mouse (Chapter 2) is interesting with this respect and may suggest that imbalance of excitation/inhibition in the Densin KO that underlies both seizure and anxiety.

No obvious seizure foci were determined after staining for the IEGs, Arc and c-fos, in brains that were perfused 30-45 minutes after injection of Nembutal. One explanation is that sampling at 30-45 minutes after seizure is not optimal timing for Arc or cfos protein to be produced at high enough levels to differentiate the WT from the

KO. Convulsants may vary in their time courses for IEG expression. We based our experiment on a previous study (Peng and Houser, 2005) where a dramatic increase in c-fos expression was seen 30 minutes after pilocarpine-induced seizures. However, some studies have allowed 4 hours for development of protein synthesis of IEGs after the seizure. The most salient explanation is that a deranged IEG response in the mutant (Chapter 3) may not allow us to efficiently identify the seizure foci by this method. This result should not be due to the anesthetic suppressing the expression of these genes. The anesthetics themselves have minimal affect on the expression of IEGs.

There are a number of explanations for the unexpected excitation induced in the Densin KO by Nembutal, the simplest being that the lack of Densin in both excitatory and inhibitory neurons disrupts the inhibitory-excitatory balance. Other explanations relate to situations where GABA activation is excitatory rather than inhibitory: 1) Under conditions where inhibitory tone is decreased, pentobarbital can act as a convulsant (Yee et al., 2003); 2) the membrane potential is altered; 3) interneuron numbers, inhibitory synapses or GABA abundance and distribution are altered to favor disinhibition of excitation or overexcitation of pyramidal neurons (Voss et al., 2008). Pentobarbital is prescribed as an antiepileptic drug, and is routinely used as an anesthetic with anxiolytic effectrs. It has, however, been shown to act as a proconvulsant in WT hippocampal slices under conditions that lower inhibitory tone. When exposed to high extracellular K+ concentrations, that increase burst probability, pentobarbital exacerbates spontaneous bursting (Yee et al., 2003). It decreases both the interval between bursts and the duration of the bursts themselves. When the burst

probability is low, pentobarbital acts as an anticonvulsant, increasing the interburst interval and decreasing the burst duration. This provides insight into circumstances where Nembutal can increase excitability in individuals with an already unsteady physiology primed for seizure (Yee et al., 2003).

Because a large change in the RNA transcript for the α2 GABA(A) receptor and other isoforms were detected by RNA seq (H. Beale, unpublished data) and alterations in GABA(A) receptors are often seen in disease states, the abundance of different GABA(A) receptors was measured in the homogenate and synaptosome fractions. The protein levels of GABA(A) receptors were however unaltered. As mentioned earlier, mutations in GABA(A) receptors are indicated in some genetic cases of epilepsy. Their levels are also sometimes altered in schizophrenia (reviewed in (Kellendonk et al., 2009). It would be worthwhile to examine the Densin KO brain for regional differences that are not apparent in total forebrain homogenates. One could probe for other GABA receptors as well. The β2 GABA(A) receptor, for example, is implicated in bipolar and schizophrenia (Chen et al., 2009).

We examined the abundance of other GABAergic markers to assess possible disturbances in inhibitory tone in the KO brain. There is converging evidence for a decrease of GAD67 and PV in schizophrenic individuals and in mice models (including mice with reduced levels of DISC1) (Shen et al., 2008; Lodge et al., 2009; Jones, 2010). To our surprise, GAD67, GAD65, and PV are increased in the Densin KO homogenate and synaptosome fractions. Increased ectopic GAD67 production has been seen in chronic epilepsy in granule cells (Schwarzer and Sperk, 1995; Sperk et al., 2009). It is thought to

be the neuron's attempt to counter excessive excitatory activity. Interestingly, antipsychotic dopaminergic agonists also cause increases in GAD-67 (Kalkman and Loetscher, 2003). The other GAD isoform, GAD65, which is found in the soma and GABAergic terminals, is also increased. GAD65 and 67 catalyze the rate-limiting step for GABA synthesis. It is ambiguous whether total GABA levels are altered or whether the increases in GAD65 and 67 correlate with an increase in inhibitory synaptic termini or numbers of inhibitory neurons. To this end, it would be useful to quantitate regional differences among inhibitory neurons and synapses by immunostaining of brain sections from WT and KO mice, which we are preparing to do in collaboration with Margarita Behrens (Salk Institute).

We have found that Densin is expressed in at least a particular subset of inhibitory interneurons. It would be informative to determine which subset by triple staining with GAD-67, Densin, and either PV, calbindin, or calretinin. These three Ca^{2+}-dependent proteins are markers for the three largest subsets of GABAergic neurons (Baimbridge et al., 1992). PV positive neurons are fast-spiking and are responsible for gamma oscillation that desynchronize neuronal networks (Lodge et al., 2009).

Inhibitory tone and seizure potential are affected by electrolyte balance that is also developmentally regulated. One way that Nembutal might have an excitatory action on neurons is if the cells in the Densin KO brain were not fully mature and had abnormal levels of cation-chloride transporters like, KCC2 and NKCC1 transporters, which can be detected by immunostaining in neuronal cultures or slices (see Chapter 4 Introduction). These channels are developmentally regulated and expression levels

facilitate the transition of GABA as an excitatory to inhibitory neurotransmitter due to differences in intracellular ion concentrations. However, KCC2 appears to be unchanged in forebrain homogenate and synaptosome from WT and KO animals (Fig. 4.3).

Imbalances in excitation that may enable the seizures we see may be related to dysfunctional BDNF signaling in the Densin KO (Chapter 2). A knockin mouse containing a mutation (CaRE3/CREm) in the CREB binding promoter region of BDNF display decreased gene expression of BDNF as expected (Hong et al., 2008). The mutant has about half the number of inhibitory synapses as the WT, without affecting the amount of excitatory synapses or number of PV and NPY positive inhibitory neurons. Unlike the Densin KO, however, levels of GAD67 (and the vesicular GABA transporter (vGAT)), markers of GABAergic neurons, are decreased in the mutant with the altered BDNF promoter (Hong et al., 2008).

Other considerations

The Nembutal-induced seizures in the WT suggest that the Densin KO brain has lower seizure threshold. It would be informative to assess seizure threshold by i.p. injection with the convulsant pentylenetetrazole (PTZ). PTZ is a GABA(A) receptor antagonist that prevents Cl^- influx through the receptor channel. In addition, drug treatments with slice electrophysiology may be a more controlled way to assess pathways that induce excitability. To investigate the balance of excitation and inhibition in the brain of the Densin KO, the spiking patterns in hippocampal slices could be studied before and after treatment with Nembutal. If spiking is more pronounced in the KO slices, subsequent experiments can be done using bicuculline (α GABA(A) receptor

anatagonist) or MK801 (an NMDA receptor antagonist), to dissect the involvement of different mechanisms of inhibition and excitation. Treating with a different GABA agonist like diazepam, that binds to the GABA(A) receptor, but does not completely overlap with the specificity of barbiturates may allow us to confirm GABA(A) receptor involvement, and to discriminate if selective GABA(A) subunits elicit this effect.

REFERENCES

Alger BE, Nicoll RA (1982) Pharmacological evidence for two kinds of GABA receptor on rat hippocampal pyramidal cells studied in vitro. J Physiol 328:125-141.

Apperson ML, Moon IS, Kennedy MB (1996) Characterization of densin-180, a new brain-specific synaptic protein of the O-sialoglycoprotein family. J Neurosci 16:6839-6852.

Bacci A, Huguenard JR, Prince DA (2005) Modulation of neocortical interneurons: extrinsic influences and exercises in self-control. Trends Neurosci 28:602-610.

Bacci A, Rudolph U, Huguenard JR, Prince DA (2003) Major differences in inhibitory synaptic transmission onto two neocortical interneuron subclasses. J Neurosci 23:9664-9674.

Baimbridge KG, Celio MR, Rogers JH (1992) Calcium-binding proteins in the nervous system. Trends Neurosci 15:303-308.

Ben-Ari Y (2002) Excitatory actions of gaba during development: the nature of the nurture. Nat Rev Neurosci 3:728-739.

Cascella NG, Schretlen DJ, Sawa A (2009) Schizophrenia and epilepsy: is there a shared susceptibility? Neurosci Res 63:227-235.

Charych EI, Liu F, Moss SJ, Brandon NJ (2009) GABA(A) receptors and their associated proteins: implications in the etiology and treatment of schizophrenia and related disorders. Neuropharmacology 57:481-495.

Chen J, Tsang SY, Zhao CY, Pun FW, Yu Z, Mei L, Lo WS, Fang S, Liu H, Stober G, Xue H (2009) GABRB2 in schizophrenia and bipolar disorder: disease association, gene expression and clinical correlations. Biochem Soc Trans 37:1415-1418.

Cohen I, Navarro V, Clemenceau S, Baulac M, Miles R (2002) On the origin of interictal activity in human temporal lobe epilepsy in vitro. Science 298:1418-1421.

Cole AJ, Abu-Shakra S, Saffen DW, Baraban JM, Worley PF (1990) Rapid rise in transcription factor mRNAs in rat brain after electroshock-induced seizures. J Neurochem 55:1920-1927.

Combi R, Redaelli S, Beghi M, Clerici M, Cornaggia CM, Dalpra L (2010) Clinical and genetic evaluation of a family showing both autism and epilepsy. Brain Res Bull 82:25-28.

DeLorey TM, Handforth A, Anagnostaras SG, Homanics GE, Minassian BA, Asatourian A, Fanselow MS, Delgado-Escueta A, Ellison GD, Olsen RW (1998) Mice lacking the beta3 subunit of the GABAA receptor have the epilepsy phenotype and many of the behavioral characteristics of Angelman syndrome. J Neurosci 18:8505-8514.

Fabene PF, Andrioli A, Priel MR, Cavalheiro EA, Bentivoglio M (2004) Fos induction and persistence, neurodegeneration, and interneuron activation in the hippocampus of epilepsy-resistant versus epilepsy-prone rats after pilocarpine-induced seizures. Hippocampus 14:895-907.

Fritschy JM (2008) Epilepsy, E/I Balance and GABA(A) Receptor Plasticity. Front Mol Neurosci 1:5.

Gulledge AT, Stuart GJ (2003) Excitatory actions of GABA in the cortex. Neuron 37:299-309.

Hagerman PJ, Stafstrom CE (2009) Origins of epilepsy in fragile x syndrome. Epilepsy Curr 9:108-112.

Harvey BD, Sloviter RS (2005) Hippocampal granule cell activity and c-Fos expression during spontaneous seizures in awake, chronically epileptic, pilocarpine-treated rats: implications for hippocampal epileptogenesis. J Comp Neurol 488:442-463.

Herrera DG, Robertson HA (1996) Activation of c-fos in the brain. Prog Neurobiol 50:83-107.

Hong EJ, McCord AE, Greenberg ME (2008) A biological function for the neuronal activity-dependent component of Bdnf transcription in the development of cortical inhibition. Neuron 60:610-624.

Hughes PE, Alexi T, Walton M, Williams CE, Dragunow M, Clark RG, Gluckman PD (1999) Activity and injury-dependent expression of inducible transcription factors, growth factors and apoptosis-related genes within the central nervous system. Prog Neurobiol 57:421-450.

Jones MW (2010) Errant ensembles: dysfunctional neuronal network dynamics in schizophrenia. Biochem Soc Trans 38:516-521.

Kahle KT, Staley KJ, Nahed BV, Gamba G, Hebert SC, Lifton RP, Mount DB (2008) Roles of the cation-chloride cotransporters in neurological disease. Nat Clin Pract Neurol 4:490-503.

Kalkman HO, Loetscher E (2003) GAD(67): the link between the GABA-deficit hypothesis and the dopaminergic- and glutamatergic theories of psychosis. J Neural Transm 110:803-812.

Kanner et al. (2008) Epilepsy-related depression. Supplement to neurology reviews.

Kellendonk C, Simpson EH, Kandel ER (2009) Modeling cognitive endophenotypes of schizophrenia in mice. Trends Neurosci 32:347-358.

Levisohn PM (2007) The autism-epilepsy connection. Epilepsia 48 Suppl 9:33-35.

Lodge DJ, Behrens MM, Grace AA (2009) A loss of parvalbumin-containing interneurons is associated with diminished oscillatory activity in an animal model of schizophrenia. J Neurosci 29:2344-2354.

Marty A, Llano I (2005) Excitatory effects of GABA in established brain networks. Trends Neurosci 28:284-289.
McNamara JO, Huang YZ, Leonard AS (2006) Molecular signaling mechanisms underlying epileptogenesis. Sci STKE 2006:re12.
Minkeviciene R, Rheims S, Dobszay MB, Zilberter M, Hartikainen J, Fulop L, Penke B, Zilberter Y, Harkany T, Pitkanen A, Tanila H (2009) Amyloid beta-induced neuronal hyperexcitability triggers progressive epilepsy. J Neurosci 29:3453-3462.
Morimoto K, Fahnestock M, Racine RJ (2004) Kindling and status epilepticus models of epilepsy: rewiring the brain. Prog Neurobiol 73:1-60.
Noebels JL (2003) The biology of epilepsy genes. Annu Rev Neurosci 26:599-625.
Peng Z, Houser CR (2005) Temporal patterns of fos expression in the dentate gyrus after spontaneous seizures in a mouse model of temporal lobe epilepsy. J Neurosci 25:7210-7220.
Qin P, Xu H, Laursen TM, Vestergaard M, Mortensen PB (2005) Risk for schizophrenia and schizophrenia-like psychosis among patients with epilepsy: population based cohort study. BMJ 331:23.
Racine RJ (1972) Modification of seizure activity by electrical stimulation. II. Motor seizure. Electroencephalogr Clin Neurophysiol 32:281-294.
Rakhade SN, Jensen FE (2009) Epileptogenesis in the immature brain: emerging mechanisms. Nat Rev Neurol 5:380-391.
Rubenstein JL, Merzenich MM (2003) Model of autism: increased ratio of excitation/inhibition in key neural systems. Genes Brain Behav 2:255-267.
Ruiz A, Campanac E, Scott RS, Rusakov DA, Kullmann DM (2010) Presynaptic GABA(A) receptors enhance transmission and LTP induction at hippocampal mossy fiber synapses. Nat Neurosci 13:431-438.
Santhakumar V, Soltesz I (2004) Plasticity of interneuronal species diversity and parameter variance in neurological diseases. Trends Neurosci 27:504-510.
Scharfman HE (2007) The neurobiology of epilepsy. Curr Neurol Neurosci Rep 7:348-354.
Schwarzer C, Sperk G (1995) Hippocampal granule cells express glutamic acid decarboxylase-67 after limbic seizures in the rat. Neuroscience 69:705-709.
Shen S, Lang B, Nakamoto C, Zhang F, Pu J, Kuan SL, Chatzi C, He S, Mackie I, Brandon NJ, Marquis KL, Day M, Hurko O, McCaig CD, Riedel G, St Clair D (2008) Schizophrenia-related neural and behavioral phenotypes in transgenic mice expressing truncated Disc1. J Neurosci 28:10893-10904.
Sieghart W, Sperk G (2002) Subunit composition, distribution and function of GABA(A) receptor subtypes. Curr Top Med Chem 2:795-816.
Sperk G, Drexel M, Pirker S (2009) Neuronal plasticity in animal models and the epileptic human hippocampus. Epilepsia 50 Suppl 12:29-31.
Stein V, Nicoll RA (2003) GABA generates excitement. Neuron 37:375-378.
Voss LJ, Sleigh JW, Barnard JP, Kirsch HE (2008) The howling cortex: seizures and general anesthetic drugs. Anesth Analg 107:1689-1703.
Yadin E, Thomas E, Grishkat HL, Strickland CE (1993) The role of the lateral septum in anxiolysis. Physiol Behav 53:1077-1083.

Yee AS, Longacher JM, Staley KJ (2003) Convulsant and anticonvulsant effects on spontaneous CA3 population bursts. J Neurophysiol 89:427-441.

Zai CC, Tiwari AK, King N, De Luca V, Mueller DJ, Shaikh S, Wong GW, Meltzer HY, Lieberman JA, Kennedy JL (2009) Association study of the gamma-aminobutyric acid type a receptor gamma2 subunit gene with schizophrenia. Schizophr Res 114:33-38.

Seconds after injection with Nembutal

WT ~84 secs **Densin KO**

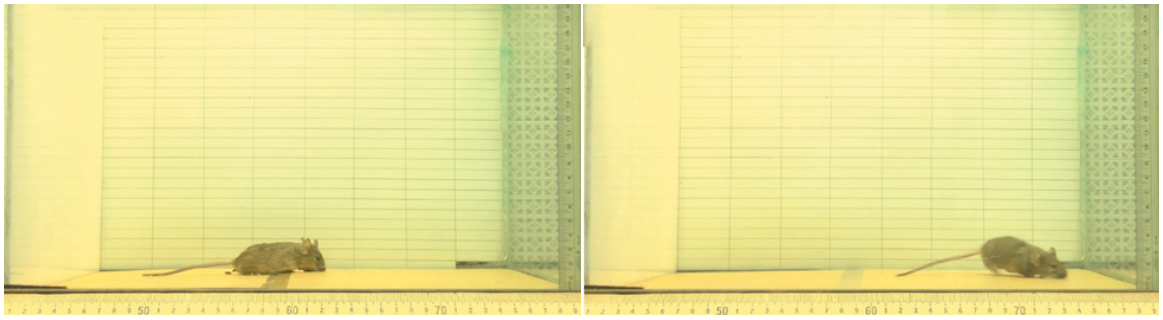

WT : Stage 0=Normal behavior and Stage 1=immobility

KO : Stage 2=Forelimb and tail extension giving appearance of rigid posture.

~93 secs

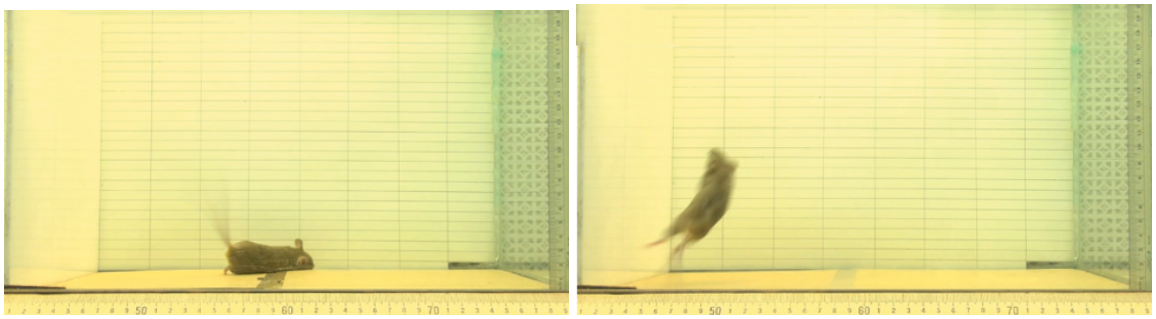

WT : Stage 2=Forelimb and tail extension giving appearance of rigid posture.

KO : Stage 6=Severe tonic clonic seizure

~94 secs

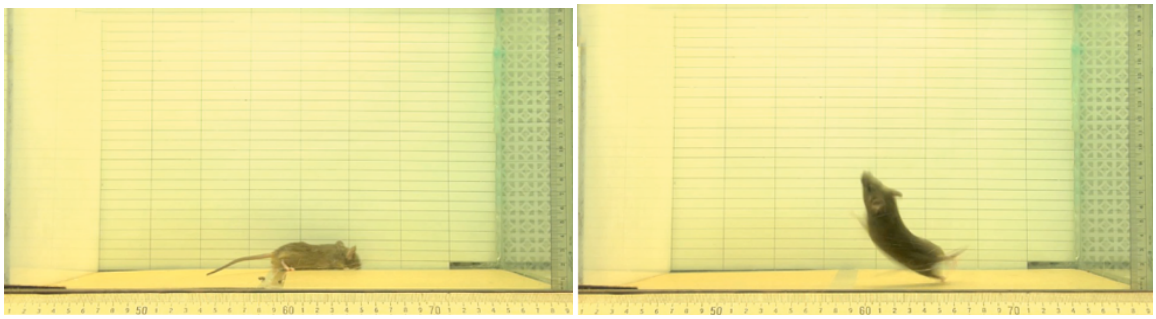

WT : Stage 2=Forelimb and tail extension giving appearance of rigid posture.

KO : Stage 6=Severe tonic clonic seizure

Figure 4.1. Nembutal induces tonic clonic seizures in the Densin knockout but not wildtype. Representative picture time course of different stages of seizures experienced in KO after injection of intraperitoneal injection of Nembutal. Staging according to the following modification of the Racine (Racine, 1972) scheme: Stage 0-Normal behavior, Stage 1-Immobility, Stage 2-Forelimb and tail extension giving appearance of rigid posture, Stage 3-Automatisms: repetitive scratching, circling, or head bobbing, Stage 4-Forelimb clonus and rearing and falling, Stage 5-Repeated forelimb clonus and rearing and falling, Stage 6-Severe tonic clonic seizures, Stage 7-death.

Seconds after injection with Nembutal

WT ~95 secs **Densin KO**

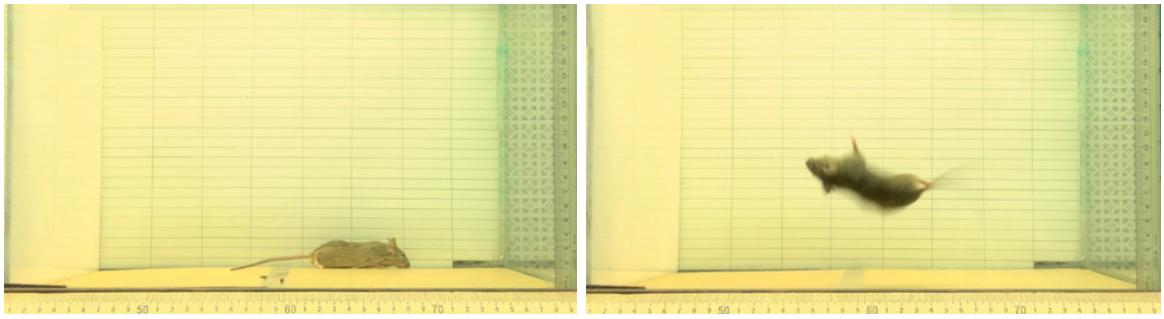

WT : Stage 2=Forelimb and tail extension giving appearance of rigid posture.

KO : Stage 6=Severe tonic clonic seizure

~100 secs

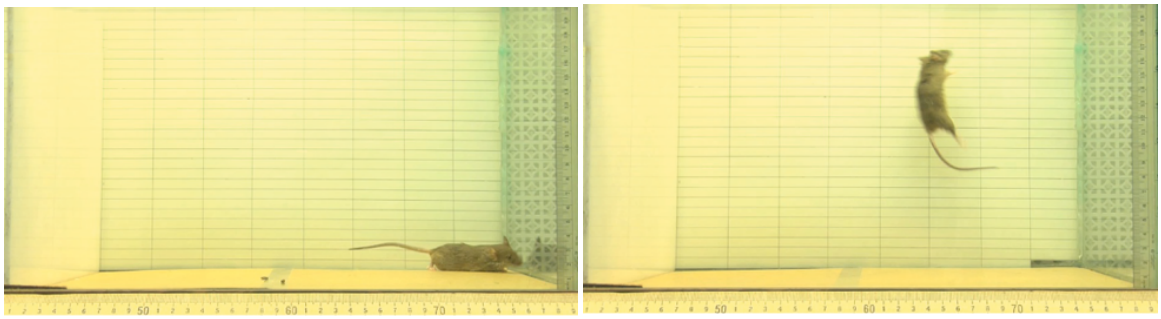

WT : Stage 2=Forelimb and tail extension giving appearance of rigid posture.

KO : Stage 6=Severe tonic clonic seizure

~101 secs

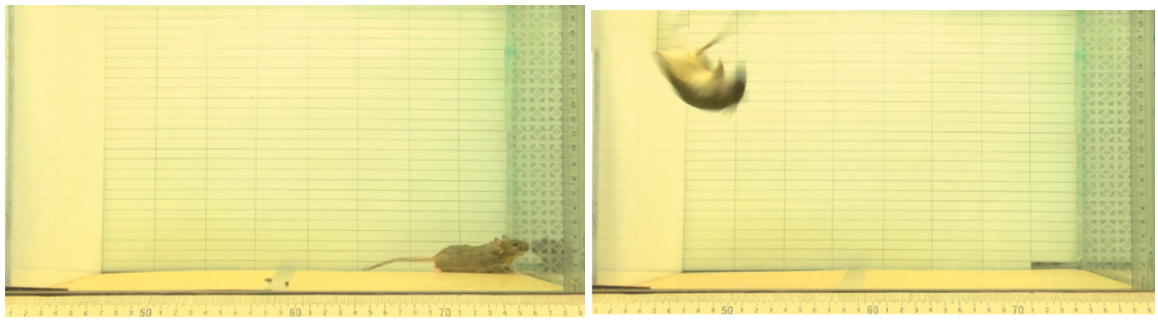

WT : Stage 0=Normal behavior

KO : Stage 6=Severe tonic clonic seizure

Figure 4.1. Nembutal induces tonic clonic seizures in the Densin knockout but not wildtype. (cont'd)

Seconds after injection with Nembutal

WT ~103 secs **Densin KO**

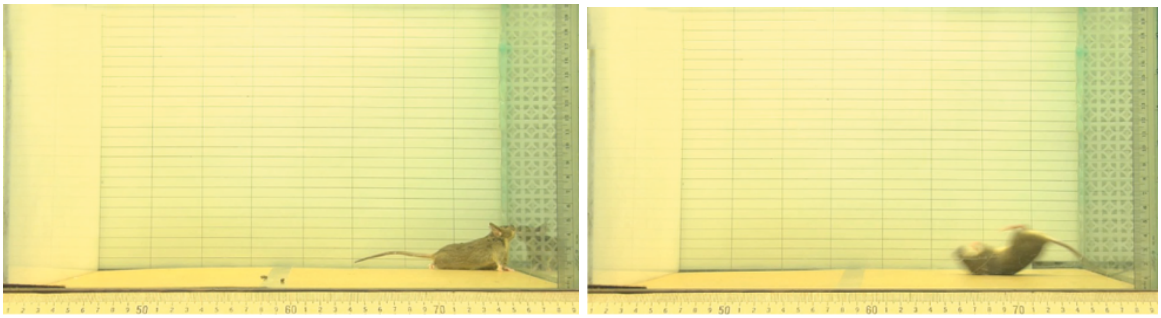

WT : Stage 0=Normal behavior

KO : Stage 6=Severe tonic clonic seizure

~105 secs

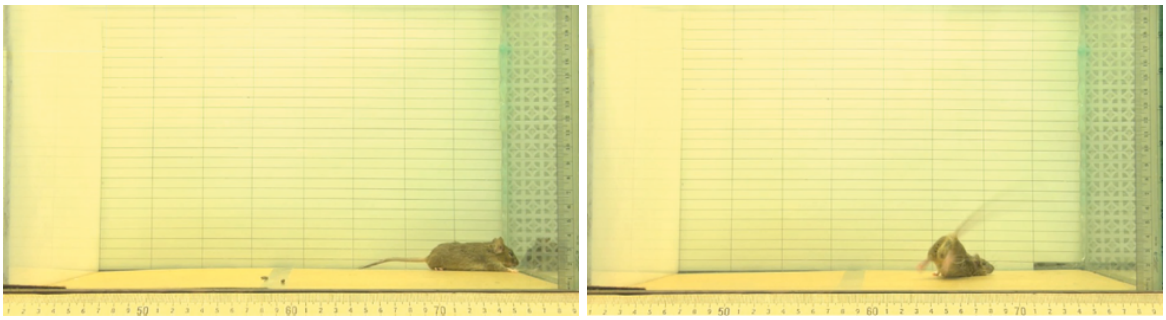

WT : Stage 0=Normal and Stage 1=Immobility

KO : Stage 2=Forelimb and tail extension giving appearance of rigid posture

~128 secs

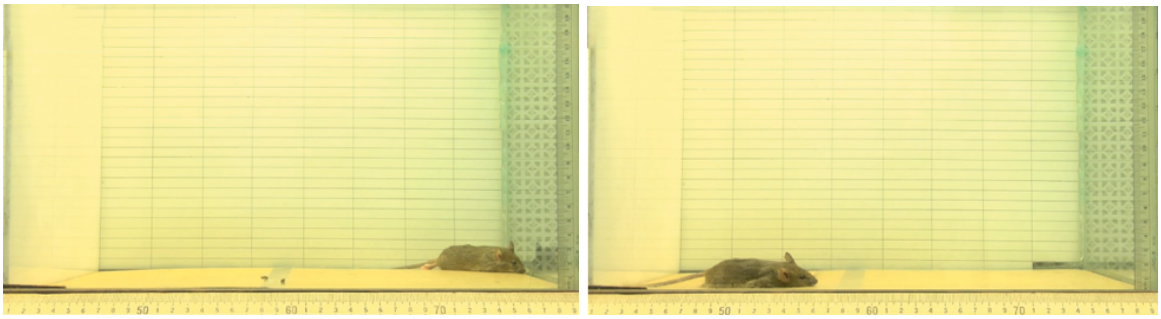

WT : Stage 0=Normal and Stage 1=Immobility

KO : Stage 0=Normal and Stage 1=Immobility

Figure 4.1. Nembutal induces tonic clonic seizures in the Densin knockout but not wildtype. (cont'd)

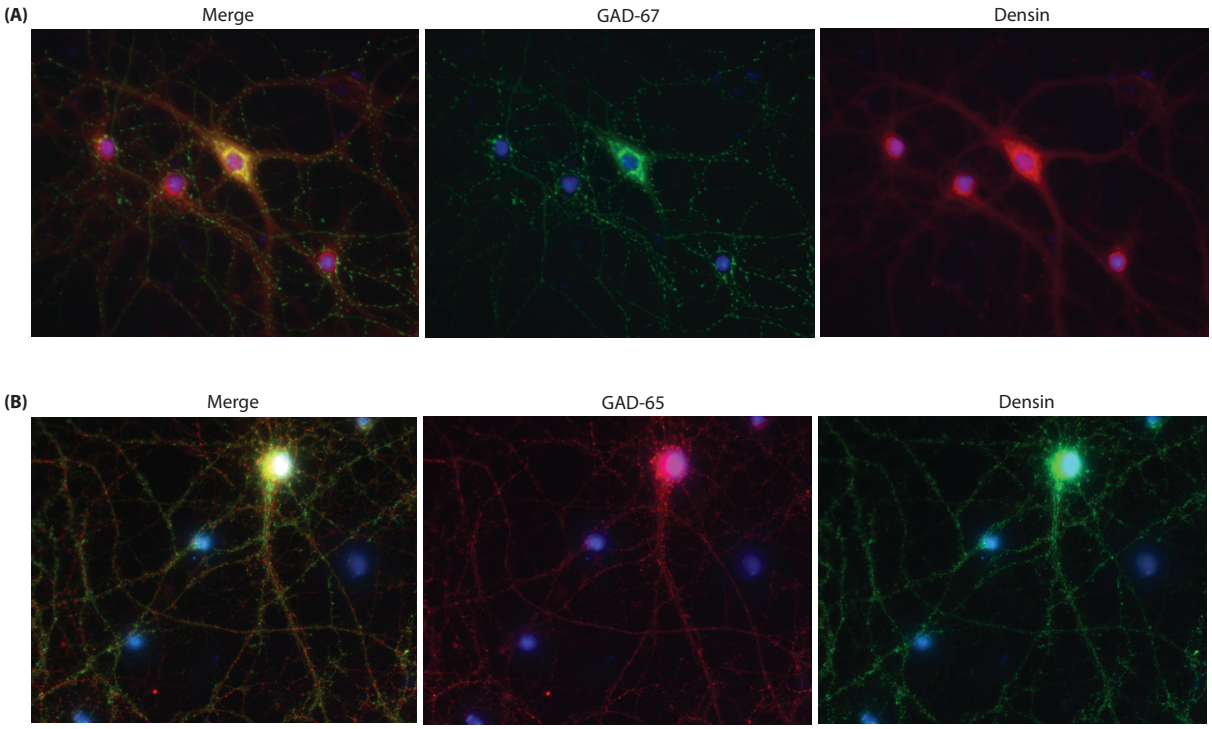

Figure 4.2. Densin is expressed in a subset of inhibitory neurons. Densin staining colocalizes with that for (A) GAD67 and (B) GAD65 in18 DIC primary hippocampal cultures. GAD67 and GAD65 are decarboxylases involved in synthesis of GABA and are found in inhibitory neurons. (A) Representative images costained for Densin (red) and GAD67 (green) (B) Representative images costained for Densin (green) and GAD65 (red). Cell bodies are indicated by nuclear staining with Dap1 (blue). GAD67 is typically found most intensely in the soma while GAD65 staining is seen in both the soma and inhibitory synaptic termini.

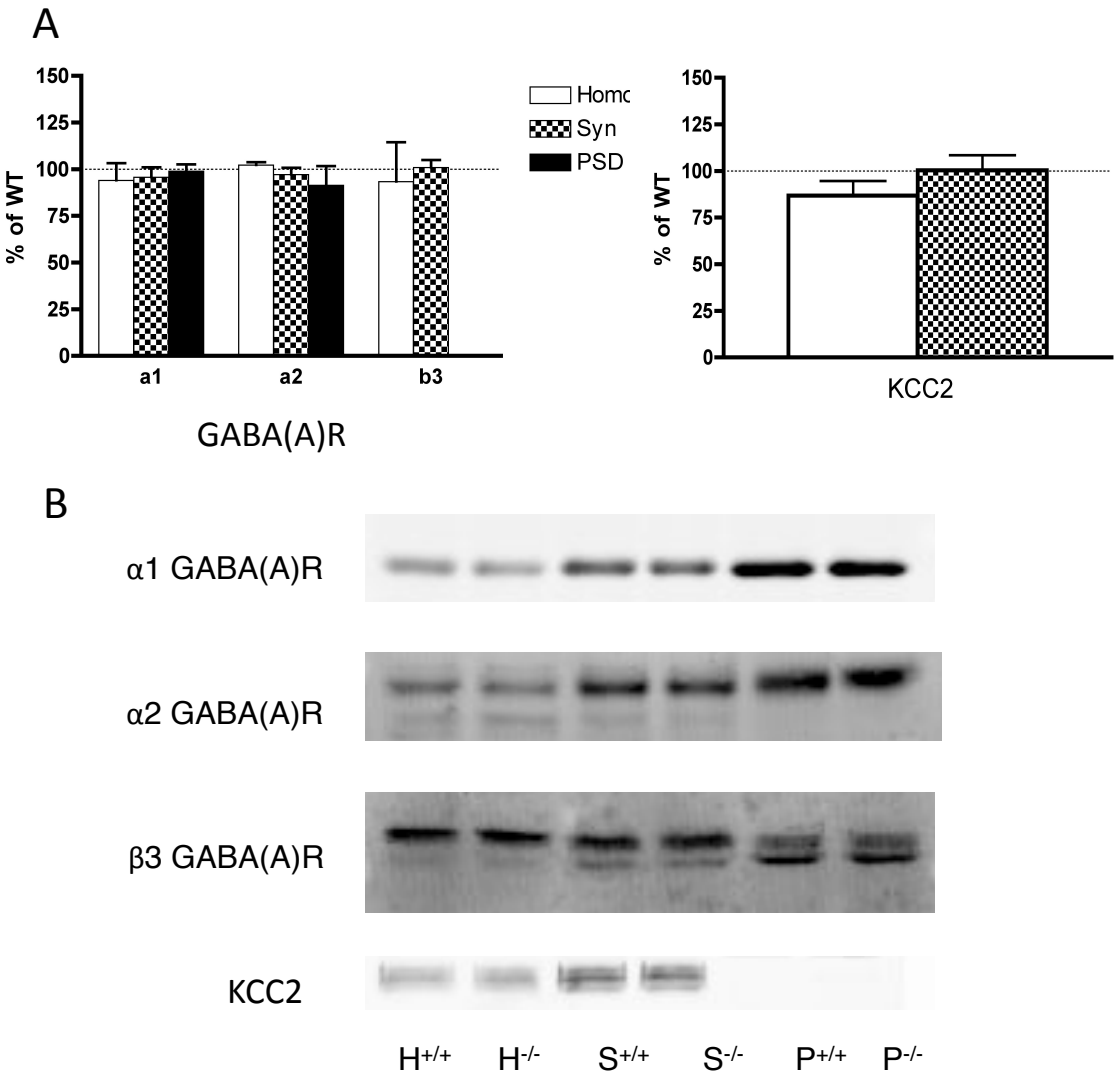

Figure 4.3. a1, a2, and b3 GABA(A) receptors and KCC2 levels are unchanged in the the homogenate, synaptosome, and PSD fractions of the Densin KO relative to the WT. (A) Quantitation of abundance of KO protein levels relative to WT (100%) based on the intensities of bands in immunoblots from gels loaded with equal amounts of protein of homogenate, synaptosome and PSD fractions. (B) Representative immunoblots are shown for a1, a2, and b3 GABA receptor, and KCC2 for homogenate (H) synaptosome (S) and PSD (P) fractions from WT (+/+) and KO (-/-) samples. Statistical significance was assessed by one-sample t-tests with a theoretical mean of 100 (n=3-4 PSD fractions each prepared from 7 or 8 age and sex-matched mice of each genotype). Error bars represent SEM.

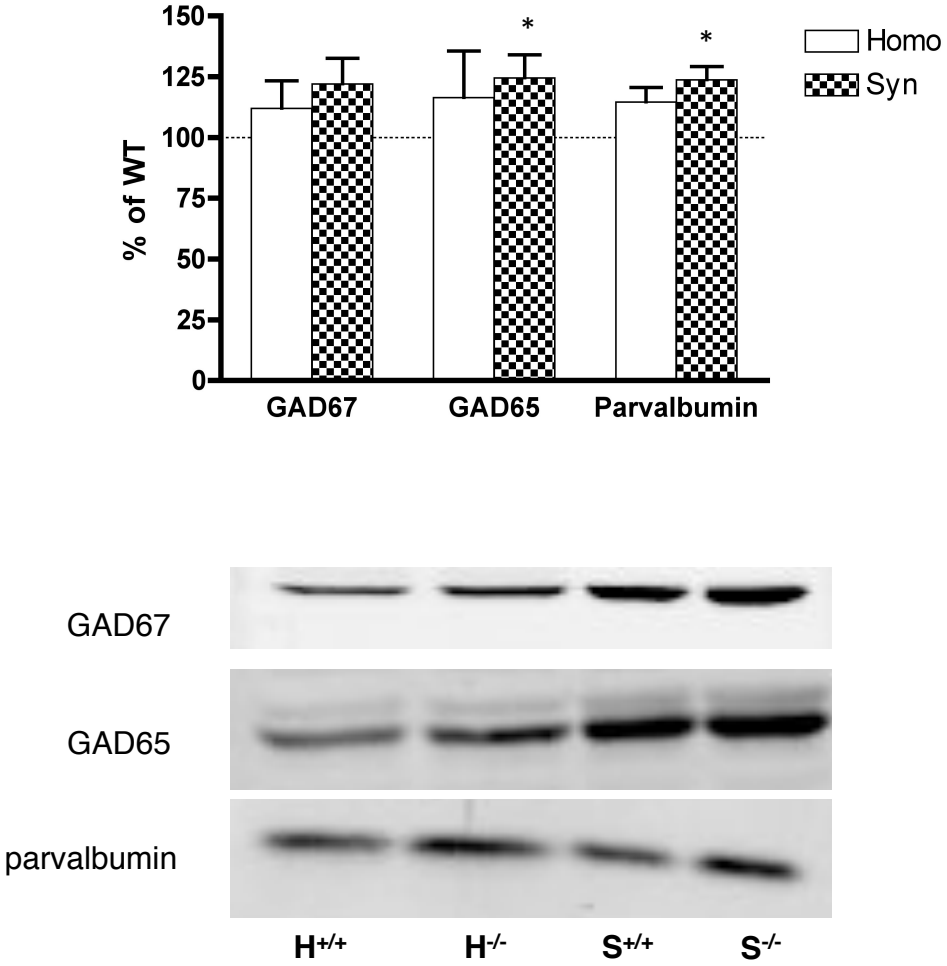

Figure 4.4. Loss of Densin results in increased GAD65, and parvalbumin protein levels in the synaptosomal fraction. Quantitation of abundance of KO protein levels relative to WT (100%) based on the intensities of bands in immunoblots from gels loaded with equal amounts of protein of homogenate and synaptosome fractions. Representative immunoblots are shown for GAD67, GAD65, and parvalbumin for homogenate (H) and synaptosome (S) fractions from WT (+/+) and KO (-/-) samples. Statistical significance was assessed by one-sample t-tests with a theoretical mean of 100 (*$p < 0.05$; n=3-4 PSD fractions each prepared from 7 or 8 age and sex-matched mice of each genotype). Error bars represent SEM.

Chapter 5
Regulation of NMDA Signaling through CaMKII and RasGRF1 by Protein-Protein Interactions and CaMKII Phosphorylation

Transmission of information underlying learning, memory, behavior, and neuronal survival relies on the response of dynamic multiprotein complexes in the postsynaptic membrane to presynaptic release of neurotransmitters. Calcium influx through NMDA receptors and the subsequent activation of Ca^{2+} sensors such as CaMKII and RasGRF1 in the PSD are critical steps in transducing membrane activity to different signaling cascades that control a broad range of cellular processes. This study investigates the interactions of CaMKII and RasGRF1 with the NMDA receptor to understand how complexes assemble under defined conditions that create specificity and avoid inappropriate cross-talk. We find that RasGRF1, CaMKII, and the NMDA receptor can be coimmunoprecipitated from brain homogenate as a complex. In HEK overexpressing functional NMDA receptors and CaMKII, the presence of RasGRF1 enhances CaMKII association with NR2B and NR1 subunits of the NMDA receptor. CaMKII phosphorylation of RasGRF1 may regulate signaling from this complex. CaMKII phosphorylates RasGRF1 at 3 preferred sites with a catalytic efficiency that is comparable to other known peptide substrates. Using LC/MS/MS, we identified Ser485, Ser745, and Ser916 were identified as CaMKII phosphorylation sites on RasGRF1. Phosphorylation of RasGRF1 by CaMKII, however, does not seem to affect the activation of Ras or Rac by RasGRF1. These results will aid our understanding of how changes in the composition of protein networks in the PSD and in signaling pathways can enhance or suppress future communication between neurons.

INTRODUCTION

One of the major signaling complexes in the PSD is anchored around the intracellular tails of the excitatory NMDA receptor which, in the hippocampus and cortex, comprises the NR1, NR2A, and NR2B subunits (Fig. 5.1). Upon stimulation of the NMDA receptor, Ca^{2+} influx activates proteins such as RasGRF1 and CaMKII that compete for the available Ca^{2+} bound to calmodulin. Instrumental in localizing CaMKII and RasGRF1 to elevated Ca^{2+} concentrations and NMDA linked signaling is the ability of both enzymes to bind NR2B directly. Disrupting the binding of these enzymes to the receptor tail has its consequences on signal transduction and synaptic plasticity

RasGRF1 is a guanine exchange factor (GEF), whose function is to promote the dissociation of GDP and allow GTP to bind, thereby activating GTPases such as Ras and Rac. In mouse models, this activity is thought to facilitate learning, memory and neuronal survival (1-3). Disruption of RasGRF1 binding to the membrane proximal region of NR2B with interfering peptides reduces ERK activation by 60-70% (4). Disruption of CaMKII-NR2B interactions with an inducible interfering peptide decreases phosphorylation of AMPA GluR1 and results in mice with hippocampal dependent learning defects (5). Overexpression of R1300Q/S1303D NR2B, which abolishes binding to CaMKII, prevents induction of long term potentiation (LTP) (6).

The binding regions of RasGRF1 and CaMKII partially overlap on the NR2B tail, but it is not known whether association of the two enzymes with the NMDA receptor is mutually exclusive. RasGRF1's binding site on the membrane proximal portion of NR2B

(aa886-1310) overlaps with at least one of the two known binding sites on CaMKII for NR2B (4). The site has not been minimized further. The region that binds NR2B on RasGRF1 has been delineated to residues 714-913, a 'neuronal domain' that comprises part of the N-RasGEF domain, and is not present in non-neuronal forms of RasGRF1 (4). CaMKII binds to the NR2 cytosolic tails, primarily through the kinase's catalytic domain to membrane proximal residues 839-1120 (7-9) and a C-terminal site minimized to aa1290-1309 (7,10,11). Clarification of whether CaMKII and RasGRF1 compete for binding should provide insight into how interactions with NR2B may modulate RasGRF1 and CaMKII transduced signals and the pathways they activate

As an upstream node from which a multitude of signaling pathways branch, various mechanisms of regulating RasGRF1 exist, such as the protein protein interactions described above, and post translational modifications. In terms of phosphorylation, RasGRF1 activity is already known to be modulated by PKA (12-14), Src (15), and Cdk5 (16). Sturani et al. (1997) observed that RasGRF1 could also be phosphorylated by CaMKII but the stoichiometry of phosphate incorporation into RasGRF1 by CaMKII was low 0.01-0.02 in contrast to the current report (12,17).

In this study, we test whether the presence of RasGRF1 interferes with CaMKII association with NR2B, exploring what complexes might be possible. The phosphorylation of RasGRF1 by CaMKII is also characterized biochemically *in vitro.* Its physiological relevance can be assessed in dissociated neuronal cultures by stimulating with bicuculline/glycine. Increased phosphorylation at Ser916 is observed with bicuculline/glycine enhancement of synaptic transmission and is attenuated by

incubating with a CaMKII inhibitor. The importance of this posttranslational modification on RasGRF1 activity towards Ras and Rac is also probed.

METHODS

Immunoprecipitation from mouse brain membrane fraction. Forebrain from adult male mice were homogenized with 12 up and down strokes at 900 rpm. The homogenate was cleared of membrane and nuclear fraction by centrifuging at 1000 xg, 10 min. The supernatant was centrifuged at 100k xg, 1 hour and the pellet was solubilized in 1% deoxycholate. The solubilized fraction was then diluted to: 50mM Tris pH 7.4, 0.15M NaCl, 1% Triton X-100, 1X Roche protease inhibitor tablet, 0.1 % SDS or 0.2% DOC and 0.540 mg was incubated with RasGRF1 antibodies (C term sc-224 or N term #3322, Cell signaling) or RbIgG isotype (Upstate) control precoupled to Protein G-magnetic dynabeads (Invitrogen/Gibco). The IPs were washed 4x with 50mM Tris pH 7.4, 0.15M NaCl, 0.1% Triton X-100 before eluting with 1X SDS loading dye. Samples were run on SDS page and a western blot performed, probing with the following antibodies: MsGluR2 Ab 1:1000 (Chemicon), RbRasGRF1 sc-863 or sc-224 1:1000 (Santa Cruz Biotechnology), RbNR2B (1:2500 Xandria), MsCaMKII (1:2000 6G9-ABR), MsPSD95 (1:2000, 7E3 ABR), Rb SynGAP (1:1000, PA1-046 ABR).

Stoichiometry and rate of phosphate incorporation by CaMKII onto RasGRF1. Recombinant Strep-RasGRF1 purified from HEK293 cells was phosphorylated by purified rat forebrain CaMKII in 50mM Tris pH 7.2, 5 mM DTT, 0.9 mg/mL BSA, 1 mM $CaCl_2$/2-4

µM CaM or 0.5 mM EGTA, 50-100 nM RasGRF1, 10-400 nM CaMKII, 100 µM ATP, 4 µCi ^{32}γP-ATP (4500 Ci/mmol MP Biomedicals), 10 mM $MgCl_2$ for 0.5-10' at 30˚C. Reactions were stopped by adding 3X SDS loading dye to 1X and heating 2.5 min at 95°C. The mixtures were separated by SDS PAGE and the band corresponding to full length RasGRF1, along with ATP standards spotted onto filter paper, exposed to a phosphorescence plate which was imaged using a Storm phosphoimager. Intensity of radioactive bands were quantified with the IQuant software. k_{cat}/K_M was determined by an approximation of the Michaelis Menten equation at low substrate concentrations.

Fluorescent activity assay-GST. Ras was preloaded with mant-dGDP (Jena Bioscience), and the decrease in fluorescence, upon release of the GDP analog, was followed at 430nm after excitation at 370nm using the Tecan Safire II plate reader and fit to a single exponential equation using Prism. Reactions were initiated with either GTP or RasGRF1. GST Rac was purified according to Karnoub et al., 2001 and Kiyono et al, 1999 (18,19). The GST-Rac1-pGEX2T plasmid (originally from Gary Bokoch's lab) was obtained from Addgene.com (plasmid 12977).

Purification of RasGRF1 and CaMKII. Rat forebrain CaMKII was purified as described in Miller, SG and Kennedy MB (1985). RasGRF1 was purified from HEK293F or 6E cells fused to an N-terminal flag or strep tag. RasGRF1 DNA (19 µg/30 mL cell culture) in pcDNA3.1 was transfected using PEI reagent into HEK293F or 6E cells and grown for 24 hours in suspension (Caltech Protein Expression Center). Cells were harvested and

frozen in liquid nitrogen and stored at -80˚C if not used immediately. Cell pellets from 1L of culture were resuspendend in 25mL 50 mM Tris pH 7.4, 150 mM NaCl, 0.1% Triton X-100, 1 ug/mL pepstatin, 1mM PMSF, and other protease inhibitors (Roche protease inhibitor tablet). After sonication (30% amplitude, Branson sonicator), the lysate was spun down at 100kxg for 1 hour. The supernatant was incubated with Flag-resin (Sigma), mixing end over end at 4˚C for 1.5 hours. The protein-resin slurry was poured onto a column and washed with 50 mM Tris pH 7,4, 0.3 M NaCl, 0.1% Triton X-100, protease inhibitors. Flag-RasGRF1 was eluted with 2 mL pH 3.5 glycine directly into a tube with 0.25 mL 1 M Tris pH 7.4 to bring the pH back up as expeditiously as possible. The eluate was exchanged into 50 mM Tris pH 7.4, 150 mM NaCl, 2 mM DTT, 10% glycerol with PD10 columns (GE Health Sciences) and concentrated using Amicon spin concentrators (Millipore). The concentrated protein was aliquoted and flash frozen in liquid nitrogen and stored at -80˚C. RasGRF1 activity was determined by a fluorescent nucleotide exchange assay with GST-H-Ras or GST-Rac1 prebound to mant-dGDP (Jena Bioscience).

Pulldown with purified protein. Purified Strep tagged RasGRF1 was immobilized on streptactin resin (IBA) and incubated with purified CaMKII from rat forebrain. The pulldown was washed with 50mM Tris pH 7.5, 0.15M NaCl, 0.1% Triton X-100 before SDS loading dye was added. Samples were run on a SDS acrylamide gel and a Western blot was performed probing with antibodies specific for RasGRF1 (sc-863) and CaMKII (6G9-ABR).

Phosphorylation of RasGRF1 at Ser916*.* Recombinant Strep-RasGRF1 purified from HEK293 cells was phosphorylated by purified rat forebrain CaMKII. Reaction conditions consisted of: 50 mM Tris pH 7.2, 10 mM $MgCl_2$, 5 mM DTT, 0.9 mg/mL BSA, 1 mM $CaCl_2$/2 µM CaM or 0.5 mM EGTA, +/-180 nM CaMKII, +/- 180 nM Strep-RasGRF1, 100 µM ATP 4' at 30˚C. ½ (15uL) of the phosphorylation reaction was run on SDS-PAGE and a western blot was done with Rb PhosphoRasGRF1 (Ser916) Antibody (#3321 Cell Signaling Technology).

Phosphopeptide mapping by tandem LC/MS/MS. Liquid chromatography-tandem mass spectrometry (LC/MS/MS) was conducted by the Protein and Peptide Microanalytical Laboratory at Caltech. 360 nM purified Strep-RasGRF1 was phosphorylated by 360 nM rat forebrain CaMKII in the presence of 50 mM Tris pH 7.2, 10 mM $MgCl_2$, 0.9 mg/ml BSA, 100 µM ATP, 1 mM Ca^{2+}, 2 µM calmodulin, for 10 minutes at 30°C. Phosphorylated protein was separated by SDS-PAGE, Coomassie stained, and the ~140 kDa RasGRF1 band (~10.8 pmol) was excised for in-gel tryptic digestion. Phospho-peptides in the digests were identified using nanoflow capillary high performance liquid chromatography (C18 column) coupled with triple quadrupole/electrospray tandem mass spectrometry (API 365, Perkin Elmer/Sciex). The MS/MS spectra were then sent to the search engine, Mascot (Matrix Science), to identify phospho-peptides from primary sequence databases with variable modification of phosphorylation on serine, and threonine. Results show observed and theoretical

mass of peptides, and their sequence. Targeted MS/MS was done, using a list of potential CaMKII phosphorylation sites on RasGRF1 based on the consensus sequence of Arg-X-X-Ser/Thr. In this way, phosphopeptides that are weaker and may not reach the threshold cutoff would still be retained for MS/MS analysis because they are likely candidates based on sequence.

Cell culture experiments using HEK293 cells. Different combinations of NR1 (pRK7), wt or R1300Q/S1303D NR2B (pCDNA3.1+), CaMKII (in pCDNA3.1+), and RasGRF1 (pCDNA3.1+-gift from R. Zippel) were expressed in HEK293H cells using the transfection reagent, Fugene 6 (Roche). R1300Q/S1303D NR2B abolishes the binding of CaMKII to NR2B (Strack et al. 2000, Barria and Malinow, 2005). Cells were washed once in PBS and scraped off petri dishes in 50mM Tris pH 7.4, 0.15 M NaCl, 0.1% Triton X-100, 1 µg/mL pepstatin, 1mM PMSF, complete protease inhibitors (Roche), 1 mM $CaCl_2$/4.5 µM CaM. The lysate was centrifuged for 15 min. at 16k xg. The supernatant was incubated with anti-CaMKII Ab (6G9-ABR) precoupled to anti-MsIgG dynabeads (Invitrogen-Gibco) end over end for 3 hours at 4ºC and then washed 4x with 0.5 mL 50 mM Tris pH 7.4, 0.15 M NaCl, 0.1 % Triton X-100, mM 1 mM $CaCl_2$/4.5 µM CaM. Mouse IgG1 (eBioscience) was used as an isotype control.

NMDA stimulation of rat hippocampal slices. Preparation of Sprague Dawley rat hippocampal slices were done according to Kindler and Kennedy (1996) (20). 500 µm slices were soaked in Ringer solution in the presence or absence of 25 µM NMDA and 5

µM okadaic acid (Calbiochem) +/- KN93 (Calbiochem). 5-6 slices were combined from each condition and homogenized (with 12 up and down strokes) in ~50 µL/slice of homogenization buffer in the presence of phosphatase inhibitors: 50 mM Tris pH 7.4, 0.15 M NaCl, 2 mM EDTA, 1% Triton X-100, 0.25% Na deoxycholate, 0.1% SDS, 1mM PMSF, Roche complete inhibitor tablet, 40 mM beta-glycerophosphate, 50 mM NaF. Homogenates were spun at 350 x g for 5 min. Protein concentration was determined by BCA assay (Pierce) and the equal amounts of protein from the homogenate were loaded onto a SDS acrylamide gel. A Western blot was done probing for phosphoSer916 (Cell signaling antibody #3321), total RasGRF1 (sc-863), CaMKII (6G9-ABR), and phosphoT286 CaMKII (22BI).

RESULTS

Immunoprecipitation of RasGRF1, CaMKII, and NR2B from brain homogenate. To see if RasGRF1 exists as a native complex with CaMKII and NR2B from brain homogenate, immunoprecipitations were done with an antibody specific for CaMKII from solubilized mouse forebrain membrane fraction. CaMKII and NR2B were both found in a RasGRF1 containing complex in the brain (Fig. 5.2). Also found in this complex were PSD-95 and SynGAP. No GluR2 was detected in the IP according to the Western blot, which served as a negative control to ensure the entire PSD was not being pulled down (21). To see what interactions were possible pairwise, immunoprecipitations were done from HEK cell lysate cotransfected with RasGRF1 and CaMKII together or alone. RasGRF1 and CaMKII appear to associate in coimmunoprecipitations from HEK cells even in the

absence of NR2B; however, RasGRF1 and CaMKII do not interact with strong affinity in pulldowns with purified protein (Fig. 5.2).

RasGRF1 enhances the association of CaMKII with NR2B in HEK293 cells. To study the effect of RasGRF1 on the NR2B-CaMKII association, immunoprecipitations (using a CaMKII specific antibody) were done from HEK cells transfected with CaMKII, NR2B in the presence and absence of RasGRF1. Signifcantly ($p<0.5$), 5 (SEM=1.6) fold more NR2B and 12.5 (SEM=5.1) fold more NR1 were detected in the immunoprecipitate with CaMKII in the presence versus the absence of RasGRF1 (Fig. 5.3).

To see if the enhancement of CaMKII association with NR2B by RasGRF1 is specific, we repeated the same experiment above but in the presence of the R1300Q/S1303D NR2B mutant, which abolishes binding of CaMKII to the NR2B tail. As expected, less R1300Q/S1303D NR2B was found in the IP with CaMKII than with wtNR2B. As with wt NR2B, more association of R1300Q/S1303D NR2B was seen with CaMKII in the presence of RasGRF1 (~2 fold enhancement, n=4); however RasGRF1 does not rescue R1300Q/S1303D NR2B-CaMKII association to that of wt levels. This suggests that this C term binding site for CaMKII on NR2B is partially responsible but not exclusively for CaMKII-RasGRF1-NR2B complex formation. However, it remains open as to whether RasGRF1 is able to increase CaMKII-NR2B association as part of a ternary complex or one that includes a protein mediator from HEK cells that can bind both CaMKII and RasGRF1 and thus facilitate the enhancement.

RasGRF1 is phosphorylated by CaMKII. ~3 mols phosphate were incorporated per mol of RasGRF1 after incubating purified RasGRF1 with CaMKII (in a 1:1 molar ratio) in the

presence of γ^{32}P-ATP and Ca^{2+}/CaM (Fig. 5.4). Increasing the ratio of CaMKII to RasGRF1 in the reaction increases the stoichiometry which plateaus at ~5-6. The stoichiometry obtained with lower CaMKII:RasGRF1 in the reaction may reflect preferred sites. The efficiency of CaMKII phosphorylation (k_{cat}/K_M = 6.6 x 10^5 M^{-1} s^{-1} Fig. 3B) of full length purified RasGRF1 is on the same order of magnitude as that for other known CaMKII peptide substrates. k_{cat}/K_M is fold lower than that for a 17 amino acid NR2B peptide (18 x 10^5 M^{-1} s^{-1}), and fold higher than that for syntide (1.2 x 10^5 M^{-1} s^{-1}), according to values by Praseeda et al., 2004 (22).

To determine the CaMKII phosphorylation sites on RasGRF1, purified RasGRF1 was phosphorylated by purified CaMKII *in vitro* and subjected to LC/MS/MS analysis. Ser 485, Ser 745, and Ser 916 were identified as phosphopeptides by targeted LC/MS/MS out of 20 possible sites based on the CaMKII phosphorylation consensus sequence of Arg-X-X-Ser/Thr (Table 5.1 and Figure 5.5). These putative sites are followed by a leucine, consistent with the observation that the Ser/Thr phosphorylated by CaMKII is often followed by a hydrophobic amino acid. Ca^{2+}/CaM dependent phosphorylation of RasGRF1 by CaMKII at Ser916 is also detected by a phosphoSer916 specific antibody (Fig. 4) on Western Blot, confirming this particular site.

Effect of CaMKII phosphorylation on RasGEF and RacGEF activity. To ascertain the effect of phosphorylation of RasGRF1 by CaMKII, we phosphorylated purified RasGRF1with CaMKII in vitro and then subjected the phosphorylated protein or nonphosphorylated control to a nucleotide exchange reaction with purified H-Ras or

Rac1. Phosphorylation of RasGRF1 by CaMKII does not appear to affect dissociation of GDP from Ras or Rac. There was little difference in rate of release of the fluorescent mant-dGDP that was precoupled to Ras or Rac in our activity assays. To ensure that phosphorylation was well controlled for, a western blot was done on the reaction mixtures after the nucleotide exchange reaction and probed for phosphorylation of Ser916.

Stimulation of hippocampal rat slices with NMDA in the presence of okadaic acid. To test whether CaMKII phosphorylation of RasGRF1 is coupled to NMDA stimulation, hippocampal slices from mature rat were treated with NMDA in the presence of okadaic acid and KN93 (a cell permeable CaMKII inhibitor). Okadaic acid is an inhibitor of protein serine/threonine phosphatase 1, 2A, and 2B and is known to accentuate CaMKII autophosphorylation (20). RasGRF1 is postulated to have a role in synaptic plasticity in mature mice. Its expression is developmentally regulated in the brain with highest levels in adult animals (day~20) which are only faintly detected by Western Blot prenatally (23). Stimulation with NMDA leads to Ser916 phosphorylation on RasGRF1 that is blocked by CaMKII inhibitors or is decreased in CaMKII knockdown. A band of higher molecular weight, corresponding to a phosphorylated version of RasGRF1 was clearly detected in slices treated with okadaic acid by an antibody recognizing total RasGRF1.

There was also an increase in Ser916 phosphorylation observed in the presence of okadaic acid indicating phosphorylation of GRF1, including that at Ser916, is regulated by PP1, 2A, and or 2B.

DISCUSSION

As shown by the IP results from solubilized brain membrane fraction, CaMKII and RasGRF1 can form a complex with NR2B in the brain. When bound to the NMDA receptor, CaMKII and RasGRF1 are situated at elevated local Ca^{2+} concentrations, facilitating their activation. A predisposition to certain complexes that cluster around the NMDA tails has repercussions on enzymatic activity and signaling. NR2B is already known to be a scaffold, modulator, and substrate of CaMKII. Increased duration of NMDA stimulation leads to more persistent binding of CaMKII to the NR2B tail (7,24). NR2B binding to CaMKII increases its affinity for CaM and suppresses the inhibitory autophosphorylation of CaMKII at T305/6. NR2B also permits kinase activity even after CaM has dissociated from the complex, possibly a contributing mechanism for molecular memory (7). In this study, the presence of RasGRF1 seems to enhance the binding of NR2B to CaMKII when the three are cotransfected together into HEK293 cells. It remains to be investigated whether RasGRF1 enriches CaMKII activity in the synapse by increasing the kinases' proximity to the NMDA receptor. RasGRF1 itself does not seem to affect CaMKII activity on its own, however (data not shown).

The enhancement of CaMKII-NR2B association in the presence of RasGRF1 seen in HEK cells also suggests that a ternary complex may be possible between CaMKII,

NR2B, and RasGRF1. However, one must also consider that a protein mediator in HEK cells may facilitate this association.

In HEK cells, it also appeared that RasGRF1 and CaMKII could associate in the absence of the NMDA receptor; however, we could not pull down purified CaMKII with immobilized purified RasGRF1. A possibility is that the interaction between CaMKII and RasGRF1 is weak and synergistic interactions might be involved in the formation of the CaMKII-RasGRF1-NR2B containing complex that otherwise would be much lower affinity pairwise. Another explanation is that a protein mediator(s) exists in HEK cells that allows CaMKII and RasGRF1 to associate.

The present study shows that ~3 mol of phosphate were incorporated per mol of RasGRF1 by CaMKII in contrast to Baouz et al.'s report of 0.01-0.02 ((12). Possible explanations for this discrepancy include differences in experimental setup. Baouz et al. performed the above experiment with full length RasGRF1 fused to maltose binding protein (~43 kDa) purified from *E. coli*. Our experiment used RasGRF1 fused to a Strep or flag-tag (~several amino acids) expressed and purified from mammalian cells (HEK293). By targeted LC/MS/MS, Ser485, Ser745, and Ser916 were also identified as being phosphorylated (Fig. 5.5). These sites are located on the PH domain, N-RasGEF domain, and between the N-RasGEF and RasGEF domains, respectively.

Redundancy in sites phosphorylated by both CaMKII and PKA has been useful in suggesting possible consequences of such modifications. Like PKA, CaMKII phosphorylates RasGRF1 at Ser916. Physiological significance has been implicated for this site from studies of PKA phosphorylation of RasGRF1. Ser916 immunostaining is

enriched in the apical dendrites of pyramidal neurons relative to soma implying activity dependent phosphorylation. Yang et al. showed that RasGRF1 truncation mutants that don't include Ser916 decrease the longest and total neurite length in PC12 endocrine cells (14). The S916A mutation prevented maximal activation of RasGEF activity after carbachol but not forskolin stimulation in NIH-3T3/hml fibroblast cells cotransfected with the mutant or wt GEF (13). Of the putative CaMKII phosphorylation sites found (as with PKA), Ser916 is the only one that doesn't exist in RasGRF2 which is 80% homologous to RasGRF1, but whose function distinct from that of RasGRF1 is unclear (14). Baouz et al. detected Ser745 as a PKA phosphorylation site amongst other sites but not 916. Mutating Ser745 to alanine or aspartate does not have an effect on activation of Ras (12). From our experiment treating rat hippocampal slices with okadaic acid, it appears that Ser916 phosphorylation is also regulated by phosphatases sensitive to okadaic acid, ie. PP1, 2A and/or 2B.

The purpose of dual regulation of RasGRF1 by PKA and CaMKII is unclear but cross talk between these two kinases are known to modulate for example, the AMPAR receptor (25,26), and in the heart, the cardiac ryanodine receptor (27), and myopodin (28). It has also been suggested that CaMKII and PKA activity may allow for synaptic tagging of different compartments of a dendrite for LTP (29). CaMKII needed for LTP in apical dendrites while PKA in the basal dendrites. Interestingly, this pattern of staining coincides with the immunostaining of phosphoSer916 is observed in (14).

RasGRF1 has dual GEF activities, and like RasGRF2 (30), it can promote the nucleotide exchange of GDP for GTP in both Ras and Rac GTPases, the latter of which is

done by the DH domain. Other members of the DBl containing family of proteins include TiamI and kalirin. Unlike TiamI and even RasGRF2, RasGRF1's RacGEF activity needs to be induced such as by phosphorylation by Src (15). Since CaMKII activity is thought to be required for NMDA stimulated spine enlargement, and can activate, for example, kalirin's RacGEF activity by phosphorylation (31), we tested the possibility that RasGRF1's RacGEF activity might be regulated by CaMKII. Although it is hard to predict the effect of phosphorylation on enzymatic activity, one of the phosphorylation sites identified by mass spec is adjacent to the DH domain and often the DH and PH domain are seen to interact cooperatively (32). Thus, it is conceivable that CaMKII could activate RasGRF1's RacGEF abilities by phosphorylation. However, this was not the case when we checked (data not shown). One promising lead is to study the effect of phosphorylation in dissociated neuronal cultures by stimulating with bicuculline and glycine in the presence of CaMKII inhibitors which enhance synaptic transmission. We are currently also assessing stimulation of neuronal cultures by bicuculline/glycine which is able to induce phosphorylation of Ser 916, that can be blocked with CaMKII inhibitors.

It remains to be investigated whether phosphorylation affects RasGRF1's intramolecular interactions, i.e. the regulation of RasGRF1's N terminus on it's catalytic C term RasGEF domain that Baouz et al. have observed *in vitro*. Several of the kinases known to phosphorylate RasGRF1 also phosphorylate NR2B and NR2A, possibly to ensure specificity at the gateway of Ca^{2+} influx. It would also be interesting to see how

RasGRF1 interaction with NR2B and the GEF's subcellular localization is affected by CaMKII phosphorylation.

REFERENCES

1. Brambilla, R., Gnesutta, N., Minichiello, L., White, G., Roylance, A. J., Herron, C. E., Ramsey, M., Wolfer, D. P., Cestari, V., Rossi-Arnaud, C., Grant, S. G., Chapman, P. F., Lipp, H. P., Sturani, E., and Klein, R. (1997) *Nature* **390**, 281-286
2. Giese, K. P., Friedman, E., Telliez, J. B., Fedorov, N. B., Wines, M., Feig, L. A., and Silva, A. J. (2001) *Neuropharmacology* **41**, 791-800
3. Tian, X., Gotoh, T., Tsuji, K., Lo, E. H., Huang, S., and Feig, L. A. (2004) *EMBO J* **23**, 1567-1575
4. Krapivinsky, G., Krapivinsky, L., Manasian, Y., Ivanov, A., Tyzio, R., Pellegrino, C., Ben-Ari, Y., Clapham, D. E., and Medina, I. (2003) *Neuron* **40**, 775-784
5. Zhou, Y., Takahashi, E., Li, W., Halt, A., Wiltgen, B., Ehninger, D., Li, G. D., Hell, J. W., Kennedy, M. B., and Silva, A. J. (2007) *J Neurosci* **27**, 13843-13853
6. Barria, A., and Malinow, R. (2005) *Neuron* **48**, 289-301
7. Bayer, K. U., De Koninck, P., Leonard, A. S., Hell, J. W., and Schulman, H. (2001) *Nature* **411**, 801-805
8. Leonard, A. S., Bayer, K. U., Merrill, M. A., Lim, I. A., Shea, M. A., Schulman, H., and Hell, J. W. (2002) *J Biol Chem* **277**, 48441-48448
9. Leonard, A. S., Lim, I. A., Hemsworth, D. E., Horne, M. C., and Hell, J. W. (1999) *Proc Natl Acad Sci U S A* **96**, 3239-3244
10. Colbran, R. J., and Brown, A. M. (2004) *Curr Opin Neurobiol* **14**, 318-327
11. Strack, S., McNeill, R. B., and Colbran, R. J. (2000) *J Biol Chem* **275**, 23798-23806
12. Baouz, S., Jacquet, E., Accorsi, K., Hountondji, C., Balestrini, M., Zippel, R., Sturani, E., and Parmeggiani, A. (2001) *J Biol Chem* **276**, 1742-1749
13. Mattingly, R. R. (1999) *J Biol Chem* **274**, 37379-37384
14. Yang, H., Cooley, D., Legakis, J. E., Ge, Q., Andrade, R., and Mattingly, R. R. (2003) *J Biol Chem* **278**, 13278-13285
15. Kiyono, M., Kaziro, Y., and Satoh, T. (2000) *J Biol Chem* **275**, 5441-5446
16. Kesavapany, S., Pareek, T. K., Zheng, Y. L., Amin, N., Gutkind, J. S., Ma, W., Kulkarni, A. B., Grant, P., and Pant, H. C. (2006) *Neurosignals* **15**, 157-173
17. Sturani, E., Abbondio, A., Branduardi, P., Ferrari, C., Zippel, R., Martegani, E., Vanoni, M., and Denis-Donini, S. (1997) *Exp Cell Res* **235**, 117-123
18. Karnoub, A. E., Worthylake, D. K., Rossman, K. L., Pruitt, W. M., Campbell, S. L., Sondek, J., and Der, C. J. (2001) *Nat Struct Biol* **8**, 1037-1041
19. Kiyono, M., Satoh, T., and Kaziro, Y. (1999) *Proc Natl Acad Sci U S A* **96**, 4826-4831
20. Kindler, S., and Kennedy, M. B. (1996) *J Neurosci Methods* **68**, 61-70
21. Tian, X., and Feig, L. A. (2006) *J Biol Chem* **281**, 7578-7582
22. Praseeda, M., Pradeep, K. K., Krupa, A., Krishna, S. S., Leena, S., Kumar, R. R., Cheriyan, J., Mayadevi, M., Srinivasan, N., and Omkumar, R. V. (2004) *Biochem J* **378**, 391-397
23. Li, S., Tian, X., Hartley, D. M., and Feig, L. A. (2006) *J Neurosci* **26**, 1721-1729
24. Bayer, K. U., LeBel, E., McDonald, G. L., O'Leary, H., Schulman, H., and De Koninck, P. (2006) *J Neurosci* **26**, 1164-1174

25. Boehm, J., and Malinow, R. (2005) *Biochem Soc Trans* **33**, 1354-1356
26. Esteban, J. A., Shi, S. H., Wilson, C., Nuriya, M., Huganir, R. L., and Malinow, R. (2003) *Nat Neurosci* **6**, 136-143
27. Kockskamper, J., and Pieske, B. (2006) *Circ Res* **99**, 333-335
28. Faul, C., Dhume, A., Schecter, A. D., and Mundel, P. (2007) *Mol Cell Biol* **27**, 8215-8227
29. Sajikumar, S., Navakkode, S., Sacktor, T. C., and Frey, J. U. (2005) *J Neurosci* **25**, 5750-5756
30. Fan, W. T., Koch, C. A., de Hoog, C. L., Fam, N. P., and Moran, M. F. (1998) *Curr Biol* **8**, 935-938
31. Xie, Z., Srivastava, D. P., Photowala, H., Kai, L., Cahill, M. E., Woolfrey, K. M., Shum, C. Y., Surmeier, D. J., and Penzes, P. (2007) *Neuron* **56**, 640-656
32. Buchsbaum, R., Telliez, J. B., Goonesekera, S., and Feig, L. A. (1996) *Mol Cell Biol* **16**, 4888-4896

Observed	Mr (experimental)	Mr (calculated)	Delta	Peptide	Site Identified
457.2629	912.5113	912.4681	0.0432	LGSLSTKK	Ser 485
478.6401	1432.8984	1432.8054	0.0930	KLSLNIPHTGGK	Ser 745
550.6012	1648.7818	1648.7028	0.0789	RMSLANTGFSSDQR	Ser 916

Table 5.1: Phosphopeptides identified by LC MS/MS. Purified RasGRF1 was phosphorylated by purified CaMKII in vitro, separated by SDS-PAGE, tryptic digested and run on LC MS/MS. Observed masses are listed as compared to experimental and calculated values (Mr), alongside the delta, which is the difference between experimental and calculated masses.

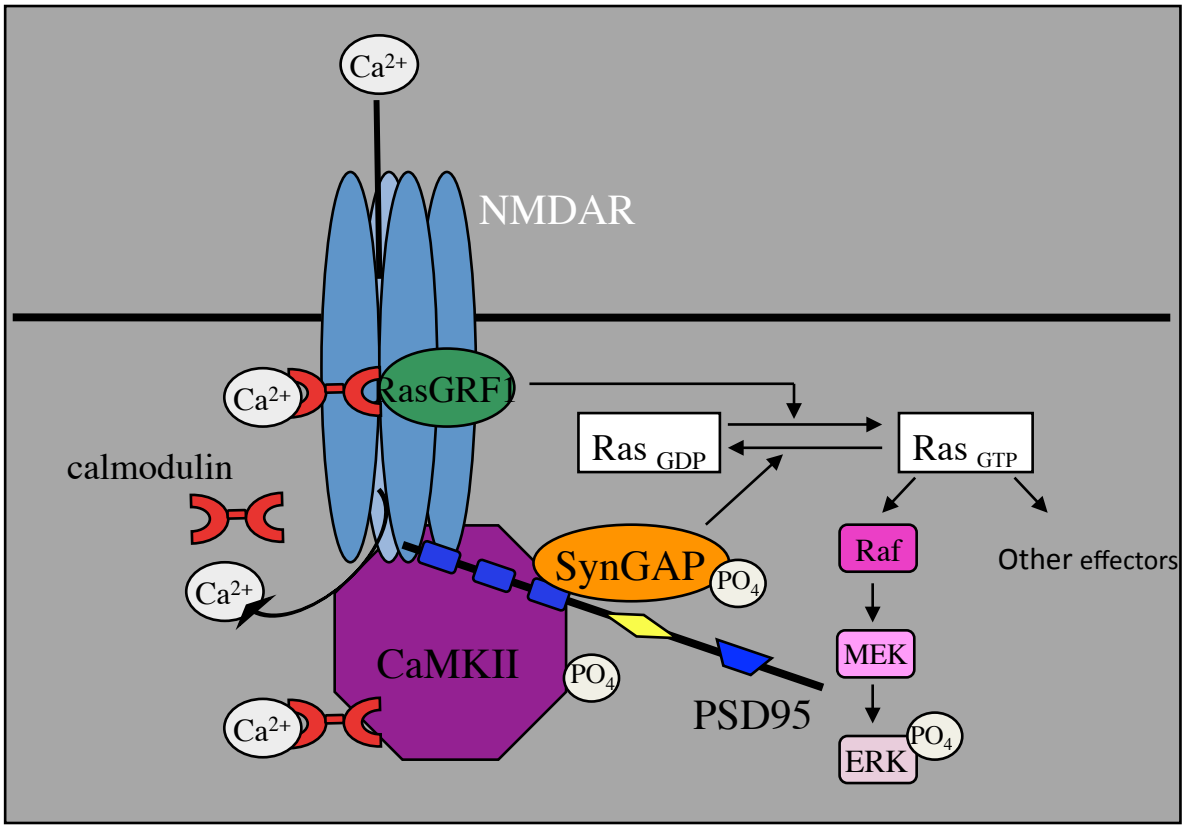

Figure 5.1. Signaling from the NMDA receptor to CaMKII and RasGRF1. Stimulation of the NMDA receptor leads to Ca2+ influx which activates Ca2+ sensitive RasGRF1 and CaMKII. CaMKII bound to Ca2+/CaM allows it to be autophosphorylated and to phosphorylate other substrates like the NMDA receptor, RasGRF1, and SynGAP. Phosphorylated SynGAP stimulates the intrinsic GTPase activity of Ras and opposes action of RasGRF1. Ca2+/CaM bound RasGRF1 activates Ras (by displacement of GDP for GTP) which activates a number of effectors, including the well known ERK pathway through Raf. Activated Raf phosphorylates the mitogen-activated protein kinase (MEK). MEK then phosphorylates the extracellular signal-related kinases 1 and 2 (ERKs 1 and 2). Erk1/2 can cross into the nucleus where it can activate transcription factors (like CREB, ATF-2, or Ap-1, etc) or promote gene expression.

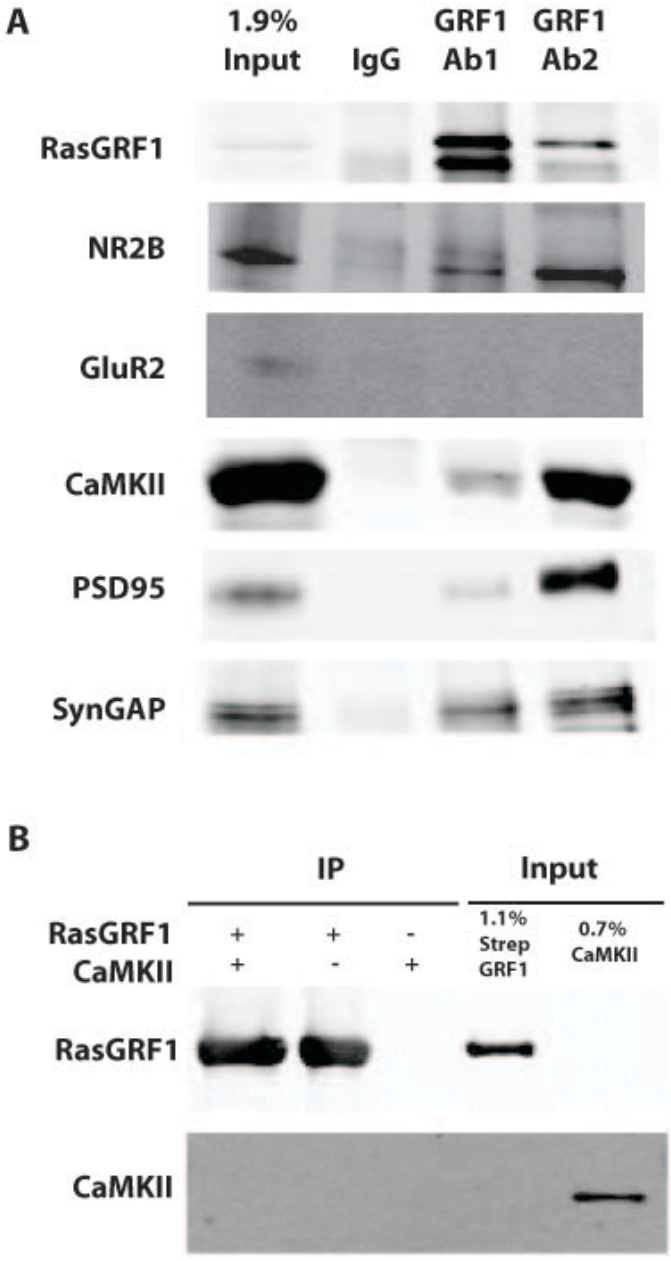

Figure 5.2. Coimmunoprecipitation of RasGRF1 and CaMKII from brain homogenate but not with purified protein (A) RasGRF1 and CaMKII is found in the co-IP with NR2B from brain homogenate. Anti-RasGRF1 antibodies (Ab1-Cterm specific and Ab2-N term specific) or RbIgG isotype control were incubated deoxycholate solubilized brain membrane fraction. Immunoprecipitates were run on SDS page alongside 1.9% solubilized brain membrane fraction as well as RbIgG isotype control. A western blot was done probing for NR2B (known binder), GluR2 (known non binder) and proteins of interest: CaMKII, RasGRF1, PSD95 and SynGAP. (B) RasGRF1 and CaMKII do not bind strongly in pulldown with purified protein. Immobilzed Strep-RasGRF1 was incubated with purified CaMKII or alone. The western blots were probed with an antibody specific for RasGRF1 or CaMKII.

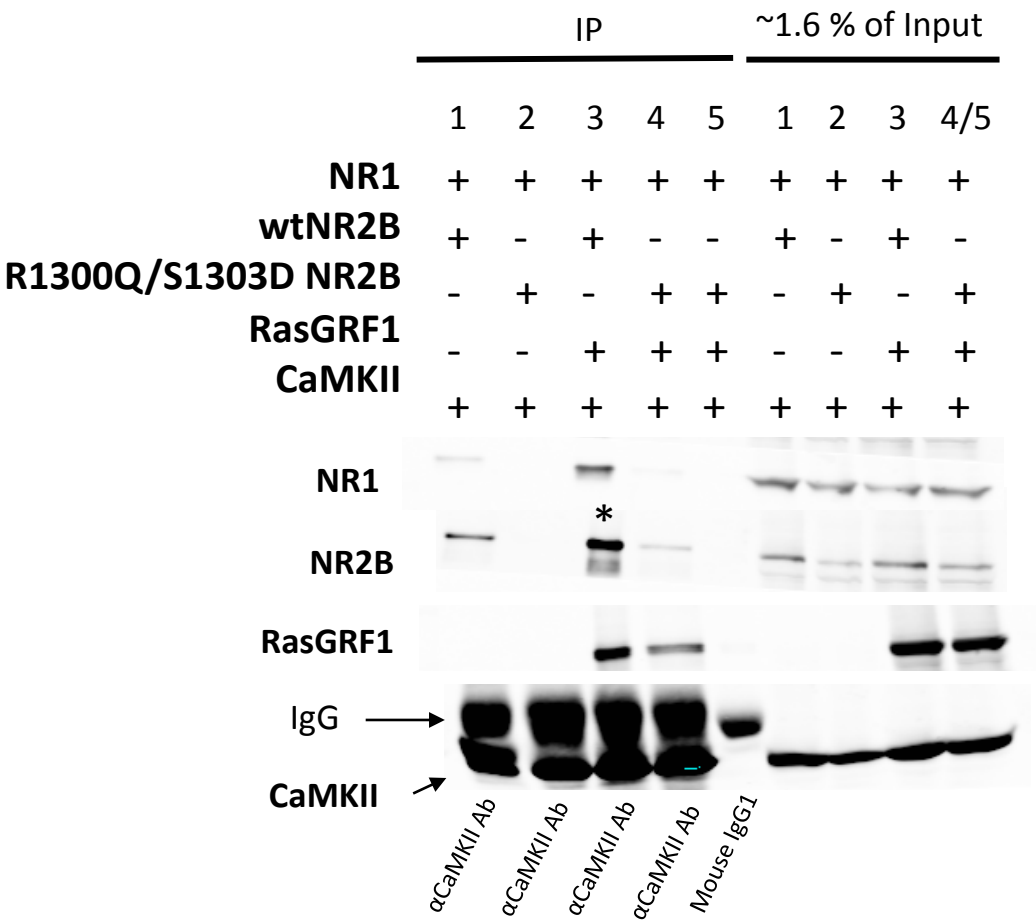

Figure 5.3. RasGRF1 enhances binding of CaMKII to NR2B in HEK cells. C-term binding site on NR2B for CaMKII is involved but not exclusively responsible for the CaMKII-GRF1-NR2B complex. The presence of RasGRF1 significantly enhances the association of CaMKII with NR2B (5 fold, SEM=1.6, n=4, p=0.04, t-test, two tailed) in immunoprecipitations with a CaMKII specific antibody. A similar result (was obtained with an NR2B mutant containing the mutations R1300Q/S1300D that abolishes binding to CaMKII. However, RasGRF1 is not able to rescue mutant binding (Lanes 2 and 4) to levels seen with wt NR2B (Lanes 1 and 3). n=3 to 4. Lysates for immunoprecipitation inputs were prepared from HEK cells cotransfected with NR1, wtNR2B or R1300Q/S1300D NR2B, CaMKII, +/- RasGRF1. NR1, NR2B, RasGRF1, and CaMKII were detected in the representative immunoblot above by specific antibodies. Immuoprecipitation with a mouse IgG1 antibody served as a negative control. Representative immunoblots from one experiment are shown.

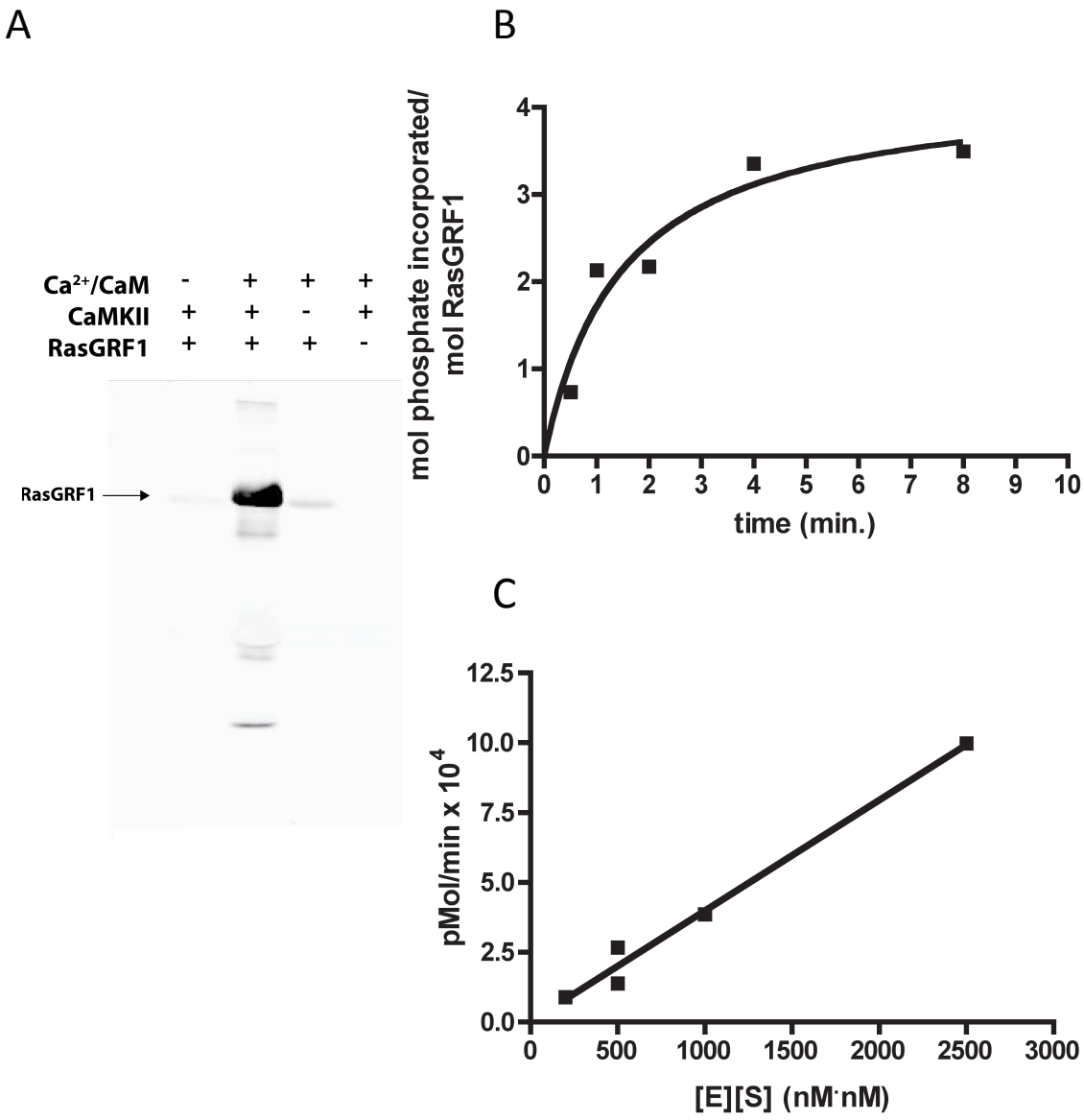

Figure 5.4. RasGRF1 can be phosphorylated by CaMKII (A) Western blot probing with phosphospecific RbSer916 antibody to detect phosphorylation of RasGRF1 by CaMKII at this particular site in the presence of 1 mM Ca^{2+}/2 μM CaM or 0.5mM EGTA. (B) Stoichiometry and efficiency of CaMKII phosphorylation of RasGRF1 (B) Stoichiometry of phosphate incorporation into 50nM RasGRF1 by 50nM CaMKII over time at 30ºC *in vitro* as measured by phosphoimaging of a gel run with the labeled reactions aside ATP standards. n=3, including experiments done with other concentrations of RasGRF1 and CaMKII that yielded similar results. (C) k_{cat}/K_M of RasGRF1 phosphorylation by CaMKII is on the same order of magnitude as that for other CaMKII substrates. k_{cat}/K_M was determined from the initial linear slope of the Michaelis Menten equation. Incorporation of ^{32}P into RasGRF1 by CaMKII was measured by phosphoimaging of a gel run with the labeled reactions.

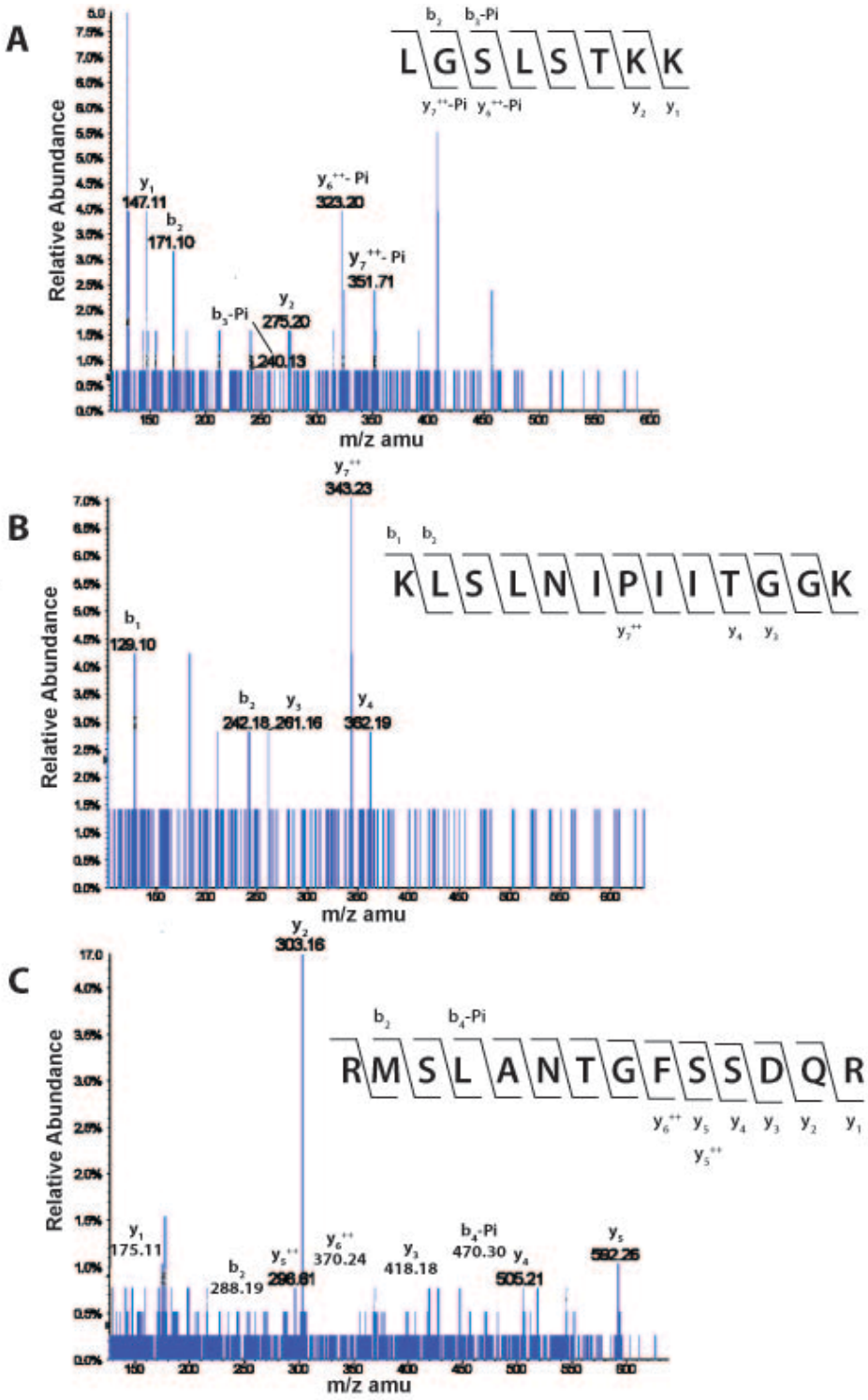

Figure 5.5. MS/MS spectrum of RasGRF1 phosphopeptides identified after phosphorylation by CaMKII *in vitro*. Loss of 98 Da, corresponding to phosphoric acid is observed in all "y or b" ions after phosphorylated residue. (A) A MS/MS fragmentation spectrum of peptide LGSLSTKK identifying phosphorylated Ser485 (B) A MS/MS fragmentation spectrum of peptide KLSLNIPHTGGK identifying phosphorylated Ser745 (C) A MS/MS fragmentation spectrum of peptide RMSLANTGFSSDQR identifying phosphorylated Ser916.

Chapter 6
Conclusions

This thesis is primarily a study of the behavioral and correlative molecular abnormalities resulting from deletion of the PSD enriched protein, Densin-180. The Densin KO exhibits severe nest building deficits, anxiety, asocial behavior, impaired sensorimotor gating, hyperlocomotion to novel objects, and hippocampal and short term memory deficits (hippocampal- and cortical- dependent). These traits are consistent with the behavior of a number of schizophrenic mouse models (Inta et al., 2009). The Densin KOs are hypoactive in their home cage relative to the WT which is seen in chronic schizophrenia, depression, and affective disorders (Steele and Gunapala, unpublished data). The Densin KO has Stage 6 tonic clonic seizures when injected with the GABA(A) agonist, Nembutal (pentobarbital). Asocial behavior, stereotypy, imbalance of excitation/inhibition, cognitive defects, and susceptibility to seizures are also associated with autism (Crawley, 2007). Disruptions in cross-linking and stabilization of PSD protein architecture may account for some of the behavioral abnormalities seen. α-actinin, a direct binding partner of Densin is decreased in the PSD fraction of the KO relative to the WT. Likely related to this deficiency is an accompanying decrease in DISC1 and mGluR5 which both directly interact with α-actinin. α-actinin is known to regulate mGluR5 surface levels (Cabello et al., 2007). Importantly, DISC1 and mGluR5 are linked to schizophrenia and affective mood disorders (Blackwood et al., 2001; Luscher and Huber, 2010). The Densin KO additionally has blunted activity dependent gene expression. Steady state levels of the immediate early genes Arc and c-fos are decreased in brain sections in both the cortex

and hippocampus. Deranged BDNF signaling in the KO may contribute to the reduction in Arc protein, aberrant spine morphology, seizure susceptibility, and problems in affect seen in the Densin KO (Tyler and Pozzo-Miller, 2003; Hong et al., 2008; Yoshii and Constantine-Paton, 2010).

DISC1 and BDNF signaling both also have roles in neuronal development and dysfunction has been associated with autism, mood disorders, and schizophrenia (Egan et al., 2003; Craddock et al., 2005; Kilpinen et al., 2008; Chapleau et al., 2009; Gadow et al., 2009; Williams et al., 2009). DISC1 is thought to facilitate neuronal migration and neurogenesis and BDNF signaling is important for neuronal maturation and plasticity in the adult brain. BDNF, DISC1 and mGluR5 mediated signaling intersect at the level of the MAPK/ERK pathway, which is normally activated by NMDA receptor stimulation. One hypothesis is that reductions in DISC1, mGluR5, and BDNF signaling, normally positive modulators of the ERK pathway, can mimic a hypoglutamatergic state, which is a mechanism of schizophrenia (Figure 2.14). DISC1 can also interact directly with the adaptor protein Grb2 and is required for neurotrophin induced axon elongation (Shinoda et al., 2007). Grb2 couples tyrosine kinase receptor (i.e. TrkB) signaling with the ERK pathway. We are in the process of assessing the activation of ERK with stimulation by BDNF and the mGluR agonist, *S* 3,5 DHPG.

Cross talk between BDNF and DISC1 signaling can also exist at the level of cAMP signaling. Phosphodiesterase 4B which degrades cAMP is normally inhibited by DISC1 under conditions of low cAMP (Millar et al., 2005). A decrease in DISC1 in the KO may alter levels of cAMP, which regulate BDNF signaling. Reduced levels of cAMP decrease

transcription of activity dependent plasticity genes such as Arc and c-fos (Figure 3.6). It would be worthwhile to investigate perturbations in PDE4B activity and signaling as related to DISC1 and BDNF.

The schizoaffective behavior in the Densin KO is consistent with reduced levels of mGluR5, DISC1, and impairments in BDNF signaling, all three of which are implicated in schizophrenia and affective disorders (Blackwood et al., 2001; Egan et al., 2003; Craddock et al., 2005; Luscher and Huber, 2010; Yoshii and Constantine-Paton, 2010). It is thought that DISC1 may be genetically more linked to psychosis end of the schizoaffective spectrum while BDNF is more associated with affective disorder, although boundaries are blurred (Sklar et al., 2002; Craddock et al., 2005; Ivleva et al., 2008). Disruption of scaffold proteins, such as Shank, that commonly stabilize multiple protein complexes in the PSD often result in such behavior that overlap with both schizophrenia, autism, and affective disorders (Durand et al., 2007; Gauthier et al., 2009; Gauthier et al., 2010). Mice with alterations in different parts of the DISC1 protein also exhibit different behavioral abnormalities with varying severity (Shen et al., 2008). The lack of Densin may create a point of weakness in the PSD architecture that is transmitted to different aspects of signaling.

While we have described behavioral abnormalities of the Densin KO mouse mostly in terms of schizophrenia for which there are currently more established mouse models, disruptions in DISC1 and BDNF and the behavioral abnormalities seen in the Densin KO mouse, are also consistent with autism. In particular, the asocial behavior, increased stereotypy (chewing, drinking, twitching), decreased prepulse inhibition,

imbalance in excitation/inhibition and seizure susceptibility, increased anxiety, and cognitive deficits exhibited by the Densin KO mice resemble autism (Crawley, 2007; Levisohn, 2007; Combi et al., 2010; Mattila et al., 2010). Mutations in DISC1 and BDNF have also been linked to the disorder (Kilpinen et al., 2008; Chapleau et al., 2009; Gadow et al., 2009; Williams et al., 2009).

We are curious whether other parts of the PSD scaffold complex that stabilize glutamate receptors in the PSD are intact and at what level DISC1, mGluR5, and BDNF signaling relate. Further investigation is needed of whether abundance and distribution of Shank and Homer are affected in the Densin KO. Mutations in Shank and Homer have roles in schizophrenia and autism (Szumlinski et al., 2005; Durand et al., 2007; Gauthier et al., 2009; Gauthier et al., 2010). Because the decreases in mGluR5 and DISC1 are related by reductions in α-actinin, it would be interesting to see if phenotypes observed in the Densin KO could be rescued by overexpression of α-actinin. We are currently assessing if surface levels of other glutamate receptors, cadherins, and TrkB (BDNF signaling) are altered in the Densin KO since Densin can directly interact with proteins that do regulate the stability of these complexes in the PSD. It would be informative to look at the effect of overexpression of Densin on these receptors and cell adhesion molecules as well.

The use of antipsychotics or amphetamine can be used to further characterize schizophrenic like behavior in mice. Amphetamine is a dopamine agonist that is administered to see whether psychosis or measurable positive or negative symptoms are aggravated in a mouse model suspected to be schizophrenic. Alternatively, future

experiments can be directed towards whether abnormal behavior is mitigated by an mGluR agonist or antipsychotic like clozapine. Because the Densin KO exhibit signs of an affective disorder and lack of pleasure in normal daily activities (i.e. nest building, hanging vertically), it would be worthwhile to test for depression using the forced swim test. Studying ultrasonic vocalizations from KO and WT mice would be interesting with respect to the communication deficits seen in autism (Crawley, 2007; Moy and Nadler, 2008).

Of the existing theories for schizophrenia, our molecular data coincide most with developmental, glutamatergic, and GABAergic mechanisms in etiology. These theories, which also include the hyperdopaminergic argument, are not mutually exclusive. There is often interplay between each of these mechanisms. Genetics and the environment also factor into the etiology of the disease. Abnormalities in the immune system, which play a role in schizophrenia and autism, may partially explain the behavioral abnormalities seen in the Densin KO. This may be due to disruptions in neurodevelopment resulting in misconnectivity of synapses (McGlashan and Hoffman, 2000). Maternal infection, for example, is associated with higher risk of schizophrenia (Smith et al., 2007; Patterson, 2009). The Densin KO runts may be immunocompromised at least before adolescence, judging from their small thymus and pale spleens at ~ 4 weeks of age (Gregory Lawson, unpublished data).

The importance of MAPK/ERK signaling in synaptic plasticity, neuronal survival, maturation, and development and the upstream molecular interactions that regulate activation of the pathway is highlighted in both studies of Densin and RasGRF1

comprising this thesis. There also appears to be some convergence on the dentate gyrus and hippocampus as regions of misregulation for the BDNF and DISC1 signaling that might partially explain the Densin KO's phenotype. The dentate gyrus, where Densin transcripts are most enriched (Allen brain map. Analysis discussed in Holly Beale's thesis), is involved in stress response, and depression due to misregulation of BDNF signaling (Bramham, 2007). A decrease in DISC1, which is seen in the Densin KO, may lead to aberrant placement of cells from neurogenesis in the dentate gyrus and thus abnormal remodeling of this layer of the hippocampus, signifying a role of DISC1 both in neuronal development and wiring. Interestingly, decrease in DISC1 leads to new cells that have increased excitability along with an increased rate of dendritic and synaptic development (Duan et al., 2007). This may increase risk for seizure activity described in Chapter 4. Decreases in DISC1 have been correlated with kindling in rodents in the dentate (Fournier et al.; Fournier et al., 2009).

We do not yet understand the mechanism behind the violent seizures in the Densin KO with administration of Nembutal. However, many mental disorders including autism, schizophrenia, and bipolar disorder have a component of imbalanced excitation and inhibition. Moreover, given that epilepsy may result from derangement in mechanisms that normally confer brain plasticity, it is not surprising that seizures are often a comorbidity of these diseases (Rubenstein and Merzenich, 2003; Qin et al., 2005; Levisohn, 2007; Cascella et al., 2009; Hagerman and Stafstrom, 2009; Combi et al., 2010). Densin is expressed in a subset of inhibitory neurons in addition to excitatory neurons (Chapter 4). Electroencephalogram studies would shed light on whether

seizures occur spontaneously in the Densin KO. The significant increases in GAD65 and parvalbumin in the KO may reflect an attempt in the Densin KO to lower excitation back to homeostatic levels (Sperk et al., 2009). It would be informative to assess seizure threshold in mice and interesting to see whether Nembutal creates higher excitability as seen by spiking in slices and what mechanisms are behind drugs that can halt this activity. The elucidation of Densin's role in inhibitory in addition to excitatory neurons would be informative. One way would be to analyze transcripts is by RNA seq analysis of RNA libraries from laser dissected inhibitory and excitatory neurons from Densin KO and WT brains.

There is uncertainty with whether developmental abnormalities or lack of Densin in the mature brain are potential mechanisms for the KO seizure phenotype. These issues can be clarified using an inducible KO generated with Cre-technology or studying the effect of antisense oligos or RNAi to knock down Densin in mature neurons in culture. One also wonders whether the ~20% of Densin KOs that died and usually exhibited the most severe runting would have resulted in a more severe phenotype had they lived to be a part of the behavioral cohort. A systemic study of other organs affected would also be of interest. Dr. Gregory Lawson (UCLA pathologist) has suggested that the gastrointestinal villi of the Densin KO may be not allow proper absorption and may lead to the runting observed in the Densin KO based on initial analysis of histology; however more thorough morphological studies would have to be done to confirm this result.

Needless to say, there is still a lot to do to clarify mechanistically how the

different signaling pathways implicated weave together and result in abnormal behavior and inappropriate response to the environment. Schizophrenia, affective disorders, autism, and epilepsy are often debilitating diseases for which there are currently unsatisfactory treatments. Side effects of drugs additionally confound the neurological disorder and an individual's sense and perception of their reality. Understanding abnormal behaviors in terms of molecular changes that are interlinked and continuous, in addition to categorizing them as a named disease, would allow better customization of treatments for individuals who cope with the physiological, psychological, and social hardships of mental illness.

REFERENCES

Blackwood DH, Fordyce A, Walker MT, St Clair DM, Porteous DJ, Muir WJ (2001) Schizophrenia and affective disorders--cosegregation with a translocation at chromosome 1q42 that directly disrupts brain-expressed genes: clinical and P300 findings in a family. Am J Hum Genet 69:428-433.

Bramham CR (2007) Control of synaptic consolidation in the dentate gyrus: mechanisms, functions, and therapeutic implications. Prog Brain Res 163:453-471.

Cabello N, Remelli R, Canela L, Soriguera A, Mallol J, Canela EI, Robbins MJ, Lluis C, Franco R, McIlhinney RA, Ciruela F (2007) Actin-binding protein alpha-actinin-1 interacts with the metabotropic glutamate receptor type 5b and modulates the cell surface expression and function of the receptor. J Biol Chem 282:12143-12153.

Cascella NG, Schretlen DJ, Sawa A (2009) Schizophrenia and epilepsy: is there a shared susceptibility? Neurosci Res 63:227-235.

Chapleau CA, Larimore JL, Theibert A, Pozzo-Miller L (2009) Modulation of dendritic spine development and plasticity by BDNF and vesicular trafficking: fundamental roles in neurodevelopmental disorders associated with mental retardation and autism. J Neurodev Disord 1:185-196.

Combi R, Redaelli S, Beghi M, Clerici M, Cornaggia CM, Dalpra L (2010) Clinical and genetic evaluation of a family showing both autism and epilepsy. Brain Res Bull 82:25-28.

Craddock N, O'Donovan MC, Owen MJ (2005) The genetics of schizophrenia and bipolar disorder: dissecting psychosis. J Med Genet 42:193-204.

Crawley JN (2007) Mouse behavioral assays relevant to the symptoms of autism. Brain Pathol 17:448-459.

Duan X, Chang JH, Ge S, Faulkner RL, Kim JY, Kitabatake Y, Liu XB, Yang CH, Jordan JD, Ma DK, Liu CY, Ganesan S, Cheng HJ, Ming GL, Lu B, Song H (2007) Disrupted-In-Schizophrenia 1 regulates integration of newly generated neurons in the adult brain. Cell 130:1146-1158.

Durand CM et al. (2007) Mutations in the gene encoding the synaptic scaffolding protein SHANK3 are associated with autism spectrum disorders. Nat Genet 39:25-27.

Egan MF, Kojima M, Callicott JH, Goldberg TE, Kolachana BS, Bertolino A, Zaitsev E, Gold B, Goldman D, Dean M, Lu B, Weinberger DR (2003) The BDNF val66met polymorphism affects activity-dependent secretion of BDNF and human memory and hippocampal function. Cell 112:257-269.

Fournier NM, Caruncho HJ, Kalynchuk LE (2009) Decreased levels of disrupted-in-schizophrenia 1 (DISC1) are associated with expansion of the dentate granule cell layer in normal and kindled rats. Neurosci Lett 455:134-139.

Fournier NM, Andersen DR, Botterill JJ, Sterner EY, Lussier AL, Caruncho HJ, Kalynchuk LE The effect of amygdala kindling on hippocampal neurogenesis coincides with decreased reelin and DISC1 expression in the adult dentate gyrus. Hippocampus 20:659-671.

Gadow KD, Roohi J, DeVincent CJ, Kirsch S, Hatchwell E (2009) Association of COMT (Val158Met) and BDNF (Val66Met) gene polymorphisms with anxiety, ADHD and tics in children with autism spectrum disorder. J Autism Dev Disord 39:1542-1551.

Gauthier J, Spiegelman D, Piton A, Lafreniere RG, Laurent S, St-Onge J, Lapointe L, Hamdan FF, Cossette P, Mottron L, Fombonne E, Joober R, Marineau C, Drapeau P, Rouleau GA (2009) Novel de novo SHANK3 mutation in autistic patients. Am J Med Genet B Neuropsychiatr Genet 150B:421-424.

Gauthier J et al. (2010) De novo mutations in the gene encoding the synaptic scaffolding protein SHANK3 in patients ascertained for schizophrenia. Proc Natl Acad Sci U S A 107:7863-7868.

Hagerman PJ, Stafstrom CE (2009) Origins of epilepsy in fragile x syndrome. Epilepsy Curr 9:108-112.

Hong EJ, McCord AE, Greenberg ME (2008) A biological function for the neuronal activity-dependent component of Bdnf transcription in the development of cortical inhibition. Neuron 60:610-624.

Inta D, Monyer H, Sprengel R, Meyer-Lindenberg A, Gass P (2009) Mice with genetically altered glutamate receptors as models of schizophrenia: a comprehensive review. Neurosci Biobehav Rev 34:285-294.

Ivleva E, Thaker G, Tamminga CA (2008) Comparing genes and phenomenology in the major psychoses: schizophrenia and bipolar 1 disorder. Schizophr Bull 34:734-742.

Kilpinen H, Ylisaukko-Oja T, Hennah W, Palo OM, Varilo T, Vanhala R, Nieminen-von Wendt T, von Wendt L, Paunio T, Peltonen L (2008) Association of DISC1 with autism and Asperger syndrome. Mol Psychiatry 13:187-196.

Levisohn PM (2007) The autism-epilepsy connection. Epilepsia 48 Suppl 9:33-35.

Luscher C, Huber KM (2010) Group 1 mGluR-dependent synaptic long-term depression: mechanisms and implications for circuitry and disease. Neuron 65:445-459.

Mattila ML, Hurtig T, Haapsamo H, Jussila K, Kuusikko-Gauffin S, Kielinen M, Linna SL, Ebeling H, Bloigu R, Joskitt L, Pauls DL, Moilanen I (2010) Comorbid Psychiatric Disorders Associated with Asperger Syndrome/High-functioning Autism: A Community- and Clinic-based Study. J Autism Dev Disord.

McGlashan TH, Hoffman RE (2000) Schizophrenia as a disorder of developmentally reduced synaptic connectivity. Arch Gen Psychiatry 57:637-648.

Millar JK, Pickard BS, Mackie S, James R, Christie S, Buchanan SR, Malloy MP, Chubb JE, Huston E, Baillie GS, Thomson PA, Hill EV, Brandon NJ, Rain JC, Camargo LM, Whiting PJ, Houslay MD, Blackwood DH, Muir WJ, Porteous DJ (2005) DISC1 and PDE4B are interacting genetic factors in schizophrenia that regulate cAMP signaling. Science 310:1187-1191.

Moy SS, Nadler JJ (2008) Advances in behavioral genetics: mouse models of autism. Mol Psychiatry 13:4-26.

Patterson PH (2009) Immune involvement in schizophrenia and autism: etiology, pathology and animal models. Behav Brain Res 204:313-321.

Qin P, Xu H, Laursen TM, Vestergaard M, Mortensen PB (2005) Risk for schizophrenia and schizophrenia-like psychosis among patients with epilepsy: population based cohort study. BMJ 331:23.

Rubenstein JL, Merzenich MM (2003) Model of autism: increased ratio of excitation/inhibition in key neural systems. Genes Brain Behav 2:255-267.

Shen S, Lang B, Nakamoto C, Zhang F, Pu J, Kuan SL, Chatzi C, He S, Mackie I, Brandon NJ, Marquis KL, Day M, Hurko O, McCaig CD, Riedel G, St Clair D (2008) Schizophrenia-related neural and behavioral phenotypes in transgenic mice expressing truncated Disc1. J Neurosci 28:10893-10904.

Shinoda T, Taya S, Tsuboi D, Hikita T, Matsuzawa R, Kuroda S, Iwamatsu A, Kaibuchi K (2007) DISC1 regulates neurotrophin-induced axon elongation via interaction with Grb2. J Neurosci 27:4-14.

Sklar P, Gabriel SB, McInnis MG, Bennett P, Lim YM, Tsan G, Schaffner S, Kirov G, Jones I, Owen M, Craddock N, DePaulo JR, Lander ES (2002) Family-based association study of 76 candidate genes in bipolar disorder: BDNF is a potential risk locus. Brain-derived neutrophic factor. Mol Psychiatry 7:579-593.

Smith SE, Li J, Garbett K, Mirnics K, Patterson PH (2007) Maternal immune activation alters fetal brain development through interleukin-6. J Neurosci 27:10695-10702.

Sperk G, Drexel M, Pirker S (2009) Neuronal plasticity in animal models and the epileptic human hippocampus. Epilepsia 50 Suppl 12:29-31.

Szumlinski KK, Lominac KD, Kleschen MJ, Oleson EB, Dehoff MH, Schwarz MK, Seeburg PH, Worley PF, Kalivas PW (2005) Behavioral and neurochemical phenotyping of Homer1 mutant mice: possible relevance to schizophrenia. Genes Brain Behav 4:273-288.

Tyler WJ, Pozzo-Miller L (2003) Miniature synaptic transmission and BDNF modulate dendritic spine growth and form in rat CA1 neurones. J Physiol 553:497-509.

Williams JM, Beck TF, Pearson DM, Proud MB, Cheung SW, Scott DA (2009) A 1q42 deletion involving DISC1, DISC2, and TSNAX in an autism spectrum disorder. Am J Med Genet A 149A:1758-1762.

Yoshii A, Constantine-Paton M (2010) Postsynaptic BDNF-TrkB signaling in synapse maturation, plasticity, and disease. Dev Neurobiol 70:304-322.

Structural Modeling of Protein Interactions by Analogy: Application to PSD-95

Dmitry Korkin[1,2,3], Fred P. Davis[1,2,3], Frank Alber[1,2,3], Tinh Luong[4], Min-Yi Shen[1,2,3], Vladan Lucic[5], Mary B. Kennedy[4], Andrej Sali[1,2,3]*

1 Department of Biopharmaceutical Sciences, University of California San Francisco, San Francisco, California, United States of America, **2** Department of Pharmaceutical Chemistry, University of California San Francisco, San Francisco, California, United States of America, **3** California Institute for Quantitative Biomedical Research, University of California San Francisco, San Francisco, California, United States of America, **4** Division of Biology, California Institute of Technology, Pasadena, California, United States of America, **5** Department of Structural Biology, Max Planck Institute of Biochemistry, Martinsried, Germany

We describe comparative patch analysis for modeling the structures of multidomain proteins and protein complexes, and apply it to the PSD-95 protein. Comparative patch analysis is a hybrid of comparative modeling based on a template complex and protein docking, with a greater applicability than comparative modeling and a higher accuracy than docking. It relies on structurally defined interactions of each of the complex components, or their homologs, with any other protein, irrespective of its fold. For each component, its known binding modes with other proteins of any fold are collected and expanded by the known binding modes of its homologs. These modes are then used to restrain conventional molecular docking, resulting in a set of binary domain complexes that are subsequently ranked by geometric complementarity and a statistical potential. The method is evaluated by predicting 20 binary complexes of known structure. It is able to correctly identify the binding mode in 70% of the benchmark complexes compared with 30% for protein docking. We applied comparative patch analysis to model the complex of the third PSD-95, DLG, and ZO-1 (PDZ) domain and the SH3-GK domains in the PSD-95 protein, whose structure is unknown. In the first predicted configuration of the domains, PDZ interacts with SH3, leaving both the GMP-binding site of guanylate kinase (GK) and the C-terminus binding cleft of PDZ accessible, while in the second configuration PDZ interacts with GK, burying both binding sites. We suggest that the two alternate configurations correspond to the different functional forms of PSD-95 and provide a possible structural description for the experimentally observed cooperative folding transitions in PSD-95 and its homologs. More generally, we expect that comparative patch analysis will provide useful spatial restraints for the structural characterization of an increasing number of binary and higher-order protein complexes.

Citation: Korkin D, Davis FP, Alber F, Luong T, Shen MY, et al. (2006) Modeling of protein interactions by analogy: Application to PSD-95. PLoS Comput Biol 2(11): e153. doi:10.1371/journal.pcbi.0020153

Introduction

Protein–protein interactions play a key role in many cellular processes [1,2]. An important step towards a mechanistic description of these processes is a structural characterization of the proteins and their complexes [3–6]. Currently, there are two computational approaches to predict the structure of a protein complex given the structures of its components, comparative modeling [6–11] and protein–protein docking [12–15].

In the first approach to modelling a target complex, standard comparative modelling or threading methods build a model using the known structure of a homologous complex as a template [7,10]. The applicability of this approach is limited by the currently sparse structural coverage of binary interactions [6]. In the second approach, an atomic model is predicted by protein–protein docking, starting from the structures of the individual subunits without any consideration of homologous interactions [12–16]. This docking is usually achieved by maximizing the shape and physicochemical complementarity of two protein structures, through generating and scoring a large set of possible configurations [13,16]. Experimental information, such as that obtained from NMR chemical shift mapping, residual dipolar couplings, and cross-linking, can also be used to guide protein docking [17–20]. While docking is applicable to any two subunits whose structures are known or modeled, both the sampling of relevant configurations and the discrimination of native-like configurations from the large number of non-native alternatives remain challenging [15].

Comparative Patch Analysis

Here, we propose a third approach to modeling complexes between two structures (Figure 1). The approach, called comparative patch analysis, is a hybrid of protein docking and comparative modeling based on a template complex, with a greater applicability than comparative modeling and a higher accuracy than docking. Comparative patch analysis relies on our prior analysis of the location of binding sites within families of homologous domains [21]. This analysis

Editor: Burkhard Rost, Columbia University, United States of America

Received June 8, 2006; **Accepted** October 4, 2006; **Published** November 10, 2006

A previous version of this article appeared as an Early Online Release on October 5, 2006 (doi:10.1371/journal.pcbi.0020153.eor).

Abbreviations: DOPE, Discrete Optimized Protein Energy; GBS, GMP-binding site; GK, guanylate kinase–like; MALDI–TOF, matrix-assisted laser desorption ionization–time of flight); PDZ, PSD-95, DLG, and ZO-1; PDB, Protein Data Bank; PRBS, proline-rich binding site; PSD, postsynaptic density; SAXS, small angle X-ray scattering; SCOP, Structural Classification of Proteins; SH3, Src homology 3

* To whom correspondence should be addressed. E-mail: sali@salilab.org

Synopsis

Protein–protein interactions play a crucial role in many cellular processes. An important step towards a mechanistic description of these processes is a structural characterization of the proteins and their complexes. The authors developed a new approach to modeling the structure of protein complexes and multidomain proteins. The approach, called comparative patch analysis, complements the two currently existing approaches for structural modeling of protein complexes, comparative modeling, and protein docking. It limits the configurations refined by molecular docking to the structurally defined interactions of each of the complex components, or their homologs, with any other protein, irrespective of its fold; the final prediction corresponds to the best-scoring refined configuration. The authors applied comparative patch analysis to predict the structure of the core fragment of PSD-95, a five-domain protein that plays a major role in the postsynaptic density at neuronal synapses. The study suggests two alternate configurations of the core fragment that potentially correspond to the different functional forms of PSD-95. This finding provides a possible structural explanation for the experimentally observed cooperative folding transitions in PSD-95 and its homologs.

indicated that the locations of the binding sites are often conserved irrespective of the folds of their binding partners. The structure of the target complex can thus be modeled by restricting protein docking to only those binding sites that are employed by homologous domains. As a result, comparative patch analysis benefits from knowledge of all interactions involving either one of the two partners.

We find that comparative patch analysis increases the prediction accuracy relative to protein docking. It is able to correctly identify the binding mode in 70% of 20 benchmark complexes, predicting the overall structure with an average improvement in all-atom RMS error of 13.4 Å, compared with protein docking. In contrast, protein docking correctly identifies the binding mode in 30% of the complexes.

PSD-95 Protein

We apply comparative patch analysis to model the structure of PSD-95 protein. PSD-95 is abundant in the postsynaptic density (PSD), a cytosolic organelle that plays a pivotal role in neuronal signaling [22–26]. PSD-95 serves as a major scaffold for other signaling proteins, participates in receptor and channel clustering, and performs a range of other diverse functions [25–31].

PSD-95 is a member of the membrane associated guanylate kinase (MAGUK) family. It is composed of three PDZ (named after PSD-95, DLG, and ZO-1) domains followed by SH3 (Src homology 3) and GK (guanylate kinase-like) domains [32,33]. Isolated structures of all three PDZ domains as well as the structure of the SH3-GK domain complex have been solved [34–38]. The complete structure of PSD-95 has not been determined, but experiments suggest that it adopts multiple conformations [39,40]. The structures of these conformations are necessary for functional insight into the regulation of PSD-95 activity [40,41].

We apply comparative patch analysis to model the structure of the complex between the third PDZ (PDZ_3), SH3, and GK domains. These domains comprise 60% of the PSD-95 mass and are the defining domains of the membrane-associated guanylate kinase family. We propose two configurations that satisfied all imposed spatial restraints, including

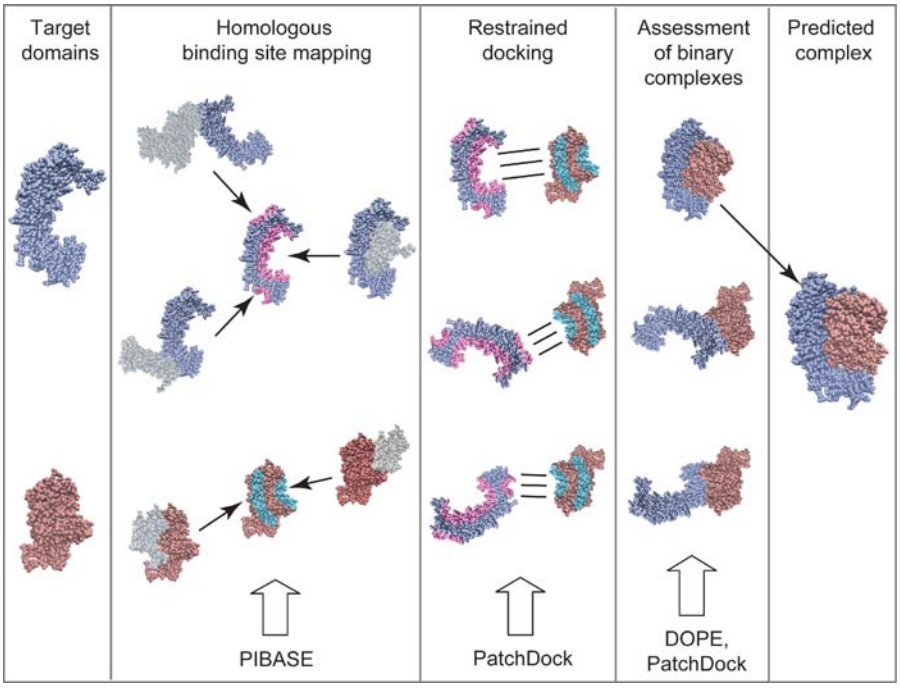

Figure 1. Basic Steps of Comparative Patch Analysis Approach

First, the binding sites of the homologs of each domain are extracted from PIBASE and superposed on its surface. Second, for each pair of the superposed binding sites, we apply a restrained docking of the domains with PatchDock to obtain a set of candidate binary domain complexes. Each of the binary complexes is then ranked using geometrical complementarity and statistical potential, and the top-ranked complex is selected to be a final prediction.

doi:10.1371/journal.pcbi.0020153.g001

previously observed binding sites, consistency with the given linker length, and physicochemical complementarity of the interacting surfaces. In addition, the prediction is in concordance with and rationalizes available biochemical, structural, and evolutionary data.

The paper begins by comparing the performance of comparative patch analysis with protein docking on a benchmark set of 20 binary protein complexes (Results). Next the application of comparative patch analysis to predicting the structure of PDZ_3-SH3-GK complex is described (Results). We combine the predictions with existing experimental evidence to propose a mechanism for the intramolecular regulation of PSD-95 (Discussion). In addition, we discuss the advantages and disadvantages of comparative patch analysis and briefly outline future directions. Finally, we present the details of the method (Methods).

Results

To assess the method, we applied comparative patch analysis to a benchmark set of 20 binary complexes of known structure (Methods). We then used comparative patch analysis to predict the tertiary structure of the PSD-95 core fragment that contains PDZ_3, SH3, and GK domains.

Assessment of Comparative Patch Analysis

Comparative patch analysis may be applied to two scenarios where binding site information is available for both or just one of the interacting subunits. We compared their performance to that of protein docking (Methods). In both scenarios, comparative patch analysis was significantly more accurate than protein docking (Figure 2). Using both (one) binding site information, the overall structure was improved for 13 (8) of the 20 complexes, with an average improvement in the all-atom RMS error of 13.4 Å (6.1 Å). The interface coverage increased by 29% (6%), and the binding site coverage by 30% (10%), on average (Table 1). In 15 (8) complexes, comparative patch analysis produced models with all-atom RMS error <3 Å, while protein docking achieved this accuracy for only six complexes. Comparative patch analysis identified the interfaces correctly in 15 (9) complexes, including 8 (7) multi-domain proteins and 7 (2) protein complexes, while protein docking achieved this for 7 complexes, including 6 multi-domain proteins and 1 protein complex. In those 15 complexes, on average 71% of the predicted residue contacts were observed in the native structures (standard error is 5%). As expected, comparative patch analysis was more accurate using binding site information for both interacting domains compared with using only one.

Application to PSD-95

Next we modeled the tertiary structure of the core fragment of rat PSD-95, which includes the PDZ_3, SH3, and GK domains (Figure 3, see Figure 3A). As this fragment contains three independent domains, there are three possible domain–domain interactions. The interaction between SH3 and GK domains were known from X-ray crystallography [37,38]. Here

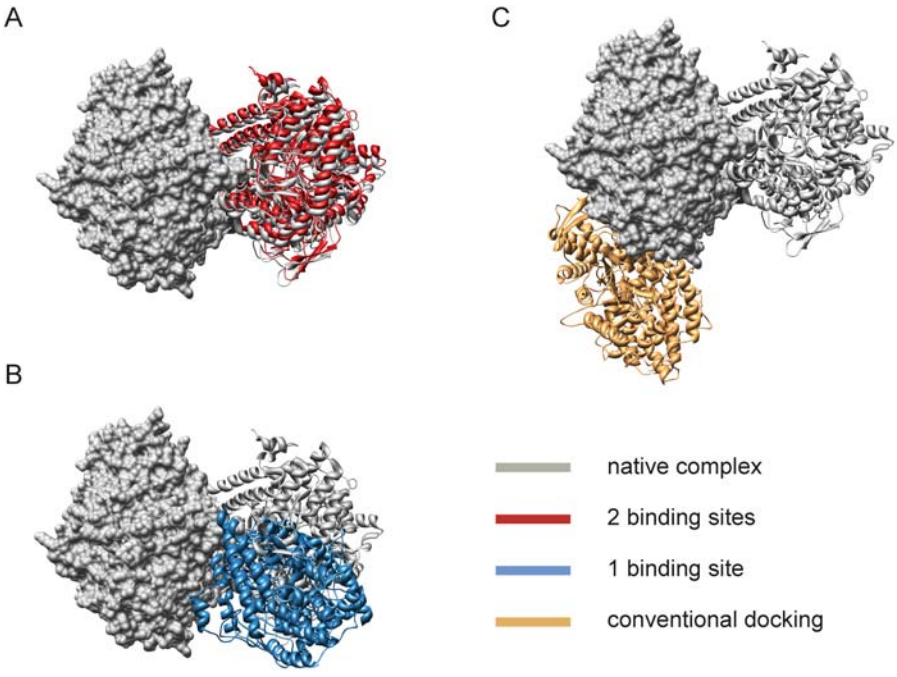

Figure 2. Examples of Predicted Protein Interface between Two Subunits for a Pyruvate Formate–Lyase Protein Complex from Our Benchmark Set
Shown are the structures of the native complex (grey) together with the best-scoring models that were predicted by comparative patch analysis using binding site information for (A) both, or (B) just one of the interacting subunits, and (C) by conventional protein docking, where no binding site information is provided. The predicted and native structures are superposed using one of the two subunits, which is represented by its accessible surface. The remaining subunits of the predicted structures are shown in the ribbon representation colored red, blue, and orange, correspondingly. In both scenarios, comparative patch analysis was significantly more accurate than protein docking. Using both binding sites, comparative patch analysis accurately predicted the protein interaction interface, including the relative orientation of subunits. The accuracy of interface prediction by our approach using only one binding site was significantly reduced, while it was still able to predict the binding sites near their native locations. The conventional protein docking failed to accurately predict either the relative orientation of subunits or the locations of their binding sites.
doi:10.1371/journal.pcbi.0020153.g002

Table 1. Assessment of Comparative Patch Analysis Approach

Number	PDB	Domain Chains and Boundaries		Restrained Docking (Two Binding Sites)			Restrained Docking (One Binding Site)			Unrestrained Docking		
		Domain1	Domain2	f_{BS}	f_{In}	RMSD	f_{BS}	f_{In}	RMSD	f_{BS}	f_{In}	RMSD
1	1l5k	A(4:349)	B(4:349)	0.96	0.88	0.64	0.23	0.00	20.45	0.05	0.00	34.35
2	1iew	A(1:388)	A(389:602)	0.92	0.85	0.64	0.92	0.83	0.71	0.79	0.48	4.20
3	1nfz	A(4:179)	B(4:183)	0.85	0.81	1.02	0.86	0.87	1.34	0.00	0.00	44.77
4	1orb	(1:149)	(150:293)	0.86	0.78	1.09	0.85	0.78	0.60	0.85	0.78	0.60
5	1cm5	A(1:759)	B(1:759)	0.86	0.73	1.10	0.37	0.00	30.41	0.00	0.00	63.34
6	1bwr	A(5:216)	B(5:216)	0.85	0.72	1.32	0.50	0.07	19.97	0.50	0.07	19.97
7	3pax	(662:796)	(797:1011)	0.77	0.66	2.07	0.77	0.66	2.07	0.77	0.66	2.07
8	1qck	A(1:89)	B(1:89)	0.91	0.68	2.47	0.10	0.00	47.82	0.02	0.00	46.01
9	1j93	A(10:352)	B(10:352)	0.43	0.02	33.02	0.25	0.00	33.02	0.08	0.00	33.02
10	1nsm	A(2:340)	B(2:347)	0.00	0.00	43.43	0.20	0.00	32.93	0.00	0.00	43.43
11	1g9a	A(862:1079)	A(1080:1289)	0.96	0.86	0.47	0.96	0.87	1.23	0.96	0.87	1.23
12	1fn7	A(9:135)	A(136:325)	0.95	0.78	0.85	0.84	0.78	0.81	0.84	0.78	0.81
13	1egu	A(171:540)	A(541:814)	0.86	0.74	0.98	0.78	0.61	3.12	0.78	0.61	3.12
14	1c97	A(2:528)	A(529:754)	0.88	0.73	1.11	0.93	0.82	0.91	0.93	0.82	0.91
15	2sic	E(1:275)	I(7:113)	0.83	0.80	1.33	0.27	0.00	26.86	0.30	0.00	13.19
16	1ltx	A(24:443)	B(6:331)	0.83	0.75	1.47	0.26	0.01	17.36	0.81	0.66	1.66
17	1pys	B(1:190)	B(191:399)	0.86	0.67	1.59	0.81	0.60	2.13	0.17	0.01	40.74
18	1e7v	A(525:725)	A(726:1094)	0.50	0.07	18.57	0.14	0.00	27.16	0.14	0.00	33.57
19	1tco	A(21:372)	C(1:107)	0.03	0.00	23.71	0.28	0.02	16.27	0.28	0.02	16.27
20	1ikn	A(19:191)	D(73:293)	0.17	0.01	39.73	0.04	0.00	36.08	0.00	0.00	40.76

The sample set of 20 binary protein complexes was used to evaluate our method. These complexes come from two groups. Each subunit of a complex in the first group is a member of a SCOP family that has been observed to interact with only one other SCOP family. In turn, each subunit from the second group of complexes comes from a SCOP family that has been observed to interact with multiple SCOP families. As expected, the accuracy of comparative patch analysis using two binding sites was higher for the first group of complexes ($\overline{\Delta RMSD}$ = 13.4 Å, $\overline{\Delta f_{IN}}$ = 29%, $\overline{\Delta f_{BS}}$ = 30%) than for the second one ($\overline{\Delta RMSD}$ = 6.1 Å, $\overline{\Delta f_{IN}}$ = 6%, $\overline{\Delta f_{BS}}$ = 10%).

doi:10.1371/journal.pcbi.0020153.t001

we focused on characterizing the other two putative interactions, namely between the PDZ_3 and SH3 as well as between PDZ_3 and GK domains. For both cases, we applied comparative patch analysis using two subunits, one containing PDZ_3 and the second one containing the interacting SH3 and GK domains. The first interaction was modeled using the binding site locations of the PDZ_3 and SH3 in all known homologs, while the second was modeled using those of the PDZ_3 and GK homologs (Methods). The results for both interactions are described next, followed by the comparison with results obtained by conventional protein docking.

PDZ_3–SH3 Interaction

The comparative patch analysis protocol was applied using the nonredundant sets of 49 PDZ_3 and 26 SH3 binding sites combined to give all 1,274 possible input pairs. The protocol resulted in an ensemble of 503 models of the PDZ_3–SH3 complex (Methods).

The interface of the best-scoring model (1493 $Å^2$) that satisfied the interdomain linker restraint consisted primarily of the C- and N-terminal residues of PDZ_3 as well as the residues of the proline-rich binding site (PRBS) and the first two beta strands of SH3 (Figure 3B). The PDZ_3 hydrophobic cleft, known to be essential for binding the C-termini of other proteins, remained accessible in this complex [42,43]. The N-terminus of PDZ_3 contains a PREP motif (P308, R309, E310, P311) which belongs to the canonical PXXP family of motifs known to interact with the PRBS of SH3 [44–47]. In the best-scoring model, this motif was in proximity to the PRBS (Figure 3B). Our confidence in this predicted binding mode was bolstered when its binding residues were found to occur in regions of high localization derived from the ten best scoring models that satisfied the linker restraint (Figure 4). Ninety-four percent of the binding residues in the best-scoring model were found to occur in no less than 70% of the ten best-scoring models.

PDZ_3–GK Interaction

The comparative patch analysis protocol was applied to the PDZ_3–GK complex using 10,731 input pairs formed by combining the nonredundant sets of 49 PDZ_3 and 219 GK binding sites. The protocol resulted in an ensemble of 1,929 models (Methods).

The interface of the best-scoring model was extensive (2729 $Å^2$), and includes, among others, residues located at the C-terminus and near the hydrophobic cleft of PDZ_3 as well as a large groove of GK formed by the GMP-binding and LID regions [48–50] (Figure 3C). The analysis of the ten best-scoring models satisfying the interdomain linker restraints revealed high localization of the binding residues for both domains (Figure 4). The residues of PDZ_3 with the highest localization were located around the domain's hydrophobic cleft and the C-terminus (Figure 4). In addition, the entire GMP-binding site (GBS) of the GK domain and part of the hydrophobic cleft of the PDZ domain became inaccessible in most top-scoring models, including the best-scoring one. Forty-six percent of the binding residues in the best-scoring model were found to occur in no less than 70% of the ten best-scoring models.

Comparison with Protein Docking Results

To evaluate the effect of binding-site information on modeling the PDZ_3–SH3–GK complex, conventional protein docking of the PDZ_3 and SH3–GK domains was performed

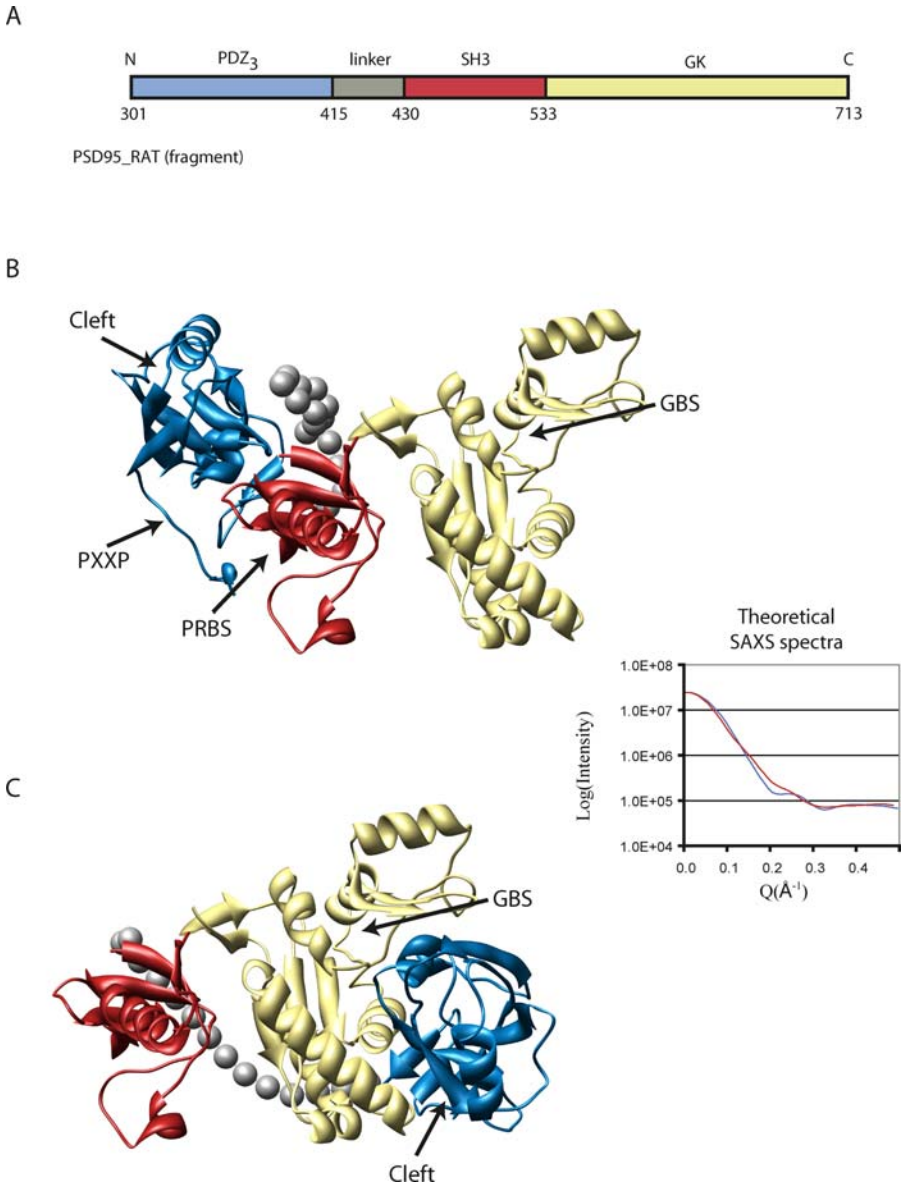

Figure 3. Two Binding Modes of the Core Fragment of Rat PSD-95

The PDZ_3 domain is shown in blue, SH3 in red, and GK in yellow. The grey spheres correspond to the residues of the interdomain linker between PDZ_3 and SH3. Locations of the hydrophobic cleft (Cleft) and PXXP motif (PXXP) in PDZ_3, PRBS in SH3, and the GBS in GK are shown by arrows. (A) The domain architecture of the core fragment. (B) The first predicted configuration. (C) The second predicted configuration. The difference between the theoretically calculated SAXS spectra of the first (red) and second (blue) configurations is significantly larger than the anticipated experimental error.

doi:10.1371/journal.pcbi.0020153.g003

(Methods). Analysis of the ten best-scoring models satisfying the interdomain linker restraint revealed that the binding sites of both PDZ_3 and SH3–GK domains were significantly delocalized compared with the comparative patch analysis models. Moreover, the binding residues of the top-scoring models almost completely covered the domain surfaces (93% and 81% of the PDZ_3 and SH3–GK domains) (Figure 4). The best-scoring model obtained using protein docking was different from both the best PDZ_3–SH3 and the PDZ_3–GK comparative patch analysis models (unpublished data).

PXXP Motif Conservation Analysis

The proximity of the PDZ_3 PXXP motif and the SH3 PRBS in the predicted model prompted a search for PXXP motifs in the sequences of six PSD-95 proteins and splice variants from four species to assess the significance of this observation. All sequences contained at least one form of a PXXP motif or noncanonical SH3-binding motif that could mimic the PXXP motif (Table 2) [47]. The human, rat, and mouse proteins all contained a PREP motif in PDZ_3; the zebrafish protein did not. Five other potential SH3 binding motifs were found outside of known domains; two at the N-terminus, one at the C-terminus, and two in the interdomain linker between PDZ_2 and PDZ_3. The conservation of the PREP sequence in PDZ_3 from the mammalian species suggests that its interaction with SH3 may be functionally significant.

Proteolysis of PSD-95

Limited proteolysis of recombinant PSD-95 with Proteinase K produces a prominent ~48 kDa band at 30 min (Figure 5).

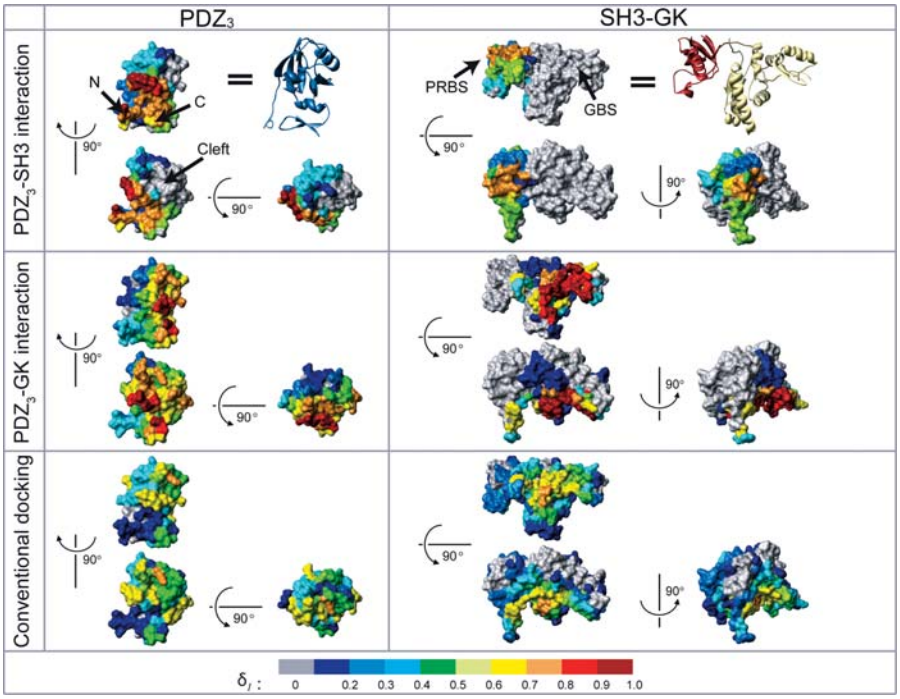

Figure 4. The Localization of Binding Sites for Both Modeled Configurations of the PDZ_3–SH3–GK Core Fragment Compared with Protein Docking

Top ten scoring models were selected for both interactions (PDZ_3–SH3, PDZ_3–GK) obtained using comparative patch analysis and using conventional protein docking. The localization index δ_I of a residue defines the relative frequency of its participation in the interaction interface. The residues that are colored grey do not participate in the interface of any of the top ten models. The PRBS in SH3 and the GBS in GK are shown by arrows.

doi:10.1371/journal.pcbi.0020153.g004

Matrix-assisted laser desorption ionization (MALDI) analysis of peptides generated by tryptic digestion of this band indicates that it represents the sequence from residues 300 to 721, which corresponds to the PDZ_3 and SH3–GK domains (mass accuracy, $\Delta ppm \leq 13$). Further digestion leads to the disappearance of the PDZ_3–SH3–GK entity and the appearance of a stable ~34 kDa fragment. The 34-kDa band was identified by MALDI analysis as the SH3–GK domains, encompassing residues 429 to 721 ($\Delta ppm \leq 10$ for all detected peptides). Cleavage with thermolysin, another nonspecific protease, generates similarly sized stable fragments (unpublished data).

Table 2. Cross-Species Analysis of PXXP Motif in PSD-95 Proteins

Motif	Position in PSD-95 Sequence	Accession ID	Species	Splice Variant?
PREP	PDZ_3 domain	P78352	Human	No
		P31016	Rat	No
		Q62108	Mouse	No
PRAP	N-terminal region	P78352–2	Human	Isoform 2
		Q62108–2	Mouse	Isoform 2
PAKP	N-terminal region	Q6R005	Zebrafish	No
PTSP	A linker between PDZ_2 and PDZ_3	P78352	Human	No
		Q62108	Mouse	No
		P31016	Rat	No
PSSP	A linker between PDZ_2 and PDZ_3	Q6R005	Zebrafish	No
RVAK	C-terminal region	Q6R005	Zebrafish	No

The human, rat, and mouse proteins all contained a PREP motif in PDZ_3; the zebrafish protein did not. Five other potential SH3 binding motifs were found outside of known domains; two at the N-terminus, one at the C-terminus, and two in the interdomain linker between PDZ_2 and PDZ_3. The conservation of the PREP sequence in PDZ_3 from the mammalian species suggests that its interaction with SH3 may be functionally significant.

doi:10.1371/journal.pcbi.0020153.t002

Discussion

We have introduced comparative patch analysis, an approach to the modeling of a complex between two subunit structures, and applied it to the protein PSD-95, a key neural-signaling scaffold. The approach relies on structurally defined interactions of each of the complex components, or their homologs, with any other subunit, irrespective of its fold (Figure 1). We assessed comparative patch analysis for its increased applicability relative to comparative modeling as well as increased accuracy relative to conventional protein docking (Figure 2, Table 1). Next, comparative patch analysis was applied to model the structure of a core fragment of rat PSD-95, containing the PDZ_3, SH3, and GK domains, resulting in two predicted configurations (Figures 3 and 4). The model was experimentally supported by limited proteolysis (Figure 5). In addition, the prediction is in concordance with and rationalizes available biochemical, structural, and evolutionary data (Figures 3 and 4, Table 2).

Comparative Patch Analysis

By limiting the configurational search to the known binding modes of the homologous subunits and applying a physical assessment of candidate complex structures, comparative patch analysis benefits from the advantages of both homology-driven and physics-driven docking. Its coverage is larger than that of comparative modeling and its accuracy is higher than that of protein docking (Figure 2), although the

A

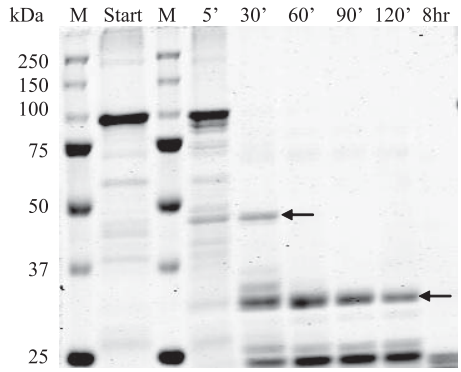

B

```
  1 mdclcivttk kyryqdedtp plehspahlp nqansppviv ntdtleapgy elqvngtege
 61 meyeeitler gnsglgfsia ggtdnphigd dpsifitkii pggaaaqdgr lrvndsilfv
121 nevdvrevth saavealkea gsivrlyvmr rkppaekvme iklikgpkgl gfsiaggvgn
181 qhipgdnsiy vtkiieggaa hkdgrlqigd kilavnsvgl edvmhedava alkntydvvy
241 lkvakpsnay lsdsyappdi ttsysqhldn eishssylgt dyptamtpts prryspvakd
301 llgeedipre prrivihrgs tglgfnivgg edgegifisf ilaggpadls gelrkgdqil
361 svngvdlrna sheqaaialk nagqtvtiia qykpeeysrf eakihdlreq lmnsslgsgt
421 aslrsnpkrg fyiralfdyd ktkdcgflsq alsfrfgdvl hvidagdeew wqarrvhsds
481 etddigfips krrverrews rlkakdwgss sgsqgredsv lsyetvtqme vhyarpiiil
541 gptkdrandd llsefpdkfg scvphttrpk reyeidgrdy hfvssrekme kdiqahkfie
601 agqynshlyg tsvqsvreva eqgkhcildv sanavrrlqa ahlhpiaifi rprslenvle
661 inkriteeqa rkafdratkl eqeftecfsa ivegdsfeei yhkvkrvied lsgpyiwvpa
721 rerl
```

Figure 5. The PDZ_3–SH3–GK and SH3–GK Domains Are Stable Fragments

(A) Coomassie-stained gel (10% acrylamide) of aliquots from limited proteolysis of PSD-95 by Subtilisin proteinase: panels 1 and 3, Precision Plus Protein molecular weight marker (Bio-Rad, http://www.bio-rad.com); panel 2, starting sample prior to proteinase addition; panels 4, Lanes 4–9, Aliquots at 5, 30, 60, 90, 120 min, and 8 h after protease addition (as labeled). Arrows point to stable fragments that were excised from the gel and analyzed by mass spectrometry as described in Methods.

(B) Sequence of Rat PSD-95: underlined are the peptide sequences identified by mass spectrometry from the ~34 kDa stable fragment corresponding to residues 429–721 (33,944 kDa). In bold are the sequences derived from the ~48 kDa stable fragment comprising residues 300–721 (47,796 kDa).

doi:10.1371/journal.pcbi.0020153.g005

coverage and accuracy are lower than those of protein docking and comparative modeling, respectively.

At least one binding site is available for 1,989 of the 3,114 total Structural Classification of Proteins (SCOP) domain families (release 1.69, July 2005). Eight hundred fifty of these families contain between ten and 100 binding sites, allowing the exhaustive pairwise docking that is currently required. Thus, the applicability of comparative patch analysis extends to approximately 41%, and in the current implementation is computationally feasible for 8%, of the ~4,850,000 theoretically possible binary domain–domain interactions. The coverage of conventional protein docking is 100%, while the comparative modeling approach is applicable to only 2,126 pairs of families, which constitutes 0.06% of the theoretically possible interactions.

When compared with protein docking, comparative patch analysis was able to correctly identify the binding mode in 40% more benchmark complexes, predicting the overall structure of the complexes with an average improvement in all-atom RMS error of 13.4 Å. The method also exhibits robustness to small errors in the locations of the specified binding sites, due to the configurational search performed by the docking procedure. In the benchmark set of complexes with known structures, a minimal threshold of 75% overlap between the initially specified and resulting refined binding sites captured all but one of the good models (LRMS error less than 3 Å), while allowing no false positives.

PSD-95 Protein: Predicting the Structure of the Core Fragment by Analogy

Evolutionary and experimental evidence for intermolecular interaction between PDZ_3 and SH3–GK domains. When modeling the structure of the PDZ_3–SH3–GK fragment, we assumed an interaction between the PDZ_3 and SH–GK domains. PDZ_3 is a good candidate for interaction with the SH3–GK domains because it is immediately upstream of SH3, separated by a relatively short 14-residue linker. To investigate whether or not PDZ_3 interacts with SH3–GK, the analysis of domain co-occurrence, as well as limited proteolysis, were applied.

A survey of the domain architectures of proteins that contain both SH3 and GK domains revealed that the proteins either do not have other domains or also contain at least one PDZ domain always preceding the SH3–GK tandem domain. The minimal architecture that contains at least one PDZ, SH3, and GK domain consists of only these three domains. This pattern strongly suggests a physical interaction between the SH3–GK tandem and the preceding PDZ domain [51,52].

The stable fragments resulting from limited proteolysis of PSD-95 by nonspecific proteases reflect the cleavage of accessible loops, rather than cleavage at a particular substrate sequence. We identified stable PDZ_3–SH3–GK and SH3–GK fragments by mass spectrometry, demonstrating susceptibility of PSD-95 to protease cleavage at sites between the PDZ_2 and

PDZ_3 domains and between the PDZ_3 and SH3–GK domains. Limited proteolysis with trypsin (unpublished data) also supports the conclusion that the PDZ_3 and SH3–GK domains are stable protein structures. These data are consistent with intramolecular interactions between the PDZ_3 and the SH3–GK domains of PSD-95.

Application of comparative patch analysis. Modeling the structure of the core PSD-95 fragment is challenging for a number of reasons. First, the structures of neither PDZ–SH3 nor PDZ–GK complexes are available, rendering comparative modeling inapplicable in this case. Moreover, conventional protein docking results were ambiguous, generating a varied ensemble of PDZ_3 and SH3–GK complexes without a predominant binding mode (Figure 3C). On the other hand, each of the domain families is known to repeatedly utilize a small number of binding sites for different protein interactions. For instance, PDZ domains bind the C-termini of several different proteins through its hydrophobic cleft [42,53]. Similarly, the PRBS of SH3 domains recognizes PXXP-sequence motifs in a variety of proteins [45,46]. These observations suggest that comparative patch analysis is suited for modeling the PSD-95 core fragment.

Functional roles of the predicted configurations. Comparative patch analysis of the PDZ_3–SH3–GK fragment found two possible configurations that satisfied all imposed spatial restraints, including previously observed binding sites, consistency with the given linker length, and physicochemical complementarity of the interacting surfaces. In addition, the ensemble of models produced by comparative patch analysis for each interaction type (PDZ_3–SH3, PDZ_3–GK) exhibited a single predominant binding mode. The binding sites forming the interaction interfaces of these models are located at the same or similar regions of the protein surface (Figure 4). Therefore, the binding modes are predicted with relative confidence. Multiple stable configurations of PSD-95 and its close homologs have recently been suggested independently based on biochemical studies [40,54] and single-particle electron microscopy experiments [41]. As we describe below, we suggest the two binding modes have clear functional implications.

The two predicted configurations exhibit structural properties that suggest unique functional roles. In the first configuration, the hydrophobic cleft of the PDZ domain and the GBS of the GK domain are both accessible, suggesting that this configuration corresponds to an active state in which binding of other proteins at these two sites can occur (Figure 3B). These binding sites are thought to mediate intermolecular interactions essential for the scaffolding role of PSD-95 [42,49,55–57]. In contrast, both binding sites are buried in the second configuration, by the interface between the PDZ_3 and GK domains (Figure 3C), which is suggestive of an alternative functional state. This second configuration points to an efficient intramolecular regulatory mechanism for switching the functional state with a single interaction. Similar regulatory mechanisms have been observed in other signaling networks, such as the TCR and MAPK systems [58,59], indicating this regulation may be a general feature of signaling pathways.

This two-state model also provides a structural explanation for the change in binding affinity between the GK domain and MAP1A protein in the presence of the PDZ_3 domain [60]. It has been shown that the GK domain alone is able to bind MAP1A. In the presence of PDZ_3, this binding affinity is dramatically reduced. The affinity is recovered upon titration of a C-terminal peptide of CRIPT known to specifically interact with the hydrophobic cleft of PDZ_3. This competitive binding suggests that binding to MAP1A and binding to PDZ_3 are mediated by the same GK binding site. Our model is in complete agreement with this hypothesis and provides a structural explanation for these observations.

It is known that SH3 domains bind proteins with PXXP sequence motifs through their proline-rich binding regions. The proximity of the PDZ_3 PXXP motif to the SH3 PRBS in the first configuration proposed by comparative patch analysis is consistent with the classical SH3–PXXP motif recognition. A similar PXXP-mediated intermolecular PDZ–SH3 interaction has been previously suggested to occur in syntenin [61]. Sequence analysis of PSD-95 from different species indicates that PXXP motifs are not found in its other two PDZ domains, although such motifs are found in the PDZ_2–PDZ_3 linkers and the flexible N-terminus (Table 2). Recent studies have demonstrated the importance of disordered regions in binding events [62], suggesting that future investigation of interactions of these PXXP motifs using recently developed flexible docking algorithms [63] should prove fruitful.

The limited proteolysis experiment (Figure 5) is a first step to verifying the intramolecular interactions suggested by comparative patch analysis. The two functional states hypothesis, outlined in the Discussion, points to a number of experiments that could shed light on the structure and function of PSD-95. First, the proposed regulation of the PSD-95 activity by PDZ_3–specific C-terminal peptides can be further tested using immunoprecipitation and yeast two-hybrid experiments similar to those performed for other GK-mediated interactions [60] (e.g., with the GKAP protein [57]). If the proposed regulation mechanism is verified, experimental control of the PSD-95 activity may become possible, enabling detailed study of the functional differences between the two states. Next, the intramolecular interactions proposed here can be tested by a variety of experimental techniques [64], including NMR spectroscopy [65], site-directed mutagenesis [66], hydrogen/deuterium exchange combined with mass spectrometry [67], and small angle X-ray scattering (SAXS) [68]. In particular, site-directed mutagenesis [66] of the interface residues in the first proposed state (see Datasets S1 and S2) could be used with pull-down assays to validate the predicted interaction interface [69]. In addition, the lack of accessibility of the GBS in the second state could be tested using nucleotide-binding assays [70,71]. Finally, the shapes of the calculated SAXS spectra for the best-scoring models in both conformations are substantially different (Figure 3). Thus, we expect the experimentally obtained SAXS spectra to be helpful in distinguishing between the two PSD-95 states.

Comparative patch analysis for characterizing the quaternary structure of protein assemblies provides a framework for combining data from known protein structures with a physical assessment of protein interactions. This framework will benefit from future developments in protein–protein docking, such as the explicit treatment of flexibility and more accurate scoring functions. We are currently developing an automated comparative patch analysis pipeline for large-scale modeling of protein complexes via a Web server. In closing, we expect that comparative patch analysis will

provide useful spatial restraints for the structural characterization of an increasing number of binary and higher order protein complexes, as it did for PSD-95.

Methods

Comparative patch analysis protocol. We start by outlining the steps in comparative patch analysis, followed by a more detailed description. First, for each partner domain in a binary complex, a set of protein binding sites of its homologs represented in PIBASE was identified [72]. Second, these binding sites were mapped onto the partner domain surface using structure-based alignments between the domain and each of its homologs. Third, all pairs of the mapped binding sites were converted by restrained docking to obtain candidate models of the binary complex. This ensemble of models was then ranked using a measure of geometric complementarity and a statistical potential score.

Extracting and mapping binding sites of domain homologs. For each of the two partner domains, we first defined a family of its homologs. Several schemes both dissect proteins into domains and cluster them into families, based on sequence, structure, and/or function [73–76]. We used the family definitions in SCOP [73]. Domains that belong to the same SCOP family usually share at least 30% sequence identity or the same biological function.

For a given SCOP family, the set of binary domain interfaces between its members and other domains was obtained from PIBASE, our comprehensive relational database of all structurally characterized interfaces between pairs of protein domains [72]. The domain–domain interfaces in PIBASE were extracted from protein structures in the Protein Data Bank (PDB) [77] and Protein Quaternary Structure (PQS) server [78] using domain definitions from the SCOP and CATH domain classification systems [73,74]. An interface is defined by a list of pairs of residues, one from each protein, that are in contact with each other. Each binding site consists of the residues that are within 6.05 Å of its partner domain, where the threshold is defined between any two nonhydrogen atoms.

The binding site residues from all domain family members were then mapped onto the partner domain using structure-based alignments obtained by DaliLite. DaliLite uses a Monte Carlo procedure to find the best alignment by optimizing a similarity score defined in terms of equivalent intramolecular distances [79].

Modeling protein complexes. The structures of binary protein complexes were predicted by restrained docking using the PatchDock software [80,81]. PatchDock uses an algorithm for rigid body docking that searches for the maximal geometric complementarity between two protein structures, optionally restrained by having to match two user-specified binding sites. Here, we provided all pairs of mapped binding sites, one from each target domain, as input for individual PatchDock runs. When a resulting refined model was inconsistent with the specified binding sites, it was discarded. More specifically, a model was considered not to correspond to a specified binding site interaction if the binding sites predicted by docking had less than 75% of their residues in common with the specified binding sites (the normalization is based on the size of the smaller of the specified and predicted binding sites).

The resulting binary complexes were scored using a combination of two independent scores, the geometric complementarity function of PatchDock and DOPE (Discrete Optimized Protein Energy) score. DOPE is a distance-dependent pairwise statistical potential calculated from known protein structures and available through the MODELLER program [82,83]. The configurations in the ensemble of models were ranked by a sum of the PatchDock and DOPE scores, first scaled to lie in the range between 0 and 1.

Assessment of comparative patch analysis. A benchmark set of 20 binary domain complexes was used to evaluate comparative patch analysis (Table 1). These complexes were divided into two groups. Each subunit of a complex in the first group is a member of a SCOP family that has been observed to interact with only one other SCOP family. In contrast, each subunit from the second group of complexes comes from a SCOP family that has been observed to interact with multiple SCOP families. The complexes were randomly selected from PIBASE such that the number of interactions available for the families of each component ranged between ten and 100. In total, there are 11 protein complexes (noncovalently linked domains) and nine multidomain proteins (covalently linked domains) in the benchmark set.

As in previous data-dependent approaches for modeling the structures of protein interactions [18,84,85], we have tested our method using a benchmark set designed within its scope of applicability. Our method is applicable only to protein complexes for which structures of the subunits or their homologs interacting with other proteins are available. This constraint on applicability also applies to the benchmark structures used to test the method. For this reason, we did not use the two benchmark sets that are generally used for protein docking methods, the set of CAPRI targets [16,86] and a benchmark set developed by Weng and coworkers [87]. The set of 19 CAPRI targets, whose structures are publicly available, was not an appropriate benchmark for our method because the majority of the structures either (i) contain subunits consisting of multiple SCOP domains ($n = 7$: T02–T07, T19), (ii) are not annotated by SCOP ($n = 4$: T09, T13, T20, T21), or (iii) there are no observed binding sites available for patch analysis ($n = 4$: T11, T12, T15, T19). This leaves five structures (T01, T08, T10, T14, T18) on which comparative patch analysis can be tested. Similarly, of the 63 rigid-body docking targets in the Weng benchmark set, 37 contain subunits with multiple SCOP domains and two contain subunits for which there are no observed binding sites available for comparative patch analysis. The remaining 24 targets contain subunits for which there is an average of 850 binding sites available for our method. This number of binding sites makes comparative patch analysis computationally very expensive, requiring on average more than two million localized docking calculations per target. There are only five targets in the Weng set that require no more than ten thousand calculations, the threshold we used in selecting our benchmark set. We are currently developing a method to cluster binding sites that would allow a significant reduction in the number of docking calculations required for a target structure, enabling the use of a more comprehensive benchmark set.

Adapting existing benchmarks to assess our method required ad hoc processing such as assigning domain boundaries and classifications, dissecting multidomain complexes into binary domain interactions, and reducing the number of input binding sites. Instead, we developed a benchmark set that is applicable to our method in an automated fashion. In addition, our benchmark set was designed to assess the performance of comparative patch analysis for domain–domain interactions in both multidomain proteins and protein complexes. The targets in the CAPRI and Weng benchmark sets are exclusively protein–protein interaction structures.

To quantify the amount of additional information provided by comparative patch analysis relative to docking, the structure of each protein complex was modeled using three independent protocols, relying on the docking program PatchDock (Methods). In the first protocol, known binding sites for the homologs of both subunits were used to restrain the docking. In the second protocol, known binding sites for the homologs of only one subunit were used to restrain the docking. In the final protocol, no binding site information was used, and conventional protein docking was applied.

Distance metrics. To evaluate the accuracy of comparative patch analysis in predicting the interaction interface and relative orientation of two structurally defined protein domains, the following three measures were used: binding site overlap, interface overlap, and RMS error.

First, we calculate the binding site overlap (O_B), which we define as the percentage of correctly predicted binding site residues:

$$O_B = \frac{1}{2}\left[\frac{N(B_1^{pred} \cap B_1^{exp})}{N(B_1^{pred} \cup B_1^{exp})} + \frac{N(B_2^{pred} \cap B_2^{exp})}{N(B_2^{pred} \cup B_2^{exp})}\right],$$

where $N(B_i^{pred} \cap B_i^{exp})$ is the number of residues in common between the predicted and actual binding sites, and $N(B_i^{pred} \cup B_i^{exp})$ is the total number of contact residues in both binding sites.

Next, we used the interface overlap (O_I), as a measure to assess the predicted interface between the binding sites:

$$O_I = \frac{N(I_{pred} \cap I_{native})}{N(I_{pred} \cup I_{native})},$$

where $N(I_{pred} \cap I_{native})$ is the number of residue contacts in common between the predicted (I_{pred}) and native (I_{native}) interfaces, and $N(I_{pred} \cup I_{native})$is the total number of residue contacts. Interfaces were deemed to be correct when at least half of the residue contacts were identified.

Finally, we calculated the all-atom RMS error between the predicted and native complexes using the L__RMS measure defined in CAPRI [88]. The predicted and native structures were superposed using the larger of the two domains, and the RMS error was calculated for the other domain.

Modeling the PDZ_3–SH3–GK complex of rat PSD-95. *Comparative patch analysis application.* Comparative patch analysis was used to predict the tertiary structure of the rat PSD-95 core fragment that

contains the PDZ_3, SH3, and GK domains. From PIBASE, 126, 298, and 517 protein binding sites were obtained for the PDZ_3, SH3, and GK domains, respectively. The binding sites were mapped onto the target structures. Redundant binding sites were removed so that no pair of binding sites shared more than 95% of their residues, leaving 49, 26, and 219 binding sites for the PDZ_3, SH3, and GK, respectively. The comparative patch analysis protocol was then applied.

We then assessed whether the models were compatible with the 14-residue linker length between the PDZ_3 and SH3 domains. To do so, the linker was modeled as a flexible chain of 14 spheres with 1.9 Å radii and a maximum distance of 3.8 A between consecutive spheres, to mimic the excluded volume of the linker and restrict the maximum spatial separation of the domains. Each model was assessed using the following protocol in MODELLER [83]. First, the positions of the 14 linker residues were placed at random coordinates and then optimized using simulated annealing molecular dynamics and conjugate gradient minimizations. The scoring function consists of terms equal to $\frac{(f-f_0)^2}{\sigma^2}$, where f is the restrained distance and σ is the parameter that regulates the strength of the term. Linker distances are restrained if $f > f_0$, where $f_0 = 3.8$ and $\sigma = 0.05$. Excluded volume restraints between the protein and the linker are imposed if $f > f_0$, where f_0 is the sum of the atomic and linker radii and $\sigma = 0.01$. The optimization of the scoring function was performed in 20 independent trials for each model, and the optimized coordinates of the linker residues with the lowest score were added to the model. As a result of assessment, those models that violated the imposed linker restraints and thus could not have an interdomain linker of such length between PDZ_3 and SH3 domains were removed from the ensemble.

Exhaustive docking. The PDZ_3–SH3–GK models built by comparative patch analysis were compared with those built by exhaustive docking using PatchDock without prior information about the potential binding site [80,81]. The model with the best PatchDock–DOPE score that satisfied the interdomain linker restraint was selected.

Sequence analysis. The SMART domain annotation tool was used to search for proteins containing the PDZ, SH3, and GK domains [89,90]. Proteins and splice variants annotated as PSD-95 proteins were obtained from the UniProt sequence database [91]. The sequences were scanned for known SH3 binding motifs (PXXP, PXXDY, RXXK [47]) using grep regular expression search.

Proteolysis of PSD-95. Rat PSD-95 was cloned into pET47b (+) and expressed as a His-tagged fusion protein (~83.4 kDa) in BL21 (DE3) pLysS cells at 37 °C. Cells were harvested 3–3.5 h after induction by 0.4 mM IPTG. The cell lysate was centrifuged at 17K RPM, and the supernatant was loaded onto a nickel NTA column (Qiagen, http://www1.qiagen.com) and eluted with an imidazole gradient (20 mM to 500 mM). The purest fractions were exchanged (using PD10 columns, Amersham Biosciences, http://www.amersham.com/) to: 20 mM Tris (pH 8), 150 mM NaCl, 5 mM DTT, 10% glycerol for limited proteolysis (protocol based on that of Stroh et al. [92]). Digests of PSD-95 were initiated by adding protease to the following final concentrations: 0.83 μg/ml sequencing grade modified Trypsin (Roche, http://www.amersham.com), 0.1 μg/ml of proteinase (Fluka, http://www.sigmaaldrich.com), or 8.3 μg/ml of thermolysin (Sigma, http://www.sigmaaldrich.com). The thermolysin reaction was also supplemented with 5 mM $CaCl_2$. Digests were incubated at 37 °C and stopped with 5 mM PMSF for trypsin and proteinase, and 10 mM EDTA for thermolysin. Aliquots were taken at 5, 30, 60, 90, 120 min, and 8 h after addition of protease and flash frozen in liquid nitrogen until analysis by SDS-PAGE. Stable fragments were excised from Coomassie-stained gels and subjected to tryptic digestion in the gel piece after reduction with DTT and alkylation with iodoacetamide [92,93]. The tryptic peptides were extracted from gel slices with 5% formic acid in 50% acetonitrile, concentrated in a SpeedVac (Savant Instruments, http://www.combichemlab.com), and desalted with the use of a Zip Tip (Millipore, http://www.millipore.com) before analysis by MALDI–TOF (matrix-assisted laser desorption ionization–time of flight) mass spectrometry. Samples were mixed with either α-cyanohydroxycinnamic acid or a "Universal" MALDI matrix from Fluka. Analyses were performed with a Voyager DE-PRO MALDI–TOF mass spectrometer (Applied Biosystems, http://www.appliedbiosystems.com) that was first externally calibrated using a calibration mix supplied by the manufacturer. The MALDI spectra were recalibrated internally with known peptide masses, e.g., trypsin autolysis peaks or expected masses obtained from in silico digests of the known protein. The software, Prospector MSFIT (University of California San Francisco), was used to identify the tryptic fragments.

The representations of proteins in Figures 1–3 were obtained using Chimera [94], and in Figure 4 with the help of MolMol software [95].

Supporting Information

Dataset S1. The Best Model of the First Configuration of PSD-95 Core Fragment

Found at doi:10.1371/journal.pcbi.0020153.sd001 (229 KB TXT).

Dataset S2. The Best Model of the Second Configuration of PSD-95 Core Fragment

Found at doi:10.1371/journal.pcbi.0020153.sd002 (229 KB TXT).

Accession Numbers

Accession numbers from the Protein Data Bank (http://rcsb.org) for the proteins mentioned in this paper are: rat PSD-95 GK (1JXM), rat PSD-95 PDZ_3 (1BE9), rat PSD-95 PDZ_3 (1BFE), rat PSD-95 SH3 and GK (1JXO), pyruvate formate–lyase protein complex (1CM5).
Accession numbers from the European Bioinformatics Institute SMART database (http://www.ebi.ac.uk/interpro/) for proteins mentioned in this paper are: PSD-95 PDZ (SM00228), PSD-95 SH3 (SM00326), and PSD-05 GK (SM00072).

Acknowledgments

We would like to thank the members of the Sali lab for their valuable comments. We also thank Dr. Friedrich Foerster for help in calculating the theoretical SAXS spectra and Dr. Mona Shahgholi for assistance with mass spectrometry and consultation with the limited proteolysis of PSD-95.

Author contributions. DK and AS conceived and designed the experiments. DK and TL performed the experiments. DK, FPD, FA, MBK, and AS analyzed the data. DK, FA, TL, MYS, VL, and MBK contributed reagents/materials/analysis tools. DK, FPD, FA, TL, MBK, and AS wrote the paper.

Funding. FPD acknowledges a Howard Hughes Medical Institute predoctoral fellowship. TL and MBK acknowledge Materials Research Science and Engineering Centers of the US National Science Foundation for providing partial funds for support of the MALDI–TOF mass spectrometer in the multiuser mass spectrometry laboratory of the Division of Chemistry and Chemical Engineering at California Institute of Technology. We are also grateful for the support of the US National Institutes of Health grant U54 RR022220, US National Science Foundation grant EIA-032645, Human Frontier Science Program, The Sandler Family Supporting Foundation, Hewlett-Packard, NetApps, IBM, and Intel.

Competing interests. The authors have declared that no competing interests exist.

References

1. Pawson T, Nash P (2003) Assembly of cell regulatory systems through protein interaction domains. Science 300: 445–452.
2. Alberts B, Miake-Lye R (1992) Unscrambling the puzzle of biological machines: The importance of the details. Cell 68: 415–420.
3. Park J, Lappe M, Teichmann SA (2001) Mapping protein family interactions: Intramolecular and intermolecular protein family interaction repertoires in the PDB and yeast. J Mol Biol 307: 929–938.
4. Edwards AM, Kus B, Jansen R, Greenbaum D, Greenblatt J, et al. (2002) Bridging structural biology and genomics: Assessing protein interaction data with known complexes. Trends Genet 18: 529–536.
5. Sali A, Glaeser R, Earnest T, Baumeister W (2003) From words to literature in structural proteomics. Nature 422: 216–225.
6. Aloy P, Bottcher B, Ceulemans H, Leutwein C, Mellwig C, et al. (2004) Structure-based assembly of protein complexes in yeast. Science 303: 2026–2029.
7. Marti-Renom MA, Stuart AC, Fiser A, Sanchez R, Melo F, et al. (2000) Comparative protein structure modeling of genes and genomes. Annu Rev Biophys Biomol Struct 29: 291–325.
8. Aloy P, Russell RB (2003) InterPreTS: Protein interaction prediction through tertiary structure. Bioinformatics 19: 161–162.
9. Pieper U, Eswar N, Braberg H, Madhusudhan MS, Davis FP, et al. (2004) MODBASE, a database of annotated comparative protein structure models, and associated resources. Nucleic Acids Res 32 (Database issue): D217–D222.
10. Lu L, Lu H, Skolnick J (2002) MULTIPROSPECTOR: An algorithm for the prediction of protein–protein interactions by multimeric threading. Proteins 49: 350–364.
11. Lu L, Arakaki AK, Lu H, Skolnick J (2003) Multimeric threading-based

prediction of protein–protein interactions on a genomic scale: Application to the *Saccharomyces cerevisiae* proteome. Genome Res 13: 1146–1154.
12. Halperin I, Ma B, Wolfson H, Nussinov R (2002) Principles of docking: An overview of search algorithms and a guide to scoring functions. Proteins 47: 409–443.
13. Smith GR, Sternberg MJ (2002) Prediction of protein–protein interactions by docking methods. Curr Opin Struct Biol 12: 28–35.
14. Wodak SJ, Janin J (2002) Structural basis of macromolecular recognition. Adv Protein Chem 61: 9–73.
15. Wodak SJ, Mendez R (2004) Prediction of protein–protein interactions: The CAPRI experiment, its evaluation and implications. Curr Opin Struct Biol 14: 242–249.
16. Janin J, Henrick K, Moult J, Eyck LT, Sternberg MJ, et al. (2003) CAPRI: A critical assessment of predicted interactions. Proteins 52: 2–9.
17. Clore GM, Schwieters CD (2003) Docking of protein–protein complexes on the basis of highly ambiguous intermolecular distance restraints derived from 1H/15N chemical shift mapping and backbone 15N–1H residual dipolar couplings using conjoined rigid body/torsion angle dynamics. J Am Chem Soc 125: 2902–2912.
18. Dominguez C, Boelens R, Bonvin AM (2003) HADDOCK: A protein–protein docking approach based on biochemical or biophysical information. J Am Chem Soc 125: 1731–1737.
19. Schulz DM, Ihling C, Clore GM, Sinz A (2004) Mapping the topology and determination of a low-resolution three-dimensional structure of the calmodulin–melittin complex by chemical cross-linking and high-resolution FTICRMS: Direct demonstration of multiple binding modes. Biochemistry 43: 4703–4715.
20. van Dijk AD, Boelens R, Bonvin AM (2005) Data-driven docking for the study of biomolecular complexes. FEBS J 272: 293–312.
21. Korkin D, Davis FP, Sali A (2005) Localization of protein-binding sites within families of proteins. Protein Sci 14: 2350–2360.
22. Cho KO, Hunt CA, Kennedy MB (1992) The rat brain postsynaptic density fraction contains a homolog of the *Drosophila* discs-large tumor suppressor protein. Neuron 9: 929–942.
23. Hunt CA, Schenker LJ, Kennedy MB (1996) PSD-95 is associated with the postsynaptic density and not with the presynaptic membrane at forebrain synapses. J Neurosci 16: 1380–1388.
24. Kennedy MB (1997) The postsynaptic density at glutamatergic synapses. Trends Neurosci 20: 264–268.
25. Hata Y, Takai Y (1999) Roles of postsynaptic density-95/synapse-associated protein 90 and its interacting proteins in the organization of synapses. Cell Mol Life Sci 56: 461–472.
26. Roche KW (2004) The expanding role of PSD-95: A new link to addiction. Trends Neurosci 27: 699–700.
27. Koulen P, Fletcher EL, Craven SE, Bredt DS, Wassle H (1998) Immunocytochemical localization of the postsynaptic density protein PSD-95 in the mammalian retina. J Neurosci 18: 10136–10149.
28. Kennedy MB (2000) Signal-processing machines at the postsynaptic density. Science 290: 750–754.
29. Romorini S, Piccoli G, Jiang M, Grossano P, Tonna N, et al. (2004) A functional role of postsynaptic density-95-guanylate kinase-associated protein complex in regulating Shank assembly and stability to synapses. J Neurosci 24: 9391–9404.
30. van Zundert B, Yoshii A, Constantine-Paton M (2004) Receptor compartmentalization and trafficking at glutamate synapses: A developmental proposal. Trends Neurosci 27: 428–437.
31. Cubelos B, Gonzalez-Gonzalez IM, Gimenez C, Zafra F (2005) The scaffolding protein PSD-95 interacts with the glycine transporter GLYT1 and impairs its internalization. J Neurochem 95: 1047–1058.
32. Anderson JM (1996) Cell signalling: MAGUK magic. Curr Biol 6: 382–384.
33. Gonzalez-Mariscal L, Betanzos A, Avila-Flores A (2000) MAGUK proteins: Structure and role in the tight junction. Semin Cell Dev Biol 11: 315–324.
34. Long JF, Tochio H, Wang P, Fan JS, Sala C, et al. (2003) Supramodular structure and synergistic target binding of the N-terminal tandem PDZ domains of PSD-95. J Mol Biol 327: 203–214.
35. Tochio H, Hung F, Li M, Bredt DS, Zhang M (2000) Solution structure and backbone dynamics of the second PDZ domain of postsynaptic density-95. J Mol Biol 295: 225–237.
36. Doyle DA, Lee A, Lewis J, Kim E, Sheng M, et al. (1996) Crystal structures of a complexed and peptide-free membrane protein-binding domain: Molecular basis of peptide recognition by PDZ. Cell 85: 1067–1076.
37. McGee AW, Dakoji SR, Olsen O, Bredt DS, Lim WA, et al. (2001) Structure of the SH3-guanylate kinase module from PSD-95 suggests a mechanism for regulated assembly of MAGUK scaffolding proteins. Mol Cell 8: 1291–1301.
38. Tavares GA, Panepucci EH, Brunger AT (2001) Structural characterization of the intramolecular interaction between the SH3 and guanylate kinase domains of PSD-95. Mol Cell 8: 1313–1325.
39. Yaffe MB (2002) MAGUK SH3 domains—Swapped and stranded by their kinases? Structure 10: 3–5.
40. Fukunaga Y, Matsubara M, Nagai R, Miyazawa A (2005) The interaction between PSD-95 and Ca2+/calmodulin is enhanced by PDZ-binding proteins. J Biochem (Tokyo) 138: 177–182.
41. Nakagawa T, Futai K, Lashuel HA, Lo I, Okamoto K, et al. (2004) Quaternary structure, protein dynamics, and synaptic function of SAP97 controlled by L27 domain interactions. Neuron 44: 453–467.
42. Kornau HC, Schenker LT, Kennedy MB, Seeburg PH (1995) Domain interaction between NMDA receptor subunits and the postsynaptic density protein PSD-95. Science 269: 1737–1740.
43. Niethammer M, Kim E, Sheng M (1996) Interaction between the C terminus of NMDA receptor subunits and multiple members of the PSD-95 family of membrane-associated guanylate kinases. J Neurosci 16: 2157–2163.
44. Ren R, Mayer BJ, Cicchetti P, Baltimore D (1993) Identification of a ten-amino acid proline-rich SH3 binding site. Science 259: 1157–1161.
45. Mayer BJ (2001) SH3 domains: Complexity in moderation. J Cell Sci 114: 1253–1263.
46. Agrawal V, Kishan KV (2002) Promiscuous binding nature of SH3 domains to their target proteins. Protein Pept Lett 9: 185–193.
47. Zarrinpar A, Bhattacharyya RP, Lim WA (2003) The structure and function of proline recognition domains. Sci STKE 179: RE8.
48. Blaszczyk J, Li Y, Yan H, Ji X (2001) Crystal structure of unligated guanylate kinase from yeast reveals GMP-induced conformational changes. J Mol Biol 307: 247–257.
49. Li Y, Spangenberg O, Paarmann I, Konrad M, Lavie A (2002) Structural basis for nucleotide-dependent regulation of membrane-associated guanylate kinase-like domains. J Biol Chem 277: 4159–4165.
50. Sekulic N, Shuvalova L, Spangenberg O, Konrad M, Lavie A (2002) Structural characterization of the closed conformation of mouse guanylate kinase. J Biol Chem 277: 30236–30243.
51. Marcotte EM, Pellegrini M, Ng HL, Rice DW, Yeates TO, et al. (1999) Detecting protein function and protein–protein interactions from genome sequences. Science 285: 751–753.
52. Vogel C, Berzuini C, Bashton M, Gough J, Teichmann SA (2004) Supradomains: Evolutionary units larger than single protein domains. J Mol Biol 336: 809–823.
53. Nourry C, Grant SG, Borg JP (2003) PDZ domain proteins: Plug and play! Sci STKE 179: RE7.
54. Wu H, Reissner C, Kuhlendahl S, Coblentz B, Reuver S, et al. (2000) Intramolecular interactions regulate SAP97 binding to GKAP. EMBO J 19: 5740–5751.
55. Zhang M, Wang W (2003) Organization of signaling complexes by PDZ-domain scaffold proteins. Acc Chem Res 36: 530–538.
56. Kim E, Sheng M (2004) PDZ domain proteins of synapses. Nat Rev Neurosci 5: 771–781.
57. Kim E, Naisbitt S, Hsueh YP, Rao A, Rothschild A, et al. (1997) GKAP, a novel synaptic protein that interacts with the guanylate kinase-like domain of the PSD-95/SAP90 family of channel clustering molecules. J Cell Biol 136: 669–678.
58. Andreotti AH, Bunnell SC, Feng S, Berg LJ, Schreiber SL (1997) Regulatory intramolecular association in a tyrosine kinase of the Tec family. Nature 385: 93–97.
59. Dueber JE, Yeh BJ, Bhattacharyya RP, Lim WA (2004) Rewiring cell signaling: The logic and plasticity of eukaryotic protein circuitry. Curr Opin Struct Biol 14: 690–699.
60. Brenman JE, Topinka JR, Cooper EC, McGee AW, Rosen J, et al. (1998) Localization of postsynaptic density-93 to dendritic microtubules and interaction with microtubule-associated protein 1A. J Neurosci 18: 8805–8813.
61. Grootjans JJ, Zimmermann P, Reekmans G, Smets A, Degeest G, et al. (1997) Syntenin, a PDZ protein that binds syndecan cytoplasmic domains. Proc Natl Acad Sci U S A 94: 13683–13688.
62. Dunker AK, Cortese MS, Romero P, Iakoucheva LM, Uversky VN (2005) Flexible nets. The roles of intrinsic disorder in protein interaction networks. FEBS J 272: 5129–5148.
63. Bonvin AM (2006) Flexible protein–protein docking. Curr Opin Struct Biol 16: 194–200.
64. Russell RB, Alber F, Aloy P, Davis FP, Korkin D, et al. (2004) A structural perspective on protein–protein interactions. Curr Opin Struct Biol 14: 313–324.
65. Burz DS, Dutta K, Cowburn D, Shekhtman A (2006) Mapping structural interactions using in-cell NMR spectroscopy (STINT–NMR). Nat Methods 3: 91–93.
66. Kube E, Becker T, Weber K, Gerke V (1992) Protein–protein interaction studied by site-directed mutagenesis. Characterization of the annexin II–binding site on p11, a member of the S100 protein family. J Biol Chem 267: 14175–14182.
67. Maier CS, Deinzer ML (2005) Protein conformations, interactions, and H/D exchange. Methods Enzymol 402: 312–360.
68. Rosenberg OS, Deindl S, Sung RJ, Nairn AC, Kuriyan J (2005) Structure of the autoinhibited kinase domain of CaMKII and SAXS analysis of the holoenzyme. Cell 123: 849–860.
69. Uchino S, Wada H, Honda S, Nakamura Y, Ondo Y, et al. (2006) Direct interaction of post-synaptic density-95/Dlg/ZO-1 domain-containing synaptic molecule Shank3 with GluR1 alpha-amino-3-hydroxy-5-methyl-4-isoxazole propionic acid receptor. J Neurochem 97: 1203–1214.
70. Kistner U, Garner CC, Linial M (1995) Nucleotide binding by the synapse associated protein SAP90. FEBS Lett 359: 159–163.
71. Song H, Endow SA (1998) Decoupling of nucleotide- and microtubule-binding sites in a kinesin mutant. Nature 396: 587–590.
72. Davis FP, Sali A (2005) PIBASE: A comprehensive database of structurally defined protein interfaces. Bioinformatics 21: 1901–1907.

73. Murzin AG, Brenner SE, Hubbard T, Chothia C (1995) SCOP: A structural classification of proteins database for the investigation of sequences and structures. J Mol Biol 247: 536–540.
74. Orengo CA, Michie AD, Jones S, Jones DT, Swindells MB, et al. (1997) CATH—A hierarchic classification of protein domain structures. Structure 5: 1093–1108.
75. Holm L, Sander C (1998) Touring protein fold space with Dali/FSSP. Nucleic Acids Res 26: 316–319.
76. Mulder NJ, Apweiler R, Attwood TK, Bairoch A, Barrell D, et al. (2003) The InterPro Database 2003 brings increased coverage and new features. Nucleic Acids Res 31: 315–318.
77. Westbrook J, Feng Z, Jain S, Bhat TN, Thanki N, et al. (2002) The Protein Data Bank: Unifying the archive. Nucleic Acids Res 30: 245–248.
78. Henrick K, Thornton JM (1998) PQS: A protein quaternary structure file server. Trends Biochem Sci 23: 358–361.
79. Holm L, Park J (2000) DaliLite workbench for protein structure comparison. Bioinformatics 16: 566–567.
80. Schneidman-Duhovny D, Inbar Y, Nussinov R, Wolfson HJ (2005) PatchDock and SymmDock: Servers for rigid and symmetric docking. Nucleic Acids Res 33: W363–W367.
81. Duhovny D, Nussinov R, Wolfson HJ (2002) Efficient unbound docking of rigid molecules. In: Guigó R, Gusfield D, editors. Lecture notes in computer science. Volume 2452. London: Springer-Verlag. pp. 185–200.
82. Shen MY, Sali A (2006) Statistical potential for assessment and prediction of protein. Protein Sci 15:: 1–18. doi:10.1110ps.062416606
83. Sali A, Blundell TL (1993) Comparative protein modelling by satisfaction of spatial restraints. J Mol Biol 234: 779–815.
84. Dobrodumov A, Gronenborn AM (2003) Filtering and selection of structural models: Combining docking and NMR. Proteins 53: 18–32.
85. Morelli XJ, Palma PN, Guerlesquin F, Rigby AC (2001) A novel approach for assessing macromolecular complexes combining soft-docking calculations with NMR data. Protein Sci 10: 2131–2137.
86. Janin J (2005) The targets of CAPRI rounds 3–5. Proteins 60: 170–175.
87. Mintseris J, Wiehe K, Pierce B, Anderson R, Chen R, et al. (2005) Protein–Protein Docking Benchmark 2.0: An update. Proteins 60: 214–216.
88. Mendez R, Leplae R, De Maria L, Wodak SJ (2003) Assessment of blind predictions of protein–protein interactions: Current status of docking methods. Proteins 52: 51–67.
89. Schultz J, Milpetz F, Bork P, Ponting CP (1998) SMART, a simple modular architecture research tool: Identification of signaling domains. Proc Natl Acad Sci U S A 95: 5857–5864.
90. Letunic I, Copley RR, Schmidt S, Ciccarelli FD, Doerks T, et al. (2004) SMART 4.0: Towards genomic data integration. Nucleic Acids Res 32: D142–D144.
91. Bairoch A, Apweiler R, Wu CH, Barker WC, Boeckmann B, et al. (2005) The Universal Protein Resource (UniProt). Nucleic Acids Res 33: D154–D159.
92. Stroh JG, Loulakis P, Lanzetti AJ, Xie J (2005) LC-mass spectrometry analysis of N- and C-terminal boundary sequences of polypeptide fragments by limited proteolysis. J Am Soc Mass Spectrom 16: 38–45.
93. Shevchenko A, Wilm M, Vorm O, Mann M (1996) Mass spectrometric sequencing of proteins silver-stained polyacrylamide gels. Anal Chem 68: 850–858.
94. Pettersen EF, Goddard TD, Huang CC, Couch GS, Greenblatt DM, et al. (2004) UCSF Chimera—A visualization system for exploratory research and analysis. J Comput Chem 25: 1605–1612.
95. Koradi R, Billeter M, Wuthrich K (1996) MOLMOL: A program for display and analysis of macromolecular structures. J Mol Graph 14: 51–55, 29–32.